A Search for Invariant Relative Satellite motion

Authors: Marco Sabatini, Mauro Pantaleoni, Riccardo Bevilacqua
Contractor: Me.Mo.Mat. Department, La Sapienza University of Rome

Technical officer: Dario Izzo, Advanced Concepts Team (ESA/ESTEC)

Contacts:

Dario Izzo
Tel: ++31 (0)71565 – 3511
Fax: ++31 (0)71565 – 8018
e-mail: act@esa.int

Ariadna id: 04/4104
Study length: 4 months.
Contract Number: 18876/05/NL/MV

Available on the ACT net (www.esa.int/act)

Index:

1. Introduction

1.1. Why formation flying

Though formation flying dates back to 1960, with the works of Clohessy and Wiltshire [10], the full potential of this technique has been studied only in the last decade.

Either for telecommunication or for navigation applications it was soon clear that not just one satellite, but a network of several satellites was necessary to reach certain requirements (such as continuous global coverage). This was the reason for the implementation of the so-called constellations of satellites. Iridium and Globalstar for telecommunications, GPS and Glonass for navigation and positioning are some of the most well-known examples.

Formations are a slightly different concept, and at present day a proper in orbit formation is not flying yet. The satellites of a constellation are in different orbits, and the station keeping or other manoeuvring is accomplished independently from the other satellites.

On the other hand the main objective when designing a formation is the relative motion: the requirements of this kind of mission concern with the maintenance of a relative position, chasing a target relative orbit. This means that a control system must act in order to govern the relative state (position and velocity), and not just the absolute motion of the single satellite.

A number of perturbations act on the satellites and cause a drift on the relative position. If particular conditions minimizing the drift are found, the control effort is greatly diminished.

The aim of the present work is to study the possibility of invariant (i.e. periodic) relative motion, and in case of affirmative answer, to find the initial conditions that would produce this invariance. In those cases in which periodic motion is not dynamically feasible, a method to minimize the drift is proposed.

Formation flying results to be attractive from different point of view.

First of all, performances can be greatly increased. This happens for example in remote sensing missions, where two satellites in a row form a larger baseline ensuring much greater resolution. This is the case of a particular operational mode of COSMO-Skymed mission, consisting of two satellites in a leader-follower configuration in order to have two SAR (Synthetic Aperture Radar) antennas scanning the same object, with great advantages in performances.

A second advantage comes from the fact that launching one big satellite may be more expensive than launching a certain number of smaller (sometimes micro) satellites that could ensure the same or better performances. Moreover if the one single satellite encounters problems once in orbit, the

whole mission is compromised. On the other hand, if the same problems occur to one satellite of the formation, is not jeopardized as in the previous case.
Other possible applications of satellites formation flying are illustrated in Chapter 7.

1.2. Planned missions

The missions described in this section present some differences with the case studied in the rest of the work: they do not orbit around the Earth, or their dimension is very large, or their configuration is just a leader follower one. The fundamentals of dynamics are still anyway very similar, and other science missions (e.g. study of magnetosphere) or for different purposes can be easily imagined around the Earth (see Chapter 7). The following information are extracted by ESA and NASA official websites and from [21].

1.2.1. LISA

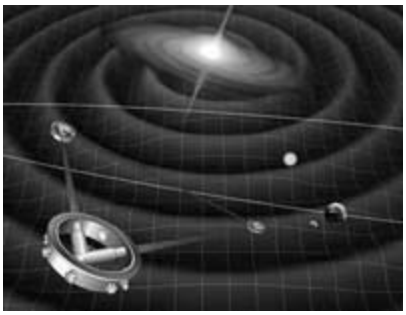

The Laser Interferometer Space Antenna (LISA) consists of three spacecraft, shaped like hockey pucks or pillboxes, freely flying (not connected to each other) five million kilometers (a little more than three million miles) apart, in an equilateral triangle. The spacecraft will carry delicate instruments to track each other and, in concert, measure passing gravitational waves. These waves, as predicted by Einstein, are space-time distortions generated from massive celestial bodies that are accelerated or disturbed. Rippling outward, gravitational waves affect any type of matter they encounter——a solid body should vibrate if a distortion of about the same size hits it. Widely separated bodies will move in and out, with respect to one another, as the distortion passes them. Although the resulting motion would be very small, it would still be measurable with modern techniques such as laser interferometry. This is the goal of the LISA mission. LISA will make measurements with 100 times greater precision than has been achieved ever before, using identical instruments in each spacecraft
LISA will operate 50 million kilometres above Earth. The center of LISA's triangle will follow Earth's orbit around the Sun, trailing 20 degrees behind. It will maintain a distance of 1 AU (astronomical unit) from the Sun, the average distance between the Earth and the Sun. LISA's operational position was chosen as a compromise between the need to minimize the effects on the spacecraft of changes in the Earth's gravitational field and the need to be close enough to the Earth for easy communication.

1.2.2. ST5

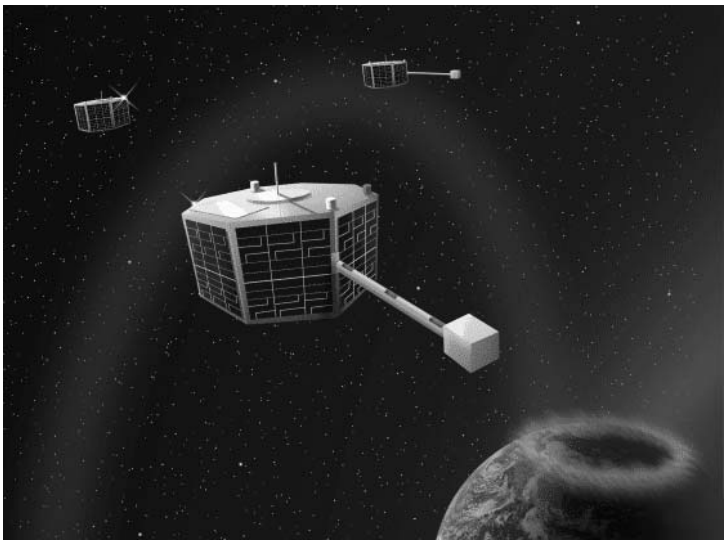

The top level mission requirements of NASA mission Space Technology 5 are focused on the design, development, integration and operation of a full service 25-kilogram class spacecraft that will implement multiple new technologies, function as a single constellation, and achieve accurate research-quality scientific measurements.

ST5's objective is to demonstrate and space-test the ability of "smart" satellites to identify scientific events and implement cooperative data-taking strategies.

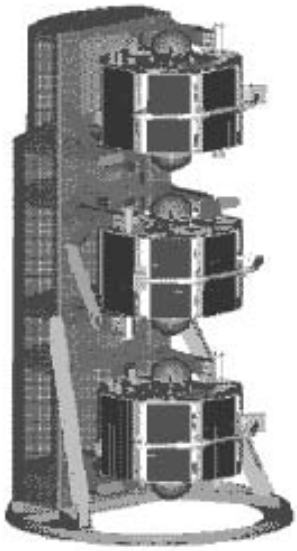

The ST5 project also developed and built the spacecraft bus that enables the mission's multiple micro-satellites to be launched from a single rocket and spun -like Frisbees - into an elliptical Sun synchronous orbit ranging from 300 km (186 miles) to approximately 4,500 kilometers (2,796 miles) above Earth. The spinning motion is required to stabilize the spacecraft and allows for optimal use of sunlight by the solar array panels on the sides of the spacecraft.

Each micro-satellite will be commanded individually from ground stations on Earth, except for a one-week period of “lights out”. During this time, the micro-satellites will fly "autonomously" with pre-programmed commands in a test to find out whether ground commanding (for 24 hours) is really necessary.

ST5's “maiden voyage” will pave the way for flying tens to hundreds of such miniature craft in future missions. These missions can be flown only if they are capable of responding to the changes in the charged particles and magnetic fields in the harsh environment of Earth's magnetosphere.

The mission is on schedule to launch from Vandenberg Air Force Base (VAFB) in late February 2006 with a mission duration of 90 days.

1.2.3. Darwin and SMART-3

ESA mission Darwin will use a flotilla of six 2-metre-diameter telescopes, flying in tight formation, to simulate a single telescope up to 250 metres across. The new formation flying technologies being developed for Darwin allow the flotilla of spacecraft to control their mutual position with high accuracy. In the case of Darwin, this enables you to analyse the atmospheres of very faraway Earth-like planets with high precision and detect the chemical signatures of life. Once this technology is developed, this could also find other applications: miniaturised versions of such technology could replace large, traditional satellites.

The technologies for control, guidance, navigation and optics/optical metrology are so advanced that there is a designated technology demonstration mission, SMART-3. Although SMART-3's exact mission requirements are still being finalised, they will undoubtedly centre on the demonstration of the high accuracy formation flying requirements. The technology requirements will be similar to those required in NASA's close formation telescope missions such as TPF and Life Finder.

For Darwin to work, the telescopes must remain in close formation and undertake centimetric precision flying. Although this sounds a challenging feature of spacecraft positional accuracy, ESA are confident of achieving this aim using a variation of the highly successful Global Positioning System (GPS) that provides so much of the satellite-based navigation on Earth. The technology involves each of the spacecraft being equipped with radio transmitters and a number of receivers. If any spacecraft begins to drift, this will show up immediately in the time it takes for signals from the other spacecraft to reach its various receivers. On board computers will then quickly compute the tiny thrust needed to correct for this and activate the propulsion system. The technical word describing this mechanism of sensing and correcting movement is metrology. The spacecraft will probably be equipped with tiny ion engines that need just 5 kg of fuel to last the entire five-year mission. Another possibility is squirting cold gas out of the thrusters. This might be a better option because ions are corrosive particles that could damage other spacecraft in the flotilla. Instead of an orbit around the Earth, Darwin will be placed far away, beyond the Moon, at a distance of 1.5

million kilometres from Earth, in the opposite direction from the Sun, in a special location, known as L2. Darwin will operate from here. L2 is one of the five points of equilibrium in an orbital system containing the two massive bodies: Sun and the Earth. One of the principal advantages of an L2 orbit is that it offers uninterrupted observations, since the Earth, Moon and Sun remain 'behind' the telescope all the time. Because the L2 point moves around the Sun, keeping pace with the Earth, the entire celestial sphere can be observed during the course of one year. The spacecraft must perform small manoeuvres every month, to ensure it stays at L2.The L2 orbit is also far away from the detrimental effects of Earth's immediate environment. Around our world, the radiation given out by the planet and the particles trapped in its magnetic field can make sensitive observations difficult or even impossible. At L2, these problems are greatly reduced. Darwin will not be the only ESA mission going to L2. When it arrives, it will join Herschel, Planck, JWST and Gaia, all of which will have already been launched. The small flotilla will be probably launched on 2 separate Soyuz-Fregat flights

1.2.4. XEUS

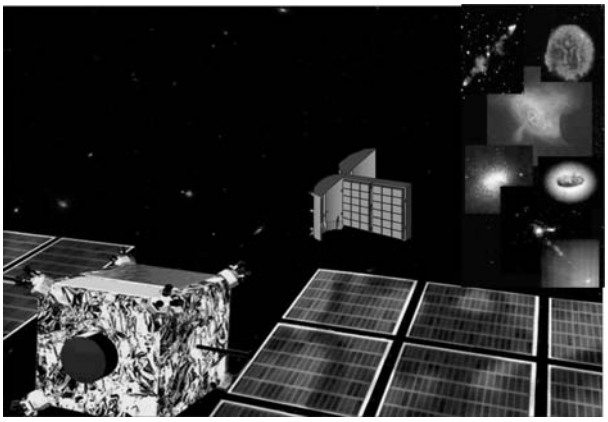

The X-ray Evolving Universe Spectroscopy (XEUS) mission is the potential follow-on to ESA's highly successful XMM-Newton mission. XEUS will consist of two spacecraft – one carrying the mirror, the other carrying the detectors – formation flying 50 metres apart to an accuracy of around 5cm. It is designed to search for the first giant black holes that formed in the Universe, over 10 billion years. This is a similar formation flying concept to NASA's MAXIM missionThe XEUS Mirrror (MSC) and Detector spacecraft (DSC) will be launched together by an Ariane V ECA. The rocket will place the XEUS spacecraft into a transfer trajectory towards the Earth-Sun L2 point. The MSC and DSC will separate and take up positions 50 m apart (the focal length of the X-ray optics) ready to commence scientific operations.

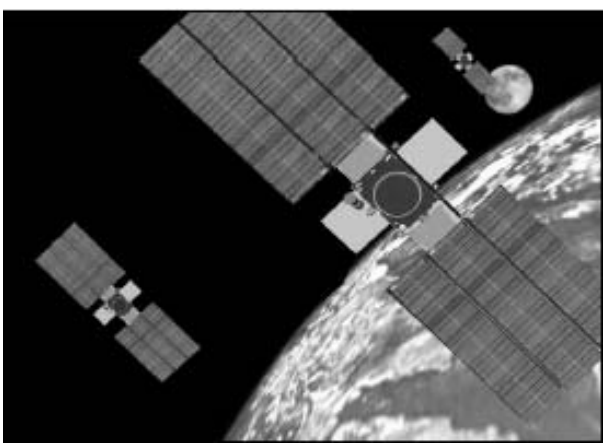

1.2.5. TechSat21

To address the technical challenges of micro-satellite formations and quantify mission

performance, AFRL (Air Force Research Laboratory) formulated the TechSat21 flight experiment consisting of three 150kg satellites in a 550km orbit. Key program objectives are to demonstrate:

1) Autonomous formation maintenance and reconfiguration of 3 satellites in non-linear formations.

2) Sparse aperture sensing for multiple missions using innovative waveforms and signal processing.

3) Validated simulation with performance modelling for broad range of missions and satellite configurations (micro-satellite formations, single large satellites, and hybrid systems in any quantities and orbits) to support future system architecture trades.

The satellites will initially be deployed from the launch vehicle in an along-track configuration separated by approximately 5km. During satellite initialization and on-orbit check out, the satellites will maintain this simple linear configuration with safe separation and no autonomous formation flying. After verifying basic GPS metrology measurements to 10m absolute position knowledge, very basic autonomy will be initiated to maintain the formation, first through monitoring of on-orbit generated command scripts and then with autonomous on-orbit execution of those scripts.

Sparse aperture sensing experiments will be initiated during this slow progression of increasing autonomy, and satellite separation will slowly decrease over the next several months until reaching 100-500m relative distance. The satellites will then move into elliptical 3-D Hill's formations where the satellites have very slight variations in altitude, inclination, and eccentricity to produce the effect of the satellites rotating around a virtual point at their center. The 3-D formation allows 2-D sparse aperture experiments to begin, and the separation of the satellites will be slowly increased in the Hill's formation until the 5km separation is again reached. At this time near the end of the 1-year experiment, the satellites will again return to closer formations to perform such higher risk experiments as autonomous formation reconfiguration and sparse aperture sensing experiments at distances under 100m separation.

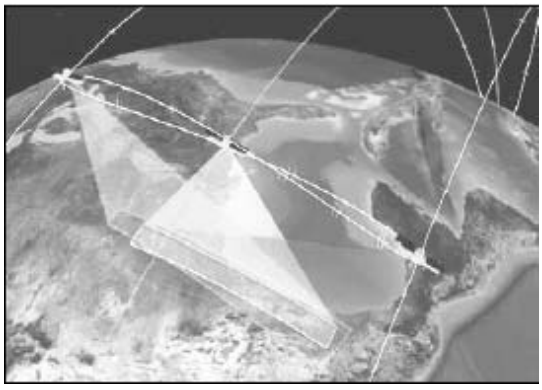

Experiment performance for different mission applications is expected to vary based on satellite separation. For example, large satellite separations are better for geolocation, bistatic synthetic aperture radar (SAR), and interferometric SAR (IF-SAR), and close proximity formations better for vernier on transmit SAR and GMTI.

1.3. Notation and reference frames

A general formation is composed by several satellites. Without loss of generality this work will focus on the case of two satellites. The formation is always formed by a reference satellite, called chief (associated with the pedex "0"), and a satellite, deputy (associated with the pedex "1"), whose relative trajectory around the chief is the object of the study. The chief satellite can also be just a geometrical point following an unfeasible dynamic. The motion is studied in the Local Vertical Local Horizontal (LVLH) reference frame. The origin (see Fig. 1) is taken as coincident with the chief satellite. The *x* axis is aligned to the Earth-to-satellite radius, the *z* axis is perpendicular to the orbital plane, and the *y* axis is such that Oxyz is a righthanded orthonormal reference frame.

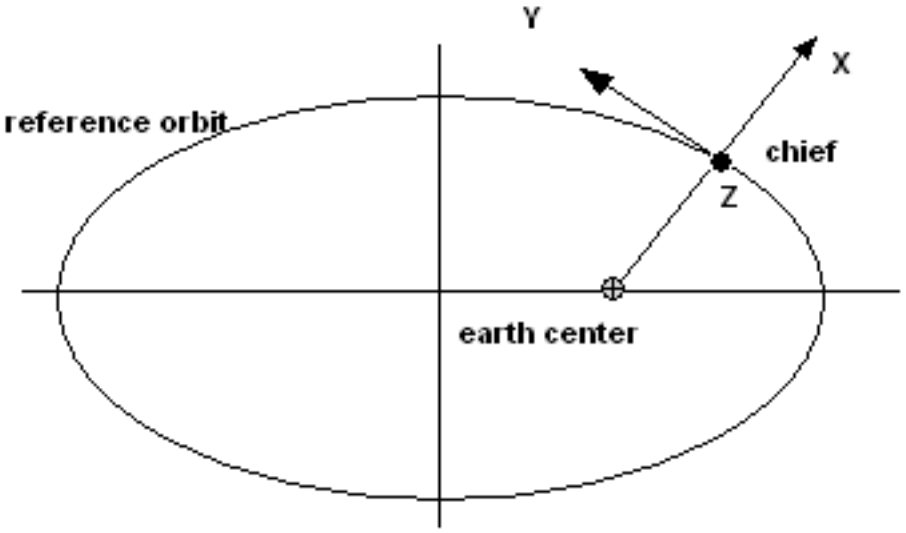

Fig. 1 LVLH reference frame

The absolute motion of the satellites is simulated by a propagator in a quasi-inertial reference frame with the origin placed in the Earth centre, the X axis aligned with line from Earth to Aries constellation (γ), Z axis coincident with polar axis and Y is consequent (Fig. 2).

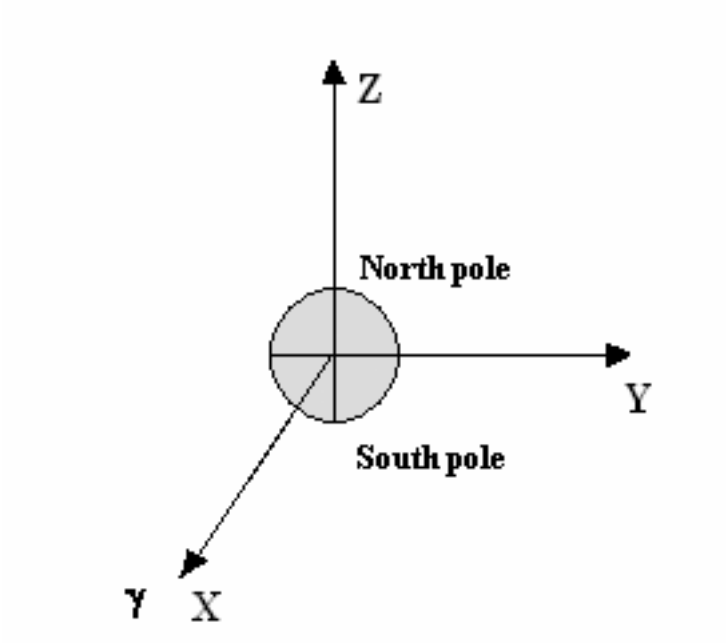

Fig. 2 Inertial reference frame

1.4. Plan of the study

As the main numerical tool used in this work is a genetic algorithm, a panoramic on the theory at the base of this methodology is offered in Chapter 2. The tuning of the algorithm for the problem of searching invariant relative orbits is widely discussed in the same Chapter 2.

A progressive approach has been used: starting from a simple model up to the complete perturbed one, the problem to find an invariant relative orbit has been investigated.

Therefore, the simplest case is analysed first in Chapter **Error! Reference source not found.**: unperturbed orbits. Under these hypotheses a periodic relative motion exists: in fact, imposing the orbits of the chief and of the deputy to have the same period, the satellites of the formation describe a closed relative trajectory. The results found using GA are compared to analytical results based on simplified dynamical models. HCW equations for circular orbits and TH equations for elliptical orbit are two of the most well known models. The conditions to obtain periodic relative motion that derive from these models are a good approximation of the period matching condition only for small formations. For larger formations their performances decrease for elliptical reference orbits, while they prove to be affordable for the circular case. The unperturbed case is used as a validation tool for the algorithm based on GA.

In Chapter 4 one of the major perturbations for satellites in Earth orbit is included in the model to be optimized by GA: the J_2 effect, due to the flattening at the Earth's poles. Though conservative, J_2 introduces non-periodic dynamics making an invariant motion of the formation possible only in very particular situations. In Chapter 5, the effects of minor gravitational perturbations are analysed.

In particular the impact on the relative dynamics of the presence of other attractive masses such as sun and moon, and of the higher harmonics of the geopotential, is analysed. The other major perturbation, which cannot be neglected for low orbits, is instead considered in Chapter **Error! Reference source not found.**. Drag influence is much more sensible as the orbit altitude is lower. As this is a dissipative perturbation, a periodic relative motion under air drag effect is not expected. In fact, in altitudes from 200 km to 500 km a closed relative orbit cannot be found with the traditional approach. In this case the aim is to maintain the formation bounded for a given number of orbits, not necessarily one as previously done when looking for invariant orbits. This means that the satellites are free to drift apart, but in such a way that after the imposed time they will be near again. This is the best that can be done to counteract drag effects.

The mentioned strategy has interesting possible applications, illustrated in Chapter 7, where two possible missions, one for the health monitoring of large space structures such as Space Shuttle and International Space Station, and one for in orbit assembly, are proposed. Moreover another use of the results is defined in this work: due to the impossibility of reaching the needed precision for the initial conditions – even with a technique such as Carrier Differential GPS – the results can be used in an indirect way, for example the invariant relative orbit found by GA as a reference trajectory for a regulator.

2. Genetic algorithms: basic theory and tuning

2.1. How do genetic algorithms work

2.1.1. Evolution and optimization

The general ideas of evolution and adaptation predate Charles Darwin's 1859 “On the Origin of Species by means of natural Selection”, but it is Darwin (and more or less simultaneously A.R. Wallace) who first identified what is still considered by most to be the primary driving mechanism of evolution: natural selection. Natural selection is the process whereby individuals better adapted to their environment (i.e., ``fitter", in the wider sense of the word) tend to produce, on average, more offspring that their less well endowed competitors in the breeding population. Darwin and his contemporaries also realized that two additional ingredients are required for natural selection to lead to evolution. The first is heredity; an offspring must inherit, in some way, some of the characteristics that make its parents fit, otherwise evolution is effectively reset to zero with each new generation. The second ingredient is variability: at any given time there must exist a spectrum of fitness among population members, otherwise natural selection simply cannot operate.

Although both these aspects remained unexplained in Darwin's lifetime, the primary processes through which heredity is mediated and variation maintained are now basically understood. Each cell of each individual (or phenotype) contains a complete set of instructions effectively defining its physical (and possibly behavioural) makeup. This information is encoded in the form of linear gene sequences stored on pairs of homologous chromosomes, which constitute the individual's genotype. Sexual reproduction involves the combination of genetic material from both parents, one half of each chromosome pair coming from each parent.

A fundamental aspect of this breeding process is that the relationship between phenotype and genotype is unidirectional; a given individual can be thought of as an external manifestation of its genotype (although there exist environmental influences in development and growth that are beyond genetic control), but the individual cannot influence its own genetic makeup. It can, however, influence the genetic makeup of subsequent generations through differential reproductive success, which is of course where natural selection plays its crucial role.

To a large extent, variability turns out to be maintained by the machinery of heredity itself. The production of reproductive cells often entails the recombination of genetic material across homologous chromosomes through the processes of crossover and inversion. Copying mistakes

and/or true random events also occasionally introduce mutations in the genotype. The ensemble of all genes existing at a given time in the breeding population makes up the gene pool. For a given gene associated with a chromosomal locus, there exist in general more than one allowed "gene value" (or allele in biological terminology). Evolution can be thought of - and mathematically modelled- in terms of temporal changes in allele frequencies throughout the gene pool.

Genetic Algorithms (hereafter "GA") are a class of heuristic search techniques that incorporate these ideas in a setting that is computational rather than biological. Strictly speaking, genetic algorithms do not optimize, and neither does biological evolution; evolution uses whatever material that is at its disposal to produce above average individuals. Evolution is blind. Evolution has no ultimate goal of "perfection". Even if it did, evolution must accommodate physical constraints associated with development and growth, so that not all paths are possible in genetic "parameter space". One could perhaps argue than evolution performs a form of highly constrained optimization, but even then it certainly does not optimize in the mathematical sense of the word.

Nevertheless, genetic algorithms form the basis of a class of extremely robust optimization method known as GA-based optimizers. The GA-based FORTRAN subroutine used in this work is a version of PIKAIA, freely available on line, modified for the purposes of this work.

2.1.2. Basics of genetic algorithms

In their simplest incarnation, genetic algorithms make use of the following reduced version of the biological evolutionary process; the gene pool -and its associated phenotypic population- evolves in response to

1) differential reproductive success in the population;
2) genetic recombination (crossover) occurring at breeding;
3) random mutations affecting a subset of breeding events.

Consider then the following generic optimization problem. One is given a "model" (in the present case, the relative dynamics of satellites flying in formation) that depends on a set of parameters **a**, and a functional relation **f(a)** that returns a measure of quality for the corresponding model; this will be called *fitness function*. The optimization task consists in finding the "point" **a*** defining a model that maximizes the quality measure **f(a)**.

For the sake of the argument suppose that one has available a target value ***F*** and define a tolerance criterion $\varepsilon > 0$ such that a "solution" **a*** satisfying

$$\left|F - f(a^*)\right| \leq \varepsilon$$

corresponds to a model deemed acceptable. Define now a population ***A*** as a set of ***K*** realizations of the parameters **a**:

$$A \equiv \{a_k\} \qquad k = 1,2...,K$$

and an operator ***R*** that, when applied to a given population A^{n-1}, produces a new population A^n. From these building blocks a basic genetic algorithm could be constructed as follows:

$$\begin{aligned}
&\text{Initialize}: \mathrm{A}^0 \equiv a_k^0 \quad \mathrm{k} = 1,...,\mathrm{K} \\
&\text{Compute}: f_k^0 \equiv f\left(a_k^0\right) \\
&n = 0 \\
&\text{do while} \left|F - f(a^*)\right| \geq \varepsilon \\
&\qquad n = n + 1 \\
&\qquad A^n = R\left(A^{n-1}\right) \\
&\qquad \text{Compute}: f_k^n, \quad \mathrm{k} = 1,...,\mathrm{K} \\
&\text{end do} \\
&a^* = a_{k_{MAX}}^n
\end{aligned}$$

Were it not that the operator R acts on a population rather than on a single individual, this would look very much like some generic Monte Carlo algorithm. The crucial difference lies with the definition of the operator R. First, R does not operate directly on the parameters a_k (the phenotypes), but rather on their encoded versions (the genotypes). Second, R applies crossover and mutation operations on the genotypes, processes that involve markedly stochastic aspects, as opposed to fully deterministic schemes such as averaging. Third, R does not operate on the existing population in a homogeneous fashion, but selects a subset of the population on the basis of their quality measure *f(a)* (their fitness). In analogy with biological systems, a phenotype is encoded in the form of a string (or chromosome) of digits. In contrast to biological systems, in basic genetic algorithms it is common to fully encode a phenotype on a single chromosome, as opposed to groups of homologous chromosome pairs with dominant/recessive character. A genotype then is made of a single chromosome, and both terms can be used interchangeably.

These considerations notwithstanding, the algorithm listed above still only defines an adaptive plan or evolution strategy. It pretty much ensures gradual improvement over successive iterations, but does not guarantee absolute maximization in anything approaching the strict mathematical sense of the word. GA-based optimizers typically implement additional strategies and techniques to improve performance in the context of numerical optimization.

Genetic algorithms have been used successfully to solve a number of difficult optimization problems arising in computer science, artificial intelligence, computer-aided engineering design,

geoseismic modelling, and are attracting increasing attention in other branches of the physical sciences. Yet, generally speaking, they are not yet a standard component of the numerical modeller's toolboxes and many think that global optimization using partially stochastic algorithms is more art than science. The benefits of these techniques are, though, huge; in fact they may approach many problems, otherwise unsolvable.

2.2. Algorithm Tuning

2.2.1. Genetic algorithms theory applied to formation flying problem

The basics of the working of the Genetic Algorithms applied to the satellite relative motion can be easily illustrated in Fig. 3.

The algorithm start with a set of possible solutions (represented by chromosomes) that represents the population. Solutions from the initial population are taken and used to form a new population. This is motivated by a hope that the new population will be better than the old one. New solutions are selected according to the value of their fitness function, the more suitable they are the more chances they have to reproduce by mating (crossover).

The scheme is quite simplified, but it can point out all the problems concerning tuning of the genetic algorithm.

1) First of all, we must establish *who* the individuals of the population are;
2) Which are their genes;
3) Which is the fitness function;
4) How many are the individuals;
5) How many generations they have to mate;
6) How can the other genetic algorithm parameters be chosen.

Moreover, a tuning of the propagator itself must be accomplished, following the main quests:

1) Which are the forces acting on the satellites;
2) Which integrator is used;
3) What is the time step size.

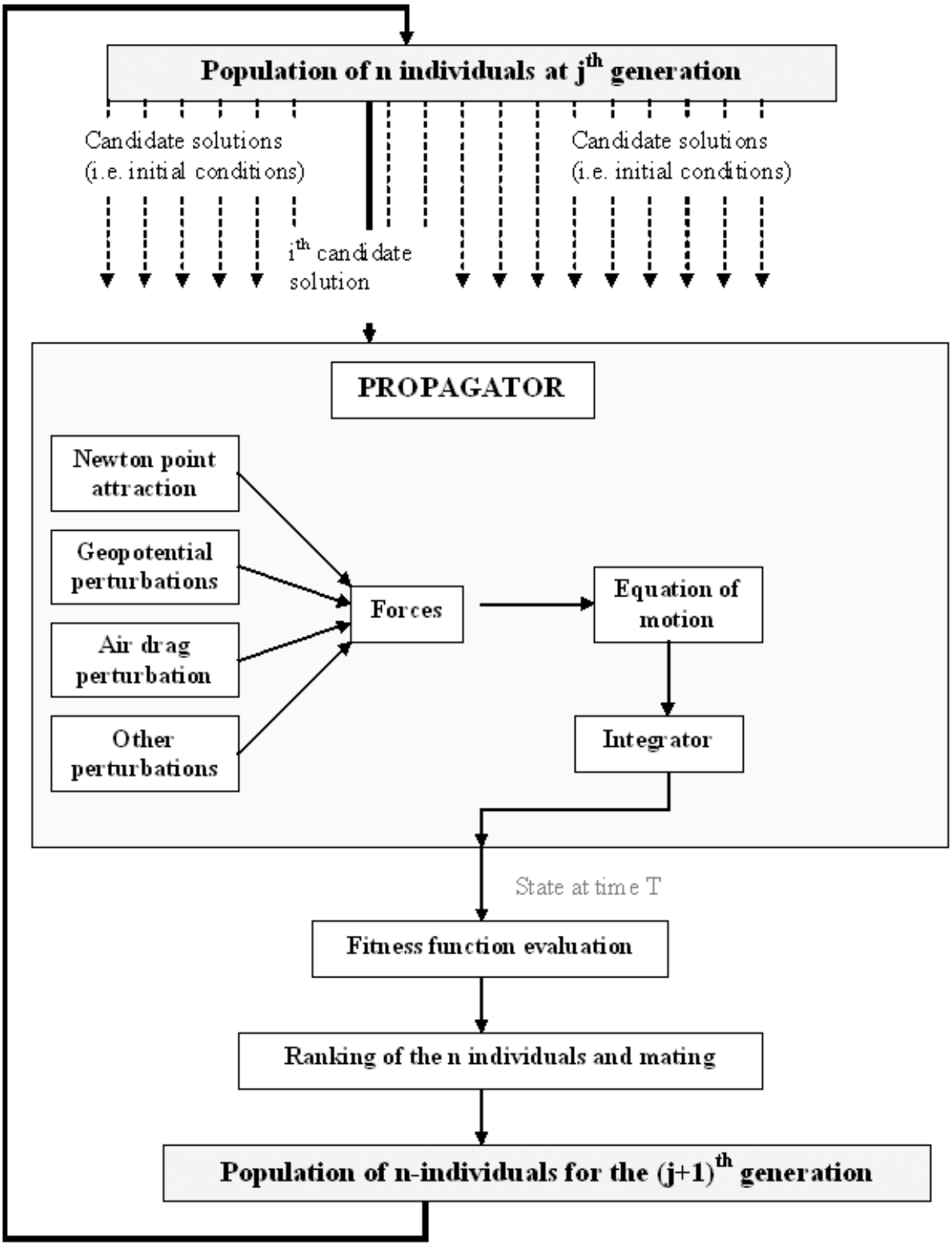

Fig. 3 Simplified scheme of the algorithm

2.2.2. Who are the individuals of the population and which are their genes

In the approach that is here proposed the individuals of the population are the relative trajectories between the Chief and the Deputy. The absolute motion of two satellites is described by the two simple equations:

$$\frac{d^2\vec{r}_0}{dt^2} = -\frac{\mu}{r_0^3}\vec{r}_0 + \vec{F}_0 \qquad + \text{initial conditions for the Chief} \qquad \textbf{Eq. 1}$$

$$\frac{d^2\vec{r}_1}{dt^2} = -\frac{\mu}{r_0^3}\vec{r}_1 + \vec{F}_1 \qquad + \text{initial conditions for the Deputy} \qquad \textbf{Eq. 2}$$

where $\vec{F}_o, \vec{F}_1$ are the forces due to perturbations – called perturbation accelerations, namely geopotential, air drag, third body and solar wind pressure effects, as shown in the scheme –. The initial conditions can be defined in various way. For the satellite 0, named chief, the initial conditions are usually given as orbital parameters at time zero, a set of six parameters that describe the shape and the space orientation of the orbit.

Eq. 1 and $\frac{d^2\vec{r}_1}{dt^2} = -\frac{\mu}{r_0^3}\vec{r}_1 + \vec{F}_1$ + initial conditions for the Deputy Eq. 2, which describe the satellite motion, are referring to coordinates in the inertial reference frame. The initial orbital parameters of the Chief must therefore be translated in initial inertial coordinates, as sketched in Fig. 4.

For the satellite 1, the initial conditions will be assigned in the form of relative state, which means:

$$[\rho, \dot{\rho}] = [x, y, z, \dot{x}, \dot{y}, \dot{z}], \qquad \textbf{Eq. 3}$$

in the orbital reference frame $[\hat{r}, \hat{\theta}, \hat{h}]$, called LVLH. This initial relative state must be again transformed in initial inertial coordinates.

The steps to perform before the actual propagation may begin, are illustrated in Fig. 4.

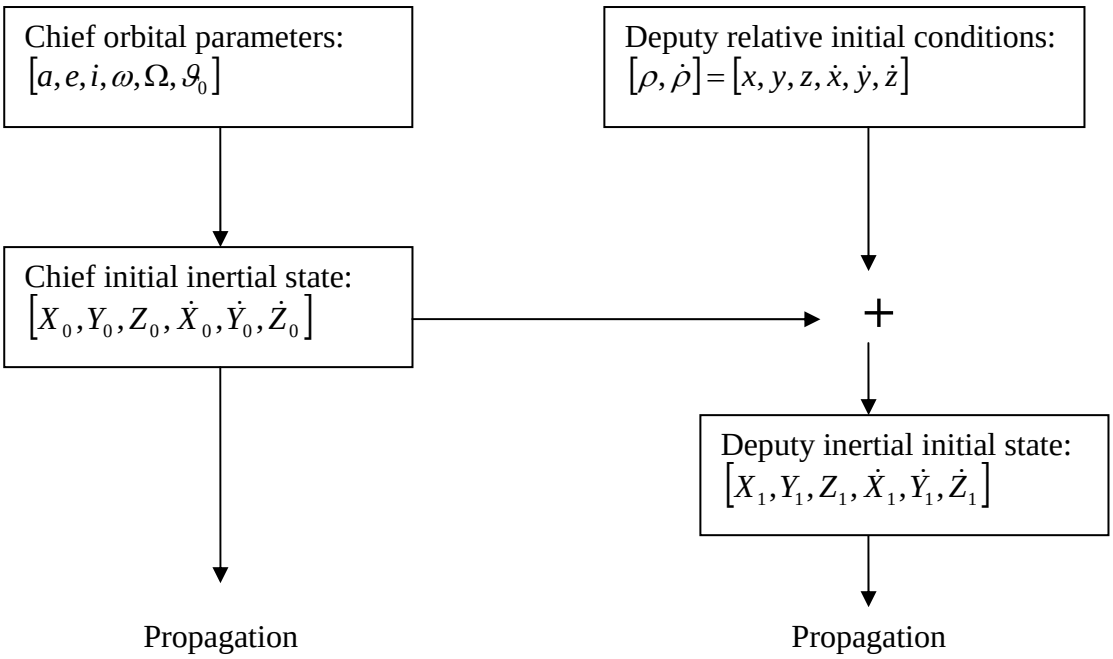

Fig. 4 Preliminary transformations

The operation indicated as a sum is not a simple sum: some manipulation is necessary have to be performed in order to obtain the deputy inertial initial state. For the space coordinates:

$$[X_1, Y_1, Z_1]^T = [X_0, Y_0, Z_0]^T + R \cdot [x_1, y_1, z_1]^T \qquad \textbf{Eq. 4}$$

where R is the matrix transforming orbital reference frame into inertial reference frame.

For initial velocities the transformation is that of Eq. 5.

$$[\dot{X}_1, \dot{Y}_1, \dot{Z}_1]^T = [\dot{X}_0, \dot{Y}_0, \dot{Z}_0]^T + R \cdot [\dot{x}_1, \dot{y}_1, \dot{z}_1]^T + R \cdot (\vec{\omega} \times [x_1, y_1, z_1]) \qquad \textbf{Eq. 5}$$

where $\vec{\omega}$ is the angular velocity of the chief satellite.

The algorithm which transform orbital parameters into inertial coordinates isn't much more complex:

$$\vec{r} = \left[\frac{a \cdot (1 - e^2)}{1 + e \cos \vartheta}, 0, 0 \right] \qquad \textbf{Eq. 6}$$

$$\vec{v} = \left[\frac{\mu}{h} e \sin \theta, \frac{\mu}{h} (1 + e \cos \theta), 0 \right] \qquad \textbf{Eq. 7}$$

These are radius and velocity in the orbital reference frame. So the inertial coordinates are simply:

$$\left[X_1, Y_1, Z_1\right]^T = R \cdot \vec{r} \quad \textbf{Eq. 8}$$

$$\left[\dot{X}_1, \dot{Y}_1, \dot{Z}_1\right]^T = R \cdot \vec{v} \quad \textbf{Eq. 9}$$

After these transformations, these two initial states are propagated. In order to obtain the relative states, the operations in Eq. 4 and Eq. 5 have to be performed in the inverse direction at each time step, so that we obtain the relative coordinates.

The relative trajectory depends only on the relative initial conditions, and these will be considered as our decision vector. Only a proper choice of these conditions can generate bounded relative orbits.

The individuals of the initial population must then represent this set of initial conditions. This means that each individual has at least six genes, three for the distances and three for the velocities. In some case, as it will be shown in Chapter 2, even just one proper initial condition can be sufficient in order to find the desired closed orbit. In more general cases, a safer approach requires that all six initial conditions are considered variables of the genetic algorithm.

A seventh genes is then added. In fact, in the purely keplerian case it's clear that if a periodic relative orbit exists, it can close only after one orbital period; in a perturbed case, trough, this is not true anymore, as an orbital period does not even exist. Therefore the final propagation time has been also considered as gene.

In other words, the DNA of the individual is representative of a single chromosome with a number of genes.

$$individual = \begin{bmatrix} x_1 \\ y_1 \\ z_1 \\ \dot{x}_1 \\ \dot{y}_1 \\ \dot{z}_1 \\ T_{end} \end{bmatrix} \quad \textbf{Eq. 10}$$

The encoding process of the algorithm here used produces, for each selected parent, a chromosome-like structure that will subsequently be used for breeding through the action of the various genetic operators to be discussed further below. The complementary process of decoding is the equivalent of development and growth in biology, i.e., the reconstruction of an individual from its defining genetic material.

More pragmatically, the aim of the encoding process is to produce a "chromosome" from the *n* parameters (seven in this case) defining the function f(x) to be maximized. Write these as

$$x \equiv (x_1, x_2, ..., x_n)$$

PIKAIA encodes these parameters using a decimal alphabet, namely the simple 1-digit base 10 integers 1 . Schematically,

$$x_k \in [0.0,1.0] \rightarrow X_k = (X_1, X_2, ..., X_{nd})_k,$$

where the $X_j \in [0,9]$ are positive integers. The encoding algorithm is simply:

$$X_j = \mathrm{mod}(10^{nd-j+1} x_k, 10), \qquad \mathrm{j} = 1,2,...,\mathrm{nd}$$

where the function mod(x; y) returns the remainder of the division of x by y.

Each of the *n* defining parameters thus becomes a sequence of *nd* 1-digit integers, so that the encoding of all *n* parameters to *nd* significant digits produces a 1-D integer array (or "chromosome") of length $n \times nd$. Each element of this array can be thought of as a "gene" having 10 possible alleles. For each encoded parameter, the complementary decoding process is simply

$$x_k = \frac{1}{10^{nd}} \sum_{j=1}^{nd} X_j \times 10^j$$

Consider the task of maximizing a function f(x; y) of two variables. In this case an individual (or "phenotype") is a point (x; y) in 2-D parameter space. The encoding process would produce

(x; y) = (0.34567890; 0.23456789) $\rightarrow$ 3456789023456789

for *nd*=8. The chromosome 3456789023456789 is made up 16 genes, and is the full genotype of the phenotype (x; y). The number of digits retained in the encoding/decoding, *nd*, is an input quantity that remains fixed throughout the run.

In order to increase the precision of the optimizator, some changes have been implemented in PIKAIA. In fact, all variables have been set to double precision, and the maximum number of digits for each gene has been brought from 6 to 9.

Because the mathematical parameters of the GA are defined as $x_k \in [0.0,1.0]$, seven parameters $[x(1), x(2), x(3), x(4), x(5), x(6), x(7)]$ are chosen to describe physical parameters, which stand for the satellite's initial conditions and time. Therefore some transformations has been operated. For the initial relative distances:

$$[x_i, y_i, z_i] = -1 + 2 \cdot [x(1), x(2), x(3)] \quad \textbf{Eq. 11}$$

Then to obtain the initial relative velocities:

$$[\dot{x}_i, \dot{y}_i, \dot{z}_i] = -1e^{-2} + [x(4), x(5), x(6)] \cdot 2e^{-2} \qquad \textbf{Eq. 12}$$

In this way initial velocities are included in the range $[-1e^{-2}, 1e^{-2}]$. In fact it can be easily shown that initial relative velocities are two order of magnitude smaller then initial distances (actually, order of the orbital angular velocity).

As for the propagation time, it will be chosen as: $T = T_{Kepler} \pm x(7) \cdot k$,where k is a constant properly chosen (some hundred of seconds).

This last one is a crucial variable, because at this time the final relative coordinates are compared to the initial relative coordinates. These two sets of relatives states (initial and final) determine the quality of the individual. It is considered as a good individual if the difference between the two relative states (initial and final) is close to zero. In this way its position in the individual ranking will be high, and so it has the chance to mate and to generate a "good" son. Its genes will survive in the next generation, and if they will be placed first, in the individual ranking at the last generation, they represent the set of initial conditions that generate a closed relative orbit, if it exists. Otherwise, they represent the set that more than other generates quasi-invariant orbits.

2.2.3. Which is the fitness function

The fitness function is the tool by which the selection process pressure is imposed. An higher value of the fitness function means an higher probability of the individual to mate. As PIKAIA uses the "roulette wheel" selection strategy, it's possible to say that the probability of success of an individual whose fitness is S_i is the same of the roulette ball to fall in an angular sector given by:

$$\frac{1}{2\pi} \frac{S_i}{\sum S_i} \qquad \textbf{Eq. 13}$$

As expected, this probability is a growing function of S_i .

In our case, the fitness function must rank an individual who generate the relative orbit in Fig. 6 as a bad individual, and the individual who generate the relative orbit in Fig. 5 as a good one.

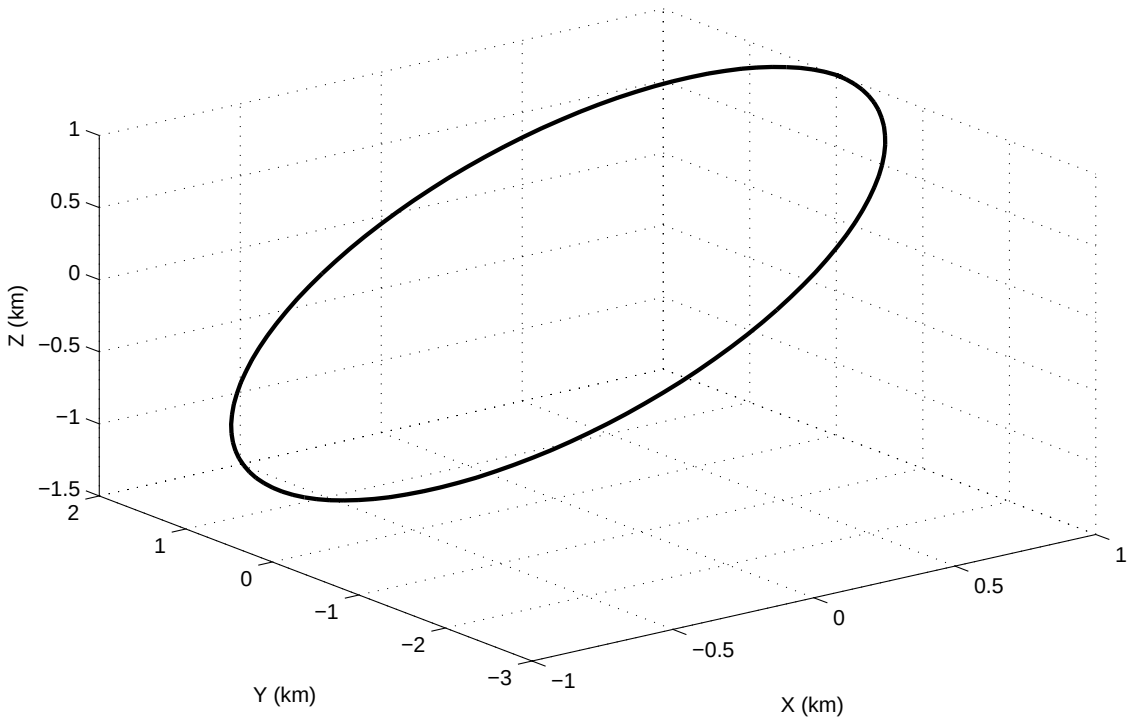

Fig. 5 Example of a relative orbit perfectly closed

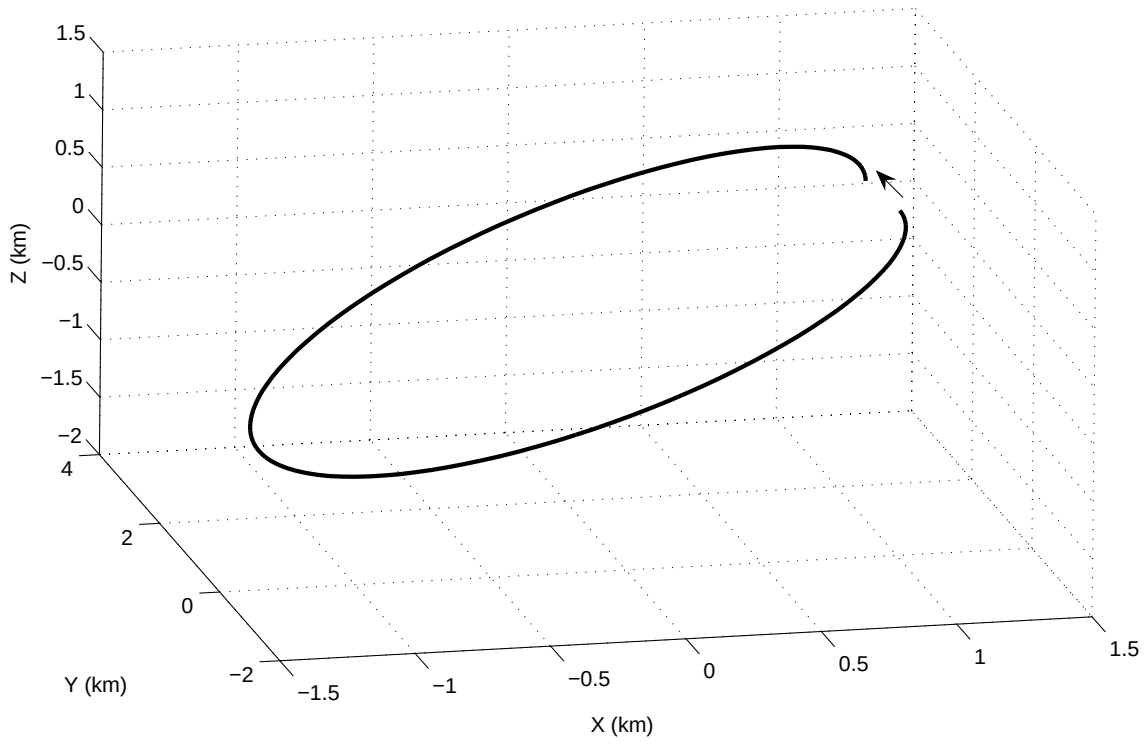

Fig. 6 Final error in a relative orbit

In Fig. 6 the black arrows shows the final error, what should be zero in order to have a perfectly closed orbit. This leads to elaborate some simple fitness function.

The distance indicated by the arrow in Fig. 6 can be calculated as:

$$d = \sqrt{\left(x_f - x_i\right)^2 + \left(y_f - y_i\right)^2 + \left(z_f - z_i\right)^2} \qquad \textbf{Eq. 14}$$

Once this parameter is defined we can proceed to determine the fitness function, as a decreasing function of *d*. Some example of fitness function could be the following:

$$f_1 = -d \qquad \textbf{Eq. 15}$$

$$f_2 = \frac{1}{d} \qquad \textbf{Eq. 16}$$

$$f_3 = -\log(d) \qquad \textbf{Eq. 17}$$

These three function are plotted in Fig. 7, Fig. 8 and Fig. 9

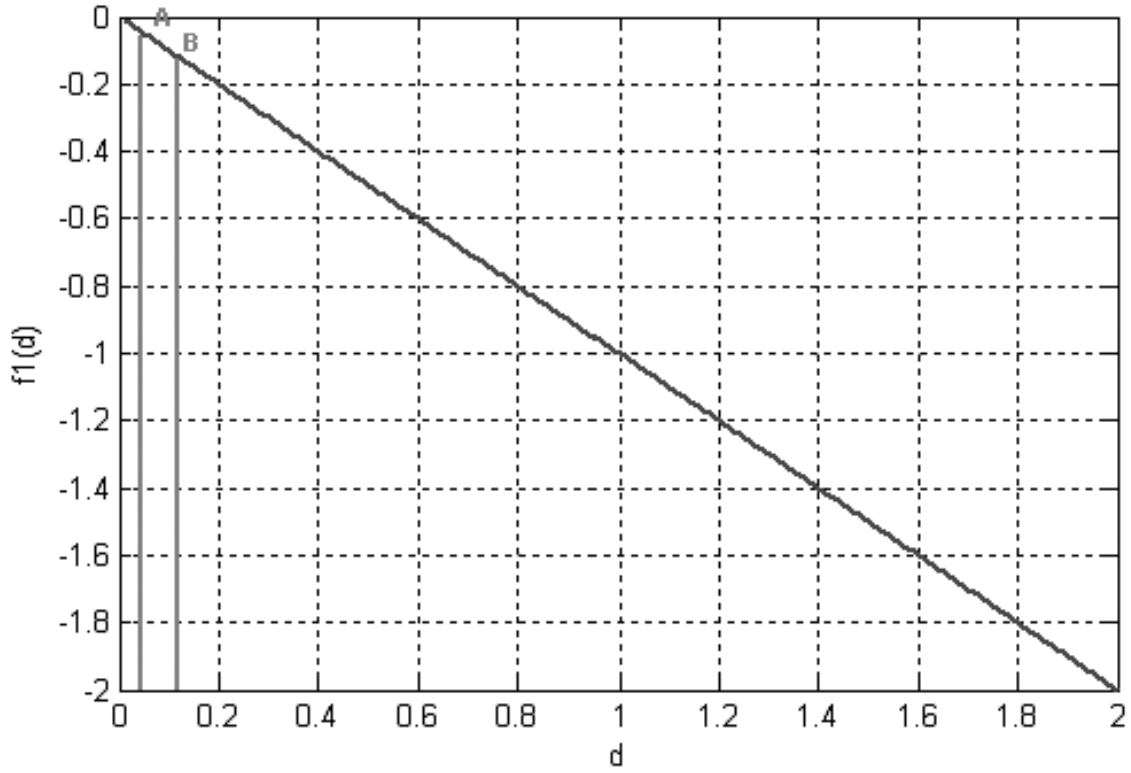

Fig. 7 Plot of Eq. 15

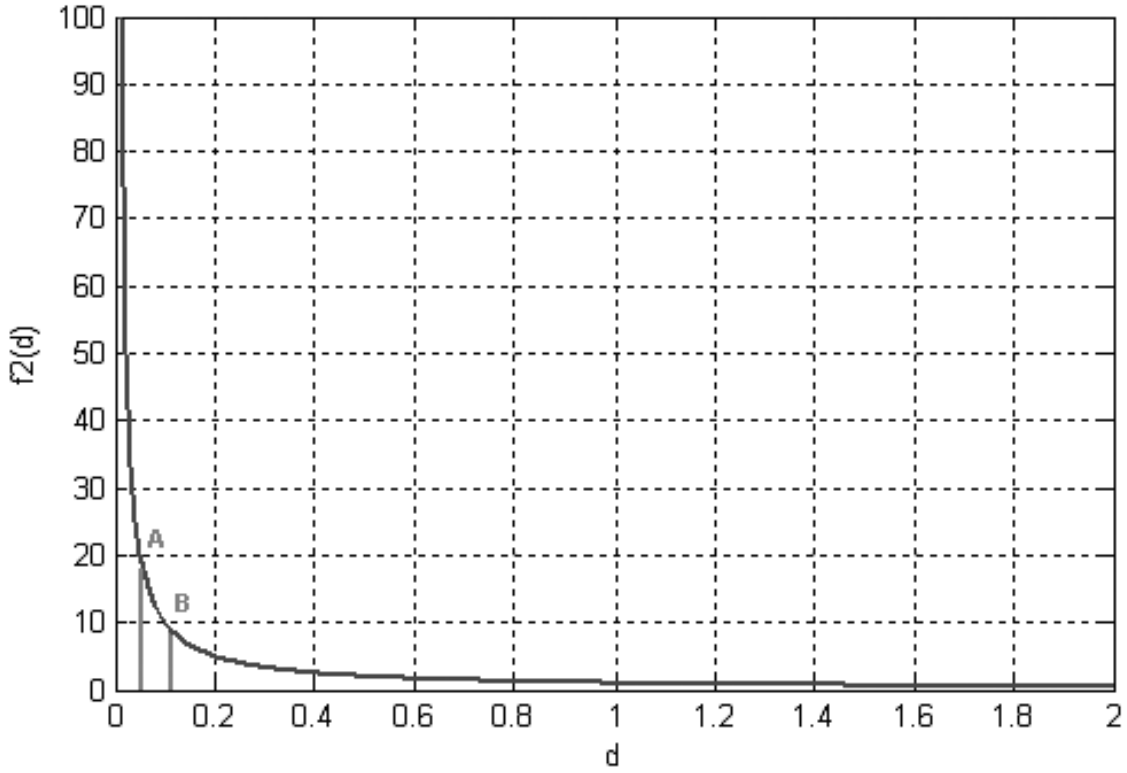

Fig. 8 Plot of Eq. 16

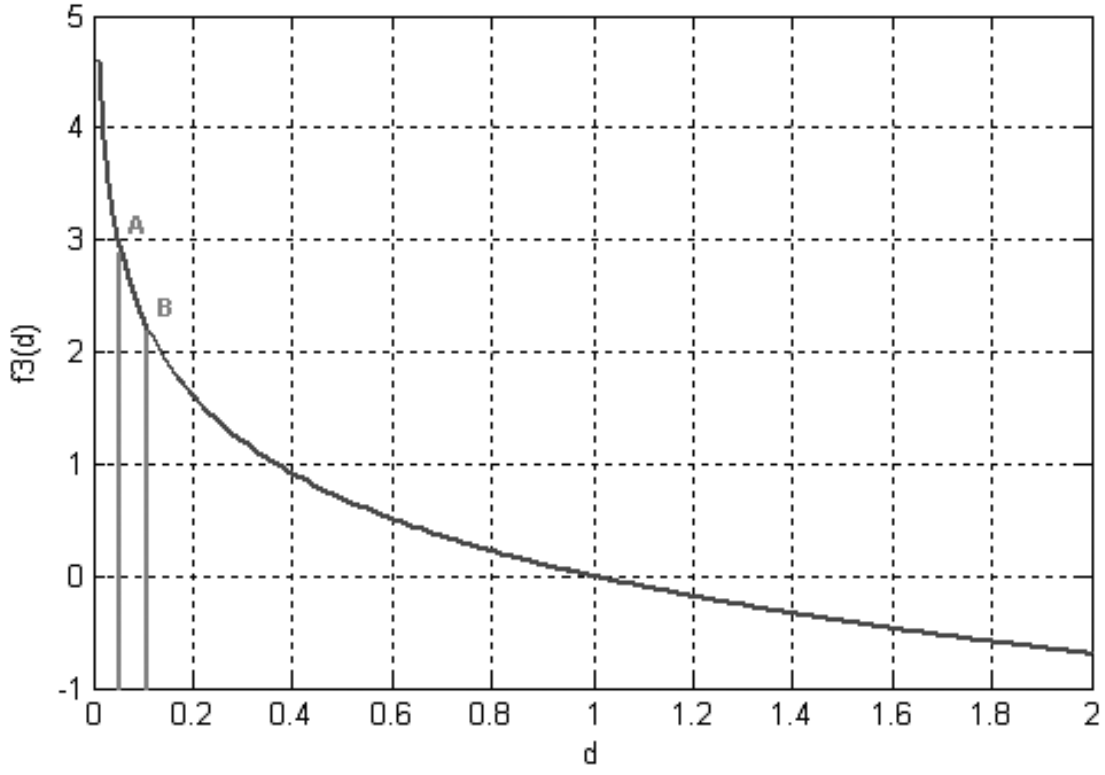

Fig. 9 Plot of Eq. 17

Function *f2* and *f3* shows a behaviour more suitable for our needs. In fact, in *f1* the difference in fitness value of two individuals *A* and *B* is linear respect to the parameter *d*, while in *f2* and *f3* an individual with lower *d* is much more likely to mate: choosing one of these, as fitness function, is an aid to the selection process.

On the other hand, *f3* is not positive for all *d*, and *f1* is always negative. This fact is not fair as it's indeed preferable to use positive definite function – even if the algorithm seems to work anyway –. This leads to the choice of function *f2*. *f2* has some problems, as well. In fact, it considers only the distance of the final position to the initial position, while the state is formed by the relative velocities as well. Saying that the best individual is the one who passes again on the starting point after a given period can be quite incorrect, because the relative velocity vector could be different.

A better way to implement the fitness function is an a-dimensional difference of the whole states, included the components of the relative velocity, and not only the difference of the distances. The function is again $f_2 = \frac{1}{d}$, but now defined as follow:

$$d = \sqrt{\left(\frac{x_f - x_i}{x_i}\right)^2 + \left(\frac{y_f - y_i}{y_i}\right)^2 + \left(\frac{z_f - z_i}{z_i}\right)^2 + \left(\frac{\dot{x}_f - \dot{x}_i}{\dot{x}_i}\right)^2 + \left(\frac{\dot{y}_f - \dot{y}_i}{\dot{y}_i}\right)^2 + \left(\frac{\dot{z}_f - \dot{z}_i}{\dot{z}_i}\right)^2} \qquad \textbf{Eq. 18}$$

2.2.4. Tuning of the integrator

Before proceeding in the tuning of the genetic algorithm itself, the propagator parameters must be established possibly one and for all the conditions.

The forces introduced in the equations of motion will be chosen according to the case study. For the following tuning of the genetic algorithm only J_2 perturbation will be included. The models adopted for each perturbation will be discussed on the following chapters (unperturbed, J_2, third body, drag effects).

The attention is then to be focused on the integrator. Though a number of numerical integrators with great precision do exist (we think in particular to a Gauss-Radau integrator of the 15th order), the most commonly used remain the simple Runge-Kutta 4th order integrator. It's main advantages are the simplicity and its being fast. On the other hand, the precision is not that great. This aspect is of capital interest in this research, has we are particularly interested in the relative motion. As the dimension of the relative trajectory are usually very small with respect to the satellite orbit, little percentage numerical error on the satellite orbit will result in very big percentage errors on the relative orbit.

To avoid this, a preliminary study on the step size of the integrator have to be performed.

As it's obvious, a smaller step results in more precise but more slow integration. To choose the proper step size, ten orbits including all perturbations are propagated with different time steps, and the errors on the final relative position are evaluated. A time step of 0.1 sec is considered to give the exact solution.

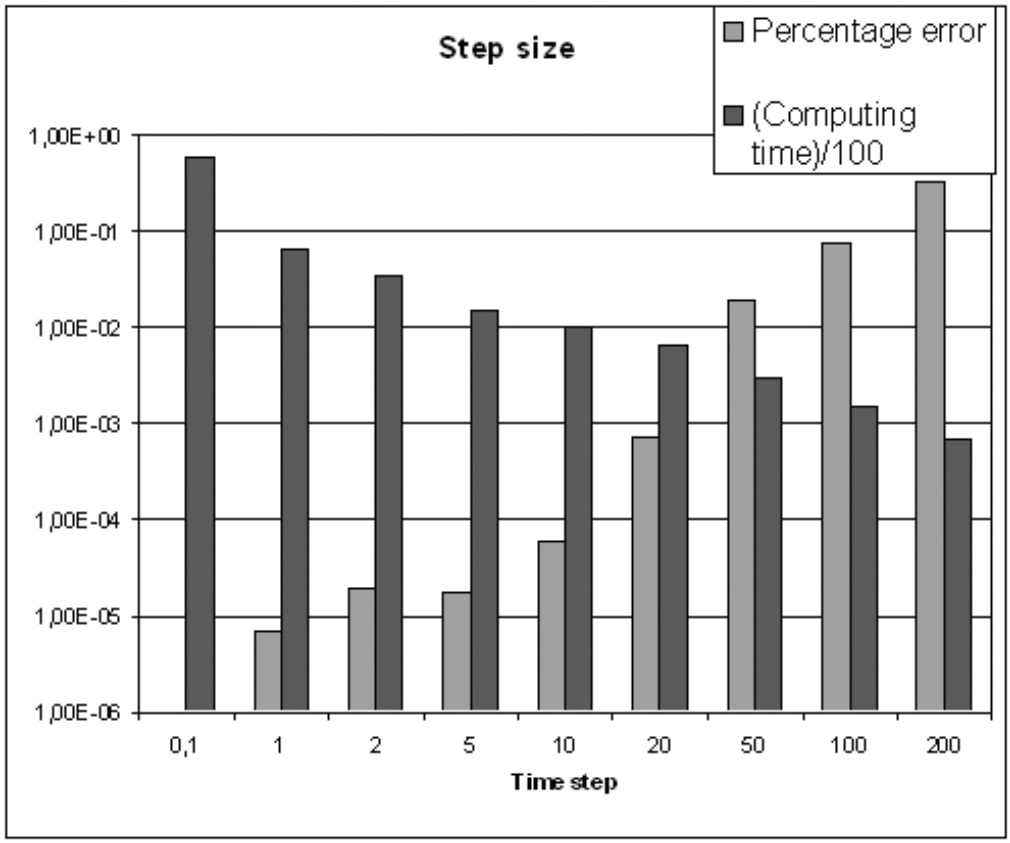

Fig. 10 Percentage error and computing time versus time step

Time steps from 1 to 10 seconds give almost the same solution. Time steps 100 seconds and 200 seconds have to be considered quite not precise, as shown in Fig. 11 and Fig. 12:

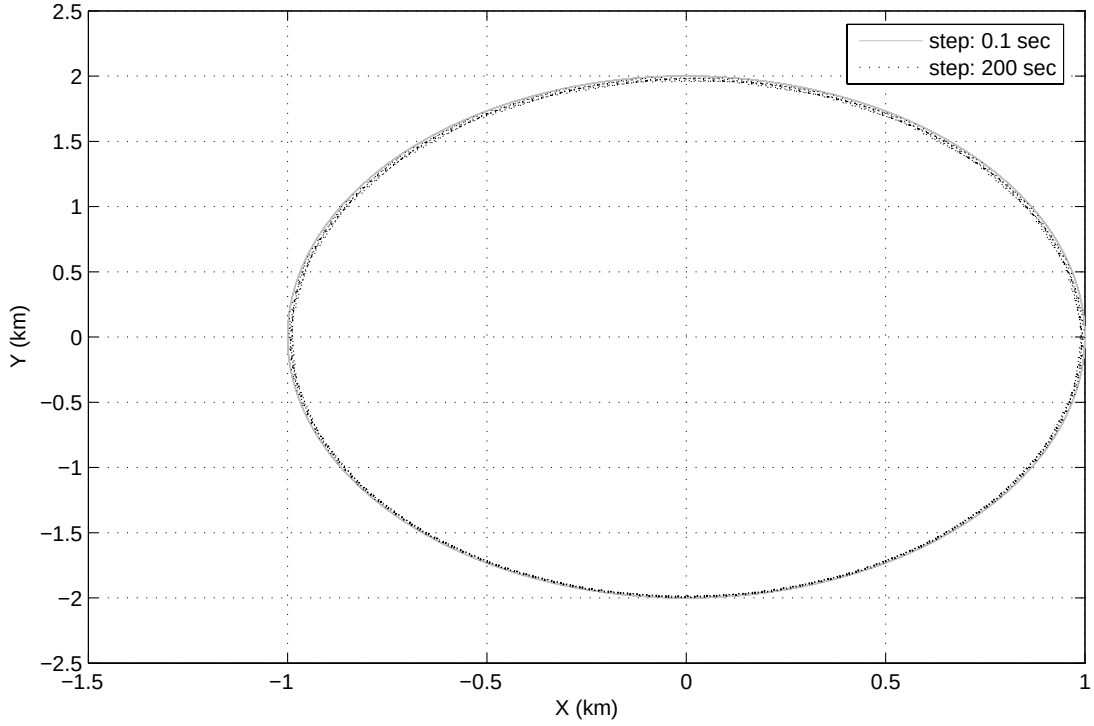

Fig. 11 Relative orbit error due to the time step of the integrator

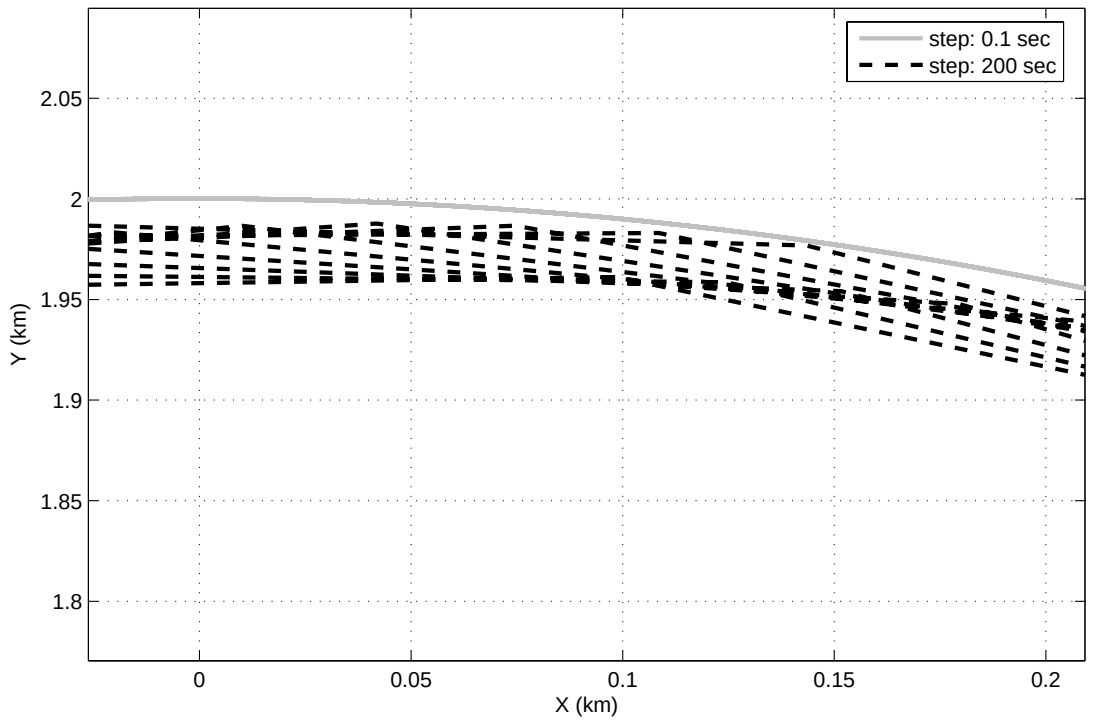

Fig. 12 Detail of relative orbit error.

The choice is between step size 20 and 50. As we consider a percentage error of 0.019% acceptable, we prefer to save computing time and that's why all the future simulation will be performed with this time step.

2.2.5. How many the individuals are and for how many generations they have to mate

The two main parameters of the genetic algorithm are surely the number of individuals of the population, and the number of generation they can mate.
Let's begin by considering a reference orbit for the chief satellite described by the following orbital parameters:

$$\begin{cases} a = 6678km \\ e = 0.00118 \\ i = 97.87° \\ \varpi = 90° \\ \Omega = 270° \\ \theta_0 = 0° \end{cases} \quad \textbf{Eq. 19}$$

This is a common sun-synchrone orbit, in particular this is the orbit planned for COSMO-Skymed remote sensing mission.
A different number of individuals of the population, 6, 10, 20, 50, 100, are chosen; the simulation is performed for 10000 generations.
To start, the algorithm needs a seed number which is used to generate an initial random population. This means that the simulations performed with same seed number will surely give the same results, while simulation performed with different seed will give probably slightly different results. It all depends on "how lucky" the first random population is. The following figures shows the behaviour of the fitness function as the generations pass: it has the typical step-like behaviour, where a sudden jump is alternated to long rest periods, as shown for example in Fig. 13.

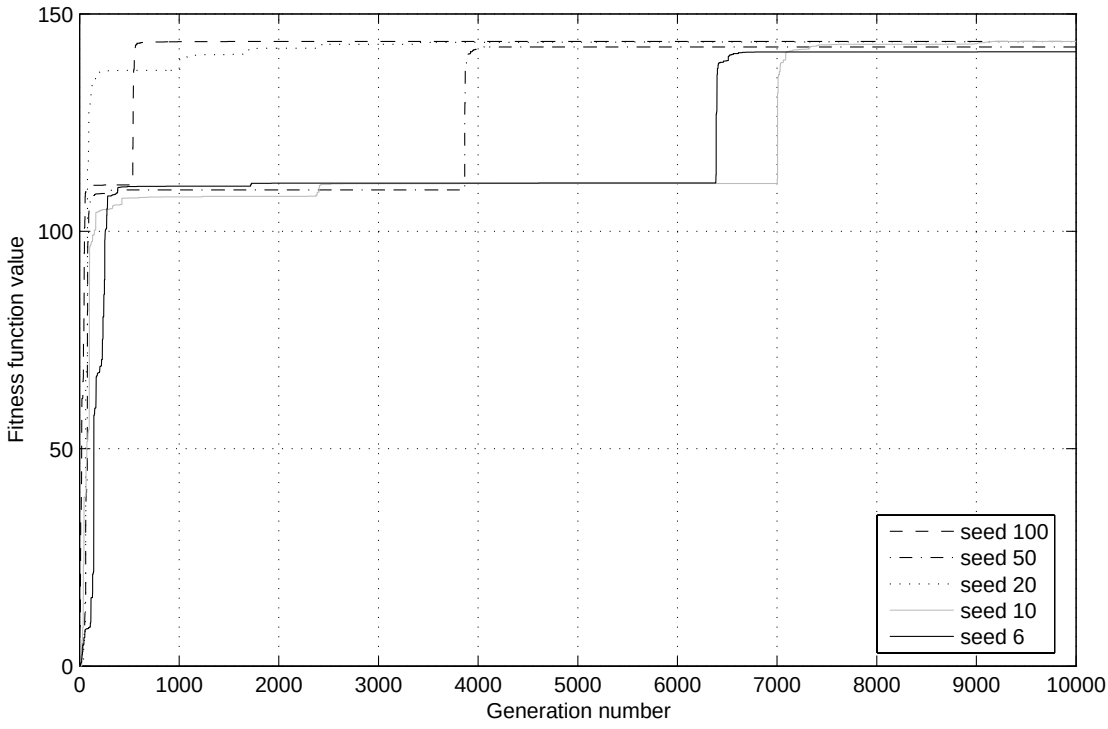

Fig. 13 Simulation results with seed = 1

In this first example, it's clear that not a direct relationship exists between the final fitness value and the number of individuals, as if it' true that the simulation with 100 individuals is the one who reach the top value for first, it' also true that 20 individuals case is faster than 50 and 6 faster than 10. So the final ranking is:

1 -	**100**
2 -	20
3 -	50
4 -	6
5 -	10

On the other hand, every generation a number of propagations equal to the individuals number has to be performed. This means that 100 individuals case requires about ten times the computing time required by the 10 individuals case.

If, as it appears from this first example, a random relation links number of individuals and fitness value, one could think to choose the minimum number of individual in order to save time. This is not that simple. In fact, a consideration must be done: an higher number of individuals in the population can sometimes hide the good qualities of one individual; a fit individual among only six

or ten individuals will emerge more easily. On the other hand, the probability that this fit individual is present in the initial population increases with the number of individuals. So, a great population can sometimes be slower in convergence than a little population, but as the generations proceed, its good results are more reliable. It' possible to say that with few individuals, the convergence is more like a fact of fortune, as we can see running the simulation with another seed:

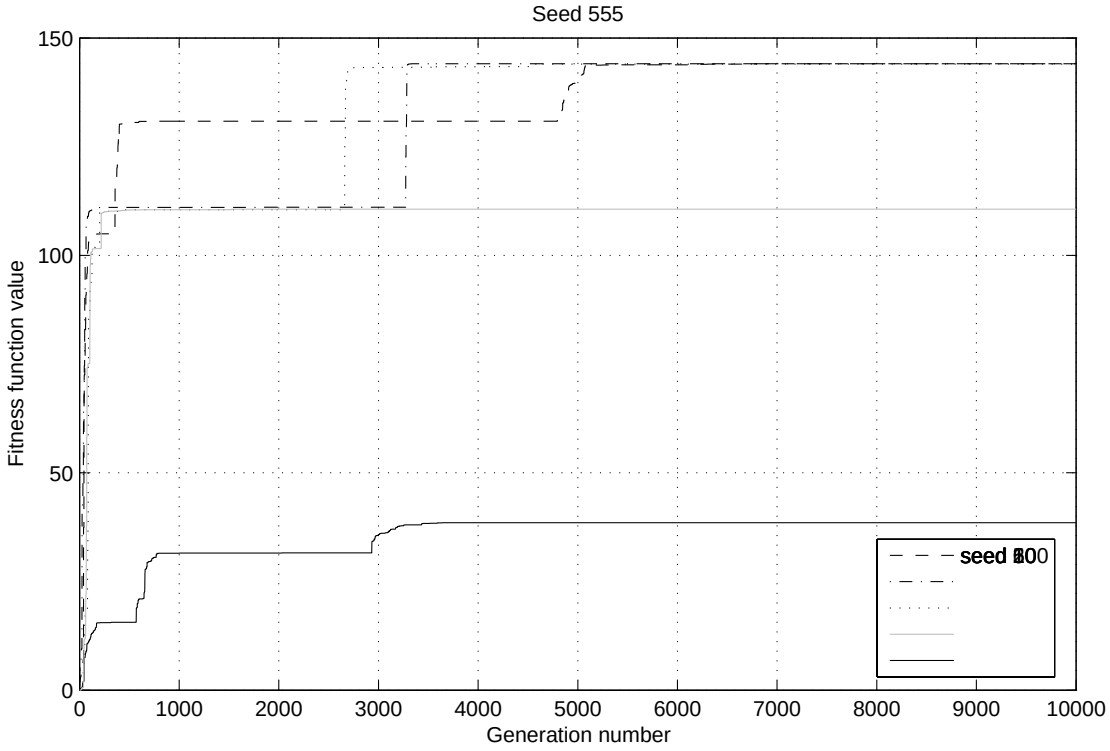

Fig. 14 Simulation results with seed = 555.

In this case, the ranking is:

1 -	**50**
2 -	20
3 -	100
4 -	6
5 -	10

Let's see another case:

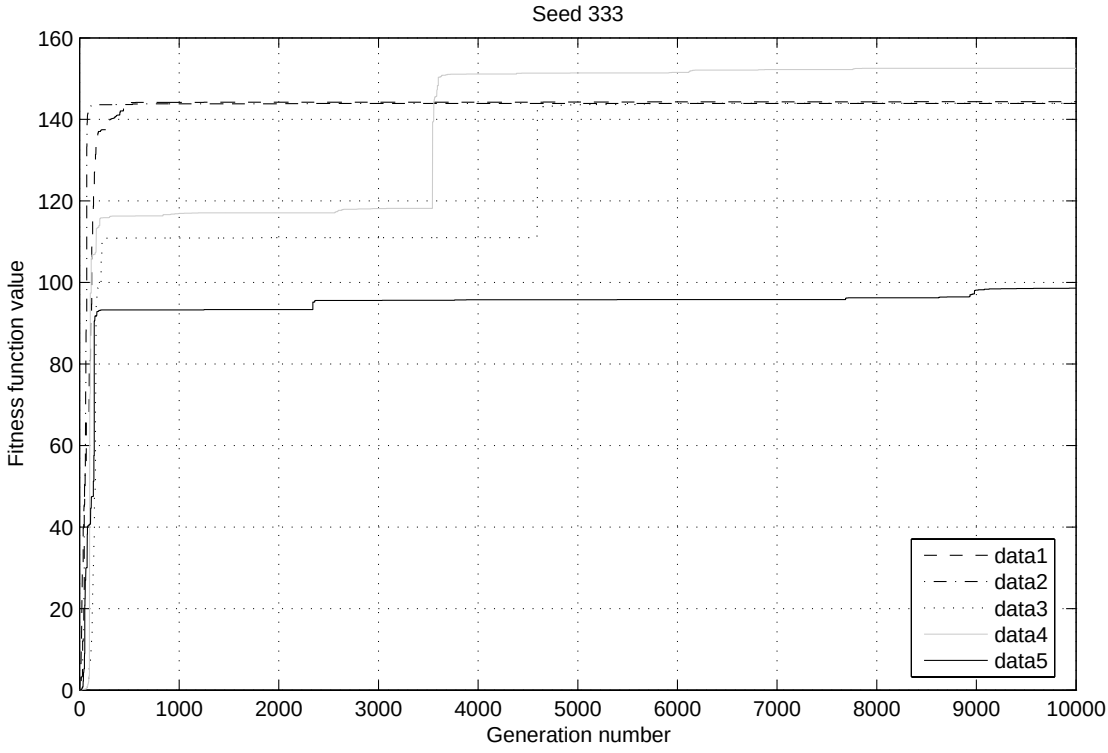

Fig. 15 Simulation results with seed = 333.

where we have:

1 -	**10**
2 -	50
3 -	100
4 -	20
5 -	6

Now 10 results to be the best, but from case of seed 123456 we can say that it's not always so: in other words, it is not confident.

A real rule cannot be established. Studying a lot of situations, we can say that a number of individuals who can ensure convergence without a great amount of computing time is 20. The number of generations when the simulation will stop is established in 5000.

Other stopping criteria can be developed and have been tested. For very simple cases (as the keplerian one), the convergence is reached far before 5000 generations. So a value for the fitness function can be established for the simulation to stop when this is reached. This results in an important time saving.

Anyway, from the considerations above, one thing remains: the possibility of the algorithm to fail. It can happen that for a given unlucky seed, a good result is not reached. Using twenty individuals is

quite uncommon, but it can happen. In this case, it's just sufficient to perform the simulation with another seed.

2.2.6. Other genetic algorithm parameters

The parameters that can influence the convergence of the algorithm are mainly three:

- crossover probability,
- maximum mutation probability,
- reproduction plan.

The crossover operator is, in essence, what distinguishes genetic algorithms from other heuristic search techniques. PIKAIA incorporates a single crossover operator known as one-point crossover. This operator acts on a pair of parent-chromosomes to produce a pair of offspring-chromosomes. Consider again two prototypical "parents", for example:

$$(x; y)_1 = (0.34567890, 0.23456789)$$

$$(x; y)_2 = (0.87654321, 0.65432198)$$

Encoding to eight significant digits (*nd*=8) would produce the corresponding parent-chromosomes:

3456789023456789

8765432165432109

The crossover operation begins by randomly selecting a cutting point along the chromosomes, for example by generating a random integer K and cutting both parent chromosomes at the corresponding locus. For example, for

K = 10:

3 4 5 6 7 8 9 0 2 3 4 5 6 7 8 9

8 7 6 5 4 3 2 1 6 5 4 3 2 1 0 9

– – – – – – – – – | – – – – – –

The chromosomal fragments located right of the cutting point are then interchanged and concatenated to the fragments left of the cutting points:

345678902-5432109 → 3456789025432109

876543216-3456789 → 8765432163456789

The two strings resulting from this operation are the offspring chromosomes. These two chromosomes decode into the two offspring phenotypes:

$$(x_1; y_1) = (0.34567890, 0.25432198)$$

$$(x_2 ; y_2) = (0.87654321, 0.63456789)$$

The resulting offspring in general differ from either parent, although they do incorporate intact "chunks" of genetic material from each parent.

In practice the crossover operator is applied only if a probabilistic test yields true. Define first a crossover rate $pcross \in [0.0, 1.0]$ and generate a random number $R \in [0.0, 1.0]$.The crossover operator is then applied only if $R \leq pcross$. If $R > pcross$, the two offspring remain exact copies of the two parents. The crossover rate *pcross* is an input quantity, and remains constant throughout the evolution.

For the crossover probability study we have the behaviour in Fig. 16:

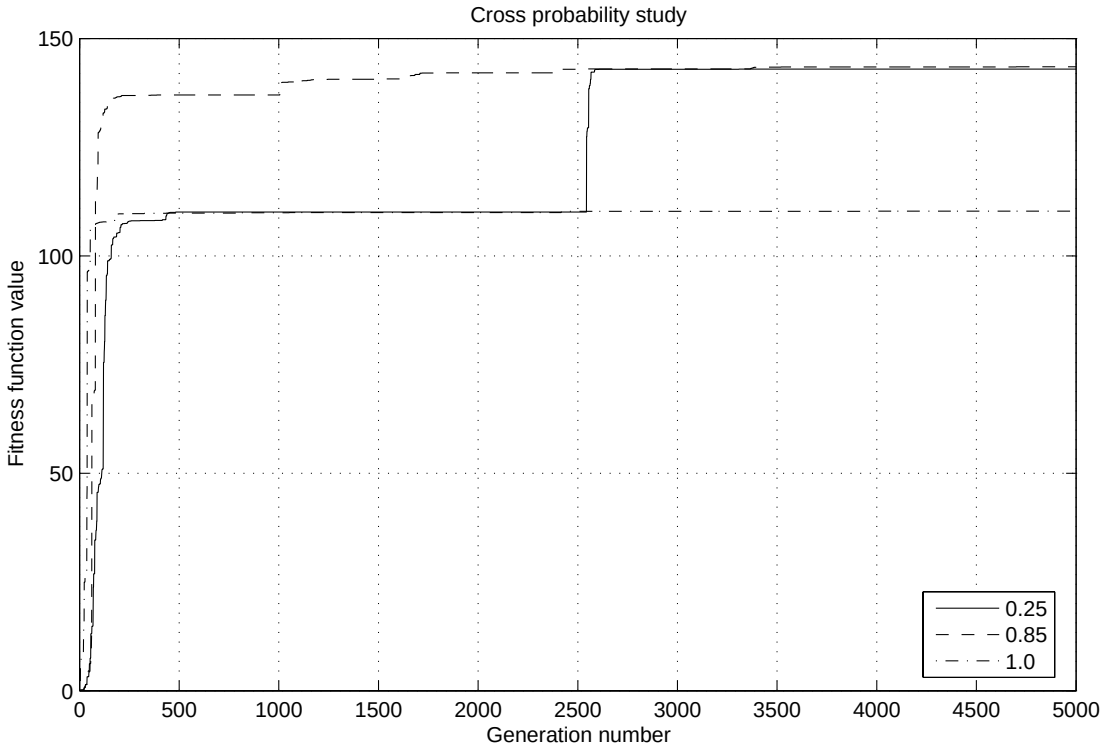

Fig. 16 Crossover probability study

The 0.85 probability, which is by the way the default value chose for PIKAIA, ensure a smoothest behaviour, though 0.25 case converge to the same value. The crossover probability is then left at its default value, that is 0.85.

Regarding the mutation probability, PIKAIA incorporates a single mutation operator known as uniform one-point mutation, but allows the mutation rate to vary dynamically in the course of the evolutionary run. The mutation operator functions as follows.

For each gene of an offspring chromosome, a random number $R \in [0.0, 1.0]$ is generated, and mutation hits the gene only if $R \leq pmut$, where $pmut \in [0.0, 1.0]$ is the mutation rate. The mutation itself consists in replacing the targeted gene by a random integer $K \in [0, 9]$

The plots of fitness value vs. number of generations for different *pmut* are completely overlapped, and they will not be reported. A maximum mutation probability of **1** will be chosen in order to ensure a greater variability in cases when the fitness function rests for long time on a plateau.

There are three possible reproduction plans: Full generational replacement, Steady-state-replace-random and Steady state-replace-worst.

The first case is perhaps the simplest reproduction plan. Throughout one iteration of the generation cycle, offspring are accumulated in temporary storage. Once a number of offspring equal to number of individuals have been so produced and stored, the entire parent population is wiped out and replaced by the offspring population , after which a new generational iteration begins. Under this reproduction plan, individuals have a fixed lifetime equal to a single generation.

Steady-state reproduction plans insert individuals as they are being bred. Criteria must be specified to decide

1) under which conditions newly-bred offspring are to be inserted;

2) how members of the parent population are to be deleted to make room for the new members

3) if any limit is to be imposed on an individual's lifetime.

PIKAIA incorporates two steady-state plans. In both cases a newly bred offspring is inserted whenever its fitness exceeds that of the least fit member of the parent population, unless it is identical to an existing member of the population.

Furthermore, PIKAIA imposes no limit on the generational lifetime of a population member; a very fit individual can survive through many iterations of the generational cycle. The two plans differ in how room is made to accommodate the offspring to be inserted. Under the steady-state-delete-worst plan, the least fit member of the parent population is eliminated and replaced by the offspring. Under the steady-state-delete-random plan, a member of the old population is chosen at random and deleted, independently of its fitness.

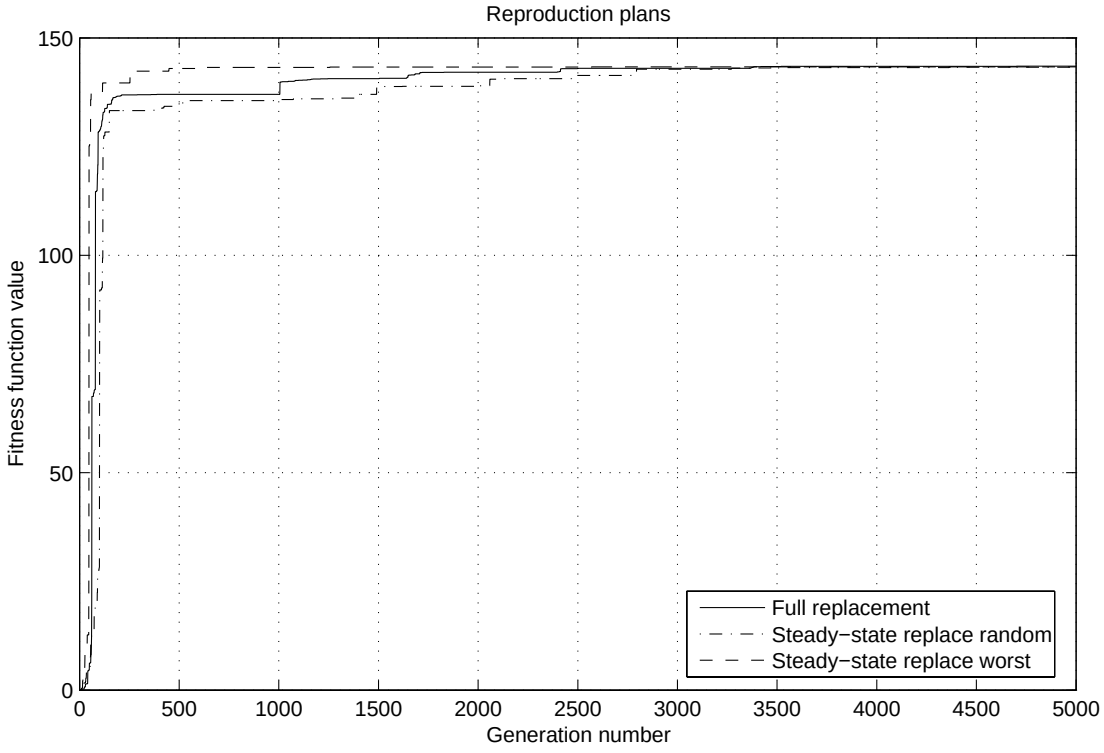

Fig. 17 Results depending on reproduction plan

As it's possible to see, there is not a great different between the three cases. Anyway the steady-state-replace-worst seems to be slightly better, and that's what we will use.

As a summary, the main parameters chosen are reported in Table 1.

Number of individuals in a population:	20
Number of generations: 5000	5000
Number of significant digit (number of genes):	9
Crossover probability:	0.85
Mutation mode:	one-point, adjustable rate based on fitness
Initial mutation rate:	0.005
Minimum mutation rate:	0.0005
Minimum mutation rate:	1
Reproduction plan:	Steady-state-replace-worst

Table 1 Genetic algorithm parameters chosen.

3. Unperturbed reference orbit

3.1. Circular reference orbit

Without any perturbation, the motion of a satellite is simply given by Eq. 20:

$$\frac{d^2\vec{r}}{dt^2} = -\frac{\mu}{r^2}\hat{r} \quad \textbf{Eq. 20}$$

For the satellites of the formation, we can write this equation in the orbital reference frame (LVLH):

$$\ddot{\vec{r}}_0 + 2\vec{\omega}\times\dot{\vec{r}}_0 + \dot{\vec{\omega}}\times\vec{r}_0 + \vec{\omega}\times\left(\vec{\omega}\times\vec{r}_0\right) = -\frac{\mu}{r_0^2}\hat{r}_0 \quad \textbf{Eq. 21}$$

$$\ddot{\vec{r}}_1 + 2\vec{\omega}\times\dot{\vec{r}}_1 + \dot{\vec{\omega}}\times\vec{r}_1 + \vec{\omega}\times\left(\vec{\omega}\times\vec{r}_1\right) = -\frac{\mu}{r_1^2}\hat{r}_1 \quad \textbf{Eq. 22}$$

Then it's possible to subtract Eq. 22 to Eq. 21 in order to obtain the following Eq. 23:

$$\ddot{\vec{\rho}} + 2\vec{\omega}\times\dot{\vec{\rho}} + \dot{\vec{\omega}}\times\vec{\rho} + \vec{\omega}\times\left(\vec{\omega}\times\vec{\rho}\right) = -\frac{\mu}{r_1^2}\hat{r}_1 + \frac{\mu}{r_0^2}\hat{r}_0 \quad \textbf{Eq. 23}$$

which is a vector equation that projected on the three axis gives:

$$\begin{cases} \ddot{x} - 2\dot{\theta}\dot{y} - \ddot{\theta}y - \dot{\theta}^2 x = -\dfrac{\mu(r+x)}{\left[(r+x)^2 + y^2 + z^2\right]^{\frac{3}{2}}} + \dfrac{\mu}{r^2} \\ \ddot{y} + 2\dot{\theta}\dot{x} + \ddot{\theta}x - \dot{\theta}^2 y = -\dfrac{\mu y}{\left[(r+x)^2 + y^2 + z^2\right]^{\frac{3}{2}}} \\ \ddot{z} = -\dfrac{\mu z}{\left[(r+x)^2 + y^2 + z^2\right]^{\frac{3}{2}}} \\ \ddot{r} = r\dot{\theta}^2 - \dfrac{\mu}{r^2} \\ \ddot{\theta} = -\dfrac{2\dot{r}\dot{\theta}}{r} \end{cases} \quad \textbf{Eq. 24}$$

where r is the radius of the reference orbit and θ refers to the latitude angle of the chief.

The previous relations describe the relative motion of the two satellites 1 and 0. The terms on the right hand give non linearity to the system. A great effort to obtain linear models describing relative motion has been done in astrodynamics research. A linear model in fact can be used much more easily to implement control systems and to better understand formation dynamics.

3.1.1. Hill-Clohessy-Wiltshire model: HCW equations

The first and most well-known attempt of linearization are the Hill-Clohessy-Wiltshire (HCW) equations:

$$\begin{cases} \ddot{x} - 2n\dot{y} - 3n^2 x = 0 \\ \ddot{y} + 2n\dot{x} = 0 \\ \ddot{z} + n^2 z = 0 \end{cases} \quad \textbf{Eq. 25}$$

where *n* is the orbital angular velocity. The hypothesis is that the reference orbit is circular. These equations, though providing an approximation of the formation's real dynamics, are still widely used thanks to their great simplicity.

As it's possible to see, the problem of searching bounded orbits using this model is extremely simple: it's in fact sufficient to impose one condition, namely:

$$\dot{y}_0 = -2nx_0 \quad \textbf{Eq. 26}$$

This is not surprising. In an unperturbed case, the only way a relative orbit can close is that the two satellites pass again in the same positions after the same time, which is the orbital period.

The orbital period is only dependant on the semi-major axis, by the formula:

$$T = 2\pi\sqrt{\frac{a^3}{\mu}} \quad \textbf{Eq. 27}$$

The condition for the non linear motion is therefore just one, and it's the period matching condition. For perturbed orbits, as it will be shown in the following orbits, this condition is no more sufficient, as the satellites never pass again in the same positions after the same time: that's why it's not clear if a bounded relative orbit does exist or not even for reference orbits subjected to conservative perturbation such as J_2.

Back at the unperturbed case, having linearized the relative motion brings as a natural consequence that the condition in $\dot{y}_0 = -2nx_0$ Eq. 26 is a better approximation as the formation dimensions are smaller.

In other words, the deputy satellite with the HCW closing condition has a period which is less and less similar to the chief as the formation dimensions grow.

The reference orbit is:

$$\begin{cases} a = 6678km \\ e = 0 \\ i = 97.87° \\ \varpi = 90° \\ \Omega = 270° \\ \theta_0 = 0° \end{cases} \quad \textbf{Eq. 28}$$

If we choose a very compact orbit, with initial spatial conditions of $[x_0, y_0, z_0] = [1e^{-2}, 1e^{-2}, 1e^{-2}]km$, the only condition that we infer from the HCW equations is that $\dot{y} = -2nx = $ -0.00002313818849 Km/s. With these initial conditions, the propagation of the non linear model is performed for one hundred orbits.

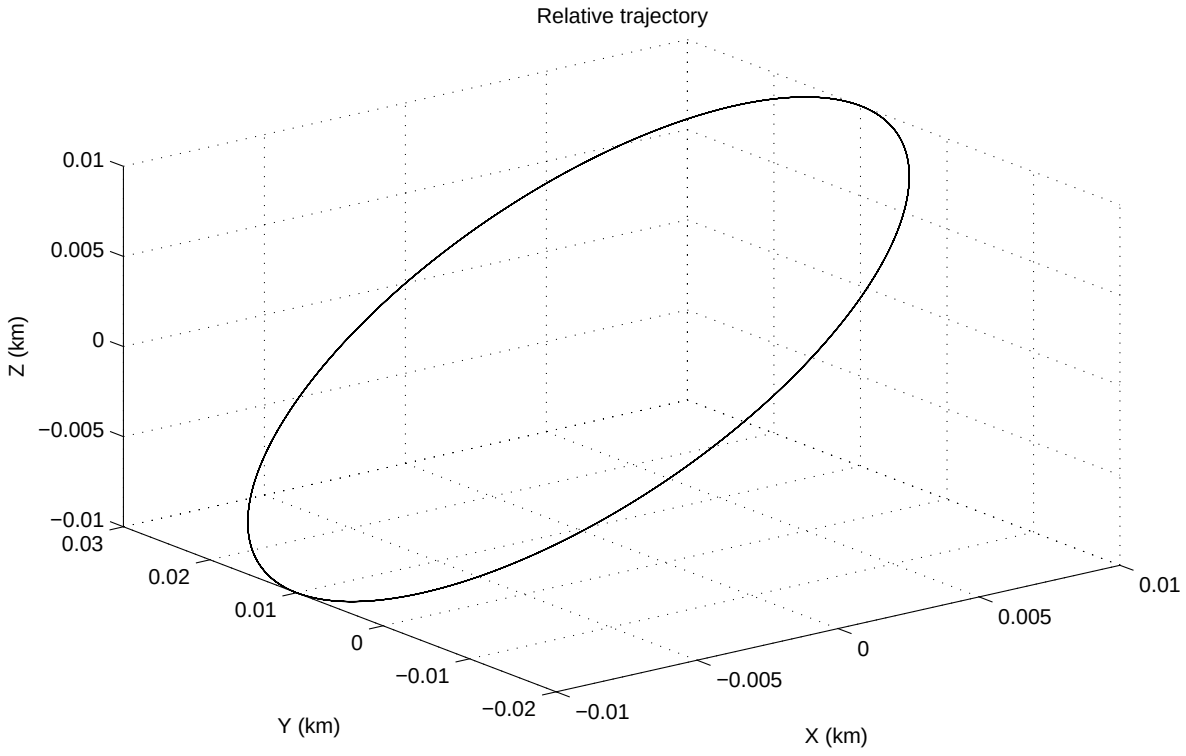

Fig. 18 Relative orbit resulting from HCW initial conditions

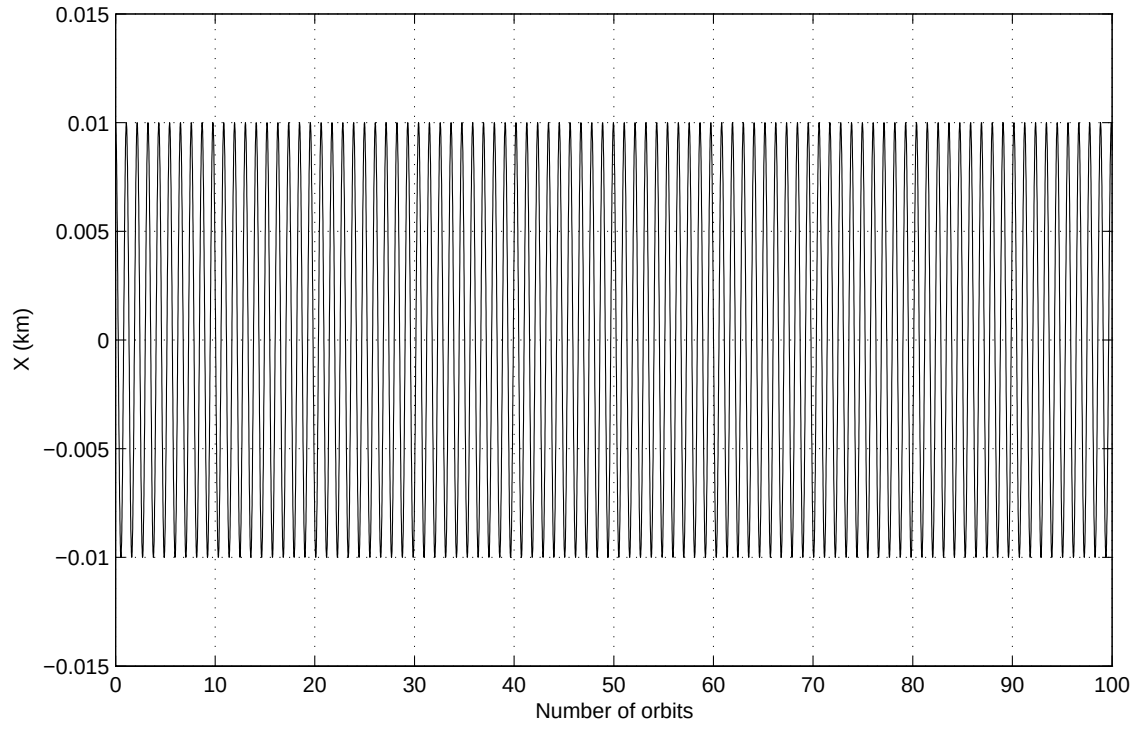

Fig. 19 X component of relative motion resulting from HCW initial conditions

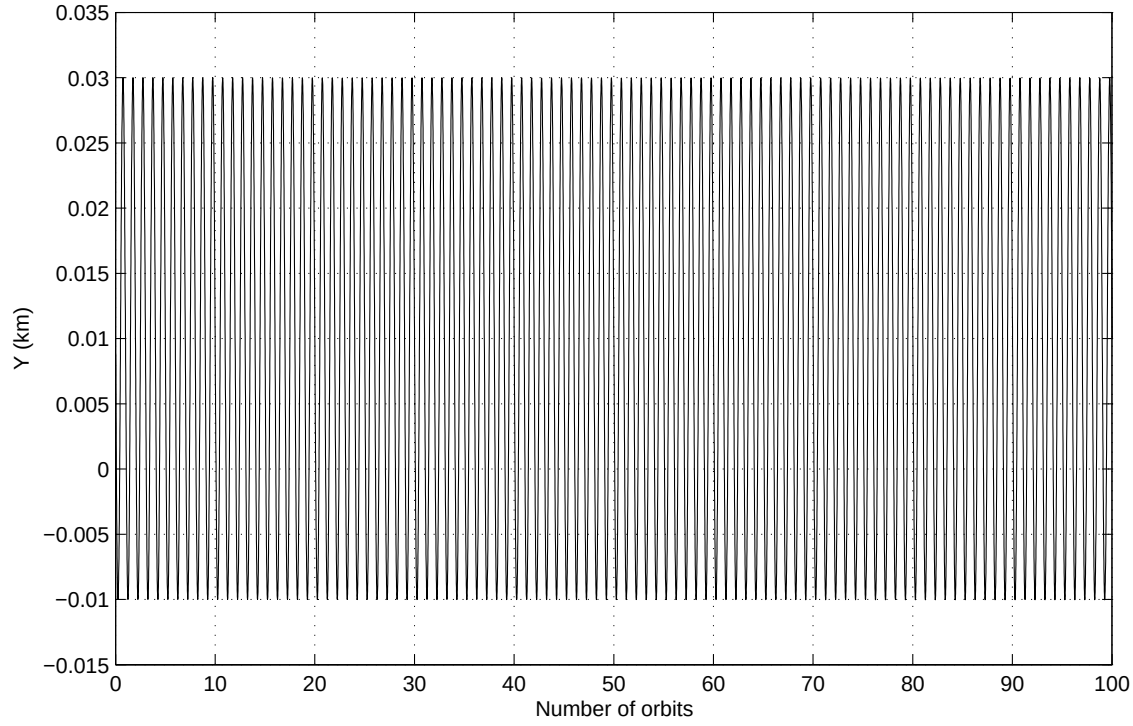

Fig. 20 Y component of relative motion resulting from HCW initial conditions

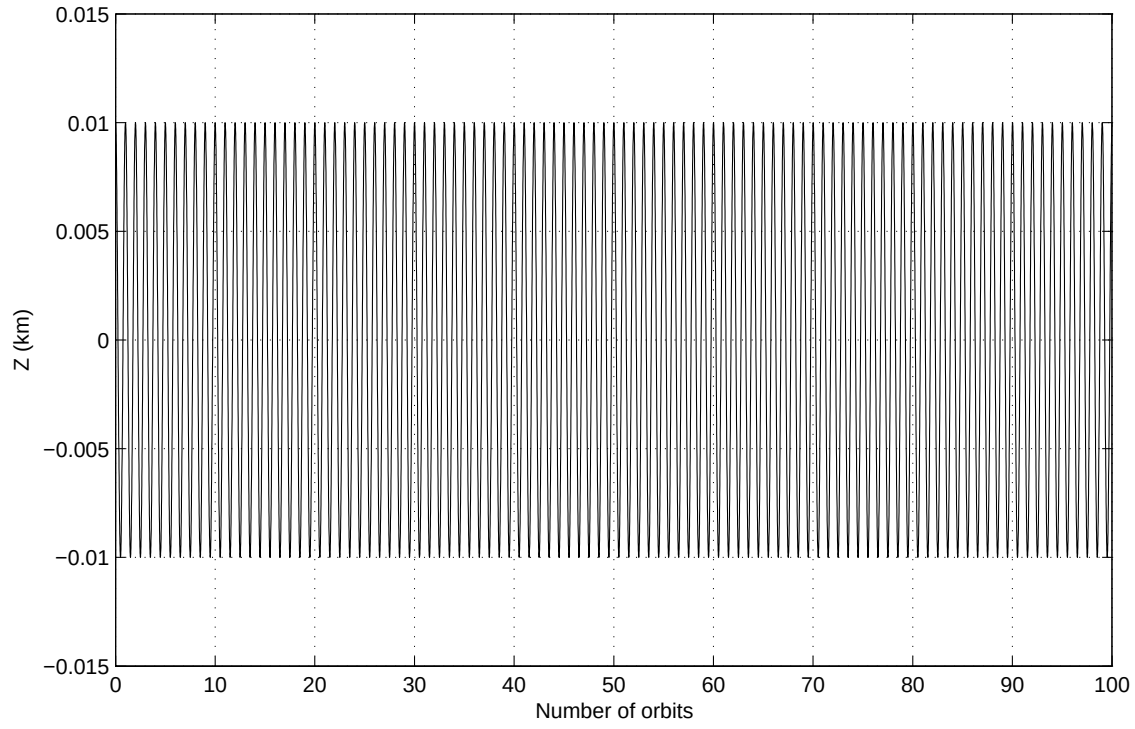

Fig. 21 Z component of relative motion resulting from HCW initial conditions

From Fig. 18, Fig. 19, Fig. 20 and Fig. 21, it's evidently a pretty good result. Difference in semi-major axis is really little, $-3e^{-5}$ m; the consequent drift can be calculated by the approximated formula: $-3\pi\delta a$=$-2.88e^{-4}$m. We can say there is not a real drift.

But the situation changes as the initial distance grows. Fig. 22 shows the drift (basically on the y axis) as the formation dimensions grow.

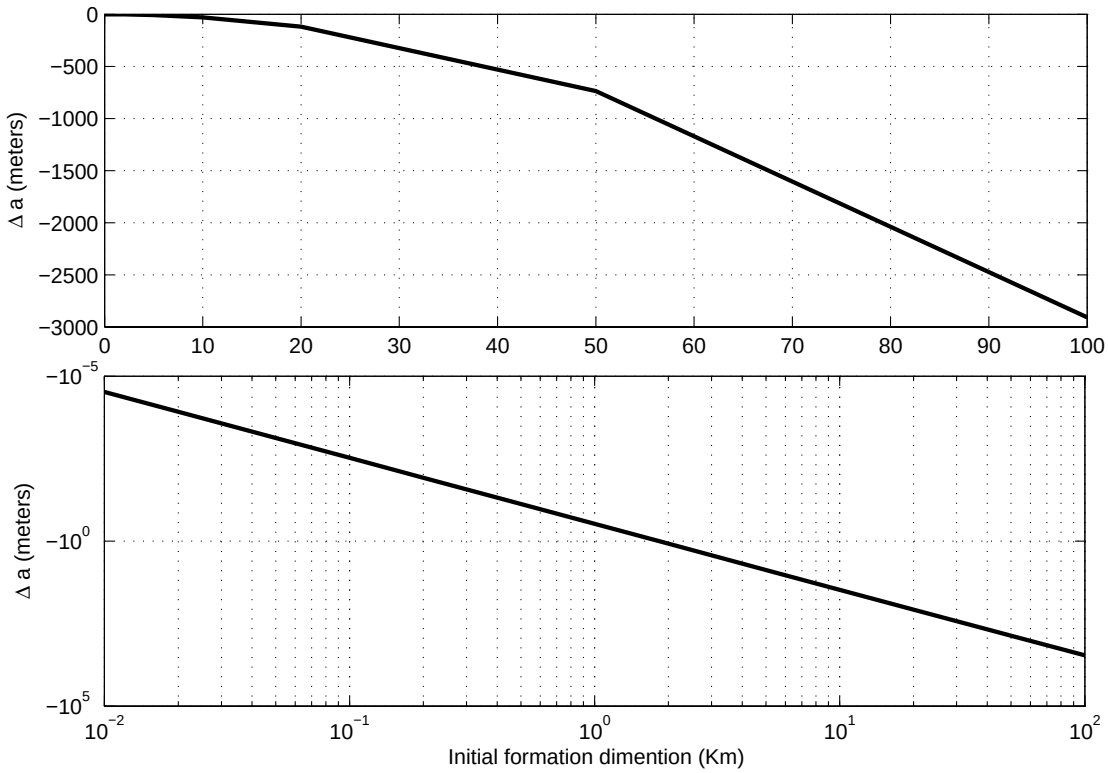

Fig. 22 Drift vs. formation dimension

The difference in semi major axis grows in an exponential way. Let's consider in fact an orbit with initial conditions much greater: $[x, y, z] = [100,100,100] km$. It's sufficient a much shorter propagation period, ten orbits, to understand that the results are completely different (see Fig. 23 to Fig. 26).

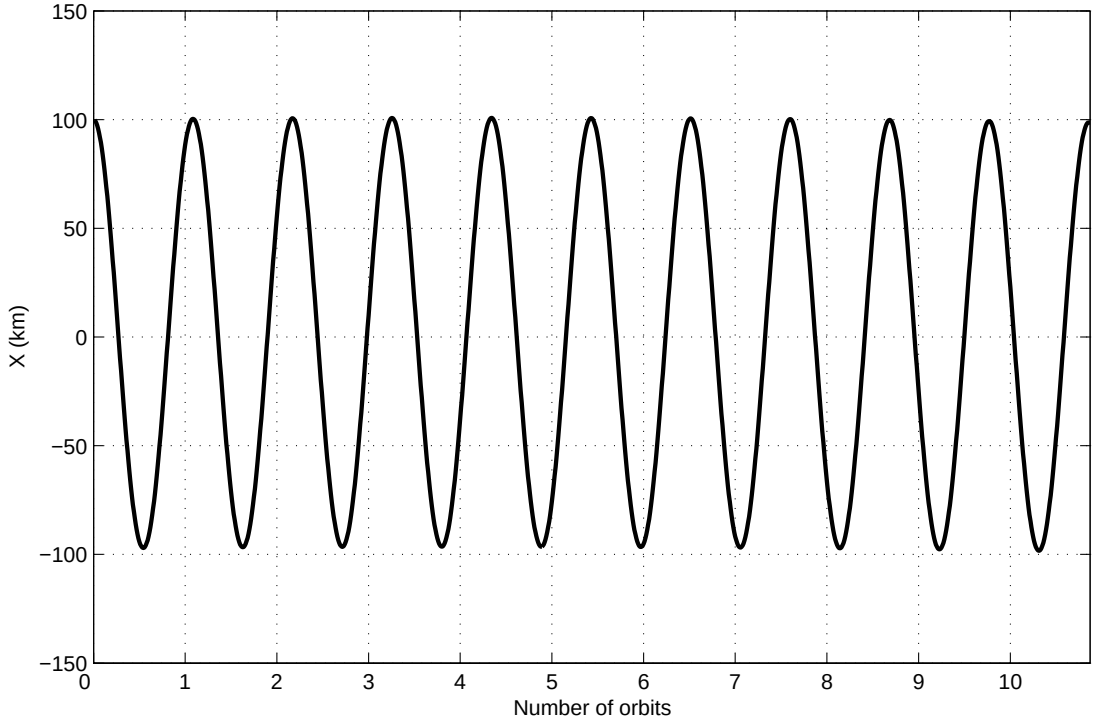

Fig. 23 X component of relative motion resulting from HCW initial conditions

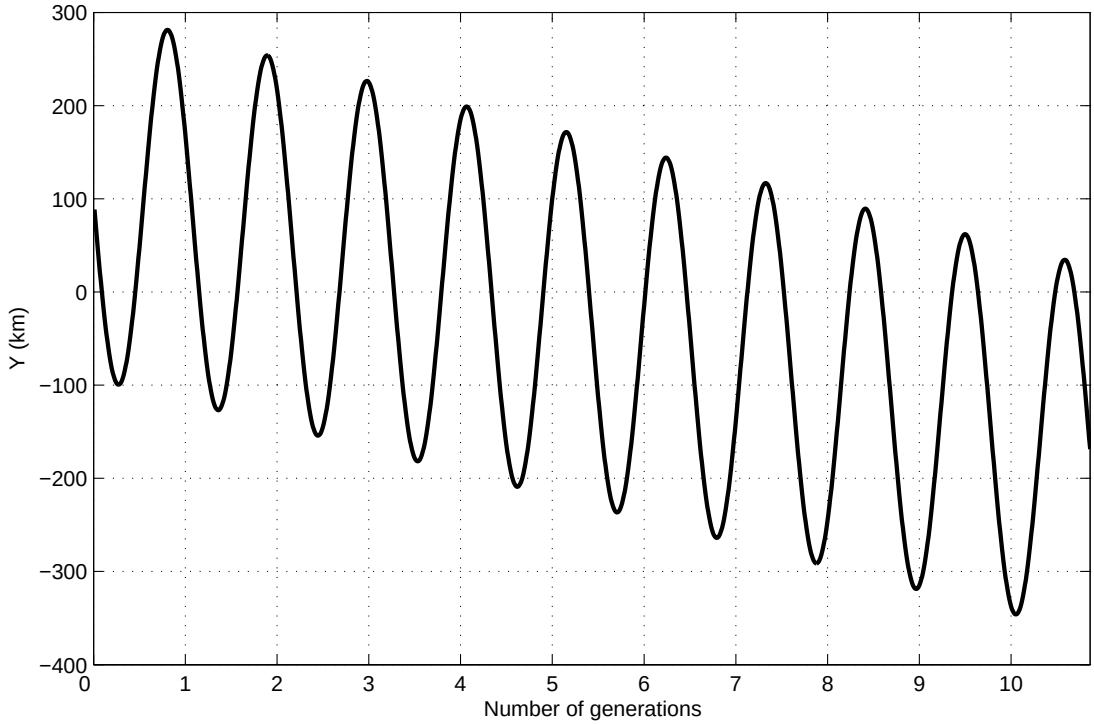

Fig. 24 Y component of relative motion resulting from HCW initial conditions

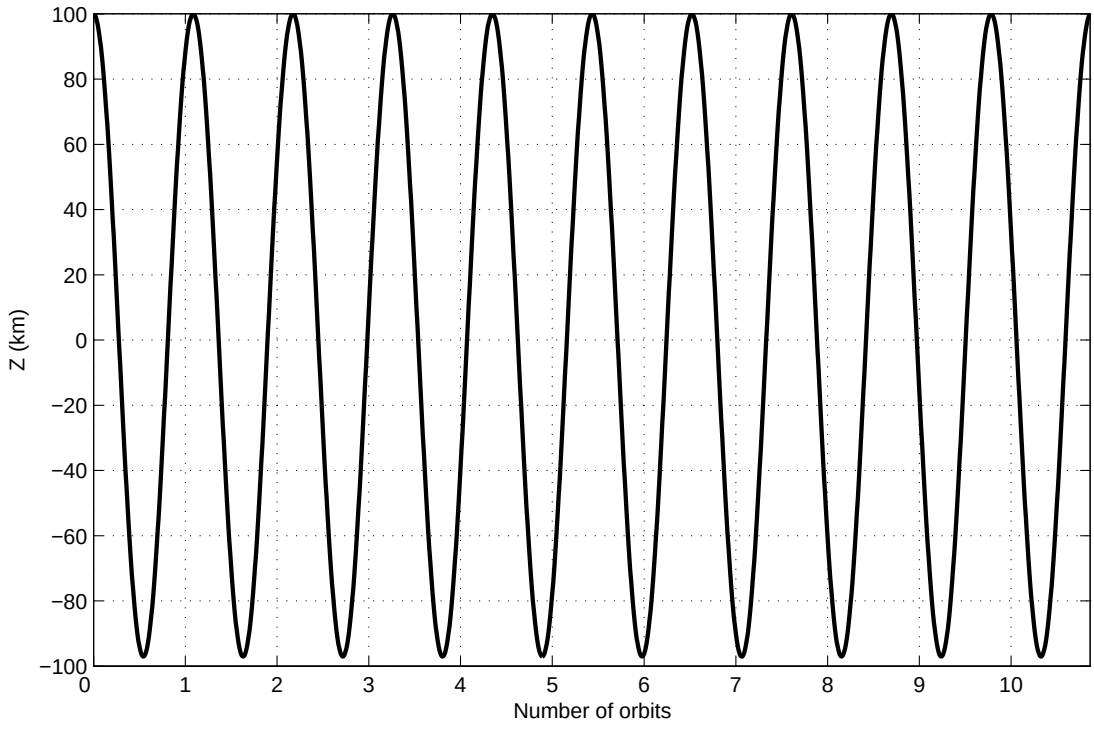

Fig. 25 Z component of relative motion resulting from HCW initial conditions

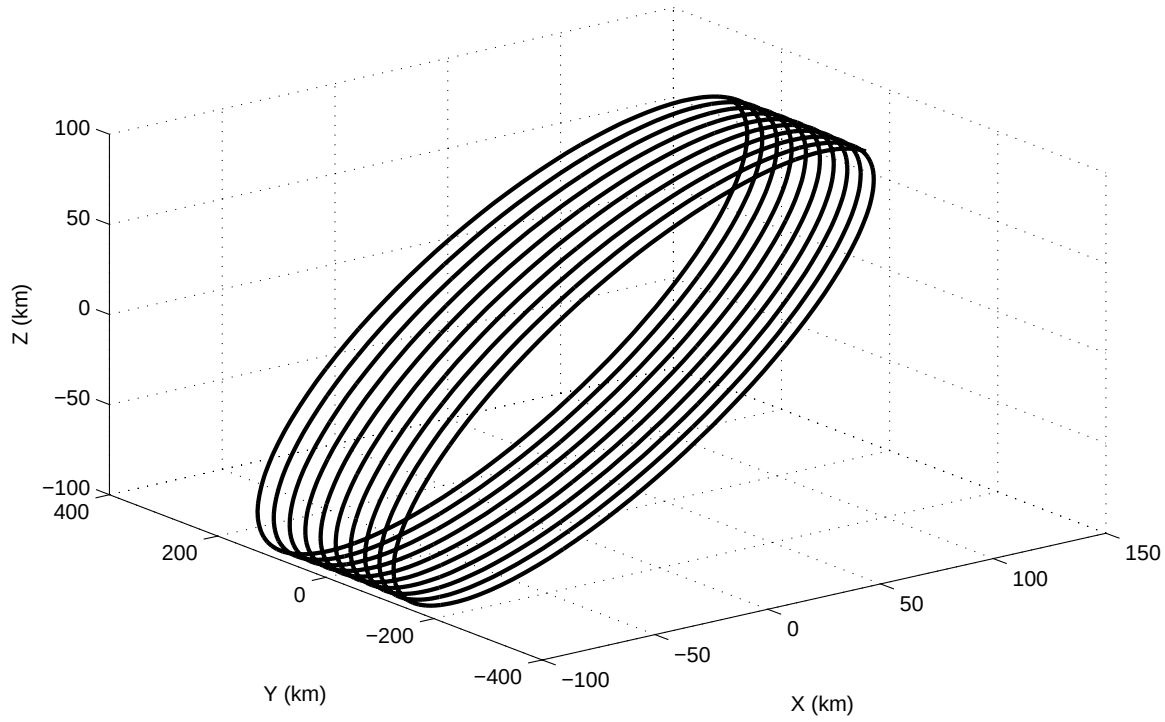

Fig. 26 Relative orbit resulting from HCW initial conditions

In case of large formations, it's clear that HCW conditions, even in absence of perturbations, cannot be used to generate periodic orbits. Fig. 27 shows the drift per orbit, which is almost entirely located on the y axis.

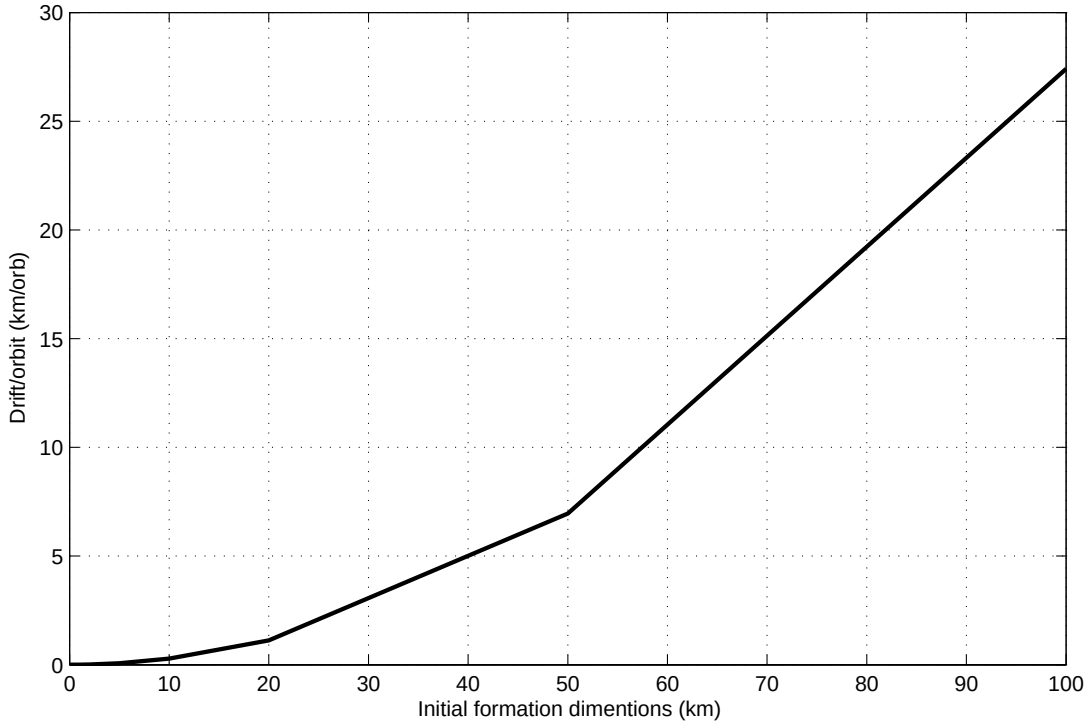

Fig. 27 Drift per orbit.

3.1.2. Non linear corrections: Vaddi, Vadali and Alfriend model

Vaddi, Vadali and Alfriend have developed a new model taking into account the effects of non linearities, both for circular and for elliptic orbits.

A Taylor's series expansion of the right-hand side of Eq. 23, retaining quadratic terms, leads to the following model:

$$\begin{cases} \ddot{x} - 2n\dot{y} - 3n^2 x = \varepsilon\left[\dfrac{y^2}{2} + \dfrac{z^2}{2} - x^2\right] \\ \ddot{y} + 2n\dot{x} = \varepsilon xy \\ \ddot{z} + n^2 z = \varepsilon xz \end{cases} \qquad \textbf{Eq. 29}$$

where $\varepsilon = \dfrac{3\mu}{a^4}$.

After some approximation, a condition for periodic relative orbits is proposed. The initial conditions are:

$$[x_0, y_0, z_0] = [\rho / 2\sin(nt + \alpha_0), \rho\cos(nt + \alpha_0), \rho\sin(nt + \alpha_0)] \quad \textbf{Eq. 30}$$

$$[\dot{x}_0, \dot{y}_0, \dot{z}_0] = [n\rho / 2\cos(nt + \alpha_0), \dot{y}, n\rho\cos(nt + \alpha_0)] \quad \textbf{Eq. 31}$$

where ρ is the relative distance and α_0 the initial phase angle. The only variable that influence the bounded-ness of the relative orbit is $\dot{y}$, which can be written as:

$$\dot{y}(0) = \dot{y}_h(0) + \varepsilon\dot{y}_{cn}(0) \quad \textbf{Eq. 32}$$

where $\dot{y}_h$ is the initial condition from HCW equation while $\dot{y}_{cn}$ is the correction for the non linearity.

$$\dot{y}_h(0) = -2nx_0 \quad \textbf{Eq. 33}$$

as we already found, while:

$$\dot{y}_{cn}(0) = -(\rho^2 / 48n)(12 + 6\cos 2\alpha_0) \quad \textbf{Eq. 34}$$

Fig. 28shows the Δa of the deputy satellite with these corrected initial conditions:

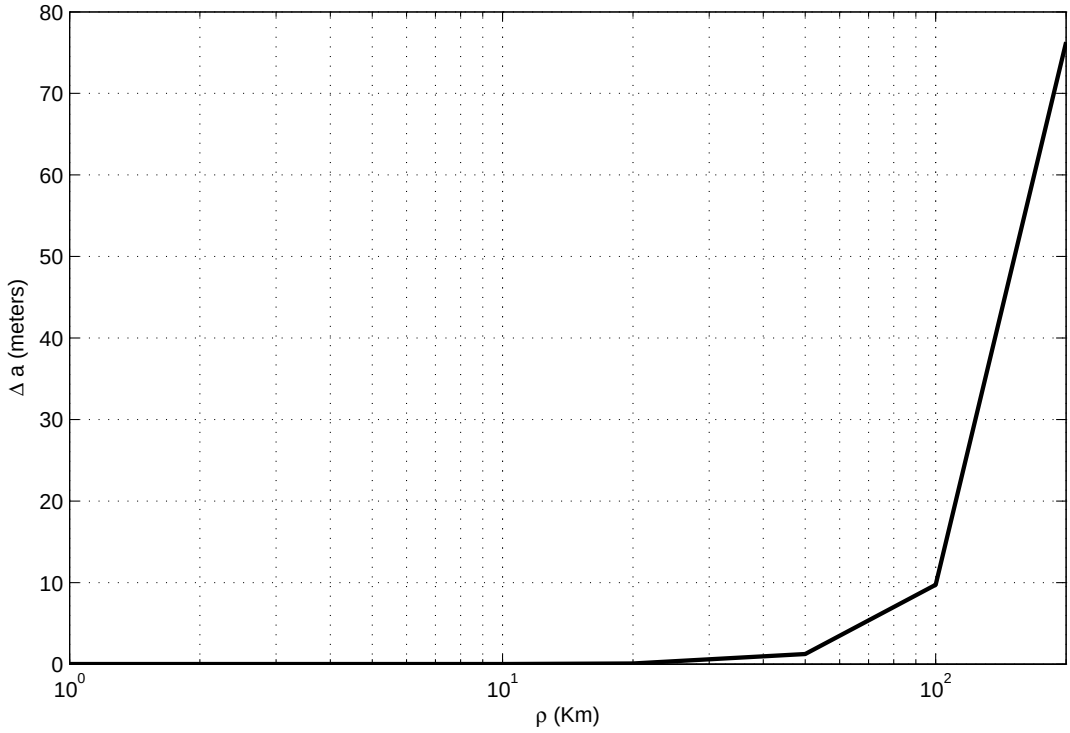

Fig. 28 Δa vs. corrected initial condition

Comparing these results with the ones shown in Fig. 22 it's possible to say that there is a great improvement. Only for very large formations a drift arise. For ρ = 200 Km, a propagation one hundred orbits long is performed and reported in Fig. 29, Fig. 30, Fig. 31 and Fig. 32.

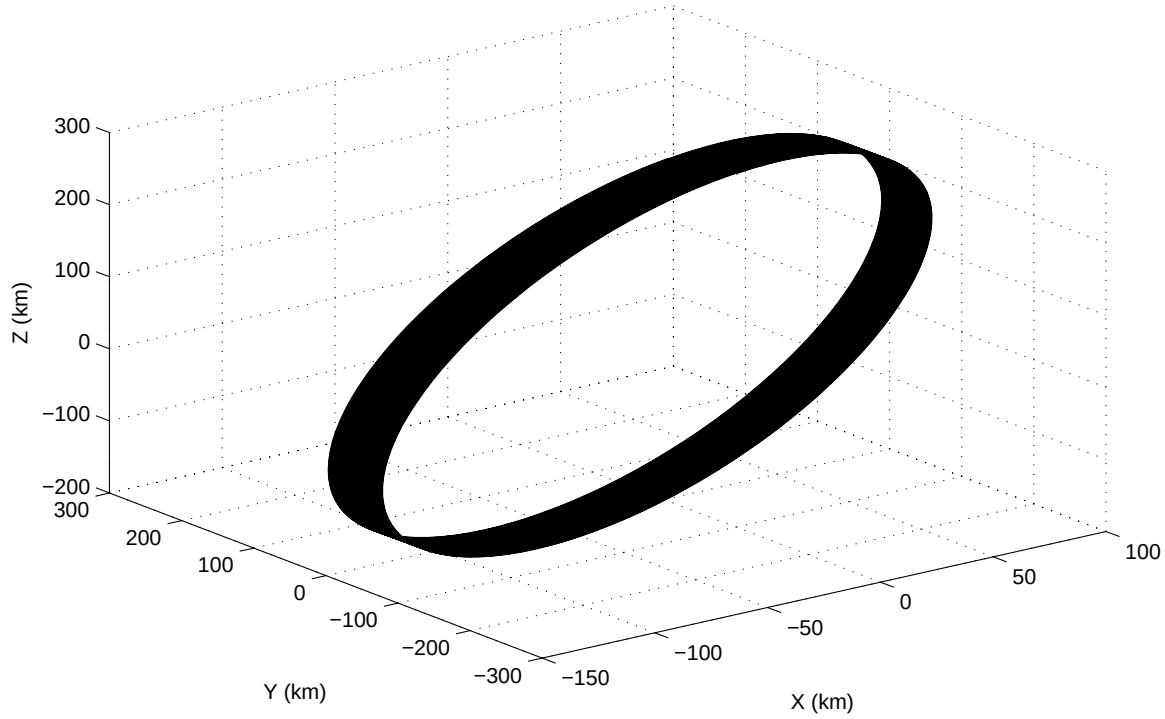

Fig. 29 Relative trajectory for 100 orbit and ρ=100 km.

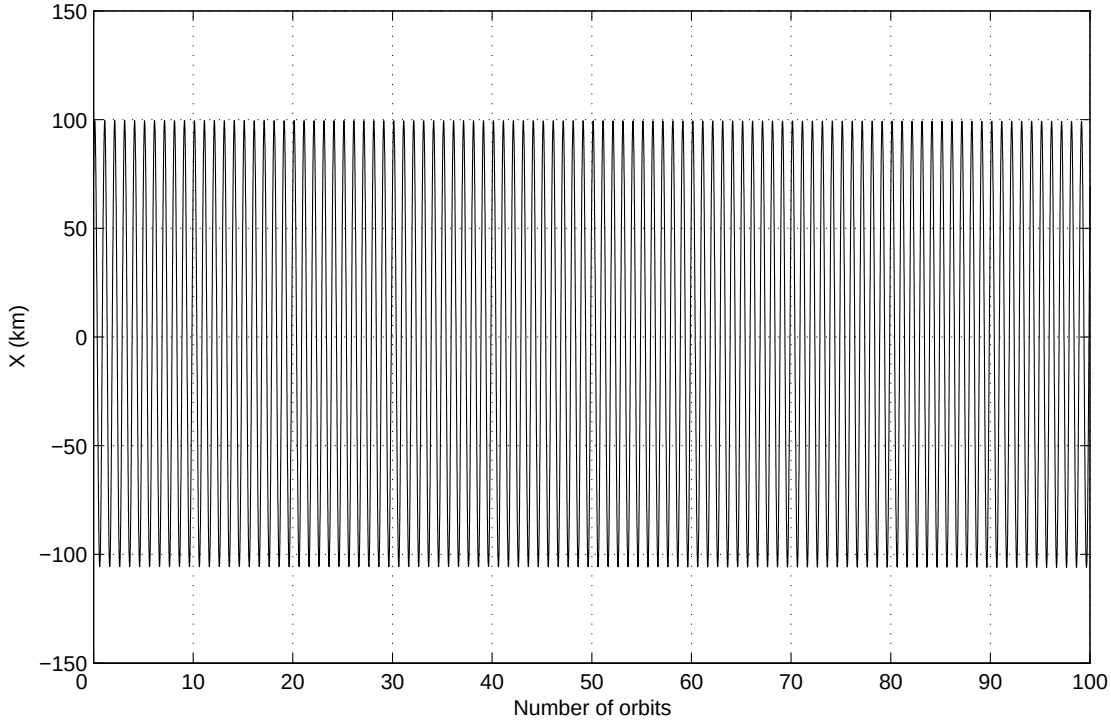

Fig. 30 X component for 100 orbit and ρ=100 km

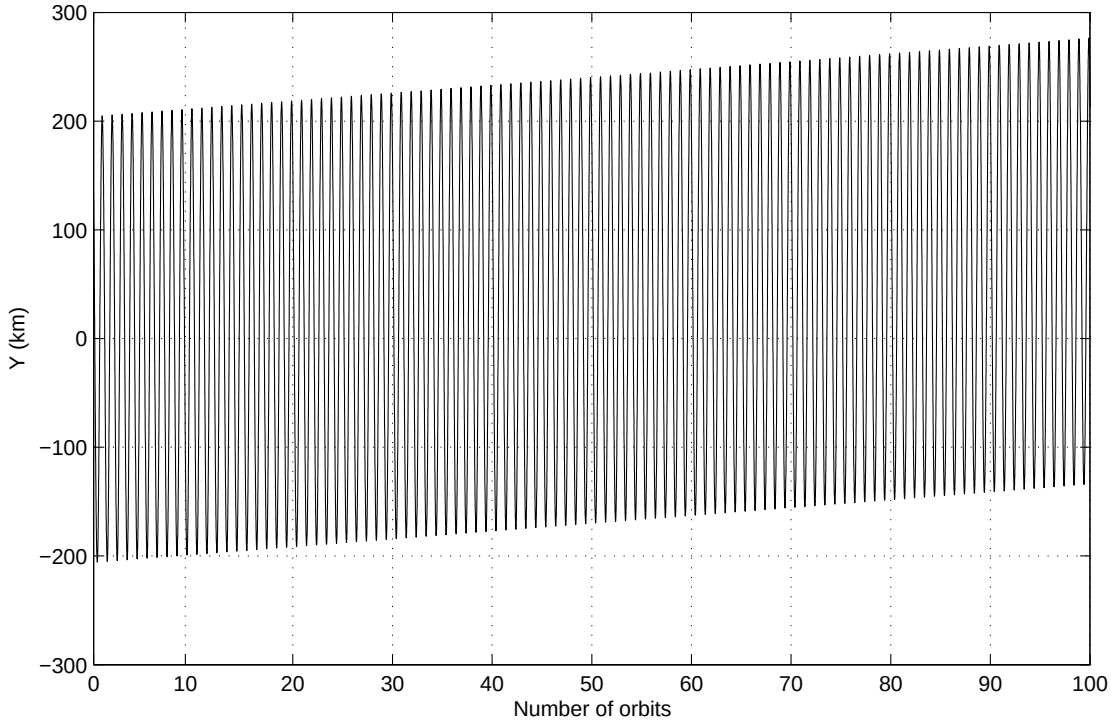

Fig. 31 Y component for 100 orbit and ρ=100 km

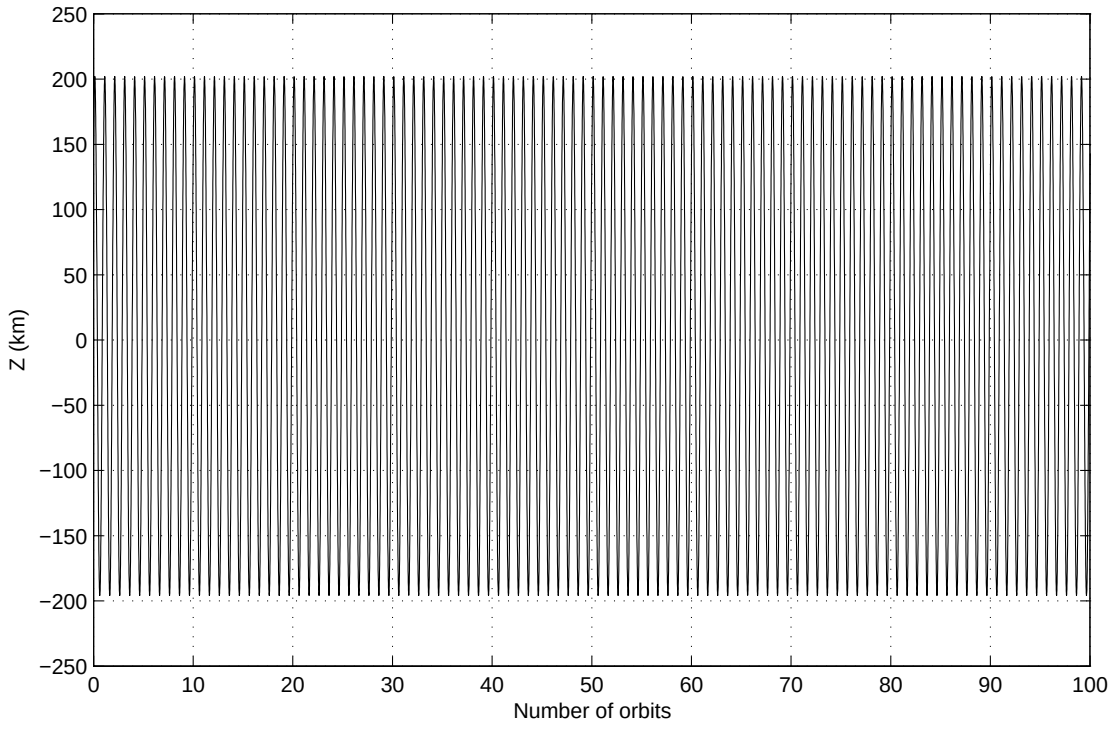

Fig. 32 Z component for 100 orbit and ρ=100 km

As the non linear correction reported in Eq. 34 is evaluated through an approximated process, there is still a residual drift for very large formation of about -0.72 km/orb.

3.1.3. Method of epicyclic elements: Kasdin and Koleman model

In their work [22], Kasdin and Koleman use a Hamiltonian approach to derive the equations of motions for an object relative to a circular or slightly elliptical reference orbit. By solving the Hamilton-Jacobi equation they develop constants of the relative motion called epicyclic elements. By means of this formalism, they derive bounded, periodic orbits in the presence of various perturbations. Non-linear effects are among this effects. Now we focus on the conditions found for the circular reference orbit case. Two formulas are given: one considering second-order terms in the series expansion for the initial conditions, and one considering also third-order terms.

$$a_3(0) = -\frac{5}{2}{a_1}^2(0) - \frac{1}{2}\left({a_2}^2(0) - {b_1}^2(0) + {b_2}^2(0)\right) - 3a_1(0)b_3(0) - {b_3}^2(0) \qquad \textbf{Eq. 35}$$

$$a_3(0) = -\frac{5}{2}{a_1}^2(0) - \frac{1}{2}\left({a_2}^2(0) - {b_1}^2(0) + {b_2}^2(0)\right) - 3a_1(0)b_3(0) - {b_3}^2(0) - \frac{3}{2}\left({a_1}^2(0)b_1(0) + {a_2}^2(0)b_1(0)\right) + \frac{1}{2}{b_1}^3(0)$$

Eq. 36

In both cases, it's:

$$
\begin{aligned}
a_1 &= \sqrt{2\alpha_1}\cos\beta_1 \\
b_1 &= \sqrt{2\alpha_1}\sin\beta_1 \\
a_2 &= \sqrt{2\alpha_2}\cos\beta_2 \\
b_2 &= \sqrt{2\alpha_2}\sin\beta_2 \\
a_3 &= \alpha_3 \\
b_3 &= \beta_3
\end{aligned}
\qquad \textbf{Eq. 37}
$$

α_i and β_i are the initial canonical momenta and coordinates, which can be written as functions of the initial conditions (in the following expressions, distances are normalized by the reference orbit semi-major axis *a*, and the rates normalized by the angular velocity *n*):

$$
\begin{aligned}
\alpha_1 &= \frac{1}{2}\left(\dot{x}^2 + \left(2\dot{y} + 3x\right)^2\right) \\
\alpha_2 &= \frac{1}{2}\left(\dot{z}^2 + z^2\right) \\
\alpha_3 &= \dot{y} + 2x \\
\beta_1 &= -\tan^{-1}\left(\frac{3x + 2\dot{y}}{\dot{x}}\right) \\
\beta_2 &= \tan^{-1}\left(\frac{z}{\dot{z}}\right) \\
\beta_3 &= -2\dot{x} + y
\end{aligned}
\qquad \textbf{Eq. 38}
$$

Imposing the conditions in Eq. 35 or in Eq. 36 (according to the order of approximation), we can substitute Eq. 37 in Eq. 38 and then solving Eq. 38 in order to find $\dot{y}$ for bounded orbits for different initial ρ.

The difference of the semi major axis can be so plotted for the three constraints on initial conditions for periodic orbits, as in Fig. 33.

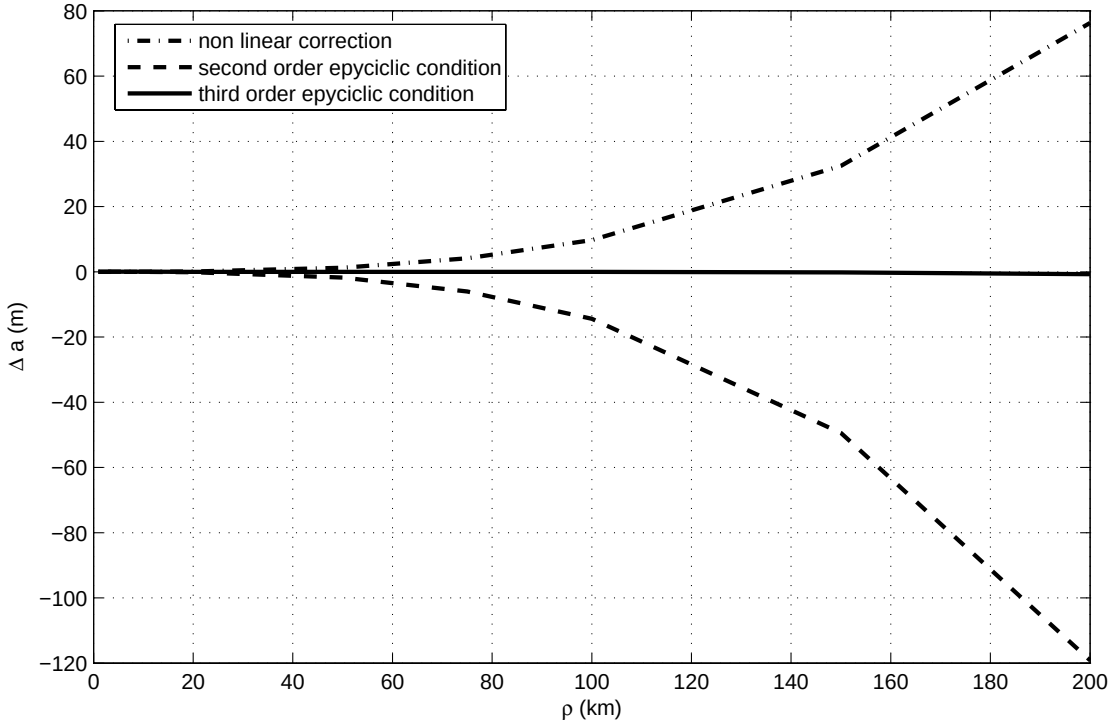

Fig. 33Difference of the semi major axis vs. initial condition

The third-order epicyclic conditions are a very good approximation of the period matching conditions, and indeed the use of the genetic algorithm tool seems not really necessary in this case. Anyway a comparison can be performed. As just one condition is necessary (on the $\dot{y}$) to ensure the period matching, the simulations with the genetic algorithm is performed with just two variables, $\dot{y}$ and T. The reason for this choice is that in this way we have a direct comparison between the resulting relative orbits, because the other five initial conditions are kept equal. Otherwise we would obtain completely different relative orbits, because relative orbits generated by GA are random in dimension and spatial orientation.

Running the simulation again with $\rho = 200Km$, so that we have:

$$x_0 = 70.710678118654 \text{ km}$$
$$y_0 = 1.41421356237310 \text{ km}$$
$$z_0 = 1.41421356237310 \text{ km}$$
$$\dot{x}_0 = 0.08180578703989 \text{ km/s}$$
$$\dot{z}_0 = 0.16361157407979 \text{ km/s}$$

the genetic algorithm returns an $\dot{y}_0 = -0.168764291999998$ km/s. The resulting relative trajectory is shown in Fig. 34, Fig. 35, Fig. 36 and Fig. 37.

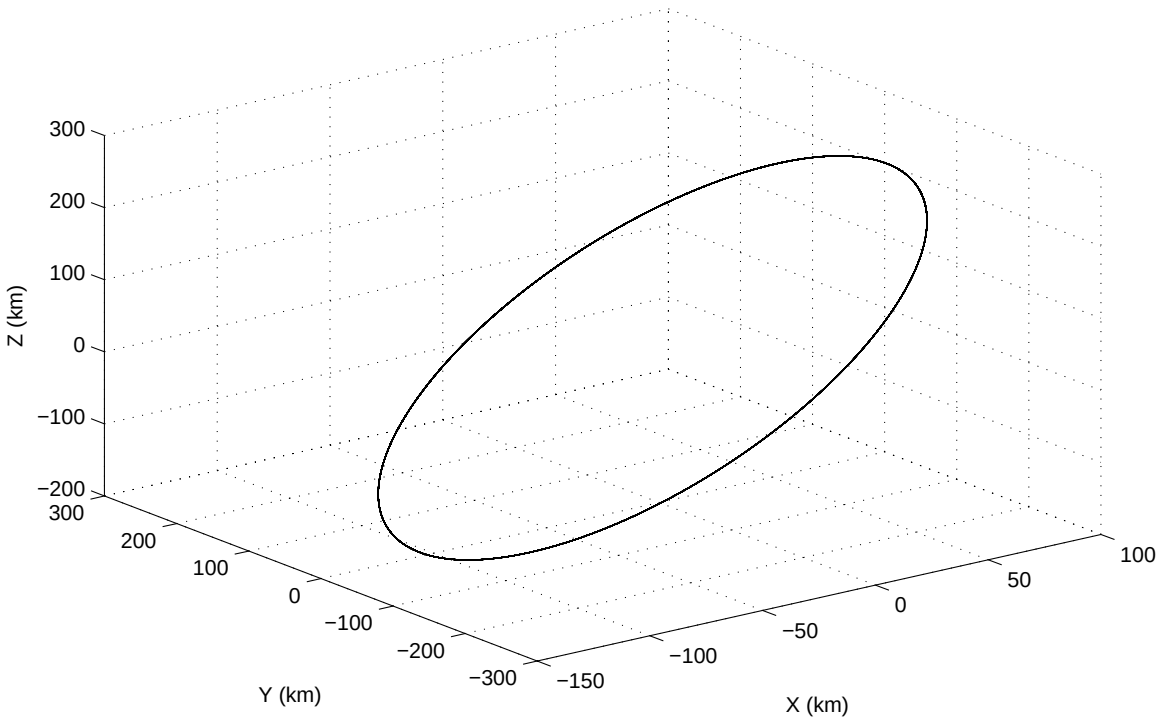

Fig. 34 Relative orbit generated with epicyclic method

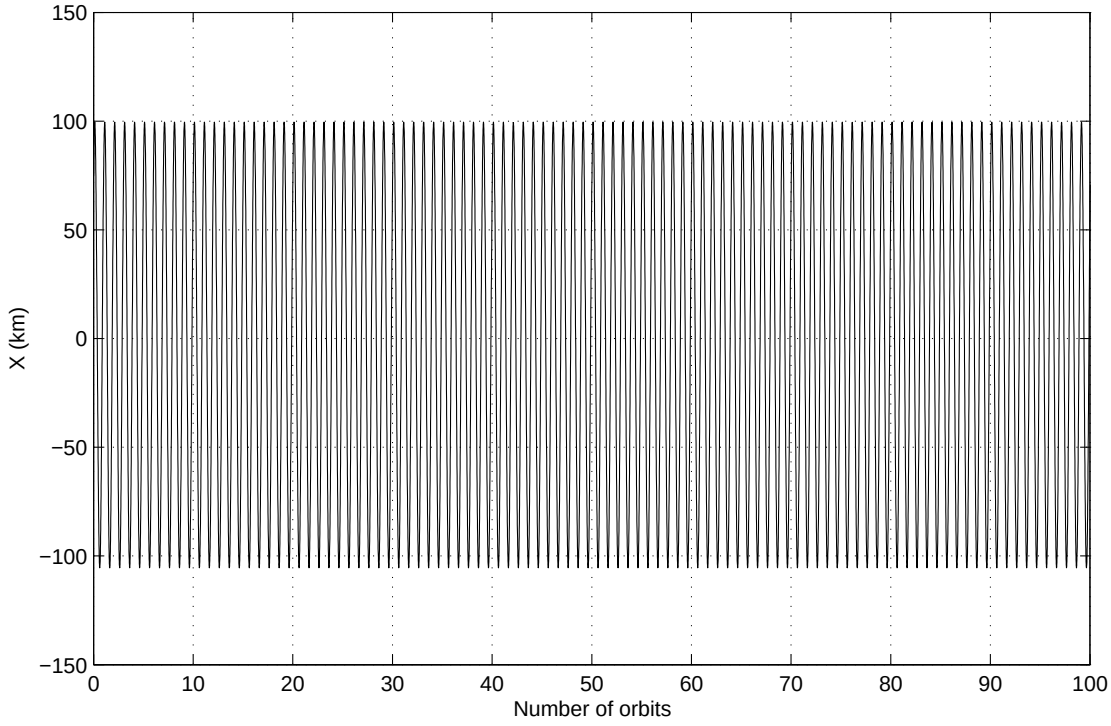

Fig. 35 X component generated with epicyclic method

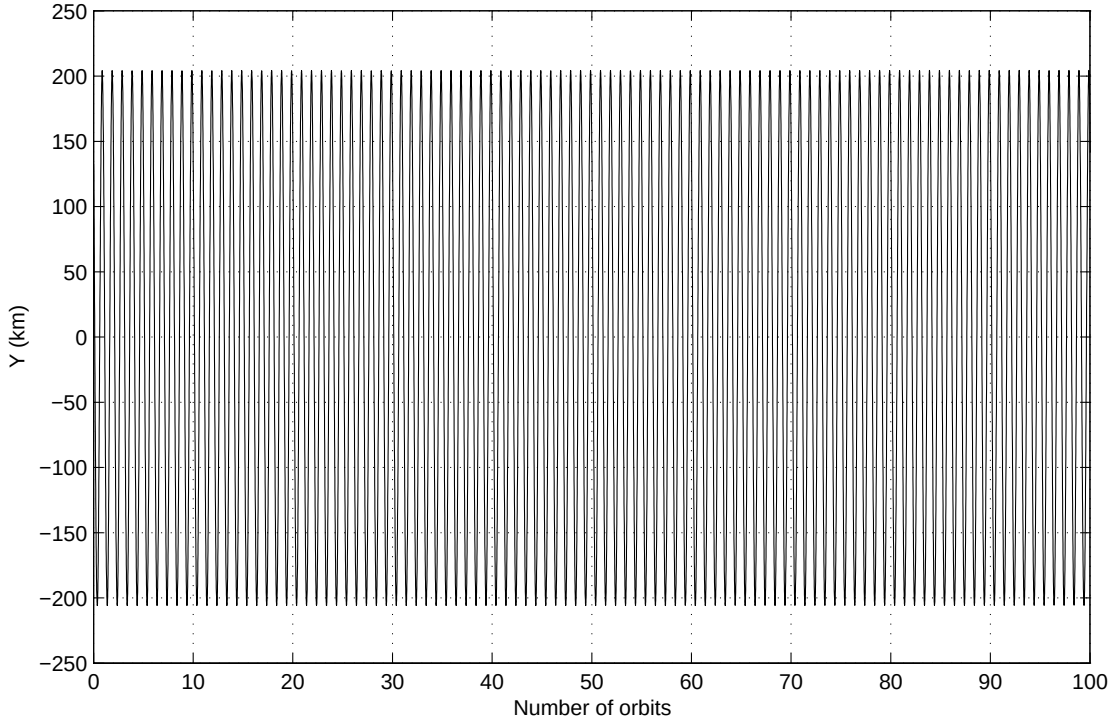

Fig. 36 Y component generated with epicyclic method

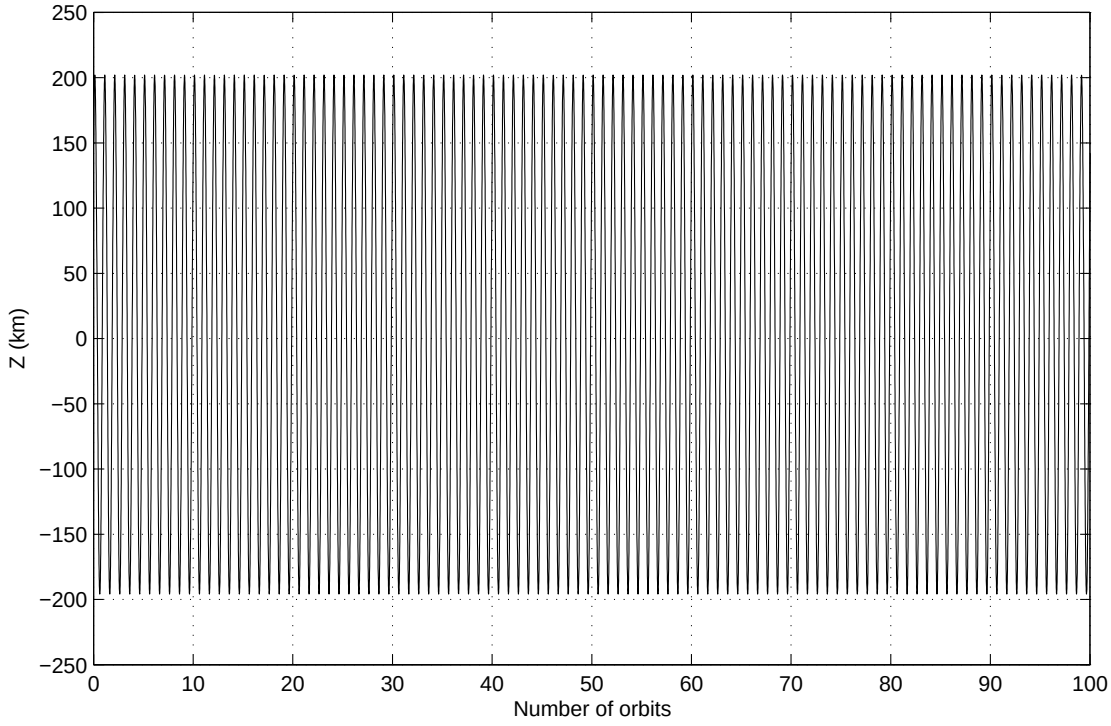

Fig. 37 Z component generated with epicyclic method

As it's possible to see, the relative orbit is perfectly closed and there is no drift on any coordinate.

A comparison among the conditions on $\dot{y}_0$ arising from the four cases, HCW, non linear correction and second and third-order conditions can be done with respect to the GA results (which can be considered as "exact"). This is shown in Fig. 38.

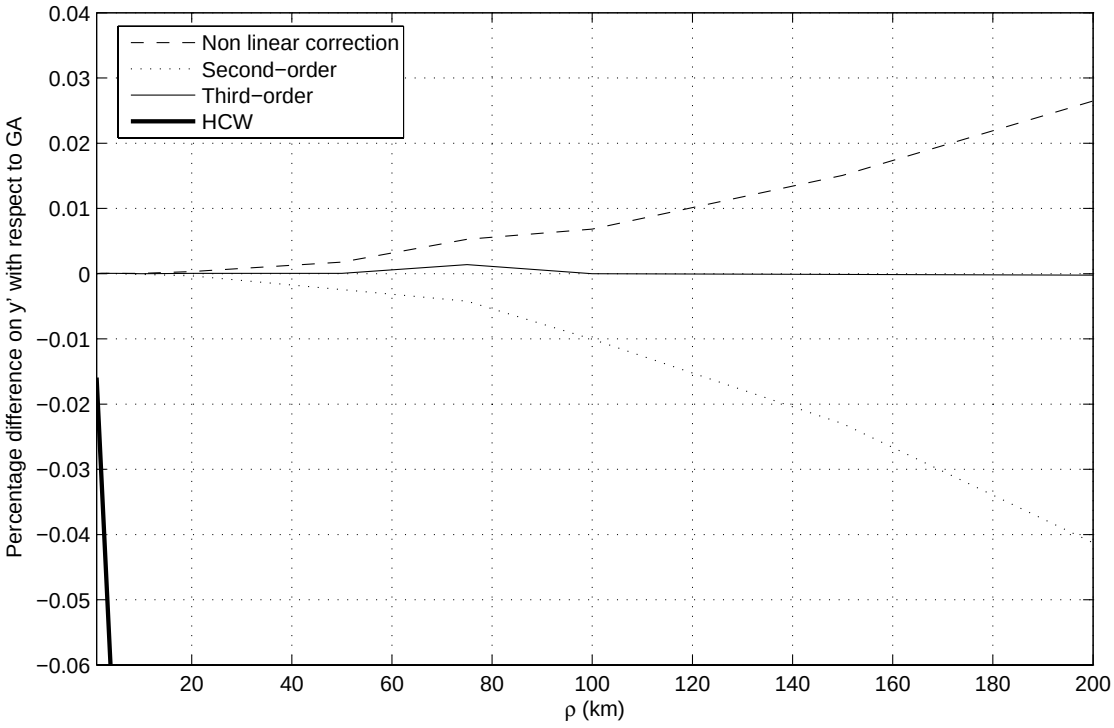

Fig. 38 Percentage difference on of different methods with respect to GA

It is notable that a percentage difference on the $\dot{y}_0$ of just -0.02647 % between the non linear correction case and the genetic algorithm, corresponding to something like -4.466e^{-5} km/s, can be responsible of the closing or not of the relative trajectory. This shows how sensitive is the dynamical system to small variation on the parameters.

The only one analytical condition which generates results that can be compared to genetic algorithm performances is the third-order one, as shown in Fig. 39.

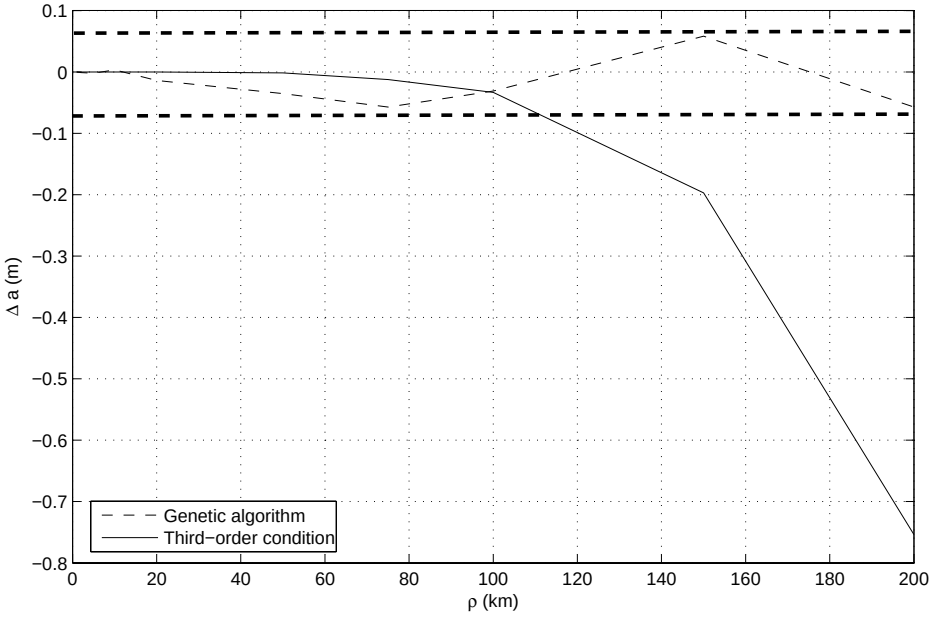

Fig. 39 Comparison between GA and third-order condition

The main difference is that Δa due to genetic algorithm conditions is oscillating and due just to numerical errors and to the random process which characterize the optimizator; instead, Δa due to third-order conditions grow as the formation is larger. Anyway, even for very large formations, its results are quite good. In fact, if we analyse the *y* component, we can say that no real drift is present, as shown in Fig. 40.

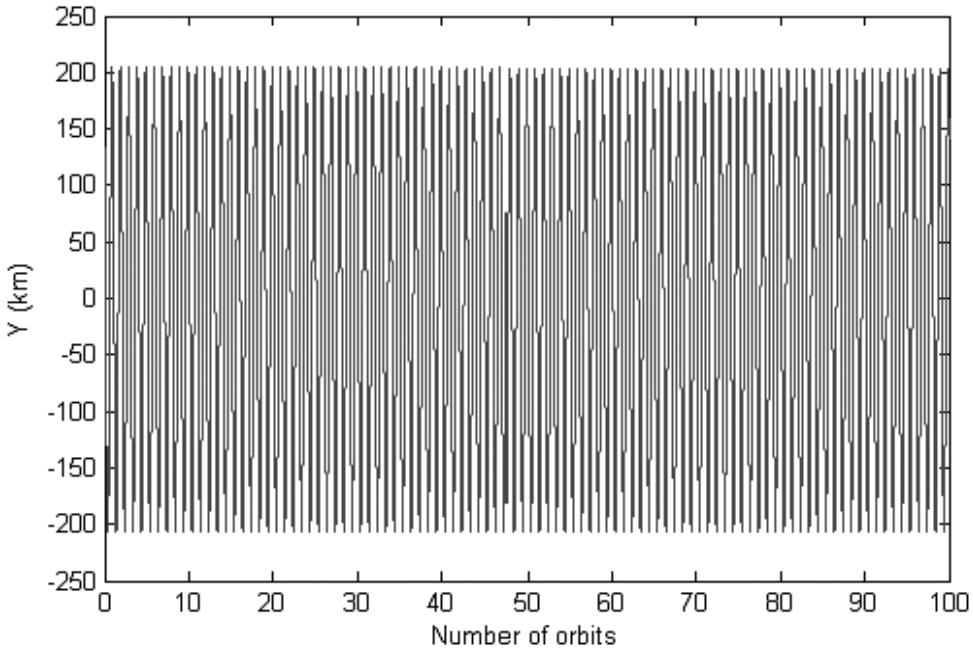

Fig. 40 Y component for a large formation

3.2. Elliptic reference orbit

3.2.1. Tschauner-Hempel model: TH equations

When HCW solution for bounded orbits is applied to formations characterized by non-circular reference orbits, results are not so reliable any more, even for very small eccentricities. Fig. 41 shows the growing of the drift per orbit as the eccentricity varies.

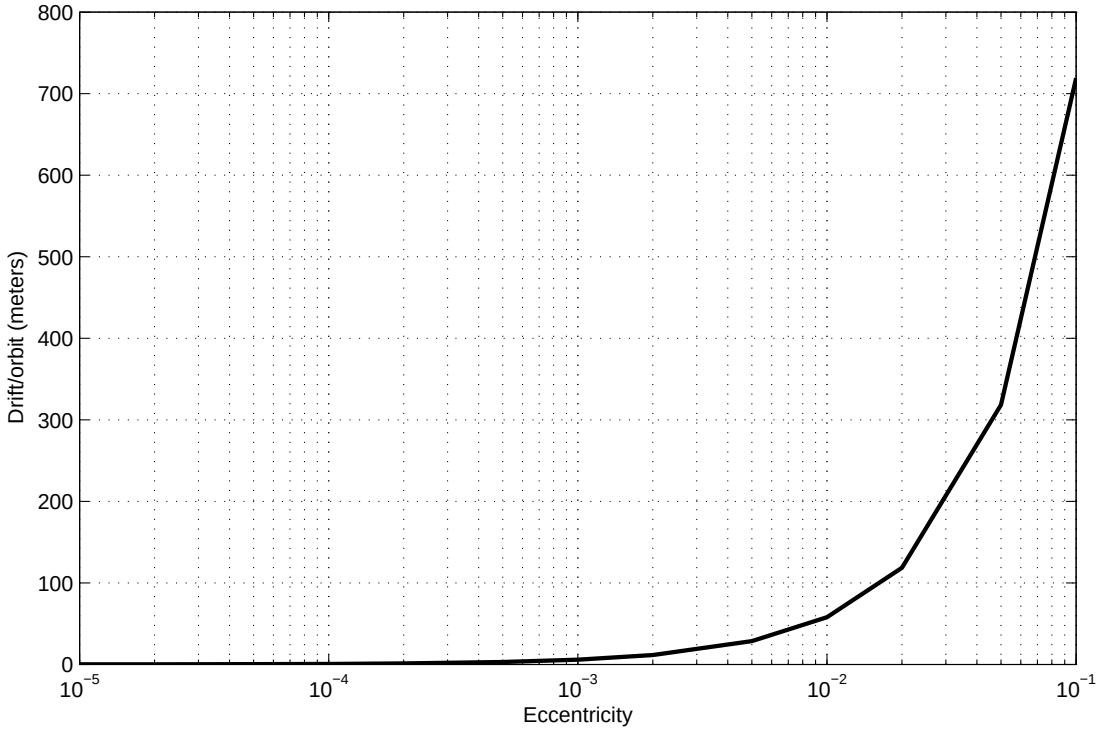

Fig. 41 Drift per orbit due to non-circularity of reference orbit

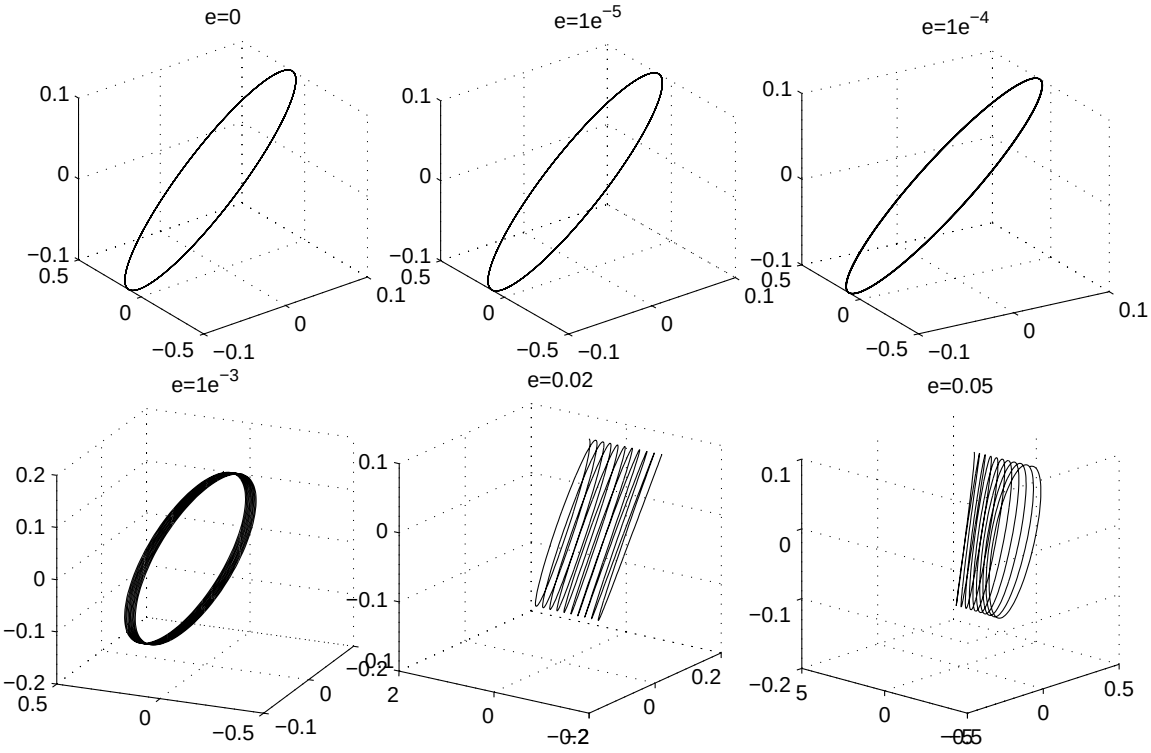

Fig. 42 Degeneration of relative orbit for non-zero eccentricity

It can be seen as even for small eccentricity, let's say more then $e = 0.001$, HCW conditions cannot be used anymore. Eccentricity is a strong perturbation for the relative motion.

Considering again Eq. 24:

$$\begin{cases} \ddot{x} - 2\dot{\theta}\dot{y} - \ddot{\theta}y - \dot{\theta}^2 x = -\dfrac{\mu(r+x)}{\left[(r+x)^2 + y^2 + z^2\right]^{\frac{3}{2}}} + \dfrac{\mu}{r^2} \\ \ddot{y} + 2\dot{\theta}\dot{x} + \ddot{\theta}x - \dot{\theta}^2 y = -\dfrac{\mu y}{\left[(r+x)^2 + y^2 + z^2\right]^{\frac{3}{2}}} \\ \ddot{z} = -\dfrac{\mu z}{\left[(r+x)^2 + y^2 + z^2\right]^{\frac{3}{2}}} \\ \ddot{r} = r\dot{\theta}^2 - \dfrac{\mu}{r^2} \\ \ddot{\theta} = -\dfrac{2\dot{r}\dot{\theta}}{r} \end{cases}$$

,

it's possible to linearize this set of equations and obtain the equivalent of the Hill-Cloesshy-Wiltshire equations for the elliptic unperturbed reference orbit.

These are the so-called Tschauner-Hempel equations. In these equations the independent variable is true anomaly:

$$\begin{cases} x'' - 2\frac{e\sin\theta}{1+e\cos\theta}x' - 2y' + 2\frac{e\sin\theta}{1+e\cos\theta}y - (1 + 2\frac{1}{1+e\cos\theta})x &= 0 \\ y'' - 2\frac{e\sin\theta}{1+e\cos\theta}y' + 2x' - 2\frac{e\sin\theta}{1+e\cos\theta}x - (1 - \frac{1}{1+e\cos\theta})y &= 0 \\ z'' - 2\frac{e\sin\theta}{1+e\cos\theta}z' + \frac{1}{1+e\cos\theta}z &= 0 \end{cases}$$

Eq. 39

If one wants to adopt time as independent variable, the resulting model is:

$$\begin{cases} \ddot{x} - 2\dot{\theta}\dot{y} - \ddot{\theta}y - \dot{\theta}^2 x - 2\dfrac{\mu}{r^3}x = 0 \\ \ddot{y} + 2\dot{\theta}\dot{x} + \ddot{\theta}x - \dot{\theta}^2 y + \dfrac{\mu}{r^3}y = 0 \\ \ddot{z} + \dfrac{\mu}{r^3}z = 0 \\ \ddot{r} = r\dot{\theta}^2 - \dfrac{\mu}{r^2} \\ \ddot{\theta} = -\dfrac{2\dot{r}\dot{\theta}}{r} \end{cases}$$

Eq. 40

In this case, an analytical solution exists, and it's exact for the linearized case:

$$\frac{\dot{y}_0}{x_0} = -\frac{n(2+e)}{(1+e)^{\frac{1}{2}}(1-e)^{\frac{3}{2}}}$$

Eq. 41

This condition is only valid if the initial conditions are given at the perigee of the reference orbit. Using Vaddi, Vadali and Alfriend notation of paragraph 3.2.1, where eccentricity is considered a perturbation of the HCW model, the constraint for bounded orbits can be written as:

$$\dot{y}_0 = \dot{y}_h + \delta(e),$$

where $\dot{y}_h$ is the usual HCW solution and $\delta(e)$the correction for the non-circularity:

$$\delta(e) = n\rho\sin\alpha_0\left\{1 - \left[\frac{(2+e)}{2(1+e)^{\frac{1}{2}}(1-e)^{\frac{3}{2}}}\right]\right\}$$

Eq. 42

This is just another way to write the initial condition Eq. 41. Let's choose as reference orbit:

$$\begin{cases} a = 9500km \\ e = -- \\ i = 97.87° \\ \varpi = 90° \\ \Omega = 270° \\ \theta_0 = 0° \end{cases}$$

The semi major axis has been chosen greater than the previous cases to permit simulations of high eccentric orbits. Initial spatial conditions are set:

$$[x_0, y_0, z_0] = [0.1, 0.1, 0.1] km \quad \textbf{Eq. 43}$$

In this way effects of nonlinearity are almost negligible, because the relative orbit is quite compact. Initial constraint Eq. 41 (or Eq. 42) is not an approximated correction for TH equations as the ones for nonlinearity were, but it's exact. Nevertheless the drift per orbit grows as the eccentricity of the reference orbit is higher:

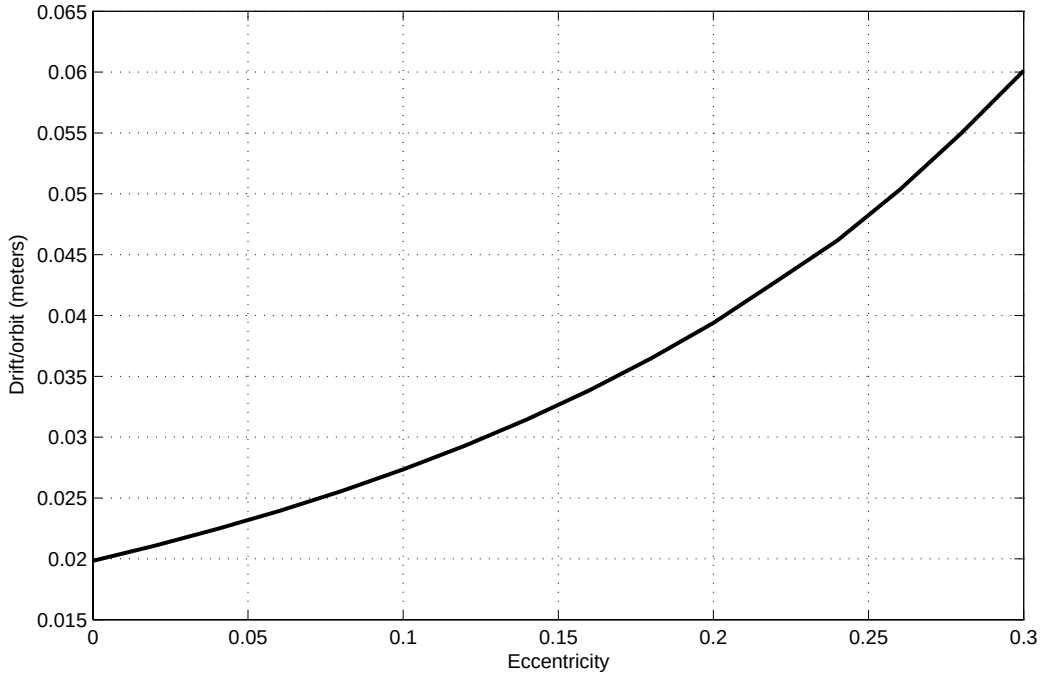

Fig. 43Drift resulting from use of TH condition at different eccentricities

The fact that the drift, though very little, is growing, is due to the fact that the initial condition used are an exact solution just for the linear model. Instead using genetic algorithm results in a very small random drift, due just to numerical errors; a comparison is reported in Fig. 44.

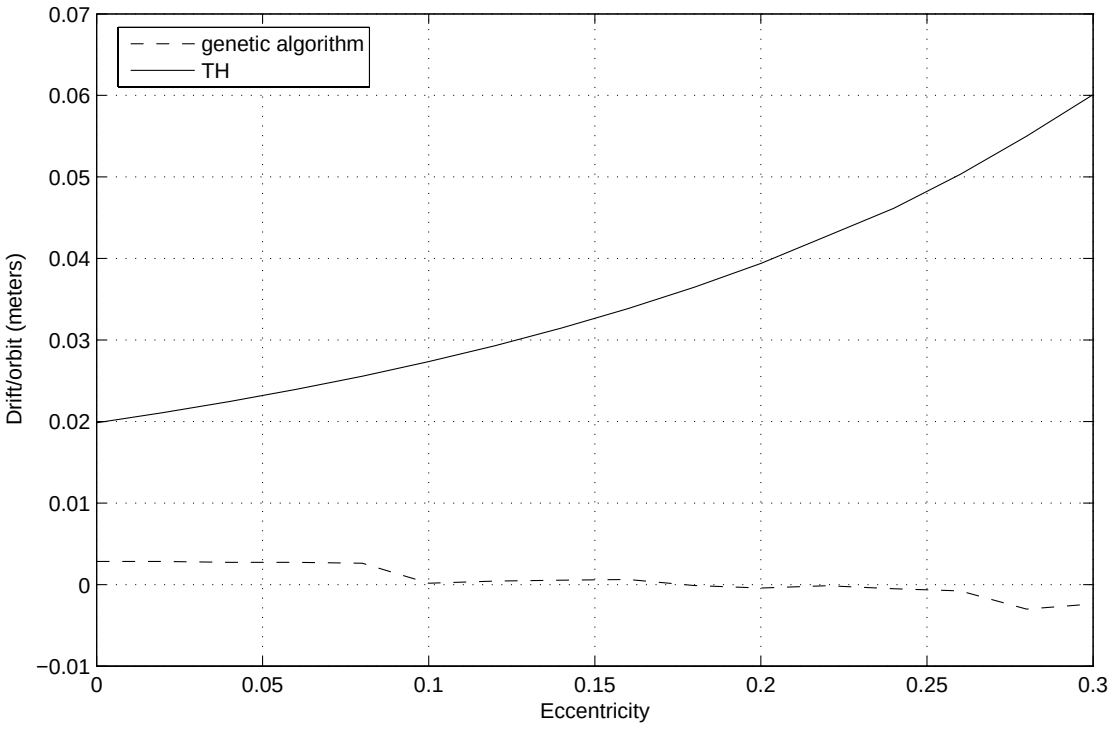

Fig. 44 Comparison between GA and TH conditions for different eccentricity

This behaviour of TH condition is due to the fact that the higher-order nonlinear perturbation effects become of the same order as eccentricity perturbation, and thus cannot be considered separately.

The dimensions of the formation studied for Fig. 43 were in fact quite small. If larger configurations are considered, the boundedness of the formation with TH condition dramatically brakes down.

3.2.2. Non linearity plus Eccentricity Correction

Vaddi, Vadali & Alfriend propose a correction for non-linear, eccentric case. The condition is simply the sum of the corrections for non linearity and for eccentricity.

$$[x_0, y_0, z_0] = [\rho/2\sin(nt+\alpha_0), \rho\cos(nt+\alpha_0), \rho\sin(nt+\alpha_0)]$$

$$\dot{y}(0) = \dot{y}_h(0) + \varepsilon\dot{y}_{cn}(0) + \delta(e) \qquad \textbf{Eq. 44}$$

where:

$$\dot{y}_h(0) = -2nx_0 \text{: HCW condition}$$

$$\dot{y}_{cn}(0) = -(\rho^2/48n)(12+6\cos 2\alpha_0) \text{ : non linear correction}$$

$$\delta(e) = n\rho\sin(\alpha_0)\left\{1-\left[\frac{(2+e)}{2(1+e)^{\frac{1}{2}}(1-e)^{\frac{3}{2}}}\right]\right\}$$: eccentricity correction.

$\varepsilon = 3\mu / a^4$, parameter for nonlinear correction.

For low eccentric reference orbits it all seems to work quite well, meaning the drift per orbit is limited for large formations as well. Let's see for example e=0.005:

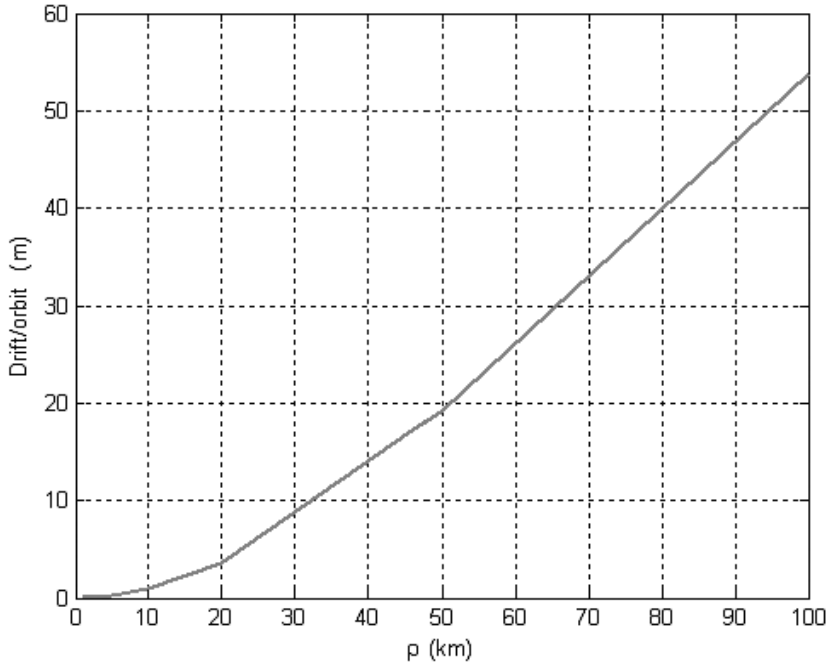

Fig. 45 Drift per orbit for different formation dimension using the method of non-linear plus eccentricity correction (low eccentricity case)

The drift per orbit seems to be same order of magnitude as in the circular case with non linear correction (consider this is a higher orbit). Actually, for other cases the correction for nonlinear effect is not so good as in the circular orbit case. In fact, for high eccentricities, as for example e=0.2, the drift per orbit is much greater then e=0.005 case:

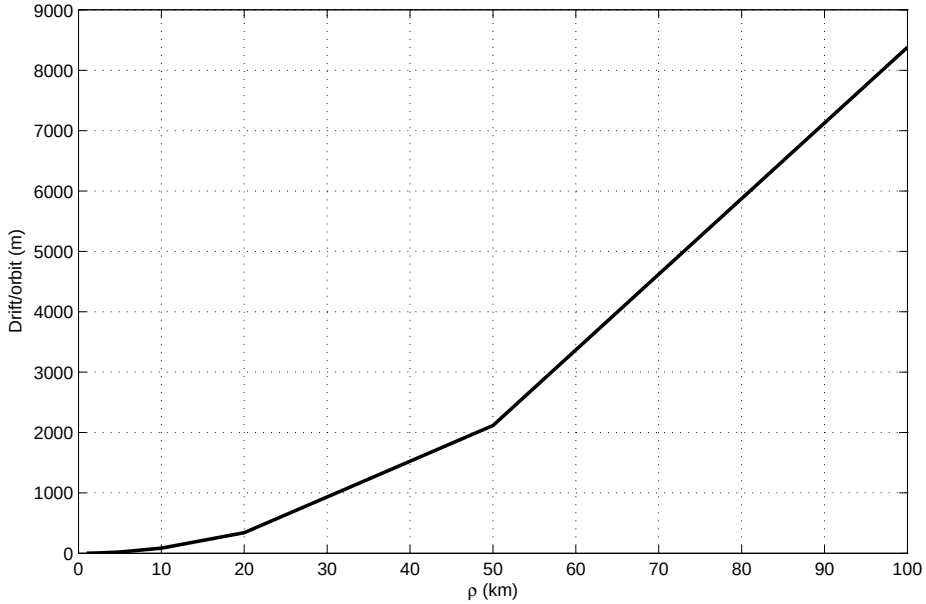

Fig. 46 Drift per orbit for different formation dimension using the method of non-linear plus eccentricity correction (high eccentricity case)

In order to have an "exact" solution, it's possible to use the genetic algorithm tool for this last situation. We can then compare the $\dot{y}$ from this analytical formulation and the $\dot{y}$ from genetic algorithm computation; this is accomplished in Fig. 47.

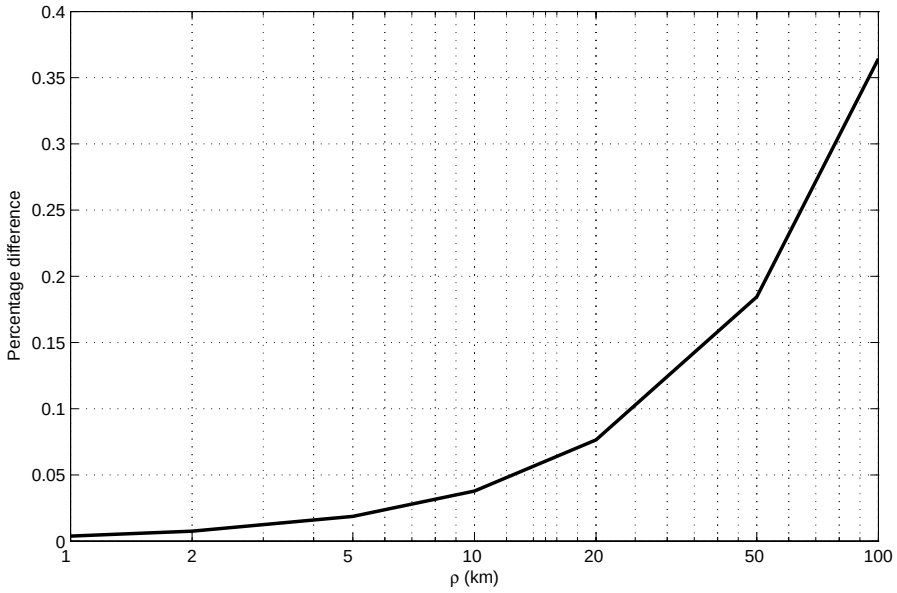

Fig. 47 Difference on $\dot{y}_0$ using GA and using he method of non-linear plus eccentricity correction (high eccentricity case)

As we already noticed, a difference of about 0.35% can seem little, but it has very serious effects, which are shown in Fig. 48and in Fig. 49.

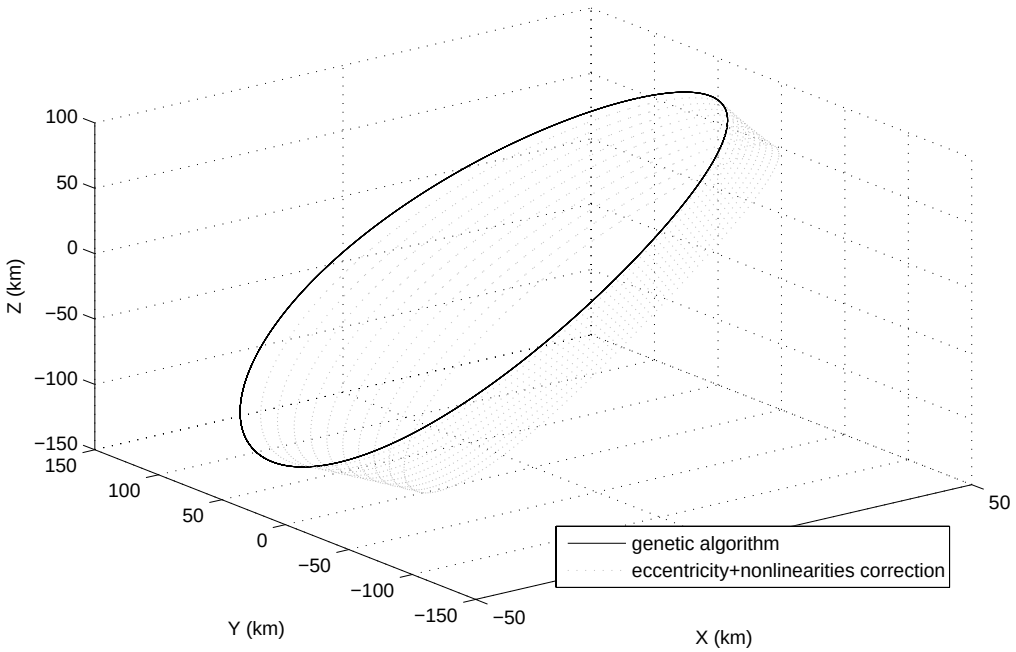

Fig. 48 Relative orbits obtained using GA conditions and conditions from the method of corrections

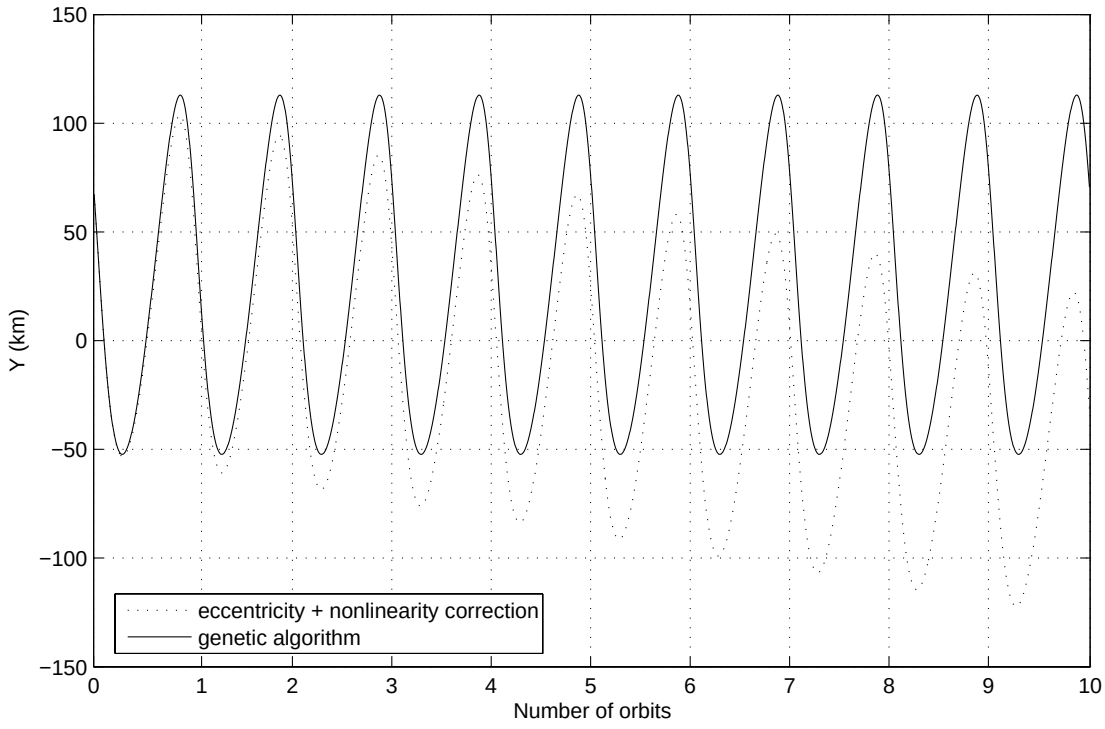

Fig. 49 Y components obtained using GA conditions and conditions from the method of corrections

Therefore we can say that the method for nonlinear plus eccentricity correction here exposed is valid just for low eccentric orbits (as the authors state), while **genetic algorithm doesn't show any drift for any eccentricity and for any formation dimension.**

While this case is very simple and could be solved with any other numerical method, because just one simple condition is to be imposed (equality of semi-major axes of the two satellites), in other cases, as perturbed ones, or multi-satellites formations case, genetic algorithm can be considered a very useful tool. Anyway, it must be noticed that random processes play a very important role in the genetic algorithm. This means that even in such simple cases, sometimes the algorithm can fail. Let's see for example one case:

$$\begin{cases} a = 9500km \\ e = 0.02 \\ i = 97.87° \\ \varpi = 90° \\ \Omega = 270° \\ \theta_0 = 0° \end{cases} \quad \text{and} \quad [x, y, z, \dot{x}, \dot{y}, \dot{z}] = [0.1, 0.1, 0.1, 0, ?, 0]$$

Performing the simulation with seed number = 1, fitness values are not so good at all; so a second run is necessary with different seed number (in the example, seed is 555), which means different initial random population.

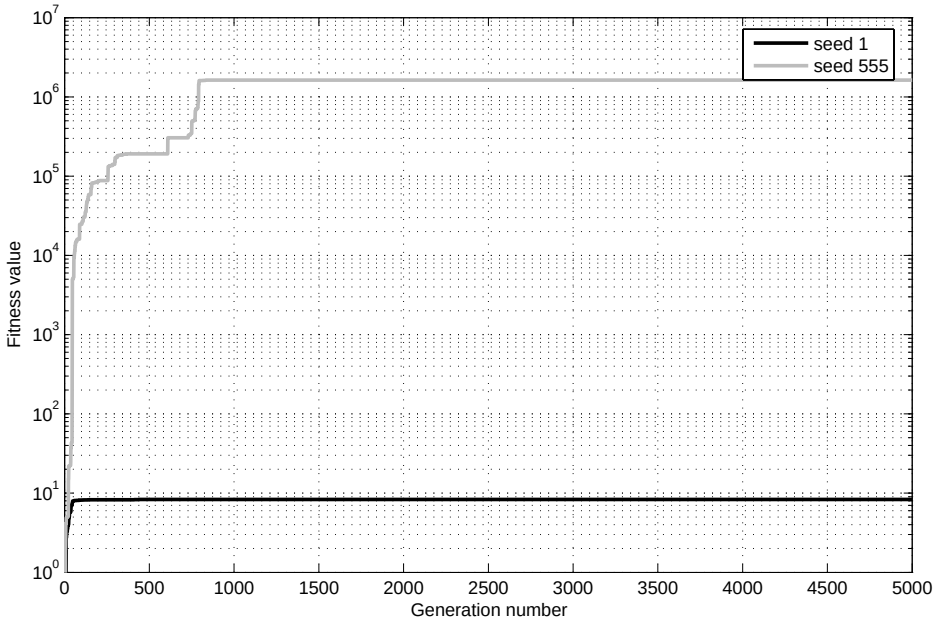

Fig. 50 Possibility of the GA to fail

Evidently, random population generated with seed number 1 is particularly unlucky. This can happen, and must be taken in consideration.

4. J_2 perturbed reference orbits

4.1. J_2 perturbation

The actual motion of a satellite is not given by the simple:

$$\frac{d^2\vec{r}}{dt^2} = -\frac{\mu}{r^2}\hat{r}$$

as supposed in Chapter **Error! Reference source not found.**. In fact, the satellite is not subject just to kepler gravitational attraction, but also to a number of forces of much lower magnitude, called perturbations. Though their intensity is not big compared to kepler attraction, their effects cannot be neglected. The equation of motion of a single satellite so becomes:

$$\frac{d^2\vec{r}}{dt^2} = -\frac{\mu}{r^2}\hat{r} + \vec{f}$$

and the relative motion of two satellites, in analogy with Eq. 23 can be rewritten as:

$$\ddot{\vec{\rho}} + 2\vec{\omega}\times\dot{\vec{\rho}} + \dot{\vec{\omega}}\times\vec{\rho} + \vec{\omega}\times(\vec{\omega}\times\vec{\rho}) = -\frac{\mu}{r_1^2}\hat{r}_1 + \frac{\mu}{r_0^2}\hat{r}_0 + \vec{f}_1 - \vec{f}_0 \qquad \textbf{Eq. 45}$$

where $\vec{f}_1$ and $\vec{f}_0$ are the perturbations acting on the two satellites.

The first perturbation which will be considered is the so-called J_2 effect. This is due to the fact that Earth is not an homogeneous perfect sphere, but it's a geoid. This means nothing but that our planet has an irregular shape which is characteristic of the Earth alone. The most evident difference from the spherical shape is the flattening at the poles. So the Earth can be modelled not as a sphere, but as a spheroid (an ellipsoid of revolution). This is the cause of the J_2 perturbation, which results to be the most important perturbation at almost every altitude. Only for very low orbits drag becomes predominant, as it will be shown in Chapter **Error! Reference source not found.**.

The acceleration due to kepler Earth attraction $\vec{f}_N$ and to J_2 effect $\vec{f}_{J2}$ can be written in the LVLH frame as:

$$\vec{f} = \vec{f}_N + \vec{f}_{J2} = \left(-\frac{\mu}{r^2} - \frac{3}{2}\frac{\mu R_\oplus^{\,2} J_2}{r^4}\left(1 - 3\sin^2 i \sin^2 u\right)\right)\hat{r} - \left(\frac{3}{2}\frac{\mu R_\oplus^{\,2} J_2}{r^4}\sin^2 i \sin 2u\right)\hat{\theta} - \left(\frac{3}{2}\frac{\mu R_\oplus^{\,2} J_2}{r^4}\sin 2i \sin u\right)\hat{z}$$

Eq. 46

The components of this acceleration must be introduced in Gauss' equations to obtain the variation of the parameters:

$$\begin{aligned}
\frac{da}{dt} &= \sqrt{\frac{p}{\mu}}\frac{2p}{\left(1-e^2\right)^2}\left[e\sin\theta\frac{f_r}{m}+\left(1+e\cos\theta\right)\frac{f_\theta}{m}\right] \\
\frac{de}{dt} &= \sqrt{\frac{p}{\mu}}\left[\sin\theta\frac{f_r}{m}+\frac{e+2e\cos\theta+e\cos^2\theta}{1+e\cos\theta}\frac{f_\theta}{m}\right] \\
\frac{d\Omega}{dt} &= \sqrt{\frac{p}{\mu}}\frac{1}{\sin i}\frac{\sin(\theta+\omega)}{1+e\cos\theta}\frac{f_z}{m} \\
\frac{d\omega}{dt} &= \sqrt{\frac{p}{\mu}}\left[-\frac{\cos\theta}{e}\frac{f_r}{m}+\frac{\left(2+e\cos\theta\right)\sin\theta}{e\left(1+e\cos\theta\right)}\frac{f_\theta}{m}-\frac{1}{\tan i}\frac{\sin(\theta+\omega)}{1+e\cos\theta}\frac{f_z}{m}\right] \\
\frac{di}{dt} &= \sqrt{\frac{p}{\mu}}\frac{\cos(\theta+\omega)}{1+e\cos\theta}\frac{f_z}{m}
\end{aligned} \qquad \textbf{Eq. 47}$$

In the unperturbed case, the condition imposed to have bounded relative orbits is the period matching. In fact, because the only force acting on both satellites is the keplerian gravitational attraction $-\frac{\mu}{r^2}\hat{r}$, which depends just on the position, it's clear that two satellites having same orbital period will find themselves after that period in the same position, with same velocity and subject to same forces. Their absolute motion will therefore be periodic and the relative motion is then ensured to repeat equal to himself in any orbital period.

This cannot be affirmed for a perturbed case. The effects of the J_2 perturbation on the orbital parameters are of two kinds: secular and periodic.

Secular variation can be found in argument of perigee and right ascension of ascending node; periodic behaviour on semi major axis, eccentricity and inclination. For parameters we choose a generic LEO:

$$\begin{cases}
a = 6678km \\
e = 0.00118 \\
i = 35° \\
\varpi = 90° \\
\Omega = 270° \\
\theta_0 = 0°
\end{cases}$$

The parameters are sown in Fig. 51, Fig. 52, Fig. 53, Fig. 54 and Fig. 55.

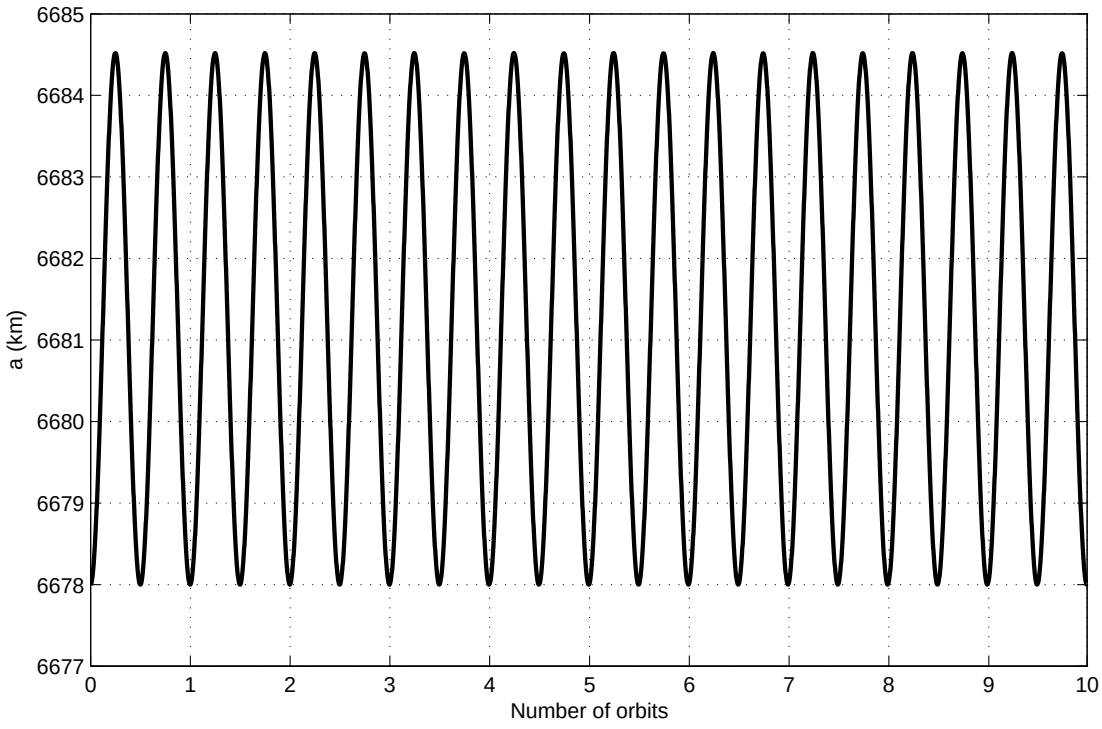

Fig. 51 Semiaxis, a

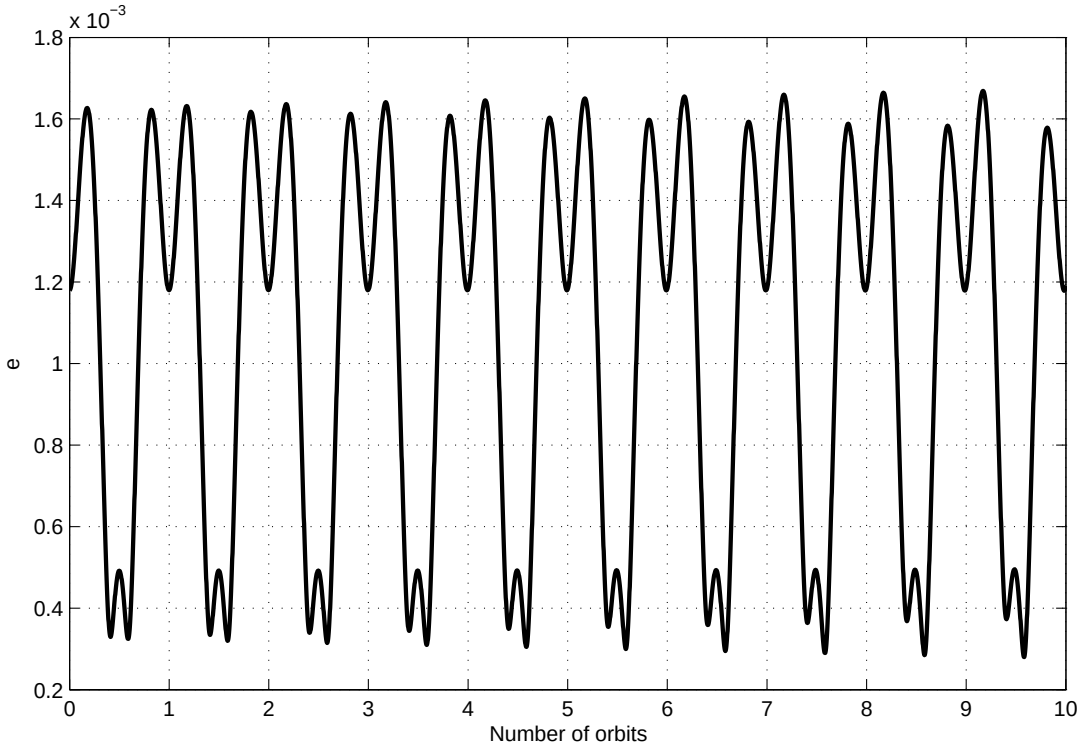

Fig. 52 Eccentricity, e

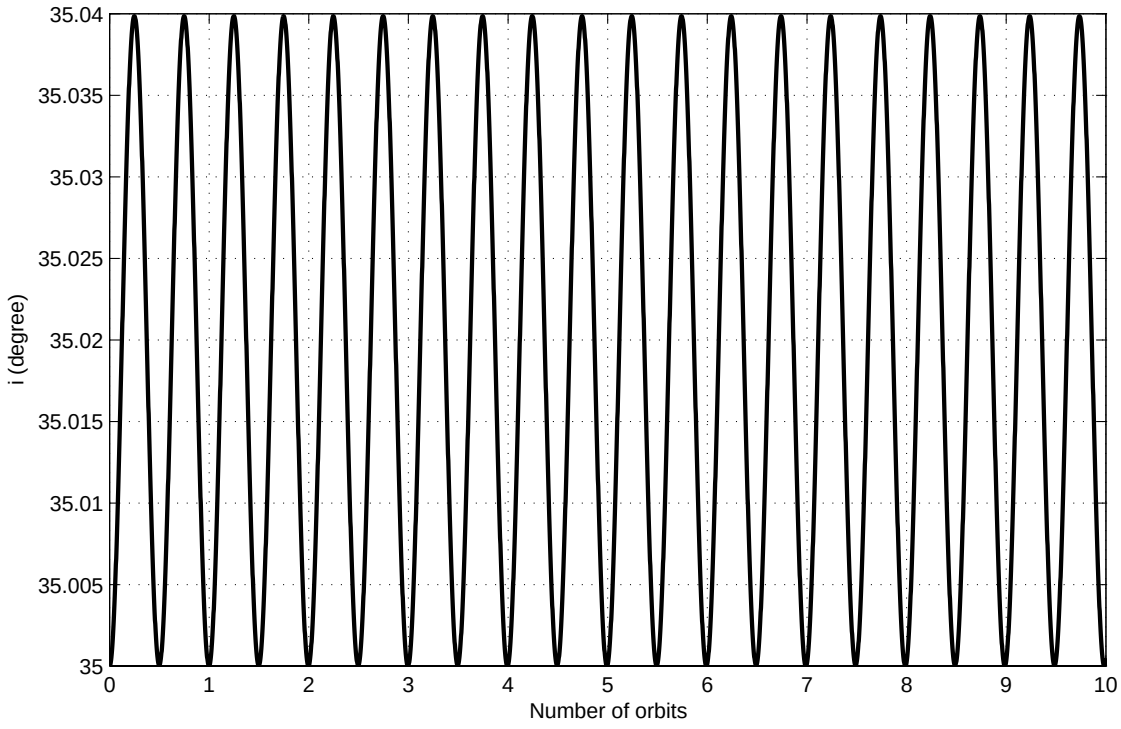

Fig. 53 Inclination, i

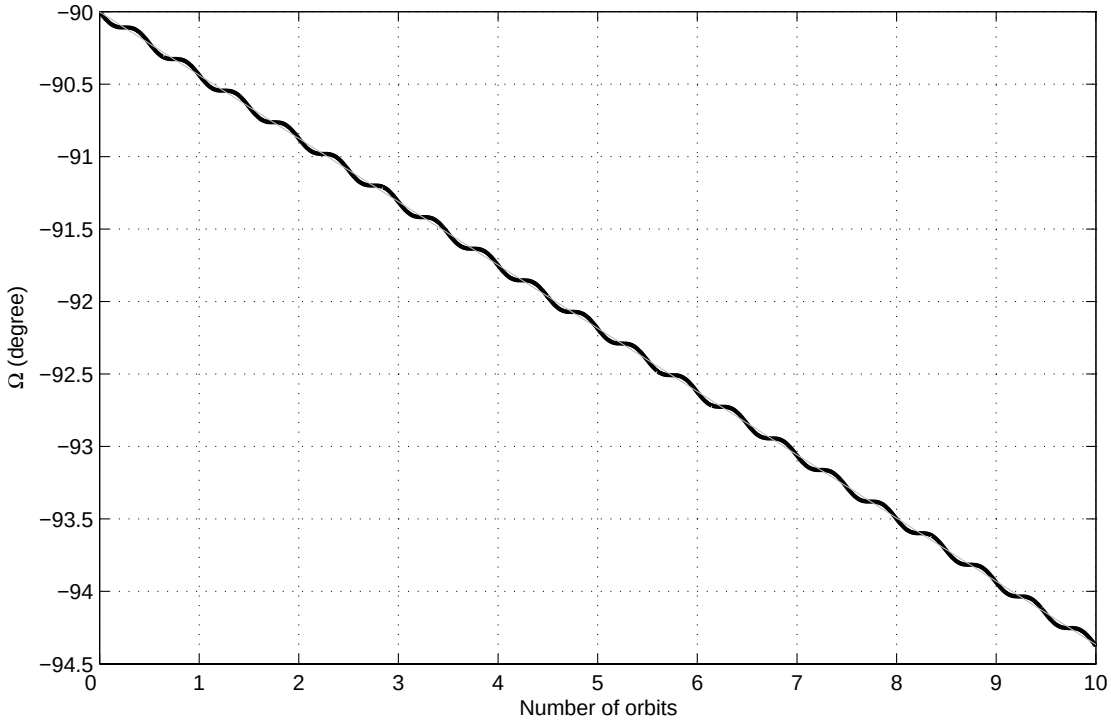

Fig. 54 RAAN, Ω

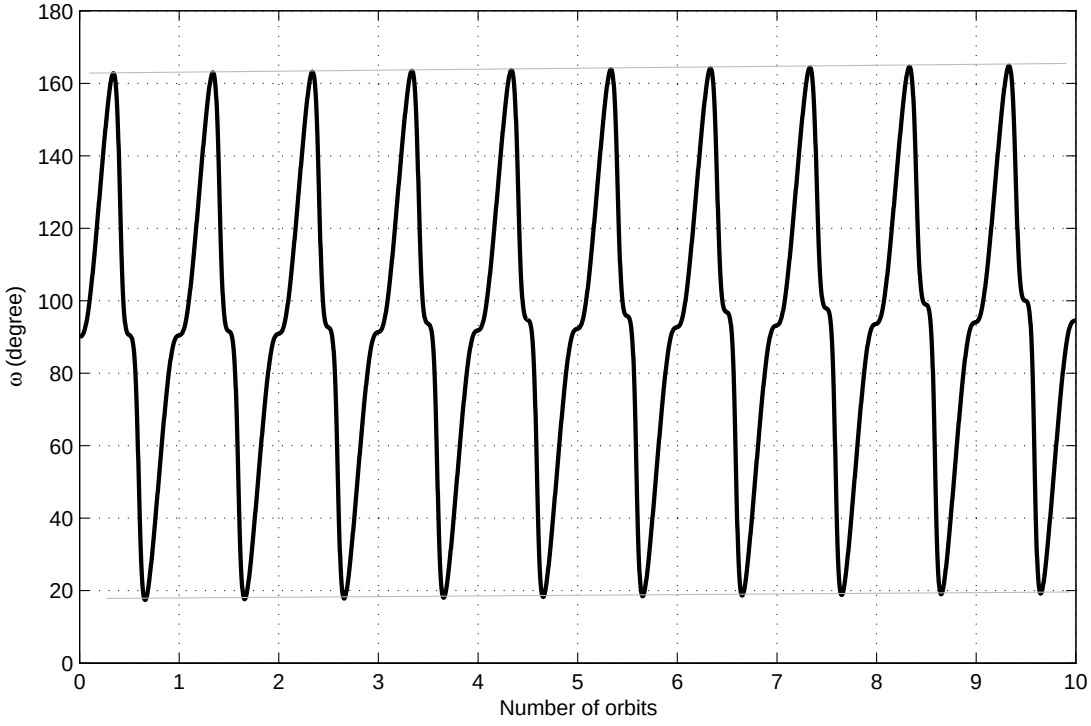

Fig. 55 Argument of perigee, ω

It's clear that the condition for the two satellites to find themselves in the same position, with same velocity and under same forces after a given period is not that easy to verify as in the unperturbed case.

First of all, a definite orbital period cannot be even defined. Fred P. J. Rimrott in [12] introduces three periods. First, an **absolute period**, which is the time required to pass through 360°; its deviation from Kepler period can be expressed as:

$$\Delta\tau_{2\pi} = -\frac{3}{4}\pi\sqrt{\frac{a^3}{\mu}}J_2\frac{R_\oplus^{\,2}}{p^2}\left(3\cos^2 i - 1\right) \quad \textbf{Eq. 48}$$

In the orbit under analysis it's $\Delta\tau_{2\pi}$ = -2.038 s . The satellite under J_2 effect is therefore slightly faster or slower according to inclination.

But other periods are introduced as well. The ascending node carries out a retrograde motion; the orbital angle from passage through ascending node to passage through the subsequent ascending node is thus smaller than 360°, and one can determine a **nodal period**:

$$\tau_\Omega = 2\pi\sqrt{\frac{a^3}{\mu}}\left[1 - \frac{3J_2R_\oplus^{\,2}\left(7\cos^2 i - 1\right)}{8a^2\left(1-e^2\right)^2}\right] \quad \textbf{Eq. 49}$$

In our case: $\tau_\Omega = 5423.573\,\text{s}$, about ten seconds shorter then kepler period, which is 5431 s.

The slow progression of the perigee affects the time between two successive passages of a satellite through the perigee (or periapsis) of its orbit, leading to the definition of an **apsidal period**:

$$\tau_{PE} = 2\pi\sqrt{\frac{a^3}{\mu}}\left[1+\frac{3}{8}J_2\frac{R_\oplus{}^2}{p^2}\left(3\cos^2 i-1\right)\right] \quad \textbf{Eq. 50}$$

In our case: τ_{PE} = 5433.046 s, that's a -$\Delta\tau_{2\pi}$ different from kepler period. Eq. 48, Eq. 49 and Eq. 50 are approximated expressions for these periods and they don't seem to be really accurate for any case.

Inclination is periodic with the nodal period, as the zoom of Fig. 53 can confirm (Fig. 56).

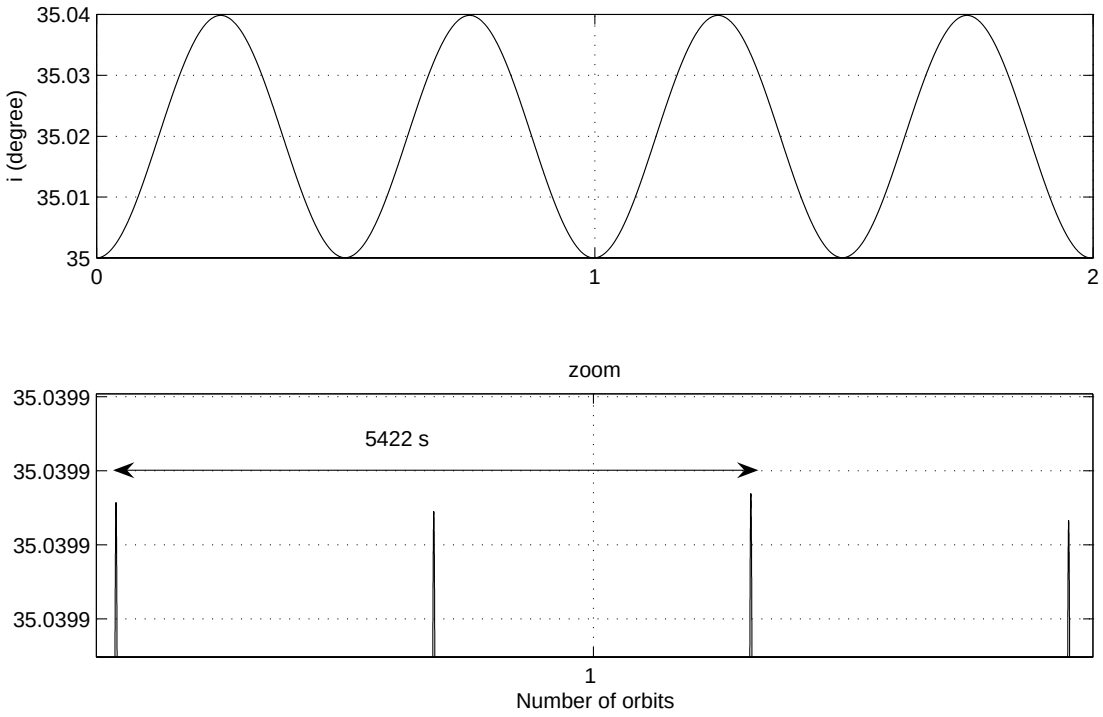

Fig. 56 Inclination period

Instead the period of *r* cannot be easily defined. It depends on the values of *e*, *a* and ω, and they all have different periods, as shown in Fig. 57.

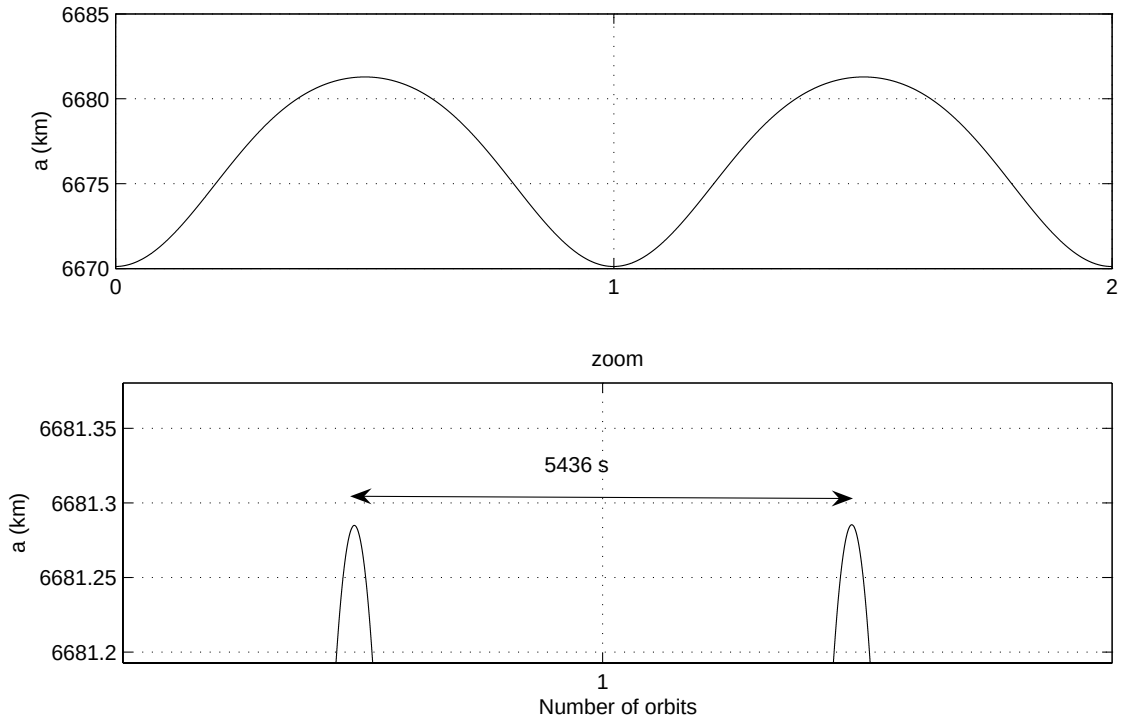

Fig. 57 Semiaxis period

Finally, we have:

$$T_i = 5422s$$
$$T_r = 5437s$$

If we consider again the formula for the J_2 perturbation (Eq. 46) :

$$\vec{f} = \vec{f}_N + \vec{f}_{J2} = \left(-\frac{\mu}{r^2} - \frac{3}{2}\frac{\mu R_\oplus{}^2 J_2}{r^4}\left(1 - 3\sin^2 i \sin^2 u\right)\right)\hat{r} - \left(\frac{3}{2}\frac{\mu R_\oplus{}^2 J_2}{r^4}\sin^2 i \sin 2u\right)\hat{\theta} - \left(\frac{3}{2}\frac{\mu R_\oplus{}^2 J_2}{r^4}\sin 2i \sin u\right)\hat{z}$$

we can say that $\vec{f}$ is function of variables which vary periodically, but with different periods. So, even if no secular growth is recognized in their behaviour, the same couple (r, i) can be obtained only after a time of $T_i \cdot T_r$. In some sense, this is like affirming that it never happens (many thousands of orbits, order of years).

So, any satellite of the formation is generally not subject to periodic forces, consequently their absolute motion is not periodic, and their relative motion is likely to be not periodic.

4.1.1. Search for physical conditions for periodic relative orbit under J_2 effect

The reason for this period mismatch in two quantities like *r* and *i* is due to the secular growth of ϖ. In fact, the secular variation of Ω isn't of any concern for the J_2 perturbation, which has an axial symmetry with respect to the polar Earth axis.

On the other hand Ω doesn't figure in any of Gauss equations Eq. 47, and its value doesn't influence the other parameters behaviour. Instead, if ϖ changes, also *r* varies and *i* as well, as it's possible to see from the Gauss equation for $\frac{di}{dt}$. And through *i*, all parameters are influenced.

The result of this interaction is the non-periodicity of the absolute satellite motion and consequently of the relative motion of the satellites.

If a proper J_2 invariant orbit is to be found, according to what exposed, this can be done for those reference orbits where ϖ doesn't have any secular growth, this means for the so-called critical inclination. This is the inclination which permits bringing to zero the drift of ϖ.

Well-known formulas which give the mean rates of change of the two secular variations per orbit are:

$$\Delta\Omega = -3\pi J_2 \frac{R_\oplus^{\,2}}{p^2}\cos i$$
$$\Delta\varpi = \frac{3}{2}\pi J_2 \frac{R_\oplus^{\,2}}{p^2}\left(5\cos^2 i - 1\right) \qquad \textbf{Eq. 51}$$

The critical inclination is therefore given by:

$$5\cos^2 i - 1 = 0 \Rightarrow \cos^2 i = \frac{1}{5} \Rightarrow \begin{cases} i = 63.435° \\ i = 116.565° \end{cases} \qquad \textbf{Eq. 52}$$

For this inclination, the variations of the parameters are:

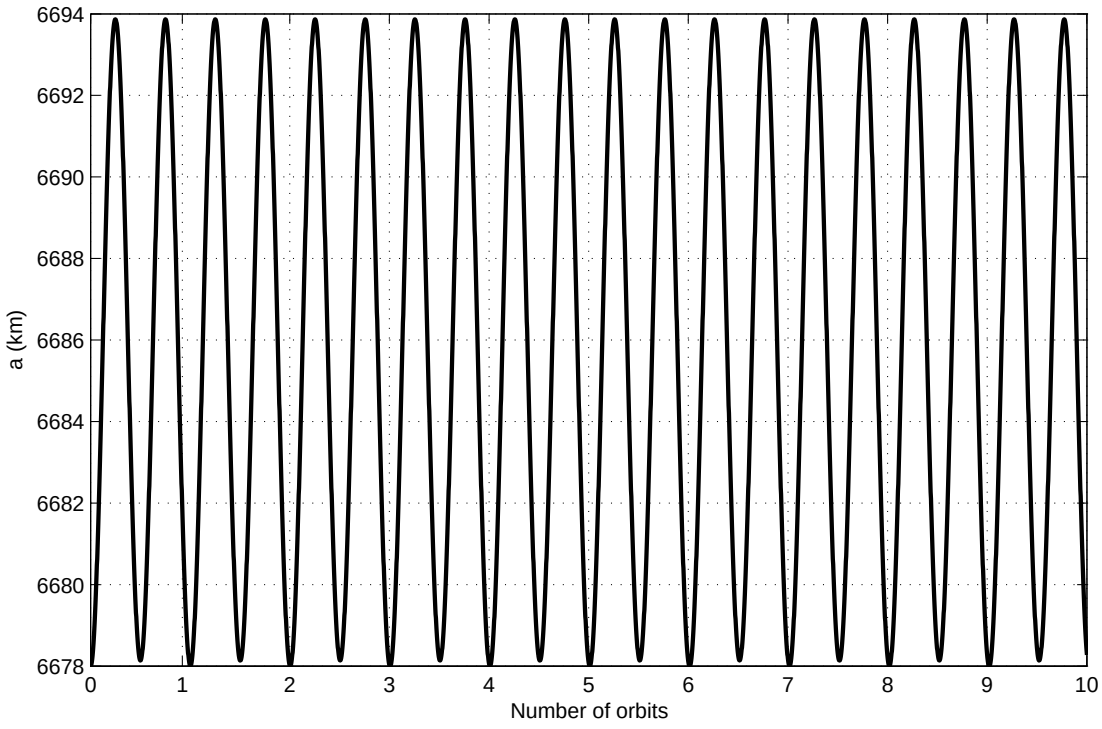

Fig. 58 Semi axis for critical inclined orbit

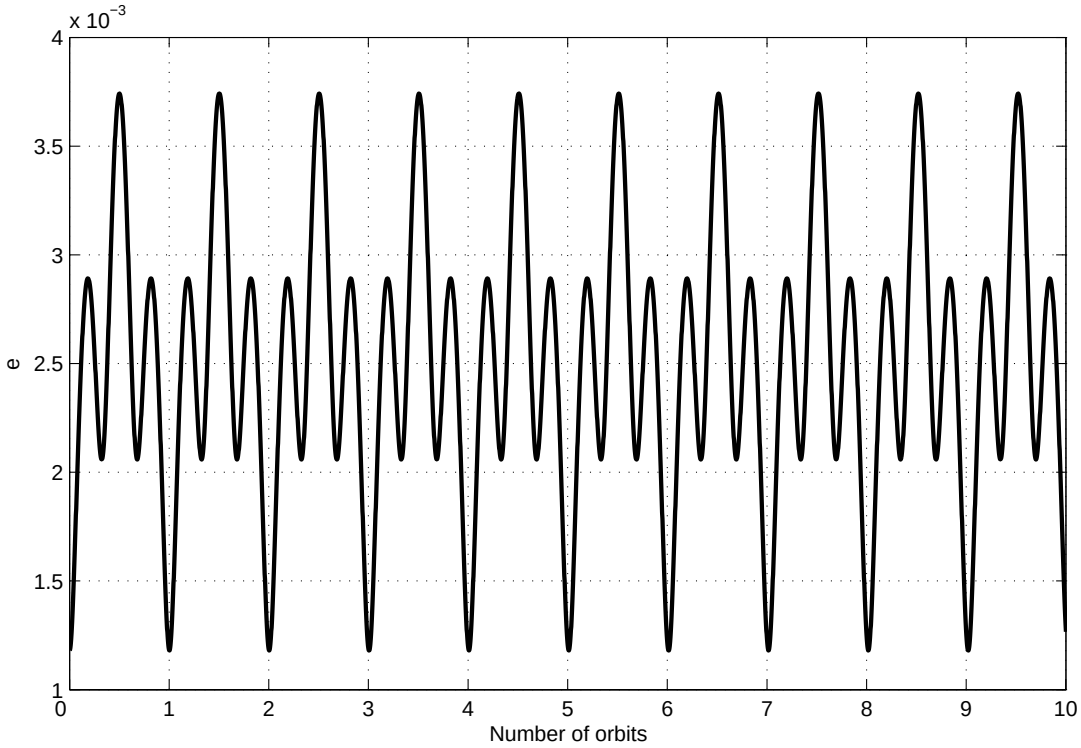

Fig. 59 Eccentricity for critical inclined orbit

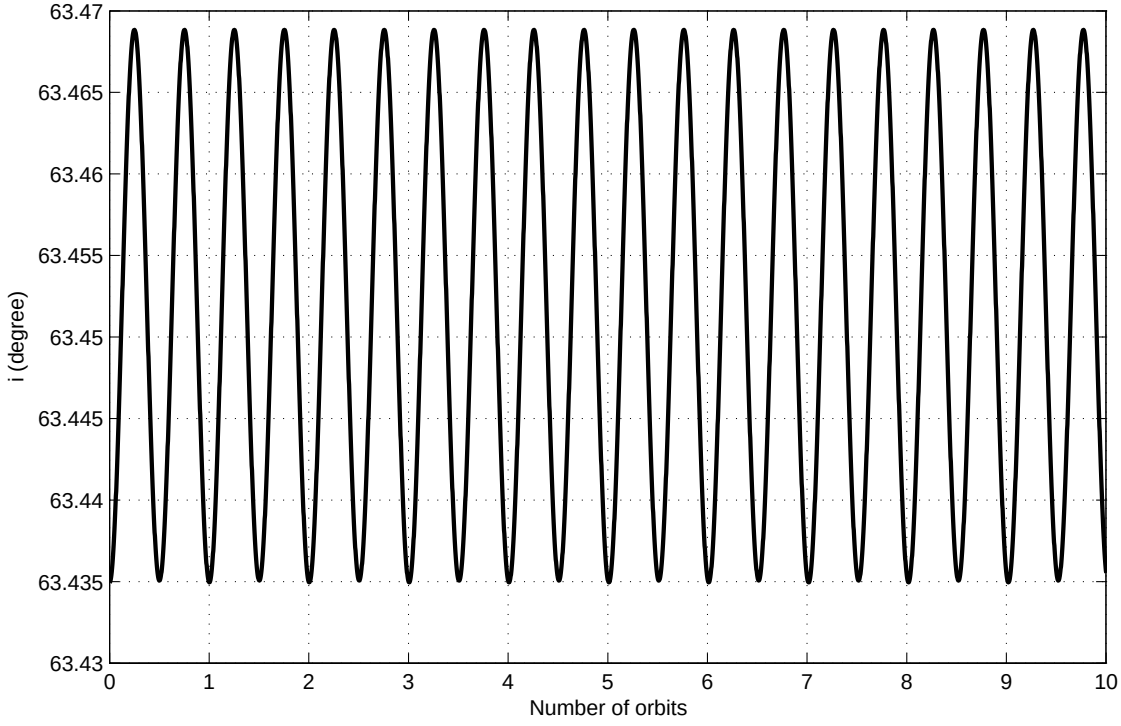

Fig. 60 Inclination for critical inclined orbit

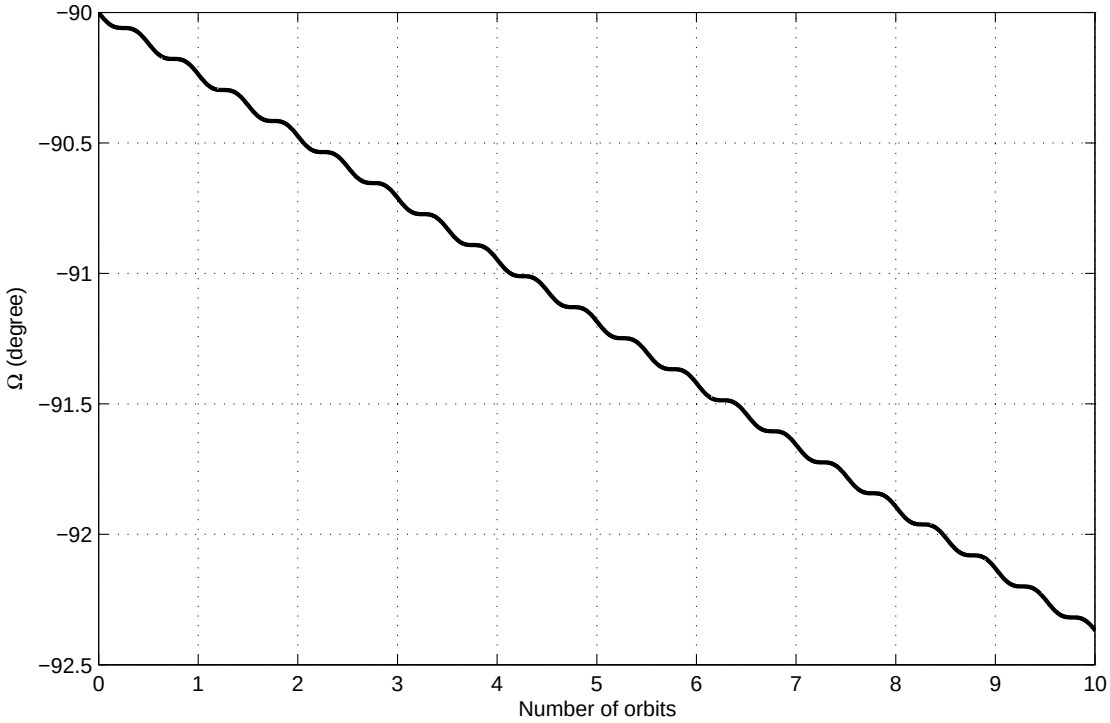

Fig. 61 RAAN for critical inclined orbit

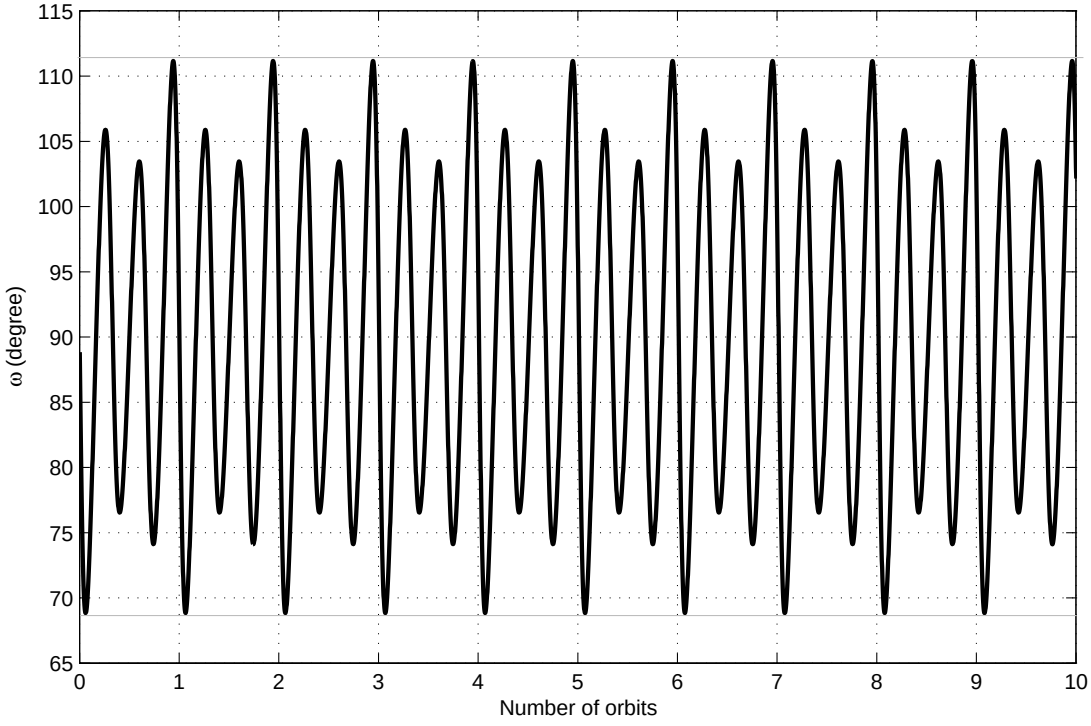

Fig. 62 Argument of perigee for critical inclined orbit

Not only ϖ hasn't any more a secular growth, but now *r* and *i* have exactly the same period. In this case:

$$T_i = T_r = 5422\,\text{sec}$$

And all the others parameters have same periodicity. In this condition, the absolute orbit is still not closing (due to Ω secular drift), but the two satellites find themselves after a certain period ($T_i = T_r$) under same forces, and a bounded relative orbit seems now possible.

4.1.2. Search for J_2 invariant orbits using GA

As a starting point for the J_2 perturbed case we analyse a reference orbit with following initial parameters:

$$\begin{cases} a = 6678km \\ e = 0.00118 \\ i = 63.43494882292201^\circ \\ \varpi = 90^\circ \\ \Omega = 270^\circ \\ \theta_0 = 0^\circ \end{cases}$$

The inclination used is the critical one. We expect therefore to find a periodic relative orbit. As a confirm, the fitness function assumes the high values, as shown in Fig. 63.

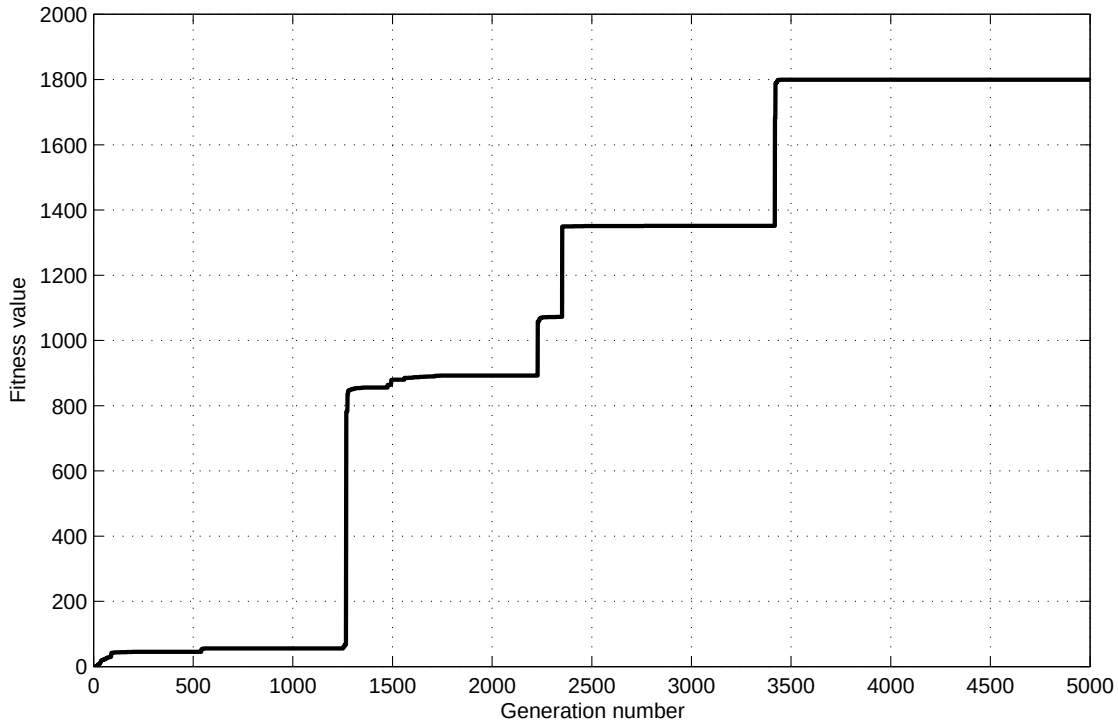

Fig. 63 Fitness function values vs. generation for the critically inclined case

The initial solutions found are reported here:

x_0 =0.601990126km

y_0 =0.848050008 km

z_0 =-6.0000002E-002 km

$\dot{x}_0$ =-5.32020246E-003 km/s

$\dot{y}_0$ =-1.4020199E-003 km/s

$\dot{z}_0$ =-9.3393759E-003 km/s

With these conditions, the two satellites have the orbital parameters shown in Table 2:

Seed 555	chief	deputy	Percentage Difference

a (km)	6678	6678.002742	0.0000411%
e	0.00118	1.28912638E-003	9.25%
i (degree)	63.43494882292201°	63.4344623°	-0.00077%
ϖ (degree)	90°	122.330753°	35.9%
Ω (degree)	270°	-90.0773537°	-0.0286%
$\theta_0 + \varpi$ (degree)	90°	90.0413827°	-0.0459%

Table 2 Percentage difference between the orbital parameters of the satellites

Note that the very little differences in some of the elements are not due to numeric errors. Setting to zero the difference in semi-major axis or inclination doesn't imply an improvement in the orbit boundedness.

The fitness value is an index of how good (meaning how bounded) is the relative orbit, and it's possible to see how the value found for a critically inclined orbit is much higher than the fitness function values found for a generic orbit shown during the tuning of the algorithm, as in Fig. 13 to Fig. 17 in Chapter 2.

A surprising behaviour is found performing the simulation for given semi-major axis and eccentricity, but varying the inclination. Instead of the expected two peaks of fitness value (corresponding to the critical inclinations), we found other two inclinations, about 50° and its supplementary 180°-50°, which give high values for the fitness.

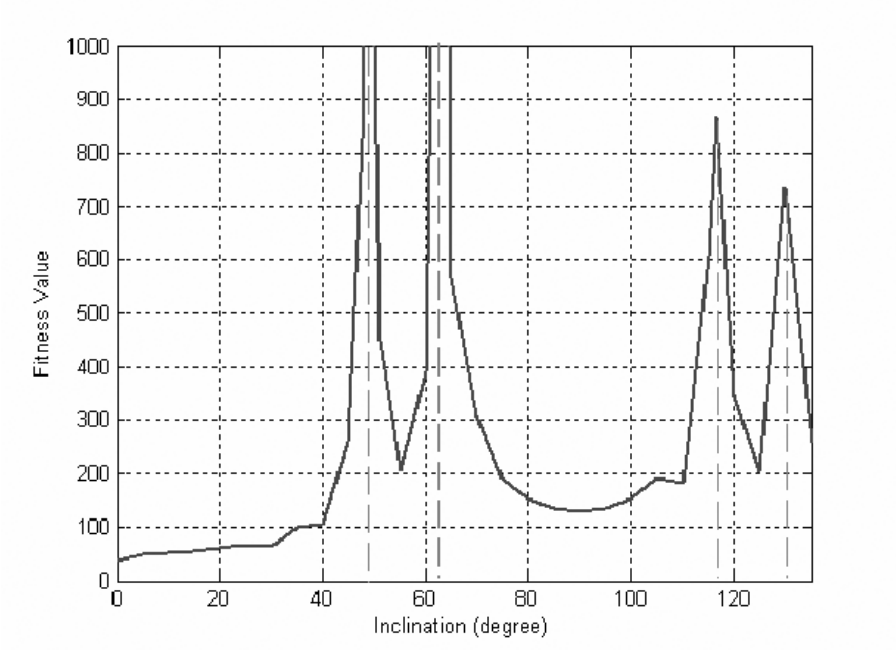

Fig. 64 Fitness function value far a wide range of inclinations

This means that for these particular inclinations, the effects of the un-periodicity due to the J_2 perturbation are weaker and easier to compensate.

The reason of the existence of this unexpected zones of easy-closable relative orbits is at present point of study still unexplained; yet, it's confirmed by the plot in Fig. 65 where it's shown how these inclinations are not sensitive to variations of semi-major axis:

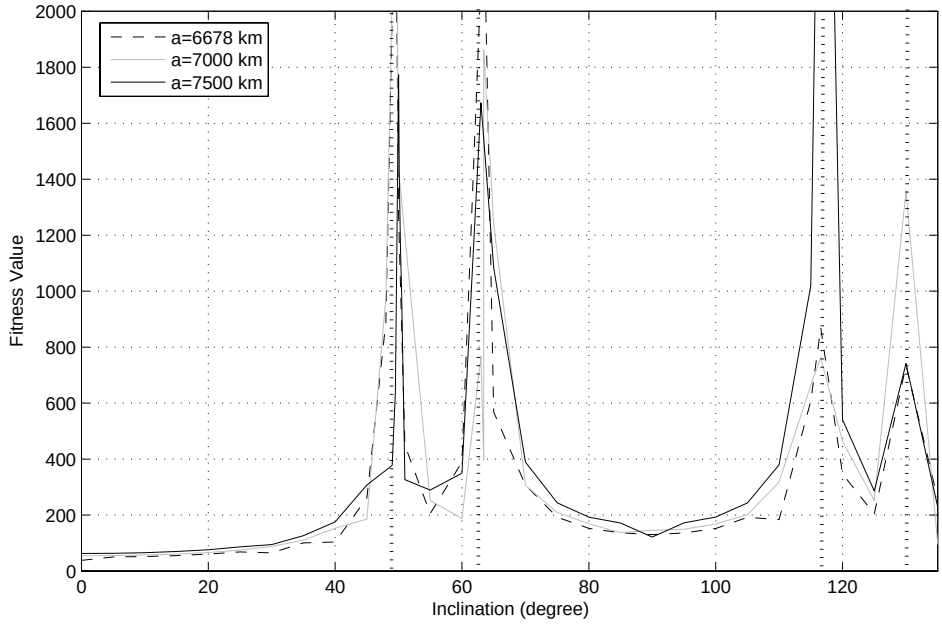

Fig. 65 Fitness function values vs. inclination for three different semiaxis

For different eccentricities, only the two really critical inclinations (63.434° and 116.565°) are confirmed, as shown by Fig. 66, Fig. 67, Fig. 68 and Fig. 69. This makes us suspect that the other two good inclinations (50° and 130°) are just indication of the existence of zones of weaker non-periodicity caused by the J_2 perturbation; at these inclinations it is easier to find closed-like orbit but they are not really periodic. In the case of Fig. 69 other inclinations for which it's easier to find quasi-periodic relative motion are in evidence.

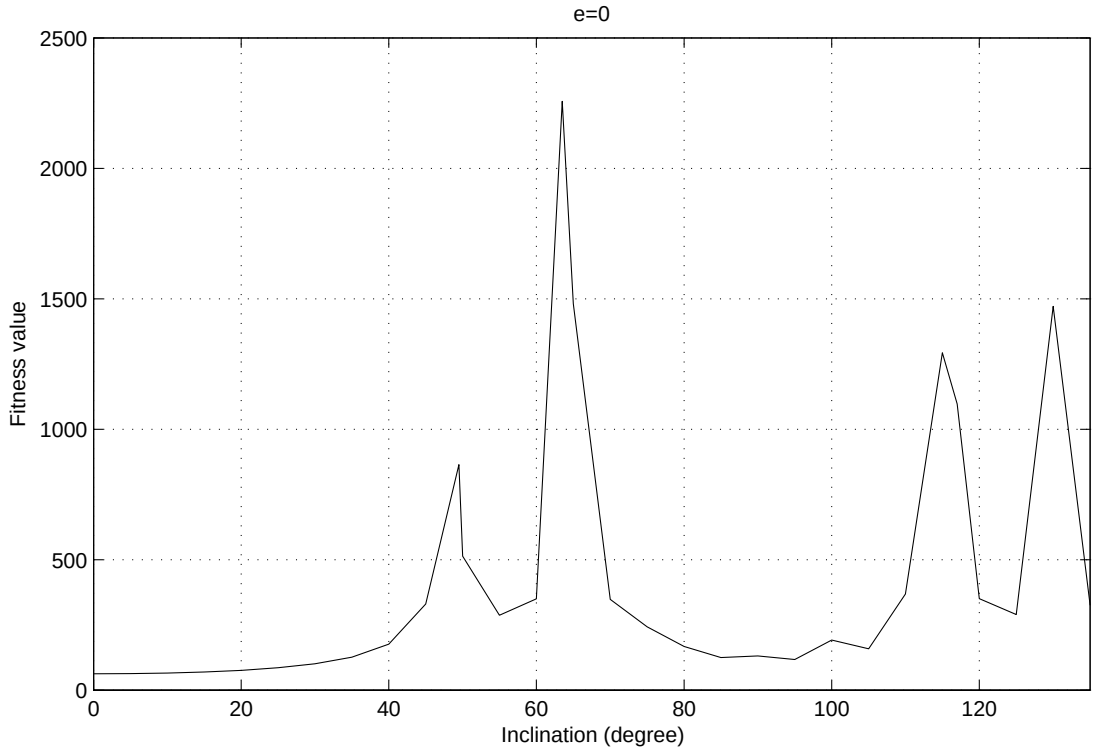

Fig. 66 Fitness function value vs. inclination: e=0

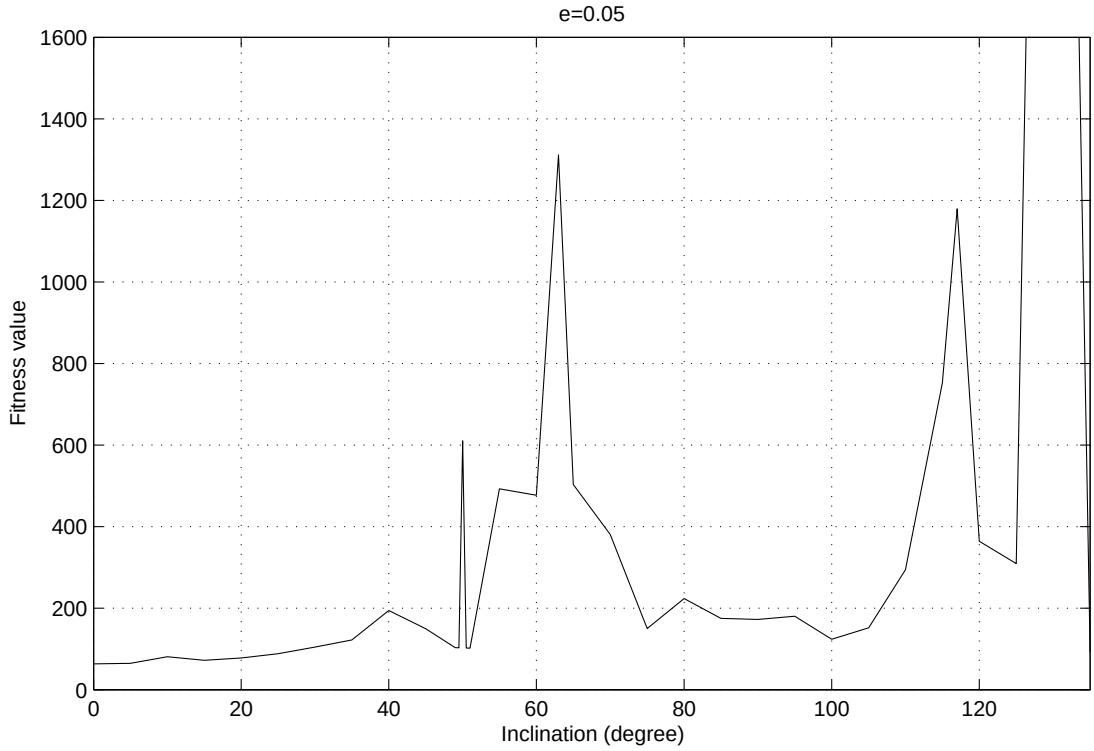

Fig. 67 Fitness function value vs. inclination: e=0.05

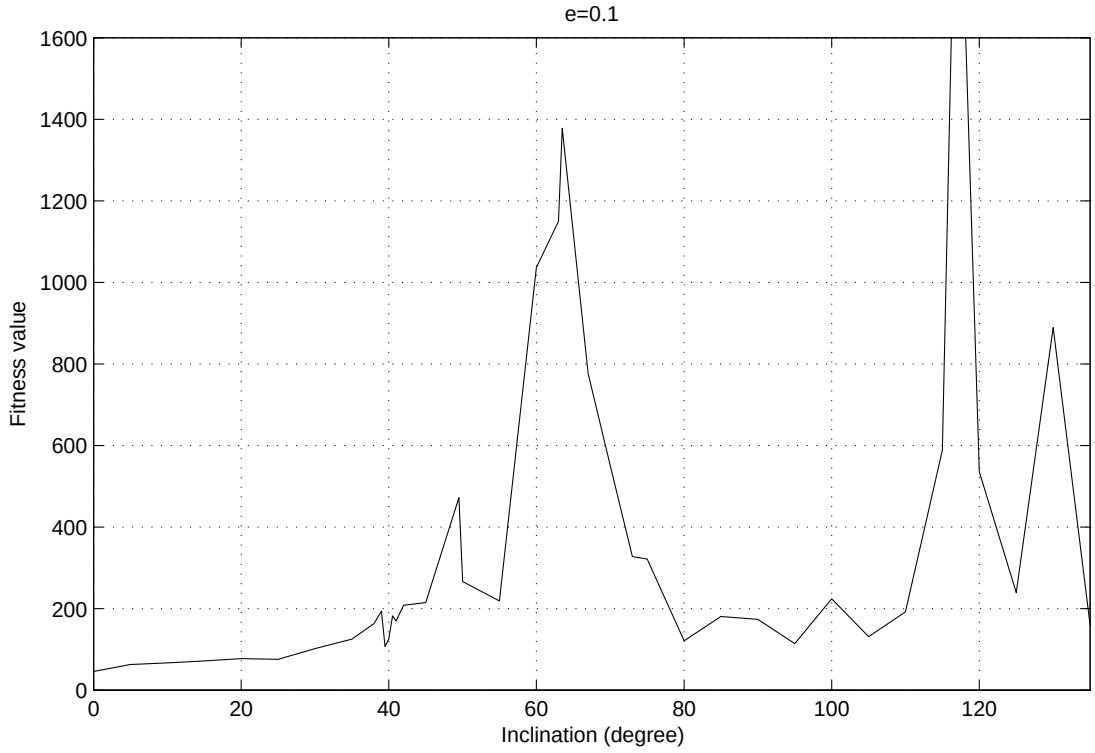

Fig. 68 Fitness function value vs. inclination: e=0.1

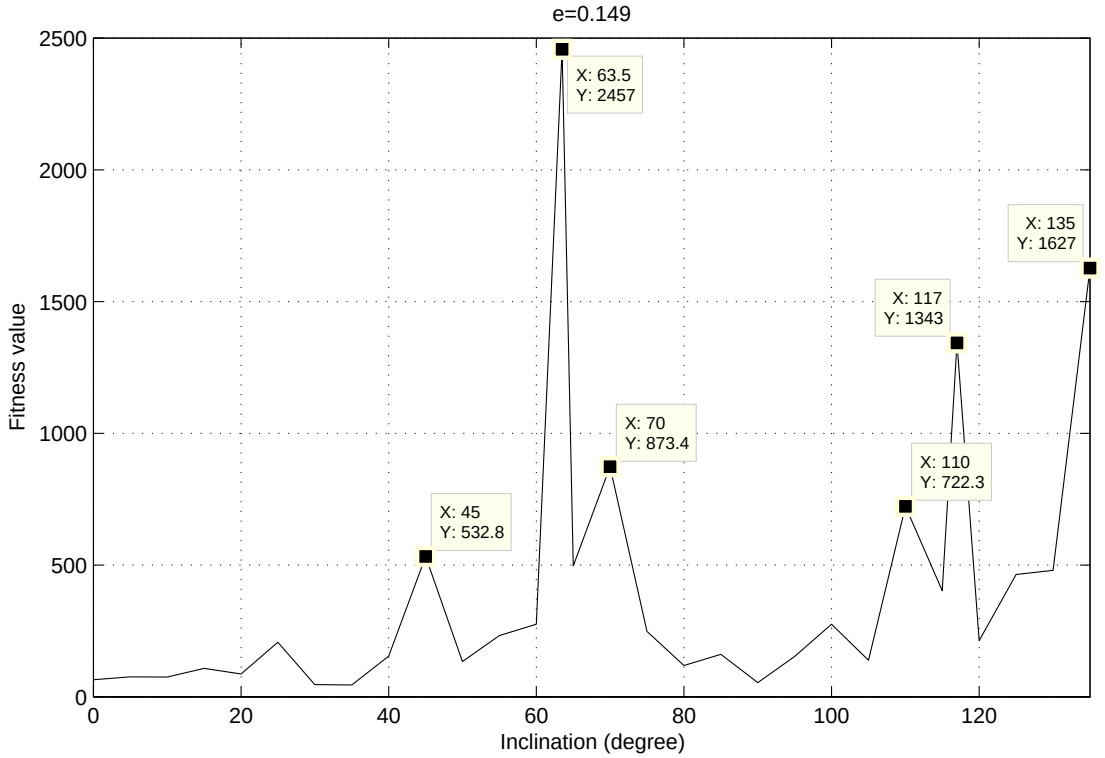

Fig. 69 Fitness function value vs. inclination: e=0.149

As we said, the unexpected critical inclinations 50° and 130° are not a true necessary and sufficient closing condition, as instead the 63.434° and 116.656° are.

A confirm comes from the study of formations of greater dimensions: in these situations the fitness value in the 50° and 130° cases decreases dramatically, while for the classical critical inclinations is quite constant. While observing Fig. 70, always consider the existence of a random component on the fitness value. So even in the 63.434° case, for some formation dimensions there seems to exist very high peaks with respect to other formation dimensions; indeed, a fitness value of order of about one thousand or more is symptomatic of a region of well-closing relative orbits. In this sense a fitness of 15000 or 1500 can only differ for a lucky or unlucky choice of initial population, i.e. initial seed number, but both fitness values are indication of closed orbits. Fig. 70 shows how the two new critical inclinations are valid only for formation dimensions which are not very large.

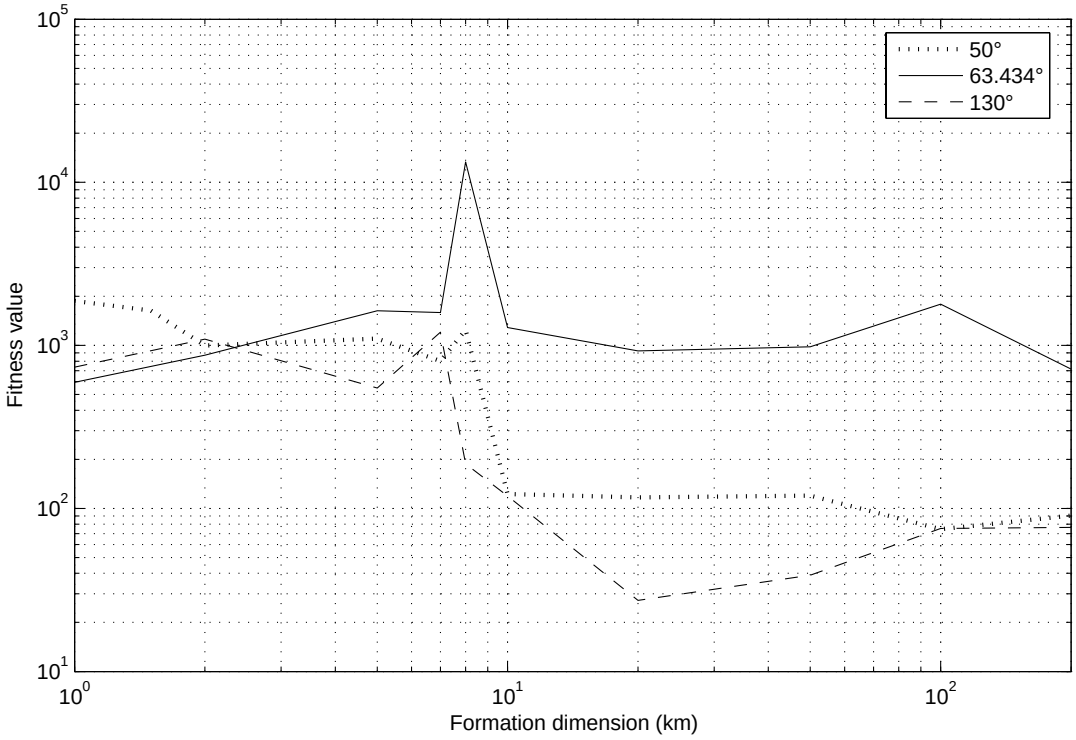

Fig. 70 Fitness values vs. formation dimensions for three different inclinations

This behaviour is probably **due to the fact that for the 50° and 130° inclination case, the relative orbits are never really closed, even if the causes of the drifting apart of the formation seem to be weaker. But for large formations these benefits slowly disappear because of the major effects of differential J_2 and non linearities.**

All these considerations do not imply that the 50° inclination cannot be useful for the designing of formations, if the reference orbit is not too eccentric and their dimensions are not very large, as this is the case of a large number of missions.

Fig. 71, Fig. 72, Fig. 73, Fig. 74, Fig. 75 and Fig. 76 show what a great improvement is reached if the critical 63.434° inclination or the newly discovered 50° inclination is used instead of a generic inclination, for not very large formations: (100 orbits propagation)

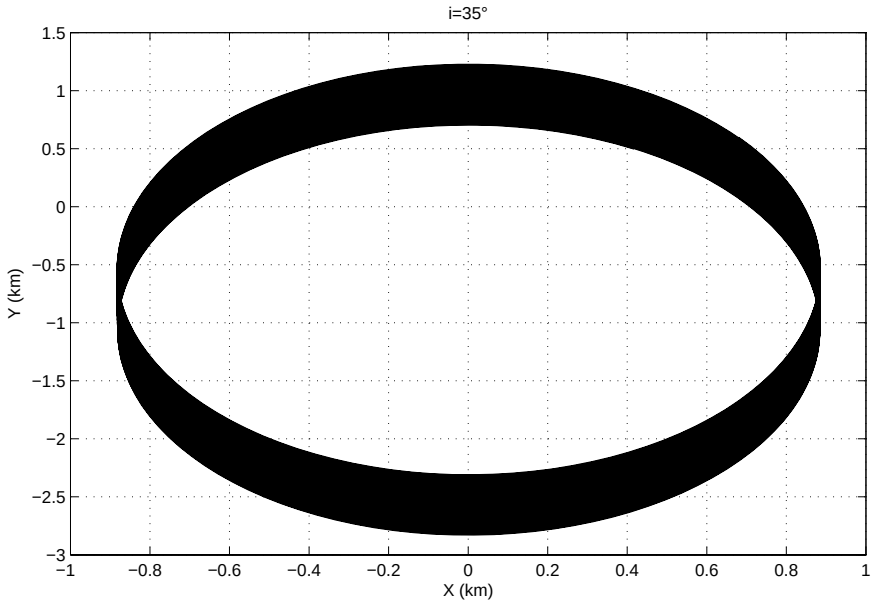

Fig. 71 Projection in XY plane of relative orbit for i=35°

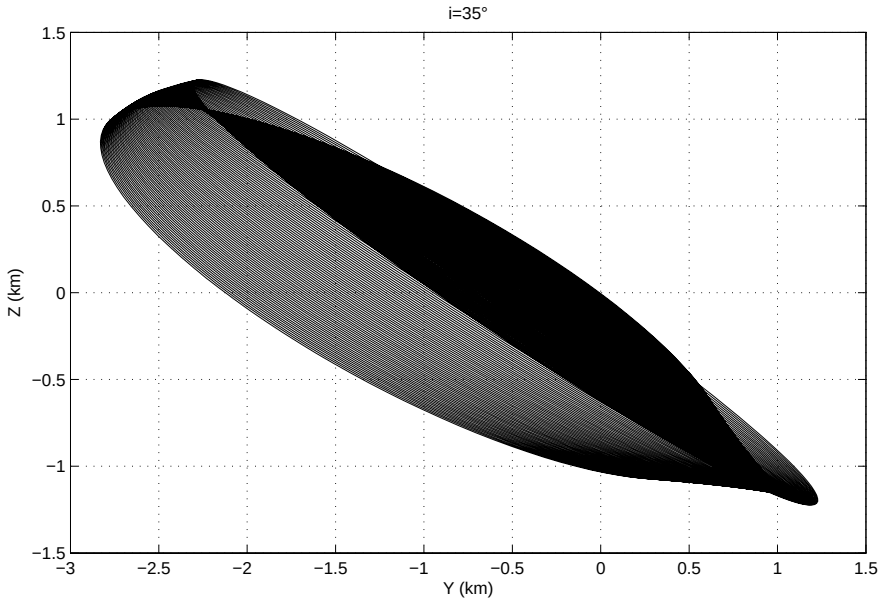

Fig. 72 Projection in YZ plane of relative orbit for i=35°

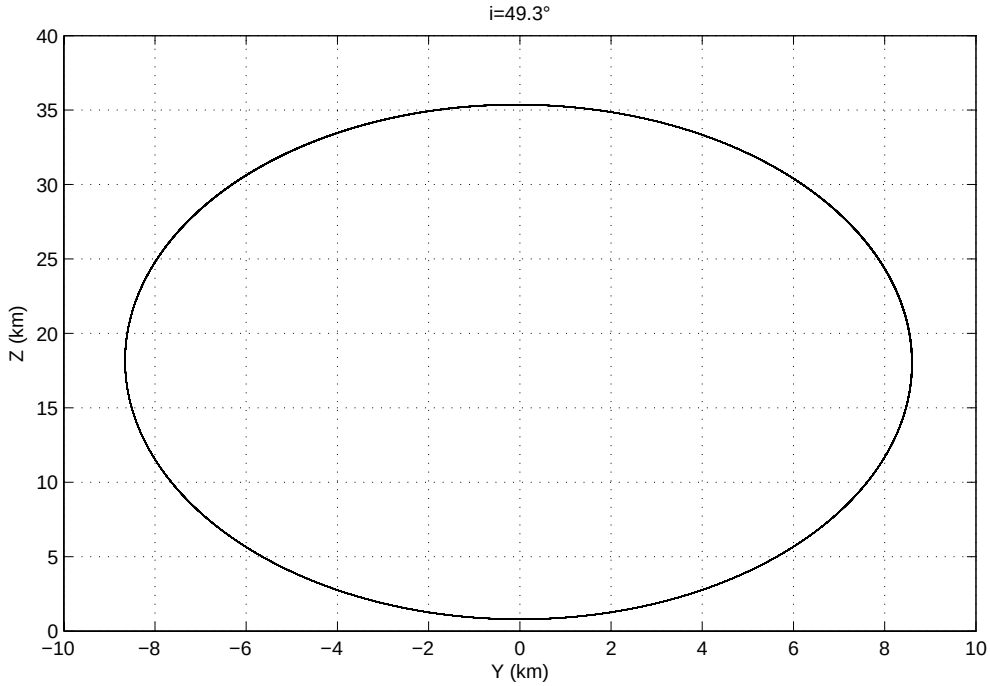

Fig. 73 Projection in XY plane of relative orbit for i=49.3°

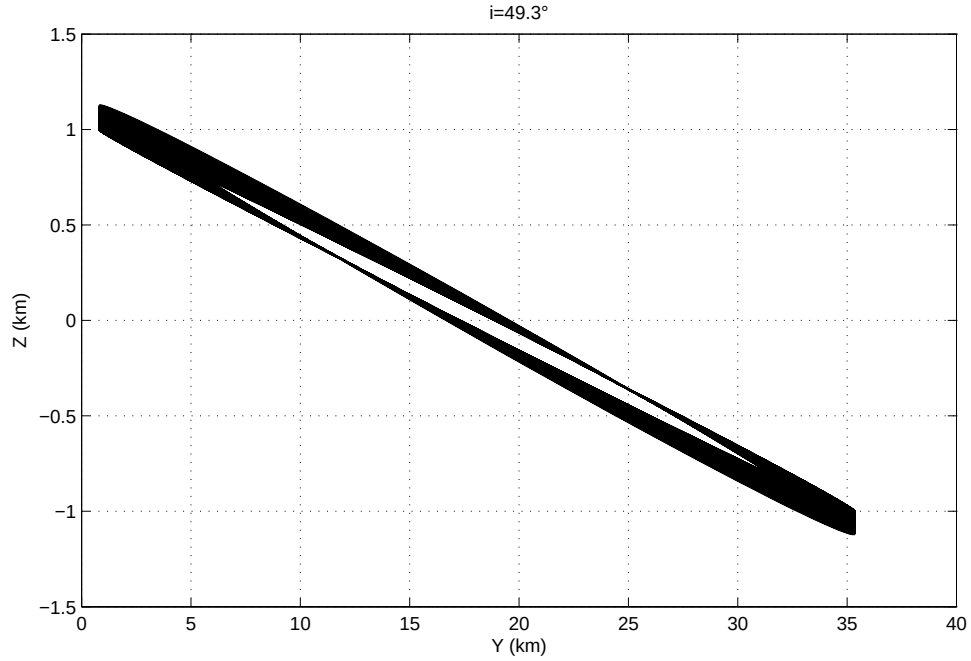

Fig. 74 Projection in YZ plane of relative orbit for i=49.3°

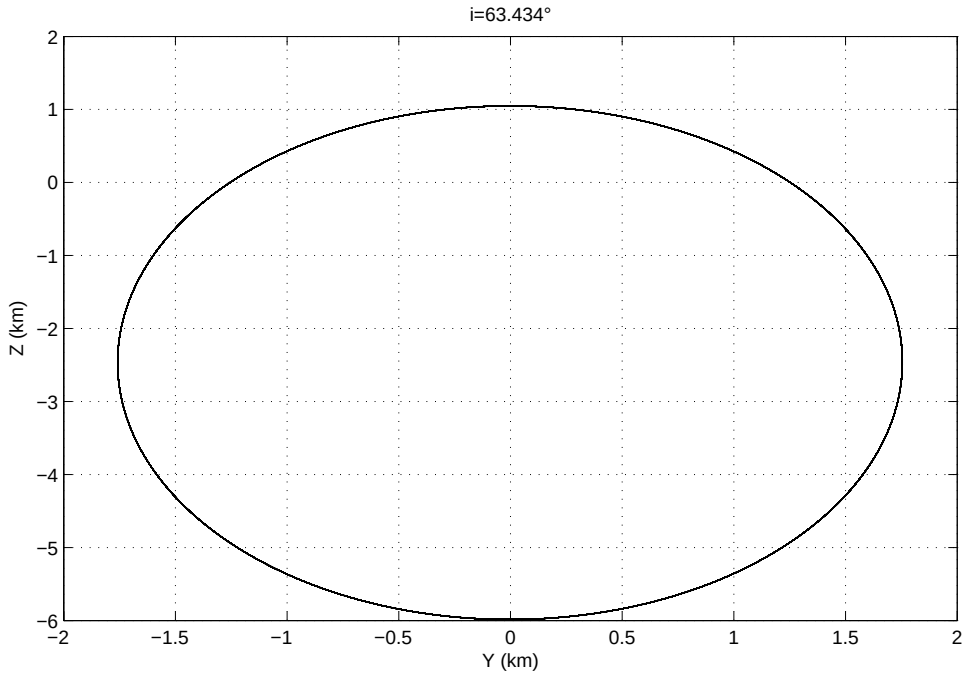

Fig. 75 Projection in XY plane of relative orbit for i=63.434°

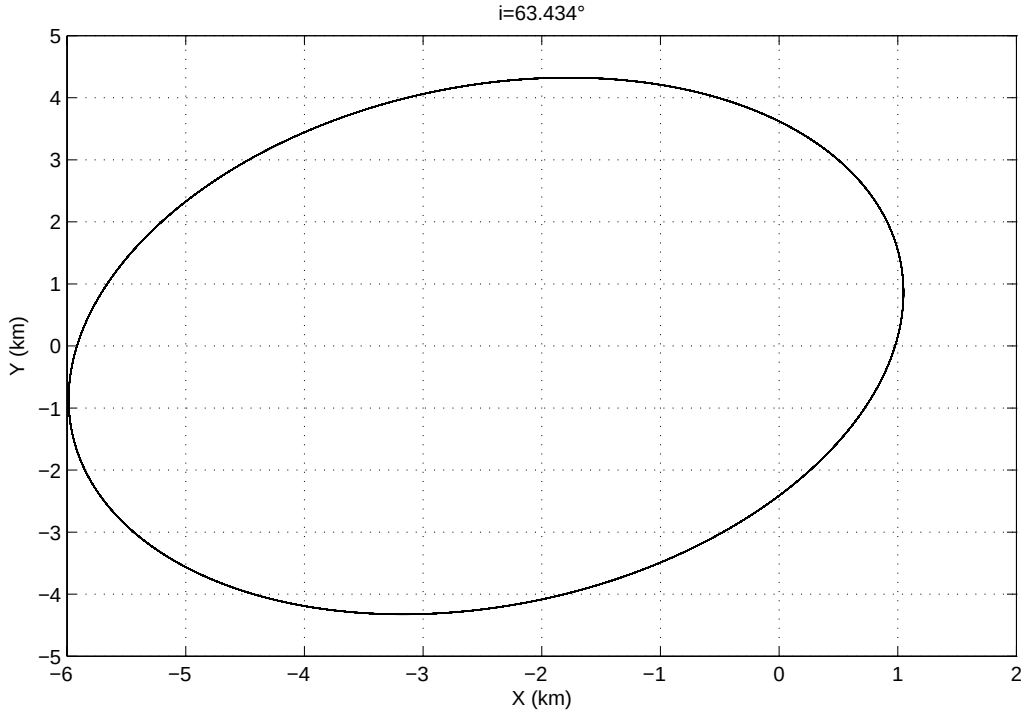

Fig. 76 Projection in YZ plane of relative orbit for i=63.434°

On the other hand, let's compare in Fig. 77, Fig. 78, Fig. 79 and Fig. 80 the relative orbits for the two cases, 50° and 63.434°, ploted using the initial conditions provided by the genetic algorithm for very large orbits. For very large formations, 50° seems to be not of particular interest anymore,

while 63.434° is always performing well, even for huge formations. The time span of all the simulation is relative to one hundred orbits.

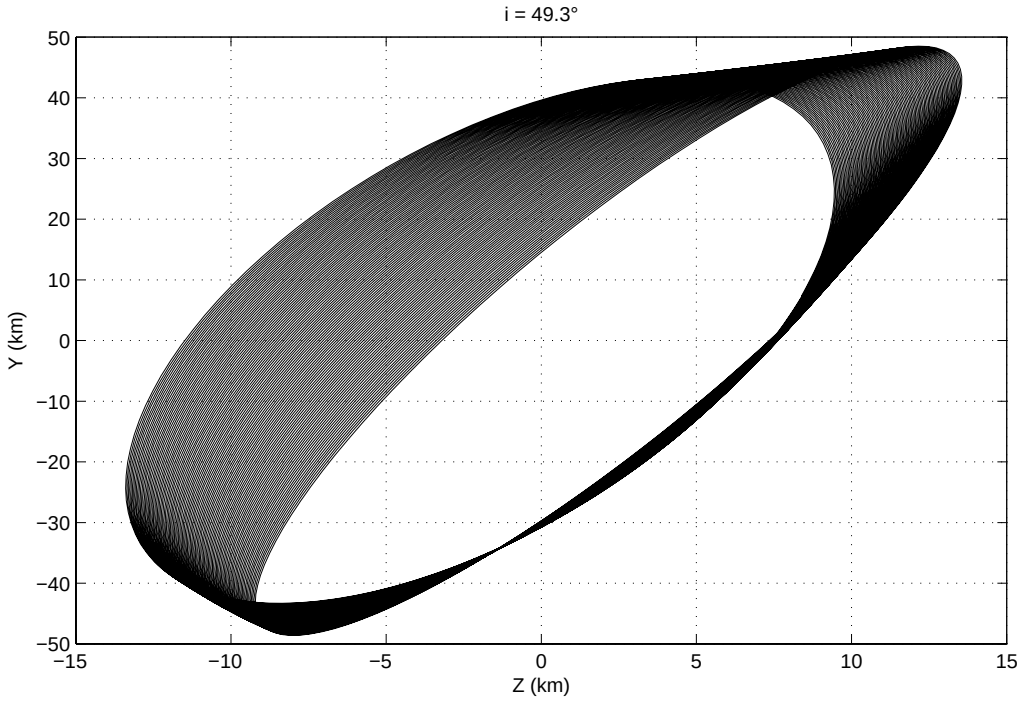

Fig. 77 Projection in XY plane of relative orbit for i=49.3° (very large formation)

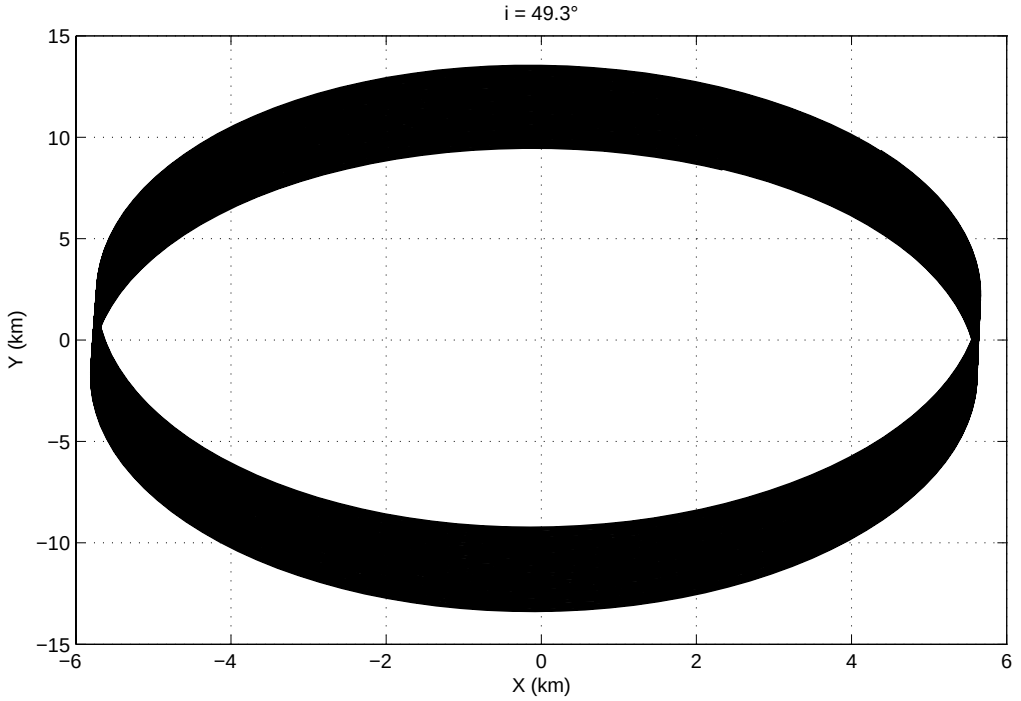

Fig. 78 Projection in YZ plane of relative orbit for i=49.3° (very large formation)

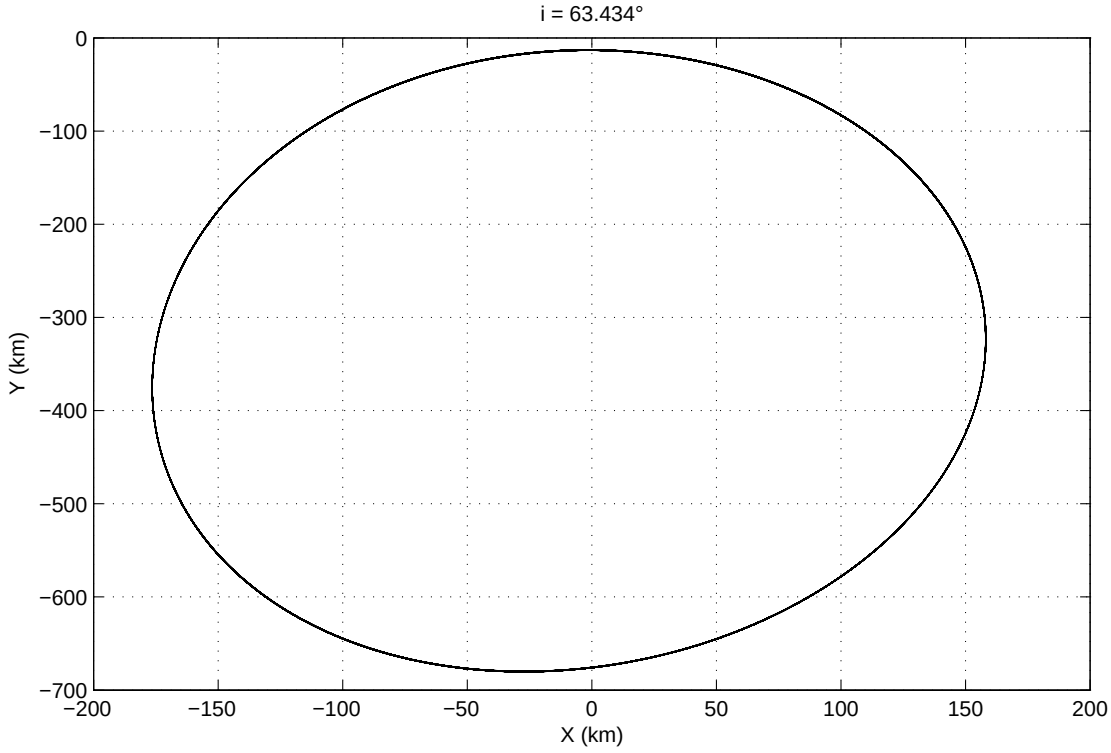

Fig. 79 Projection in XY plane of relative orbit for i=63.434° (very large formation)

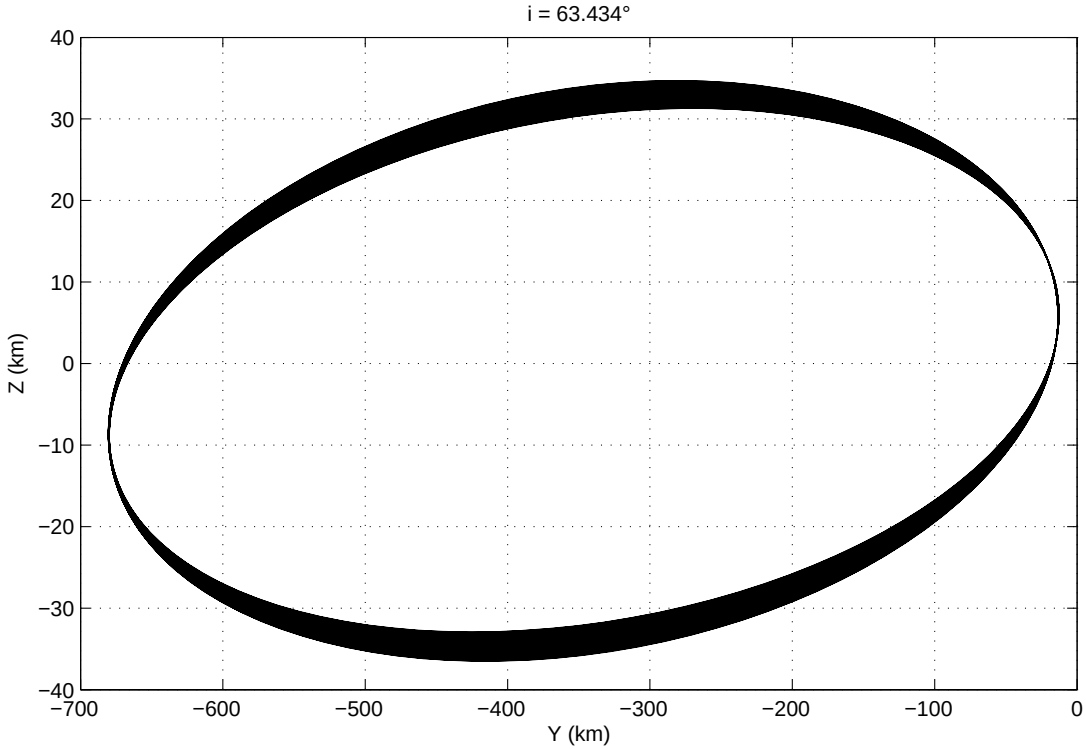

Fig. 80 Projection in YZ plane of relative orbit for i=63.434° (very large formation)

In the case of the critically inclined large orbit, the difference in initial orbital parameters is reported in Table 3:

	chief	deputy	Difference
a (km)	6678	6677.7091	-0.290900518
e	0.00118	1.57268670E-2	0.014546867
I (degree)	63.4349488°	63.391239°	-0.0437097926°
ϖ (degree)	90°	50.1256522°	-39.87434778°
Ω (degree)	270°	-89.1230105°	0.876989483°
θ (degree)	0°	40.332954°	40.33295446°
$\varpi + \theta$ (degree)	90°	90.458607°	0.458606679°

Table 3 Difference in the parameters of the members of a large formation

It must be noticed that in the hypothesis of pure keplerian motion, the drift per orbit could be measured as $-3\pi\Delta a$, which in this case would mean a great drift of about 3 km per orbit. This is a confirm that **the period matching condition is no longer valid in the J_2 perturbed case.**

Many papers try to find an analytical formulation for J_2 invariant orbits. We present here some of the most recent.

4.2. Analytical solutions to the problem

4.2.1. A linearized model including J_2 effect

Sedwick and Schweighart find in their paper [20] a linear model describing the relative dynamics of a formation. The assumption is of circular reference orbit. The resulting equations are:

$$\begin{aligned} &\Delta\ddot{x} - 2(nc)\Delta\dot{y} - (5c^2 - 2)n^2\Delta x = 0 \\ &\Delta\ddot{y} + 2nc\Delta\dot{x} = 0 \\ &\Delta\ddot{z} + q^2\Delta z = 2lq\cos(qt + \phi) \end{aligned} \qquad \textbf{Eq. 53}$$

where:

$$\begin{aligned} c &= \sqrt{1+s} \\ s &= \frac{3J_2 R_e^{\,2}}{8r^2}(1 + 3\cos 2i) \\ q &= f(r, c, i_1, i_0, \Delta\Omega_0) \\ l &= g(r, c, i_1, i_0, \Delta\Omega_0) \end{aligned}$$

These simple linear differential equations result to have periodic solution when two conditions are satisfied:

$$\Delta\dot{x}_0 = \frac{n\Delta y_0(1-s)}{2\sqrt{1+s}} \qquad \textbf{Eq. 54}$$
$$\Delta\dot{y}_0 = -2n\Delta x_0\sqrt{1+s}$$

Anyway, these conditions (named SS hereafter) are of no use when inserted in a non-linear model. Fig. 81, Fig. 82 and Fig. 83 compare for a generic inclined (i=35°) circular reference orbit the relative trajectories obtained using genetic algorithm conditions and the two conditions from Sedwick and Schweighart model (the other four are the same as the genetic algorithm):

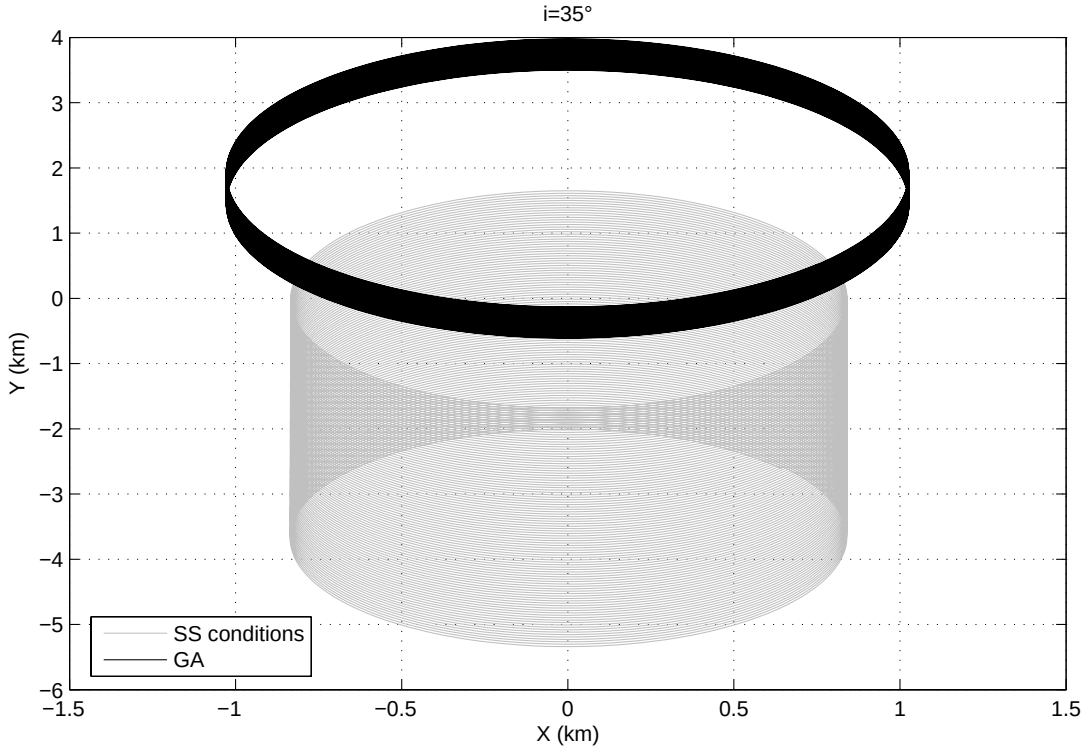

Fig. 81 Projection in XY plane of relative orbits generated using GA and SS initial conditions

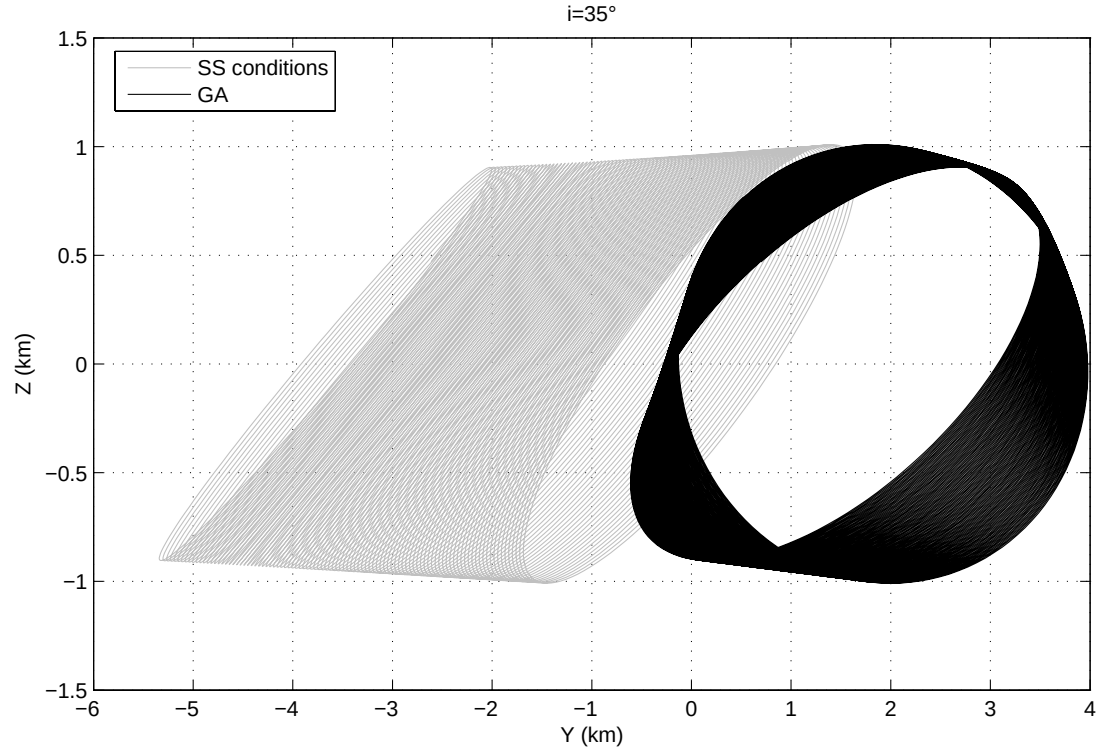

Fig. 82 Projection in YZ plane of relative orbits generated using GA and SS initial conditions

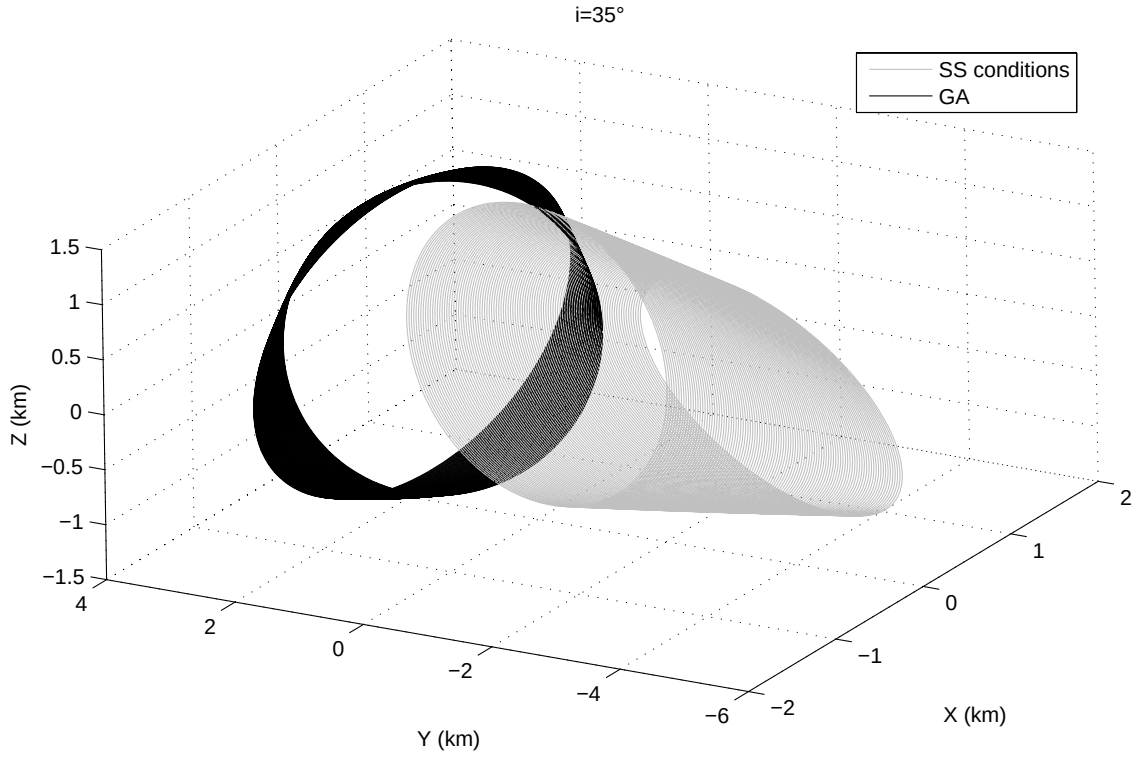

Fig. 83 Relative orbits generated using GA and SS initial conditions

Actually, there is just a slight improvement using these Sedwick and Schweighart conditions instead of the classic HCW condition, as Fig. 84 can show about the drift on the Y axis.

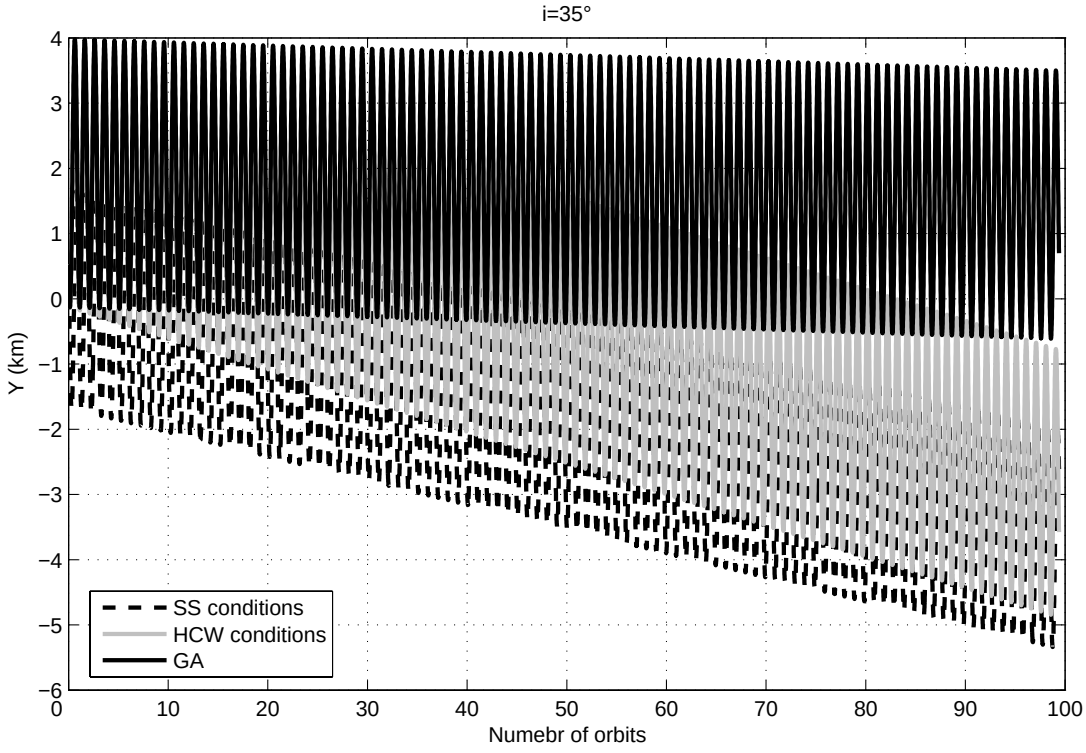

Fig. 84 Comparison of the drift along the Y axis using GA, HCW and SS conditions

4.2.2. J_2 invariant orbits analytical conditions

An analytic method is presented by Schaub and Alfriend in [7] to establish J_2 invariant relative orbits. Working with mean orbit elements, the secular drift of the longitude of the ascending node and the sum of the argument of perigee and mean anomaly are set equal between two neighbouring orbits. By having both orbits drift at equal angular rates on the average, they will not separate over time due to the J_2 influence. Two first order conditions are established among the differences in momenta elements (semi-major axis, eccentricity and inclination angle):

$$\delta a = 2Da_0\delta\eta$$
$$\delta e = \frac{\left(1-e^2\right)\tan i}{4e}\delta i \qquad \textbf{Eq. 55}$$

where:

$$\delta\eta = -\frac{\eta_0}{4}\tan i_0\delta i \qquad \textbf{Eq. 56}$$
$$\eta = \sqrt{1-e^2}$$

Combined, Eq. 55 and Eq. 56 provide the two necessary conditions on the mean element differences between neighbouring orbits to yield a J_2-invariant relative orbit. When designing a relative orbit using the mean orbit element differences, either $\delta i, \delta e$ or δa is chosen, and the other two element differences are then prescribed through the two constraints. The remaining mean orbit element differences $\delta\Omega, \delta\omega$ and δM can be chosen at will without affecting the J_2-invariant conditions. Further, note that these two conditions are not precise answers to the nonlinear problem but are only valid up to a first order approximation. Thus, relative orbits designed with these two conditions will still exhibit some small relative drift.

The comparison is performed through two parameters, defined as:

- normalized in-plane angular distance: $\dfrac{(\theta+\varpi)_1-(\theta+\varpi)_0}{\max\left[(\theta+\varpi)_1-(\theta+\varpi)_0\right]}$
- normalized out-of-plane distance: $\dfrac{z_1-z_0}{\max(z_1-z_0)}$

Given these definitions, what is important to observe in the following figures for the comparison between GA and analytical relative orbits is not the amplitude of the oscillations of these two measures (which depends on the dimensions of the formation), but the trend of their envelope.

Case of generic inclination (35°):

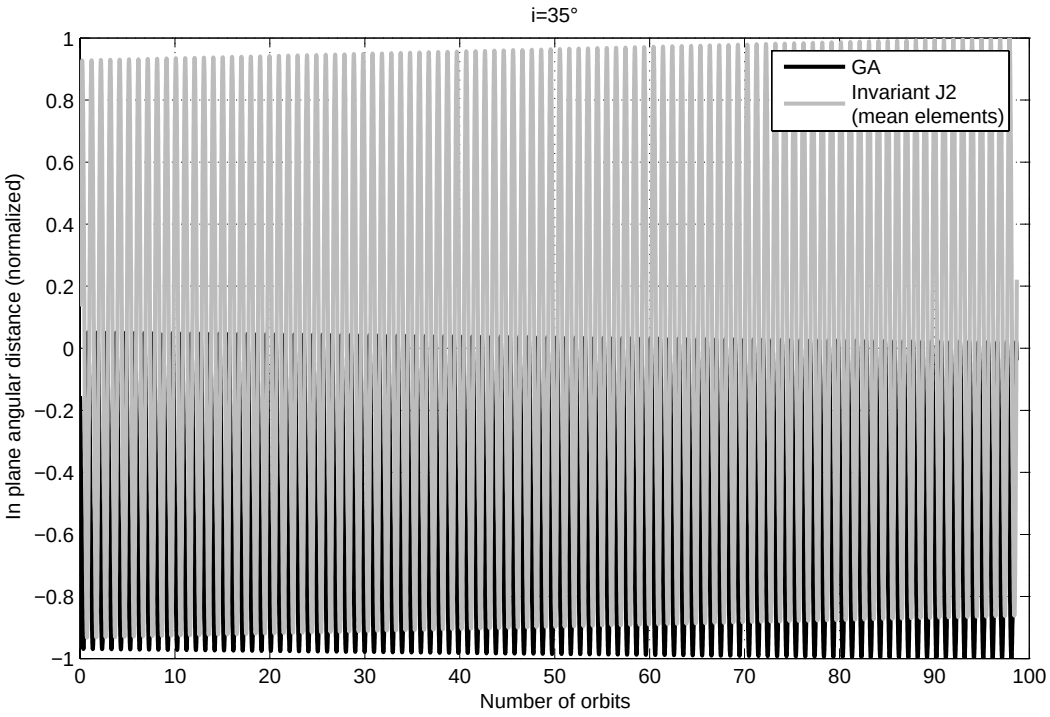

Fig. 85 In-plane normalized angular distance for GA and Invariant J2 orbits (i=35°)

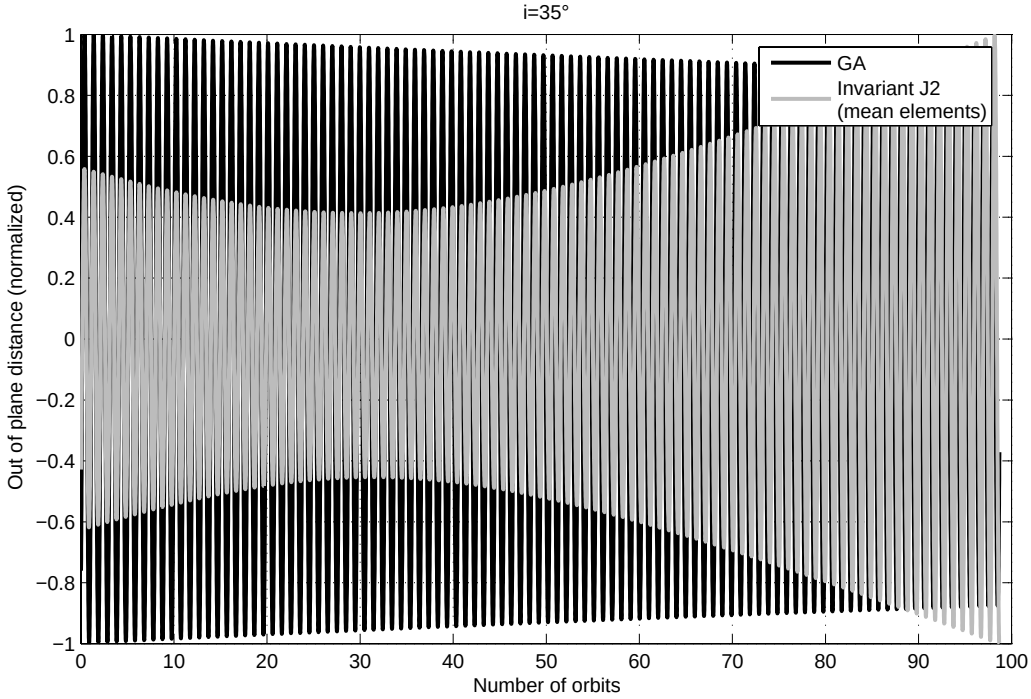

Fig. 86 Out-of-plane normalized angular distance for GA and Invariant J2 orbits (i=35°)

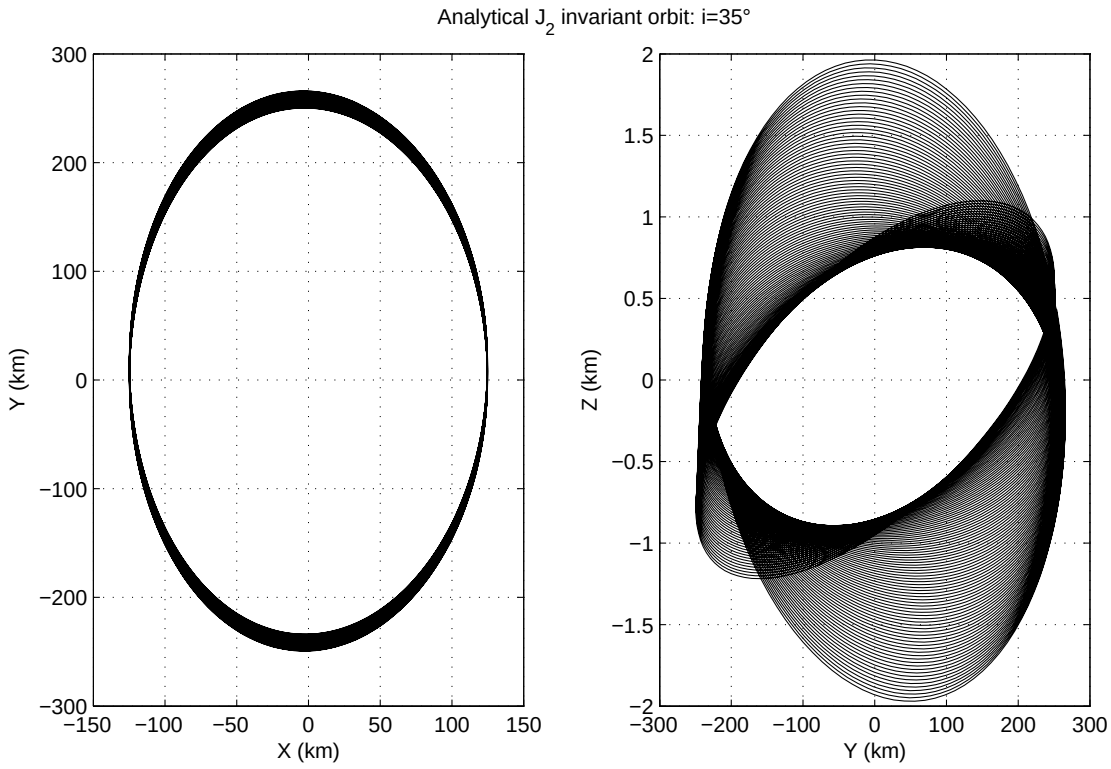

Fig. 87 XY and YZ projections of relative orbits generated with analytical J2 invariant conditions (i=35°)

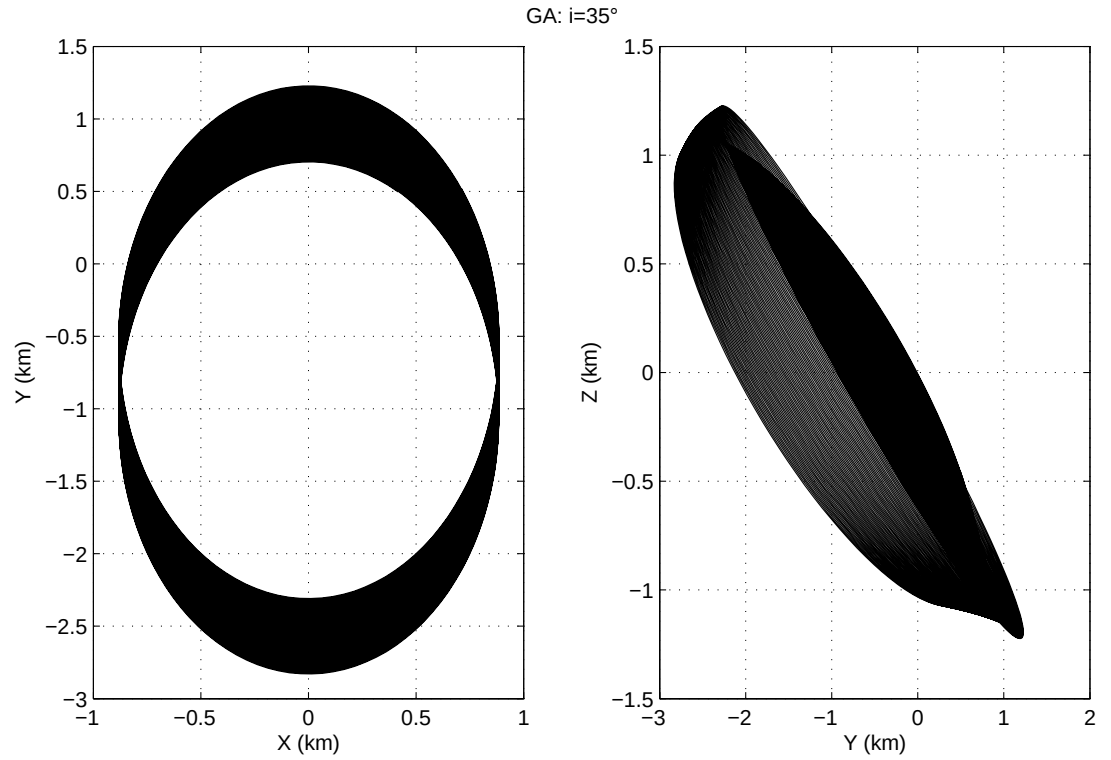

Fig. 88 XY and YZ projections of relative orbits generated with GA conditions (i=35°)

It must be noticed that, according to our theory, for generic inclinations such as 35° no formula can catch the condition for a closed relative orbit not because of the approximations necessary to have analytical formulas, but because closed relative orbits simply doesn't exist. Anyway, in this case, GA conditions have a better performance, both in the in-plane distance and n the out-of-plane distance. Note also that analytical conditions results in very large relative orbits, maybe due to the little eccentricity, which makes the conditions unstable.

Case of weak un-periodicity inclination (49.3°):

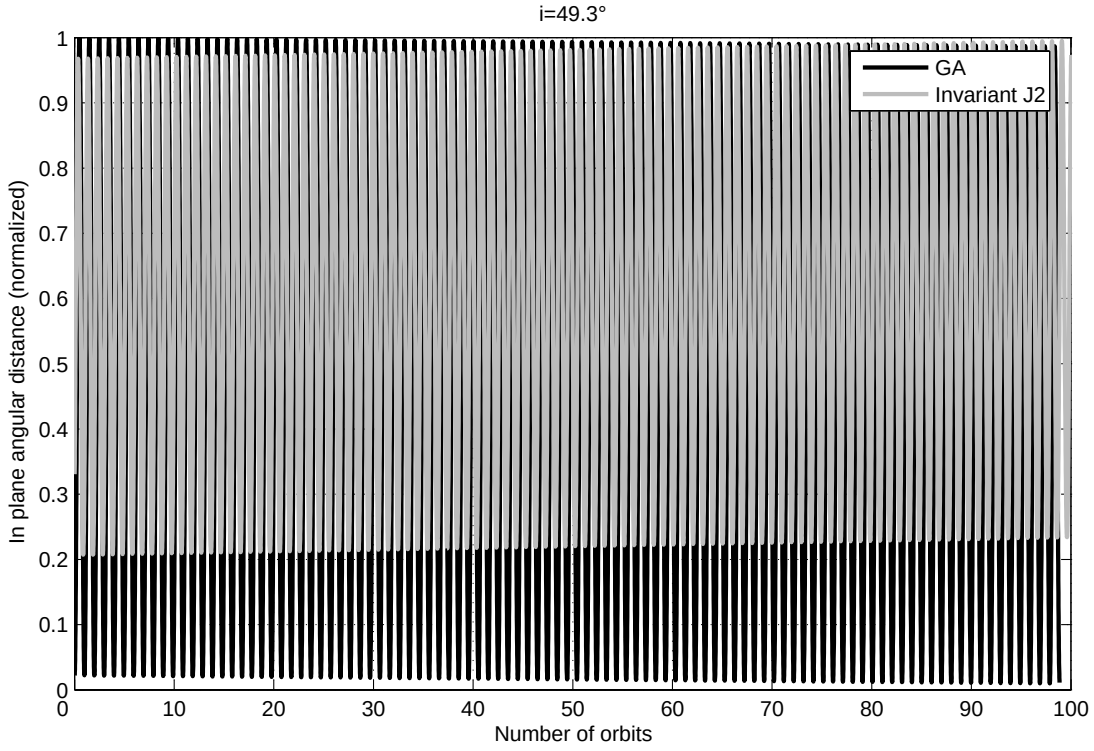

Fig. 89 In-plane normalized angular distance for GA and Invariant J2 orbits (i=49.3°)

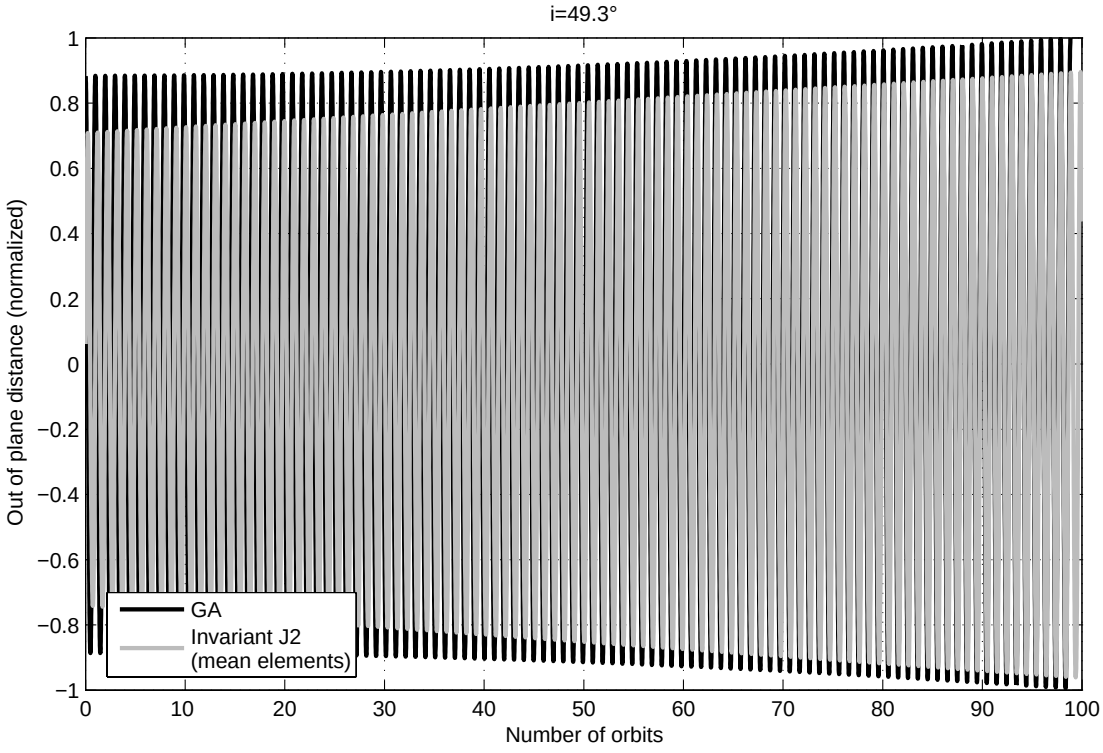

Fig. 90 Out-of-plane normalized angular distance for GA and Invariant J2 orbits (i=49.3°)

Also in this second case, analytical formulation seems to have performances which are lower than the GA case.

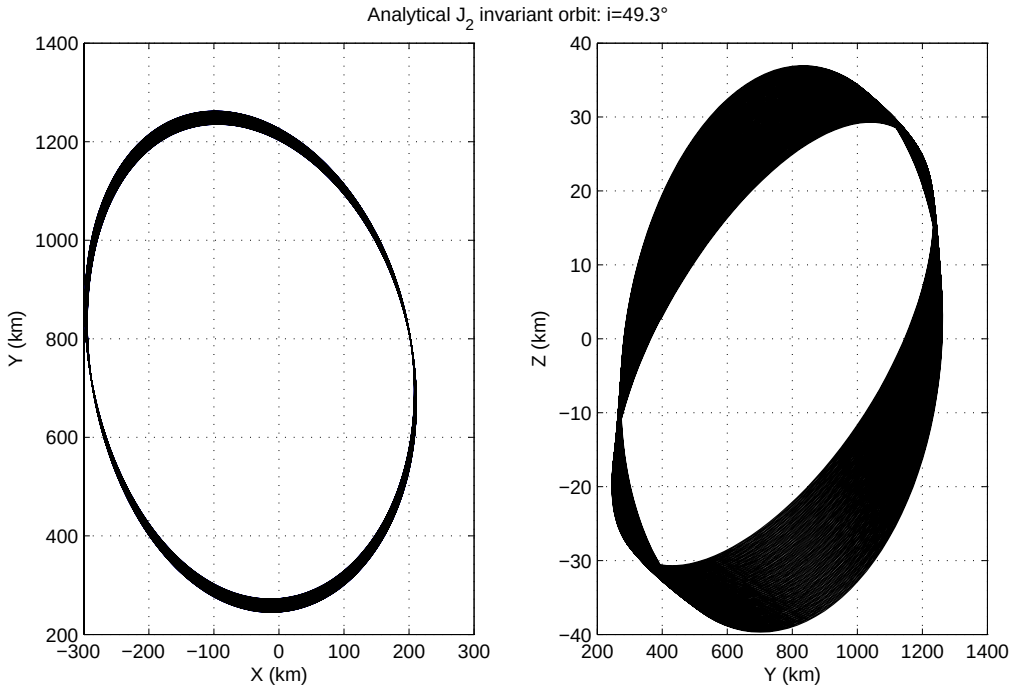

Fig. 91 XY and YZ projections of relative orbits generated with analytical J2 invariant conditions (i=49.3°)

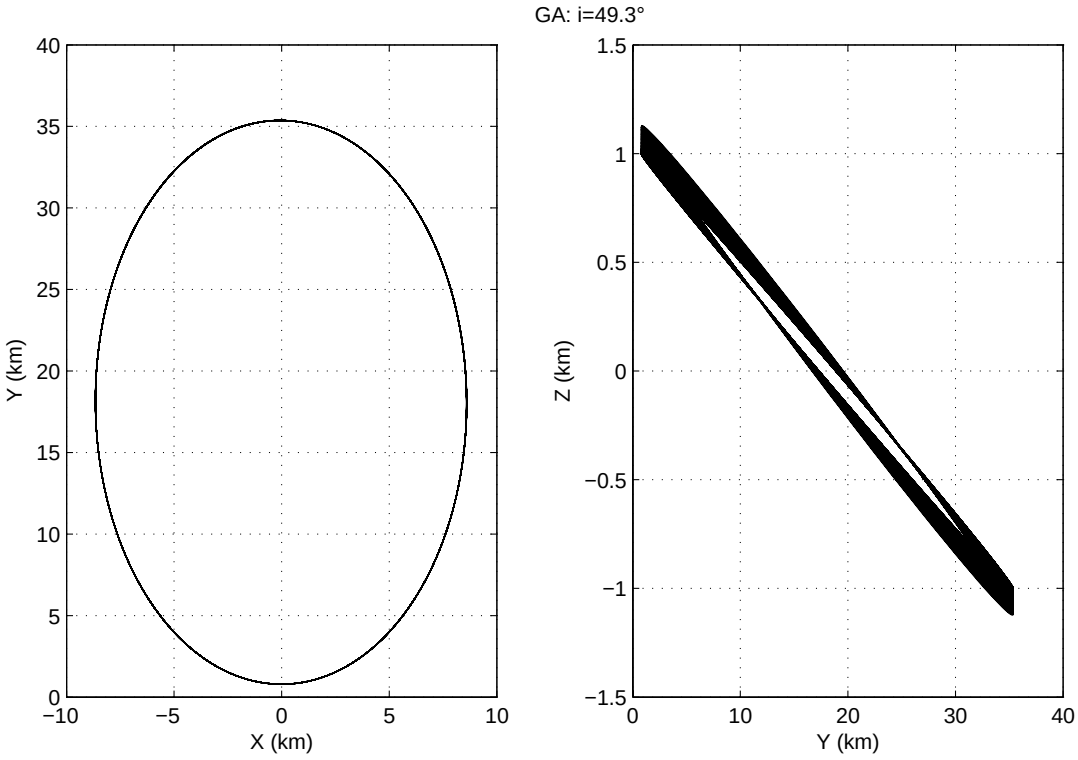

Fig. 92 XY and YZ projections of relative orbits generated with GA conditions (i=49.3°)

Case of critical inclination:

Among the limitations of the conditions Eq. 55 and Eq. 56 there is the need to transform the set of mean elements in osculating elements. This cannot be easily accomplished, specially for circular orbits and for orbits at critical inclination, which are two cases of great interest for what said in this chapter. In these cases, the mean elements have to be used as osculating elements and the results are not so good anymore.

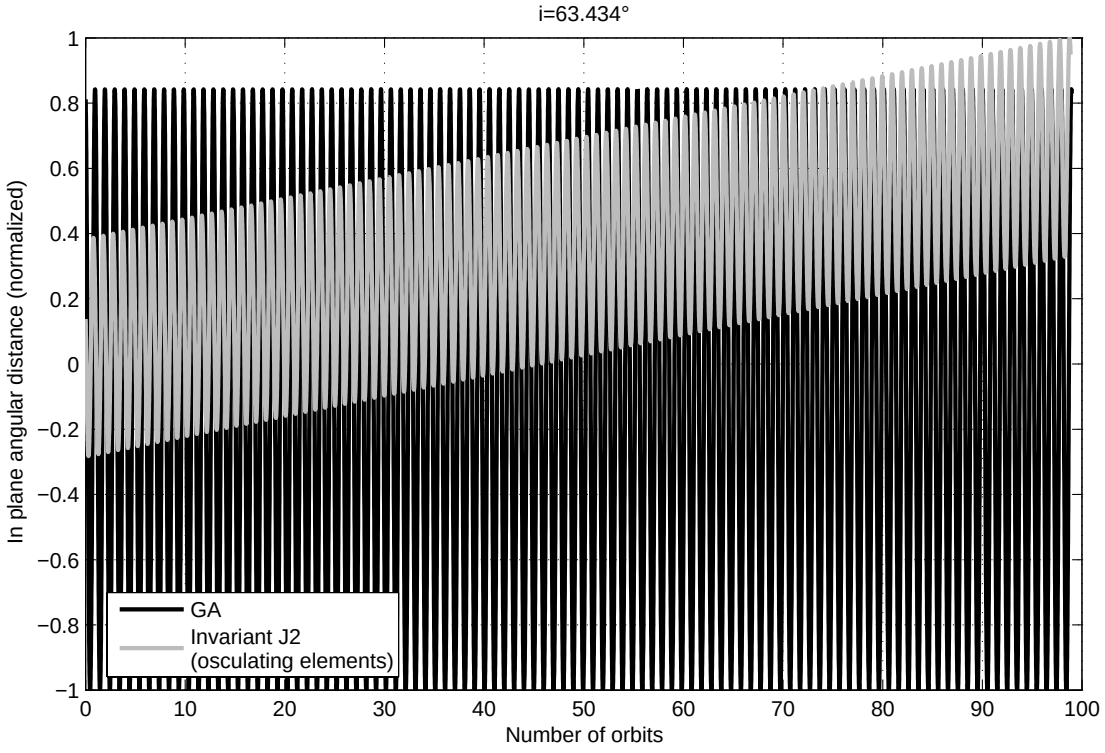

Fig. 93 In-plane normalized angular distance for GA and Invariant J2 orbits (i=63.434°)

The out of plane distance is actually overlapped and will not be reported, but the difference in the in plane distance is sufficient to show how GA can be considered an universal tool, while even the best performing analytical formulation has important limits. In fact the relative orbits calculated with osculating elements is no more satisfactory, as from Fig. 94 and Fig. 95.

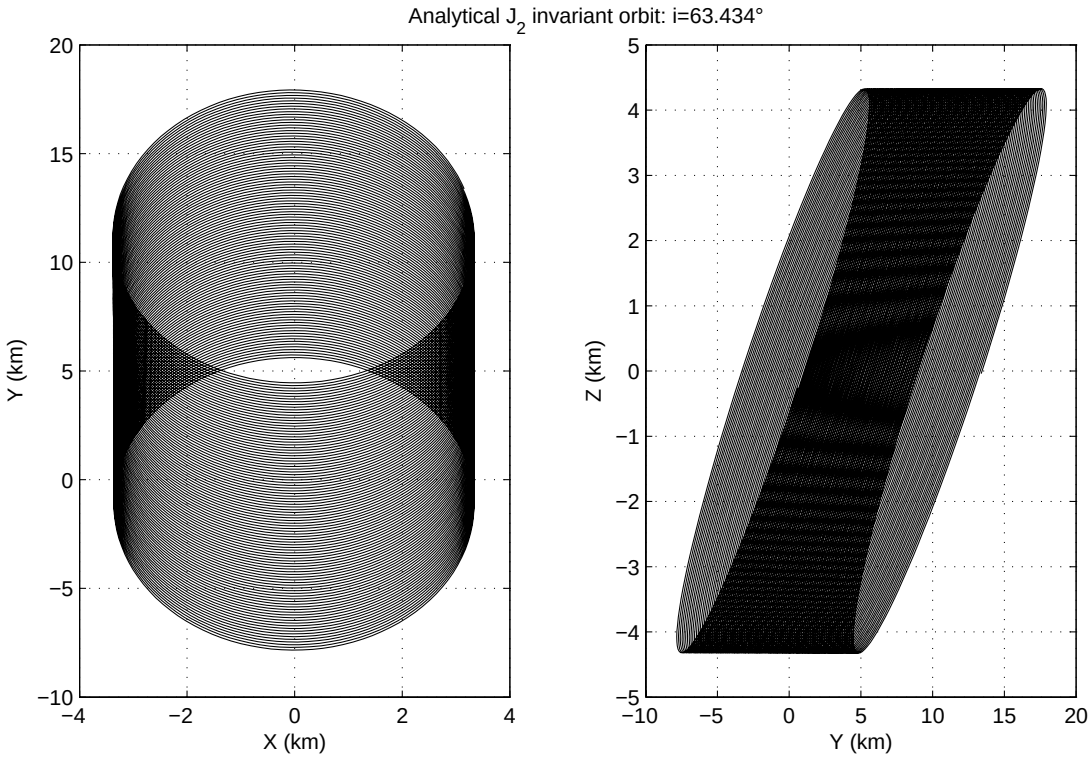

Fig. 94 XY and YZ projections of relative orbits generated with analytical J2 invariant conditions (i=63.434°)

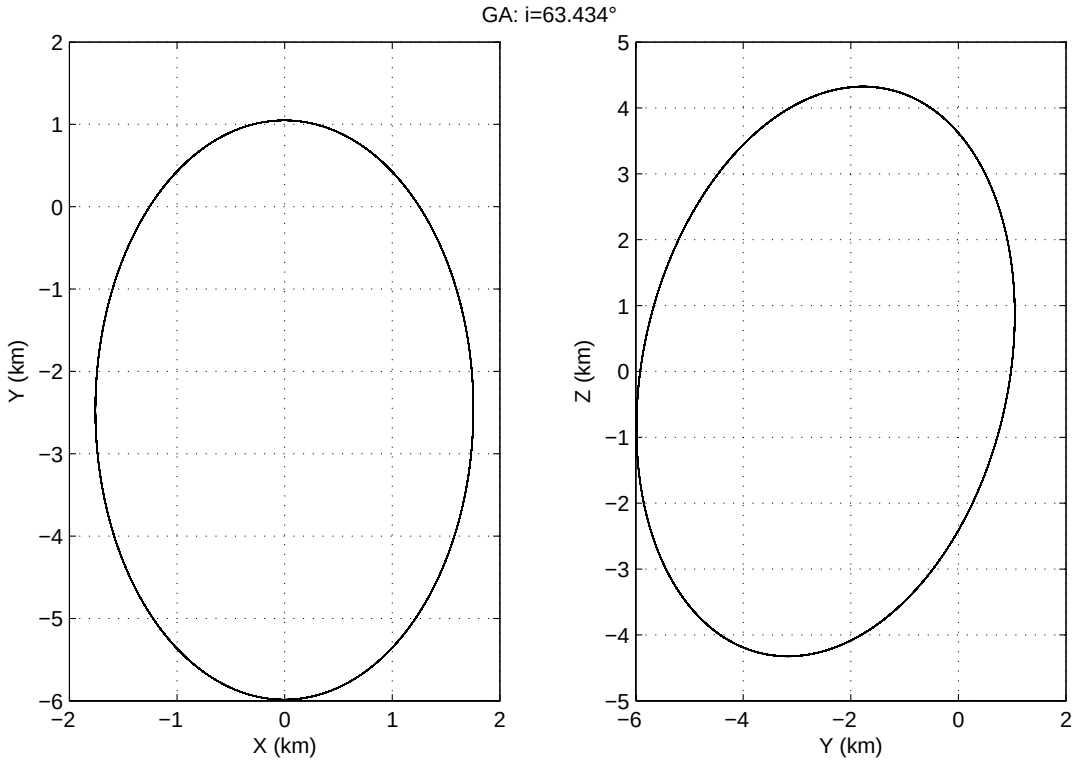

Fig. 95 XY and YZ projections of relative orbits generated with GA conditions (i=63.434°)

5. Minor gravitational perturbations

5.1. Higher terms of the Earth potential.

In Chapter 4 we referred to the shape of the Earth as a *geoid*. As approximations for the geoid, simple mathematical models are used. The first approximation, and a very good one for numerous applications, is that of a sphere.

The potential surrounding a spherical mass is equal to a potential surrounding a point mass, and it's the keplerian potential:

$$U = -\frac{\mu m}{r} \qquad \textbf{Eq. 57}$$

If, as in Chapter 4, the flattening at the poles is considered, the potential of that spheroid of slight ellipticity have to be introduced:

$$U = -\frac{\mu m}{r}\left\{1 - \frac{1}{2}\frac{R_\oplus^2}{r^2} J_2 \left(3\sin^2 \delta - 1\right)\right\} \qquad \textbf{Eq. 58}$$

where δ is the elevation angle above the equator. From this expression, the accelerations in the LVLH frame illustrated in Eq. 46 (Chapter 4) are found using:

$$\vec{f} = -\text{grad}\, U \qquad \textbf{Eq. 59}$$

A more general representation is obtained by superposing deviations from the perfect sphere, represented by coefficients in spherical harmonic series expansions. There are altogether three classes of harmonic expansion coefficients. *Zonal* coefficients, which assume symmetry about the spin axis; *tesseral* ("cube shaped") coefficients; and *sectorial* coefficients, which refer to orange-section-shaped sectors.

An expression for the potential surrounding a body of arbitrary shape can be written, using Legendre polynomials:

$$U = -\frac{\mu}{r}\left\{1 + \frac{1}{M}\sum_{n=2}^{\infty}\left[\frac{R_\oplus}{r}\right]^n J_n P_n \left(\sin\delta\right)\right\} \qquad \textbf{Eq. 60}$$

P_n are the Legendre polynomials, expressed by means of the Rodrigues formula:

$$P_n(\chi) = \frac{1}{2^n n!}\frac{d^n}{d\chi^n}\left(\chi^2 - 1\right)^n \quad \textbf{Eq. 61}$$

and J_n are the coefficients mentioned above.

5.2. Effects of higher terms of the Earth potential.

We now include in the propagator a very high number of coefficients. Like in any series expansion, the precision is the description of the phenomenon is depending on the number of coefficient considered, but the influence of these coefficients becomes lower and lower as the order of the term is higher.

23 zonal coefficient and 8 tesseral coefficients are here considered. One fundamental step is to verify if including these harmonics has or not a great impact on formation dynamics.

Let's start from a case when a periodic relative motion under J_2 effect alone has been found possible, i.e. for critically inclined orbits:

a=6678 km

e=0.00118

i=63.43494882292201°

ω =90°

Ω =270°

θ_0 =0°

The conditions obtained using GA in Chapter 4 to optimize a model with just J_2 perturbation, are now propagated considering first J_2 perturbation alone, then the full geopotential model. The results are reported in Fig. 96 and Fig. 97.

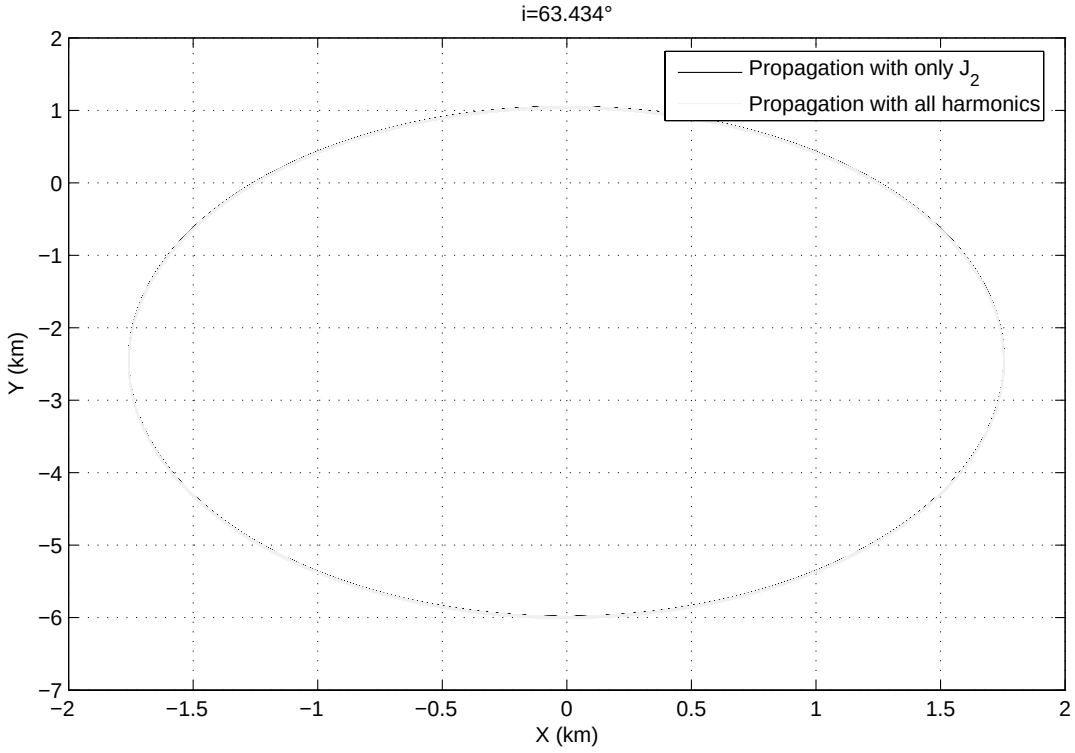

Fig. 96 Propagation with and without including higher harmonics terms (XY projection)

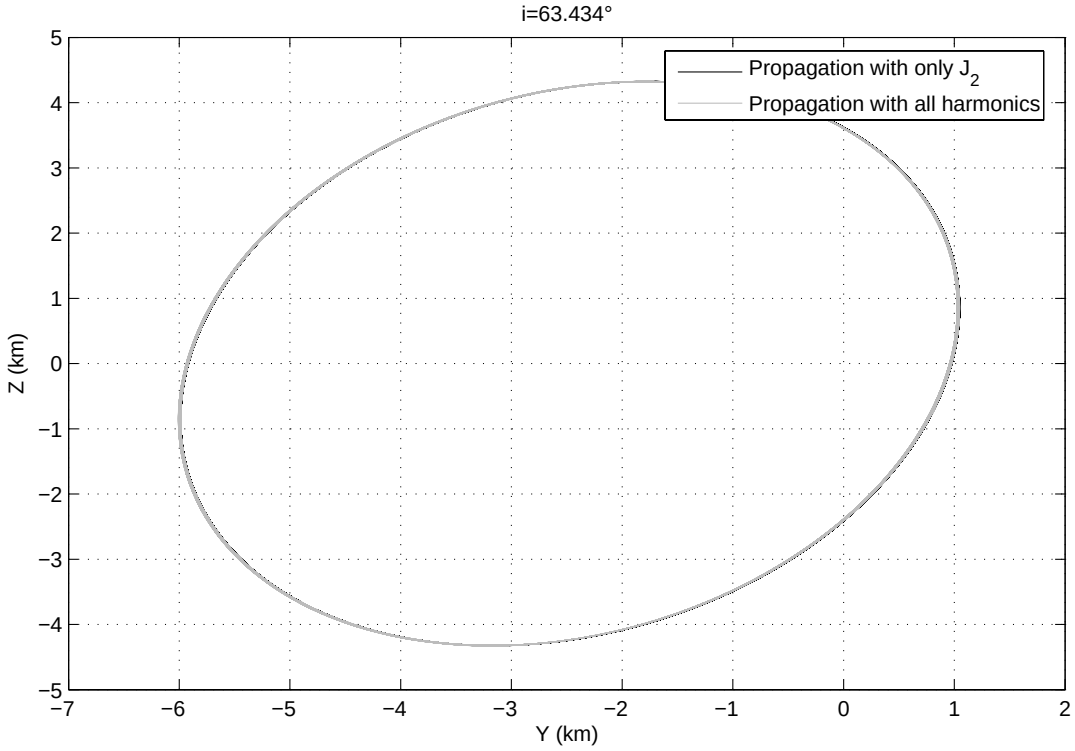

Fig. 97 Propagation with and without including higher harmonics terms (YZ projection)

A deep zoom is necessary in order to find out the differences (Fig. 98).

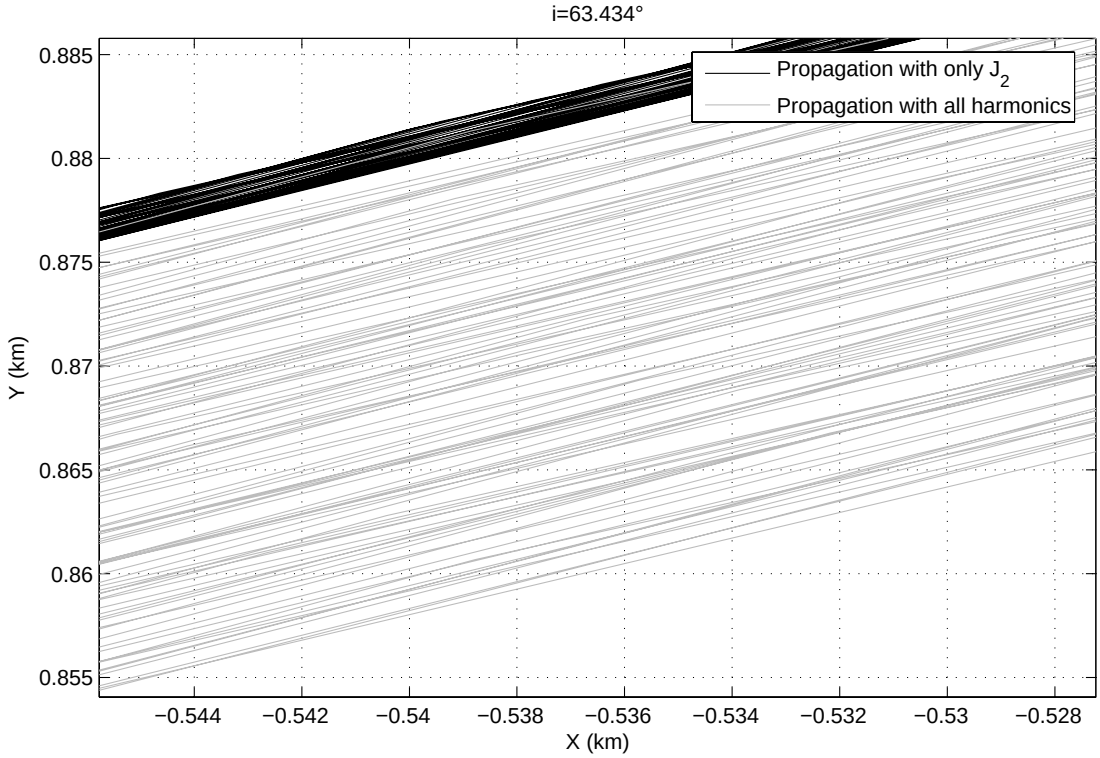

Fig. 98 Propagation with and without including higher harmonics terms (zoom of XY projection)

The simulation is run for one hundred orbits and the relative orbit is still bounded and periodic, with very good approximation.

Also for a generically inclined orbit (for example 97.87°, sun-synchronous orbit), the difference is really little. The fitness value after one orbit with just J_2 perturbation is 142, while with all the harmonics is 135: the effects of this difference on fitness value are insignificant, and the plot are not reported.

It's now possible to investigate if these very little effects are worth a simulation of PIKAIA with all the harmonics. In fact, the computing time increases a lot with respect to the case where only J_2 acceleration is considered in the model optimized by the PIKAIA.

Let's compare the two cases, named **case A** and **case B**.

In case A: the initial conditions are found optimizing with PIKAIA a model with just J_2 effects, and then propagated in a simulator with all the harmonics;

In case B: the initial conditions are found optimizing with PIKAIA a model with all the harmonics, and then propagated in a simulator with all the harmonics;

The orbit considered has the parameters in Chapter 4, but with sun-synchronous inclination (97.87°):

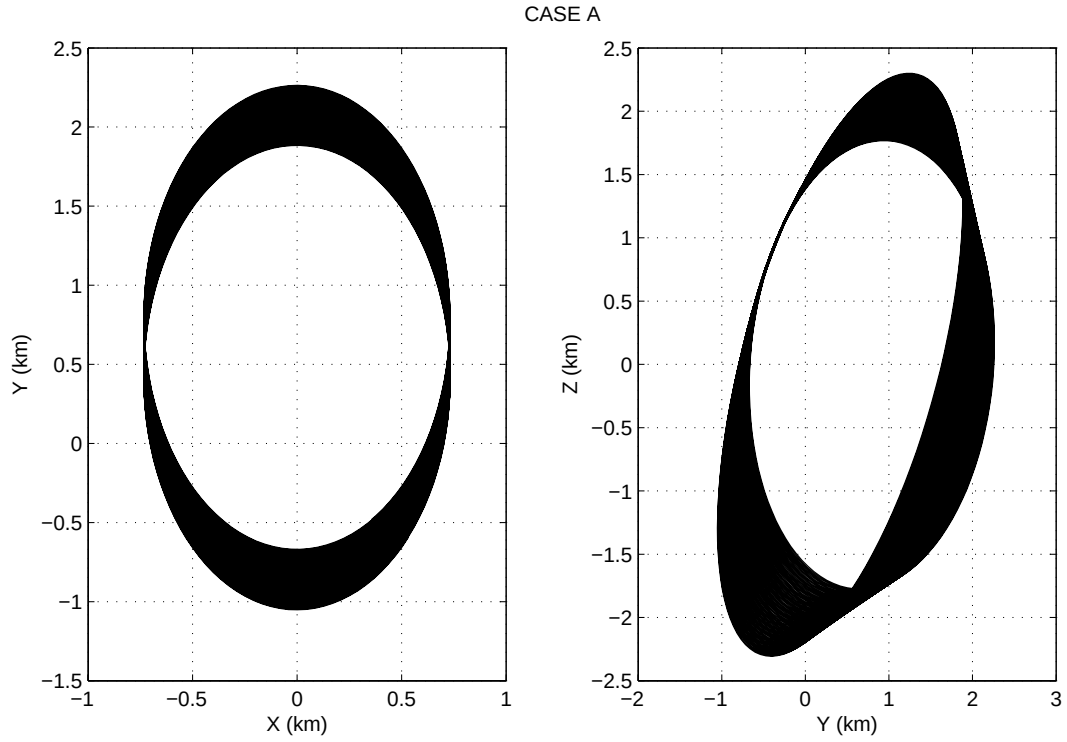

Fig. 99 The initial conditions are found optimizing with PIKAIA a model with just J2 effects, and then propagated in a simulator with all the harmonics

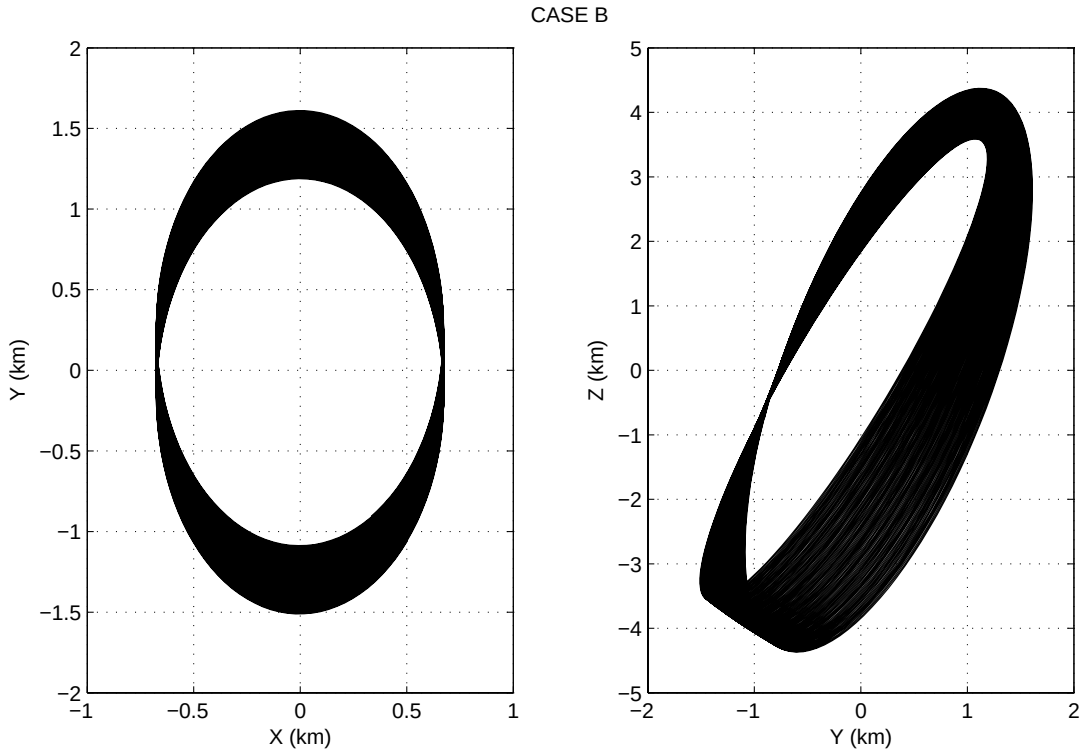

Fig. 100 The initial conditions are found optimizing with PIKAIA a model with all the harmonics, and then propagated in a simulator with all the harmonics

It’s quite clear that no advantage in terms of boundedness of the relative orbit is not corresponding to the higher computing effort.

For a confirm, in Fig. 101 a study of the fitness function resulting from the optimization of the model comprehensive of all the harmonics is performed for various the inclination.

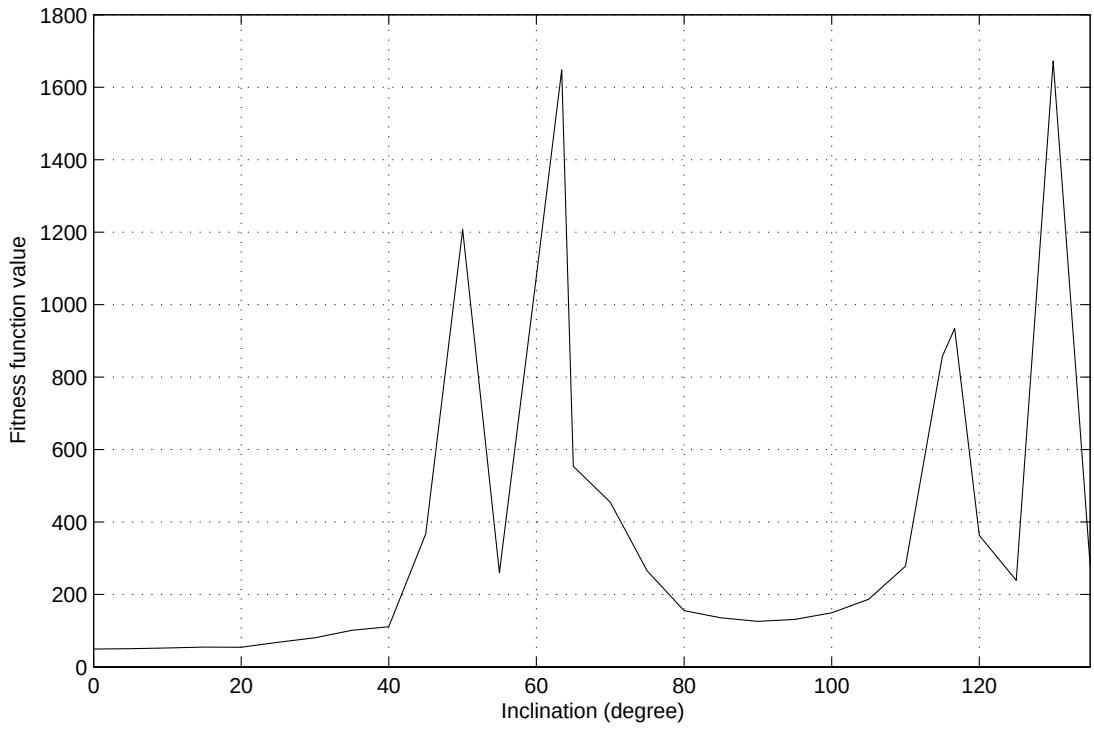

Fig. 101 Fitness function value for a wide range of inclination when higher harmonics are included

The behaviour is very similar to the plots studied in Chapter 4 (in particular Fig. 64 and Fig. 65), with two peaks at the critical inclinations representing the only possibility for a periodic relative orbit, and two peaks at 50° and 180°-50°, representing zones of weaker effects of J_2 perturbation. The higher terms of the Earth potential have no impact on the relative orbits.

Just one final check can be performed to verify if there could be a real need to introduce higher terms of the Earth potential. In fact, all these simulations refer to LEO. But higher order terms of the geopotential have a deeper impact on geostationary orbits, namely the J_{22} effect.

J_{22} effect produces the existence in a GEO of two points of stable equilibrium and two point of instable equilibrium. This results in a slow migration of the satellites from instable to stable zones. The slowness of this phenomenon brings us to consider not just one hundred orbits, but a huge number of orbits, for example one thousand. This means about 2.75 years. Of course the small drift present in the relative orbit will lead to more evident consequences due to this very long propagation time. Three situations are here compared:

Case A: the initial conditions are found optimizing with PIKAIA a model with just J_2 effects, and then they are propagated in a simulator with just J_2 effect.

Case B: the initial conditions are found optimizing with PIKAIA a model with just J_2 effects, and then they are propagated in a simulator with all the harmonics.

Case C: the initial conditions are found optimizing with PIKAIA a model with all the harmonics, and then they are propagated in a simulator with all the harmonics.

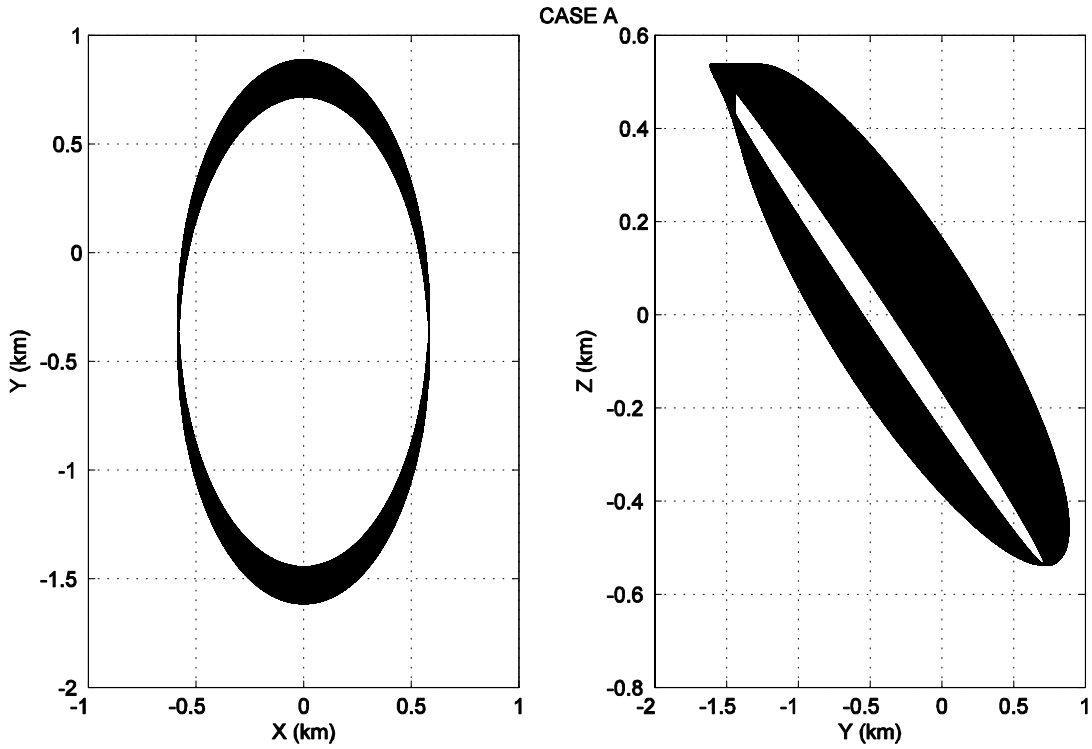

Fig. 102 The initial conditions are found optimizing with PIKAIA a model with just J2 effects, and then propagated in a simulator with just J2 effect.

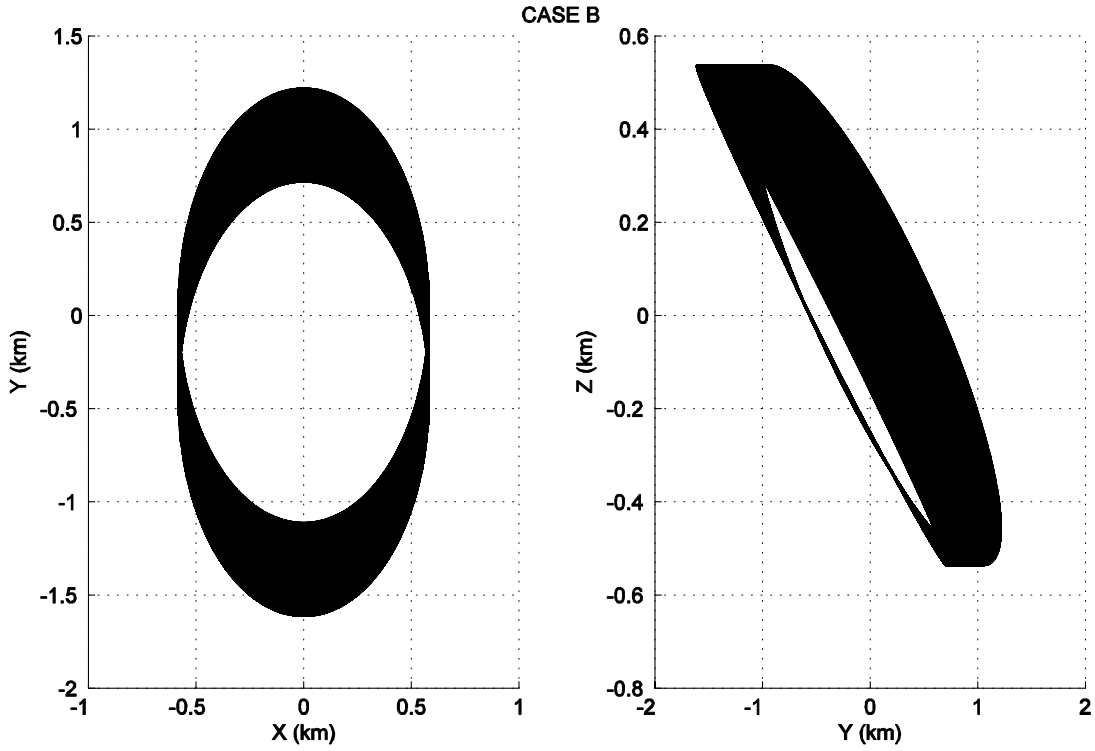

Fig. 103 The initial conditions are found optimizing with PIKAIA a model with just J2 effects, and then propagated in a simulator with all the harmonics

It can be seen from Fig. 102 and Fig. 103 that if higher terms of the geopotential are included in the propagator, the relative orbits result to be worse, but from Fig. 104 it's clear that performing the optimization with all the harmonics does not improve the situation.

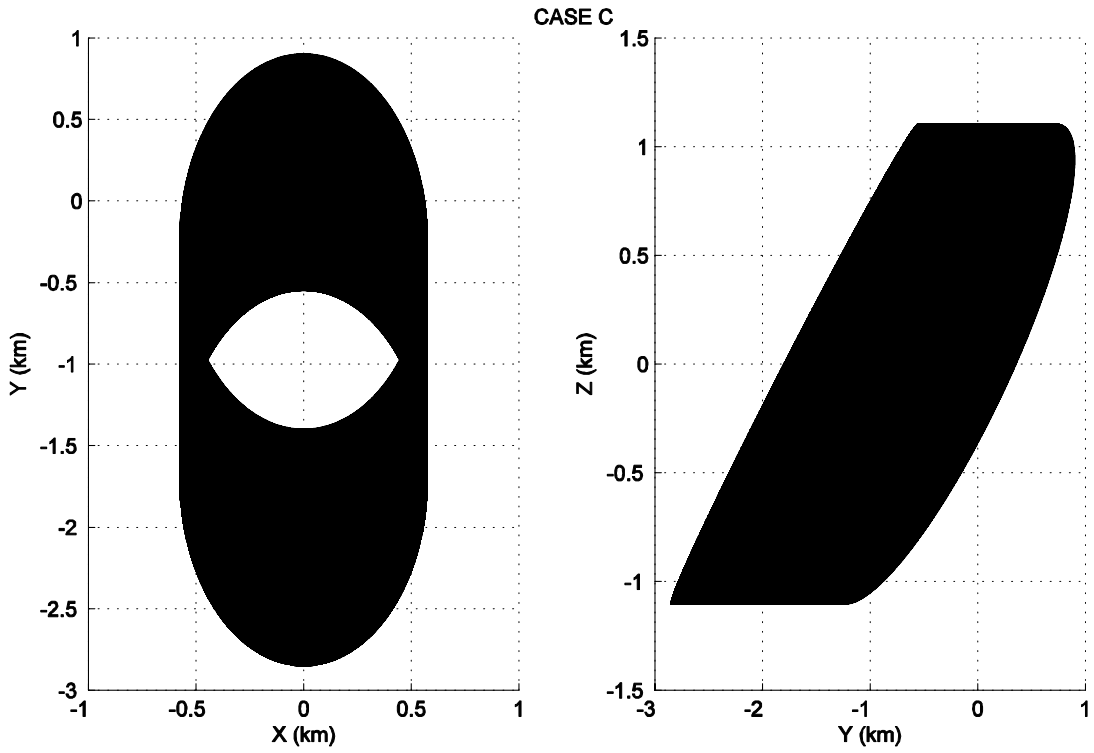

Fig. 104 The initial conditions are found optimizing with PIKAIA a model with all the harmonics, and then propagated in a simulator with all the harmonics

So it's possible to say that **even if higher terms of the Earth potential do influence the relative orbits, their impact is minimal even after something like one thousand orbits, and it cannot be corrected by introducing these higher terms in the model optimized in PIKAIA**.

The relative orbits are not periodic, but still stay bounded.

5.3. Moon-sun attraction

A satellite orbiting around the Earth is not subjected only to the Earth attraction, but also to the attraction of all the other celestial bodies.

In particular, sun and moon are by far the most relevant from this point of view. Their effect is anyway very little and it can be neglected for low orbits, where J_2 and, as it will be shown in Chapter **Error! Reference source not found.**, drag, are by far predominant. A major effect acts on high orbits, in particular on geostationary orbits. In this paragraph we proceed in the same manner as in the last paragraph, examining three cases:

Case A: the initial conditions are found optimizing with PIKAIA a model with just J_2 effects, and then propagated in a simulator with just J_2 effect.

Case B: the initial conditions are found optimizing with PIKAIA a model with just J_2 effects, and then propagated in a simulator with J_2 and third bodies perturbations.

Case C: the initial conditions are found optimizing with PIKAIA a model J_2 and third bodies perturbations, and then propagated in a simulator with J_2 and third bodies perturbations.

If case B is not much different from case A, there's no need to perform the optimization including moon and sun effect, as in case C.

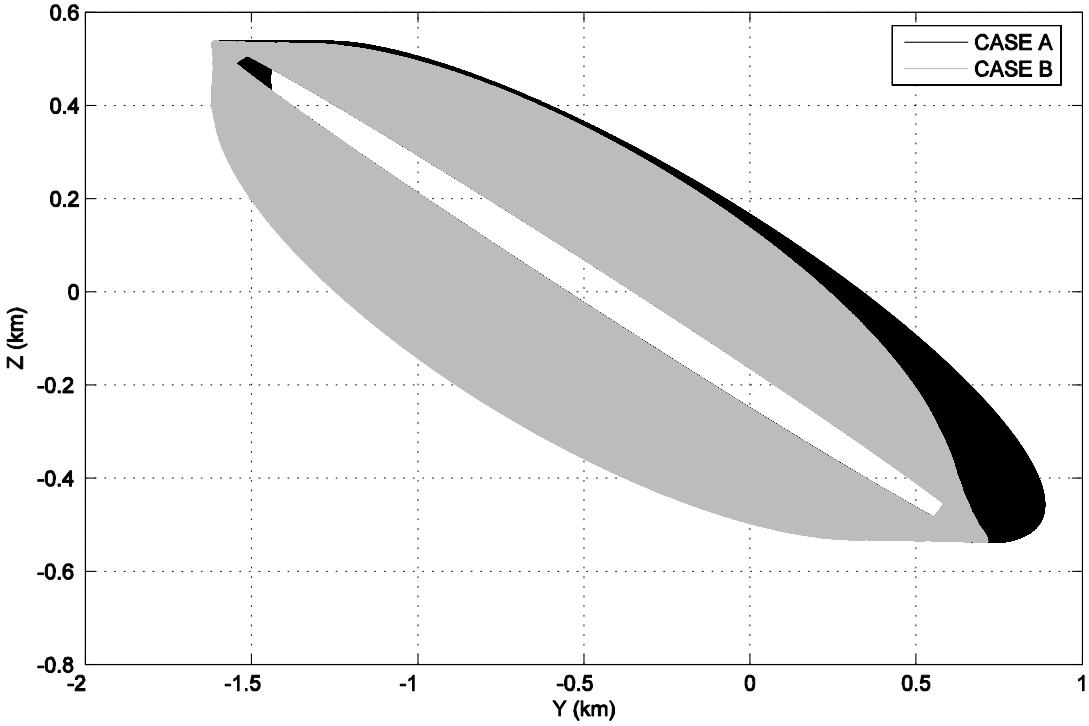

Fig. 105 The initial conditions are found optimizing with PIKAIA a model with just J2 effects, and then propagated in a simulator with just J2 effect.

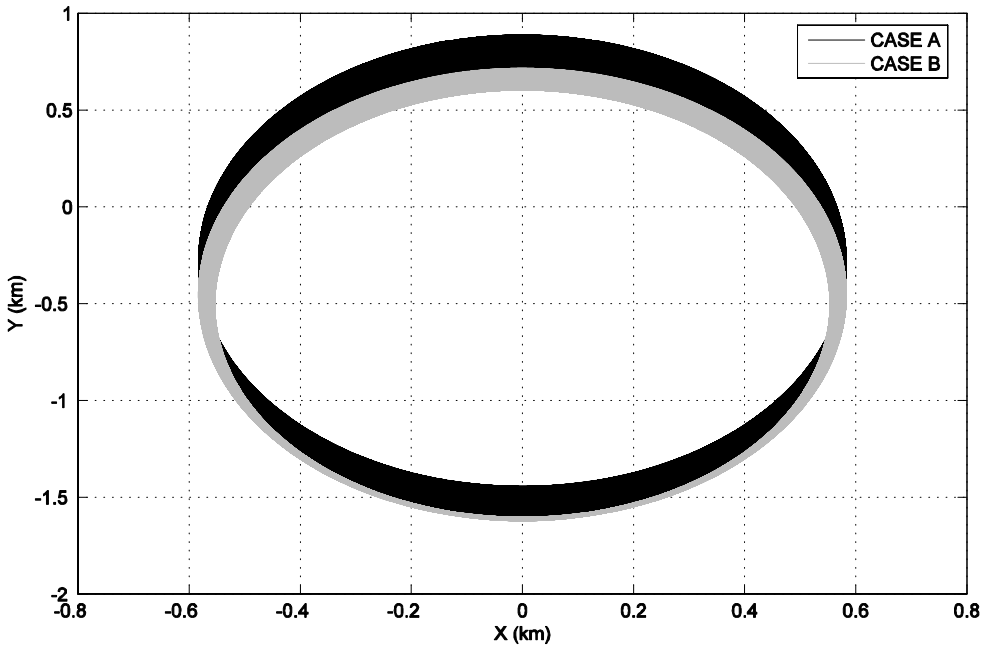

Fig. 106 The initial conditions are found optimizing with PIKAIA a model with just J2 effects, and then propagated in a simulator with J2 and third bodies perturbations

Again, it's evident that even after one thousand orbits, the effects of perturbations different from the J_2 effect are negligible. Just as a confirm, the optimization performed with a model including moon and sun presence is run, and the resulting trajectory propagated for one thousand orbit is reported in Fig. 107 (Case C)

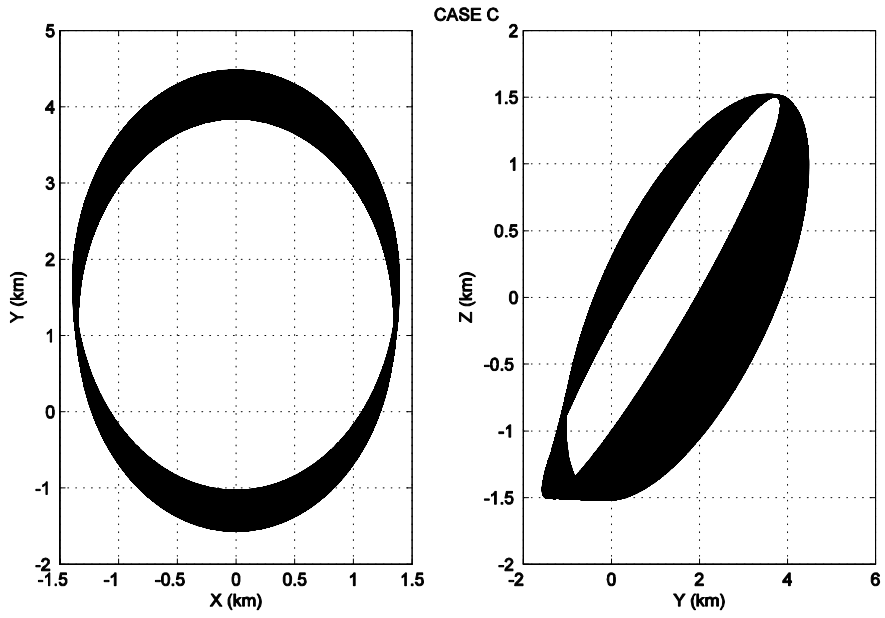

Fig. 107 The initial conditions are found optimizing with PIKAIA a model J2 and third bodies perturbations, and then propagated in a simulator with J2 and third bodies perturbations.

Again, an improvement is not reached by adding perturbation other than J_2 to the model optimized by PIKAIA.

6. Drag perturbation

6.1. Air drag and satellite's physical parameters

A detailed description of the Earth atmosphere's highest layers is not straightforward due to continuous and rapid changes of different conditions.

Air density value reduces as the height above the Earth's surface increases. The so-called upper atmosphere is the region beginning at 80 km above the surface. Density's behaviour in the upper atmosphere is pretty unpredictable, subject to large variations, depending on locality and time, and it's strongly different from what happens at the surface proximity.

Density vs. satellite's altitude for a given day time and period of the year is plotted in Fig. 108.

According to Fig. 108, the effects of drag are expected to be almost insignificant above 500 km, while they are very important for heights lower than 300 km. At 100-150 km a satellite is usually considered lost because the air drag will cause very fast orbit decay.

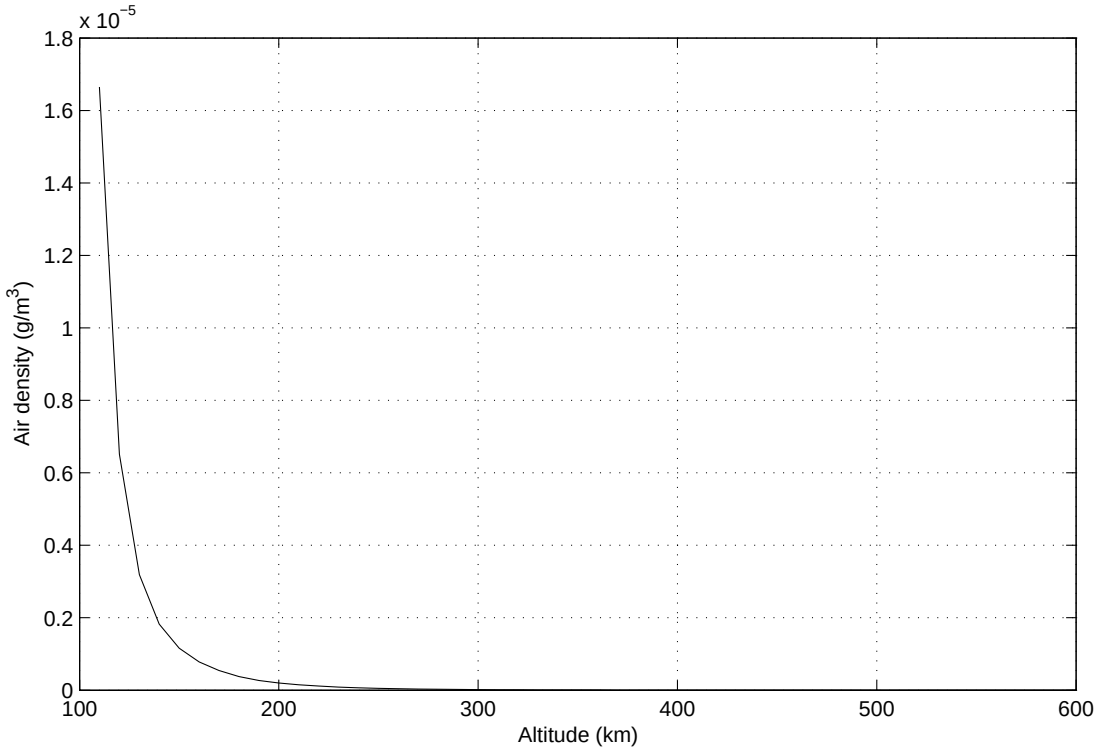

Fig. 108 Variations of air density with altitude

The following perturbation force per mass unit (acceleration):

$$\vec{f} = -\frac{1}{2}\frac{C_d A}{m}\rho v^2 \hat{v}$$

Eq. 62: drag perturbation force per mass unit

acting on the satellite, represents the drag due to air resistance. ρ is the air density, v is the relative speed of the satellite with respect to the Earth atmosphere, *A* and *m* are the frontal area and the mass of the satellite, C_d is the air drag (or resistance) coefficient, ranging between 2.0 and 2.6 for typical satellites in orbit 150 to 400 km above the Earth's surface, and $\hat{v}$ is the orbit tangential versor.

ρ is the most difficult quantity to evaluate. Different approximated models are available. The one used here is a JACCHIA model for high altitudes (100 km <h< 600 km), considering a great number of variables affecting ρ: mainly altitude, day of the year and time of the day.

When a perturbation like air drag is considered the satellite's orbital parameters are not sufficient. Physical parameters have to be taken into account:

- mass=1850 Kg;
- Equivalent diameter D=2.52 m;
- Frontal area $A = \pi\frac{D^2}{4} = 5m^2$;
- Drag coefficient $C_d = 2.2$.

6.2. Effects of the air drag

The approach will follow the guidelines of Chapter 5. First of all, it is necessary to verify if these perturbations have a significant impact on the satellites' relative dynamics. To begin a very low orbit is chosen in order to emphasize the effects of the drag. For example, a set of parameters already studied in Chapter 5, but with an altitude of just 200 km:

a=6578 km

e=0.00118

i=97.87°

ω =90°

Ω =270°

θ_0 =0°

An optimization using the GA is then performed. The model still includes the only J_2 gravity perturbation. So the usual set of initial conditions is obtained:

$$x_0 = \text{-0.242225928 km}$$

$$y_0 = \text{-0.9796673 km}$$

$$z_0 = 0.203639494 \text{ km}$$

$$\dot{x}_0 = \text{-2.4134562E-004 km/s}$$

$$\dot{y}_0 = 5.73640408\text{E-004 km/s}$$

$$\dot{z}_0 = \text{-9.99775084E-004 km/s}$$

These conditions propagated for 100 orbits in a model including J_2 result in the bounded orbits shown in Fig. 109 and Fig. 110.

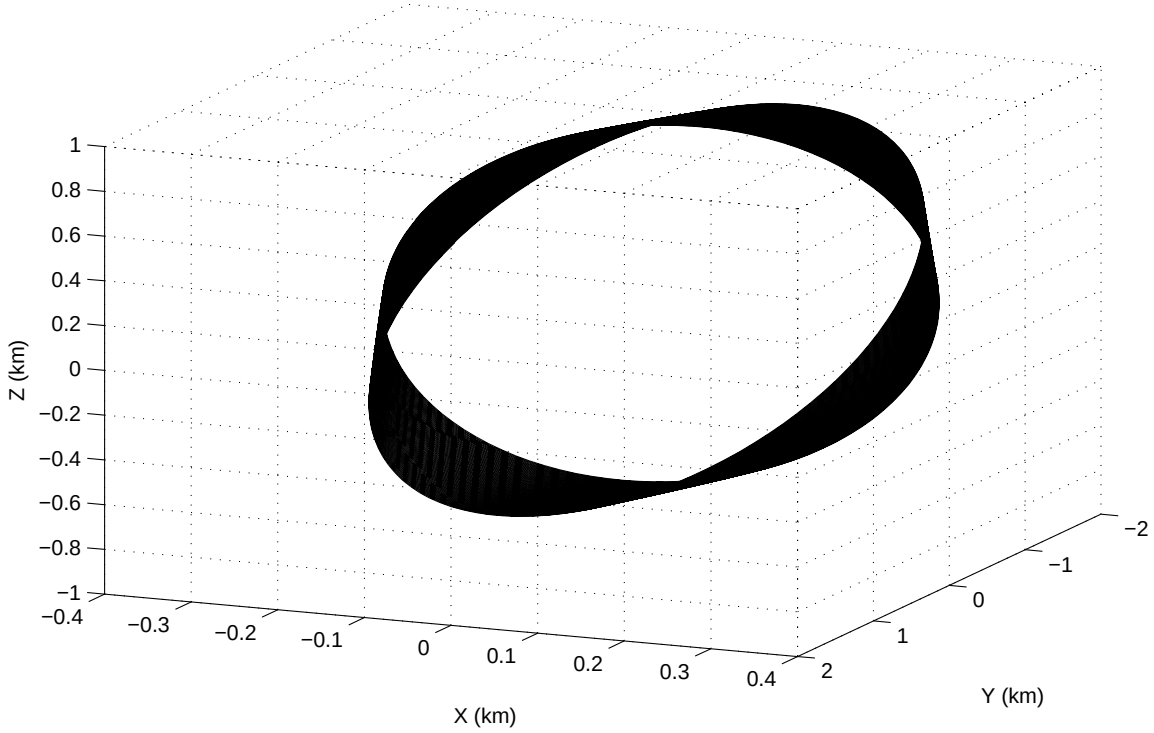

Fig. 109 Relative orbit under the only J_2 effect

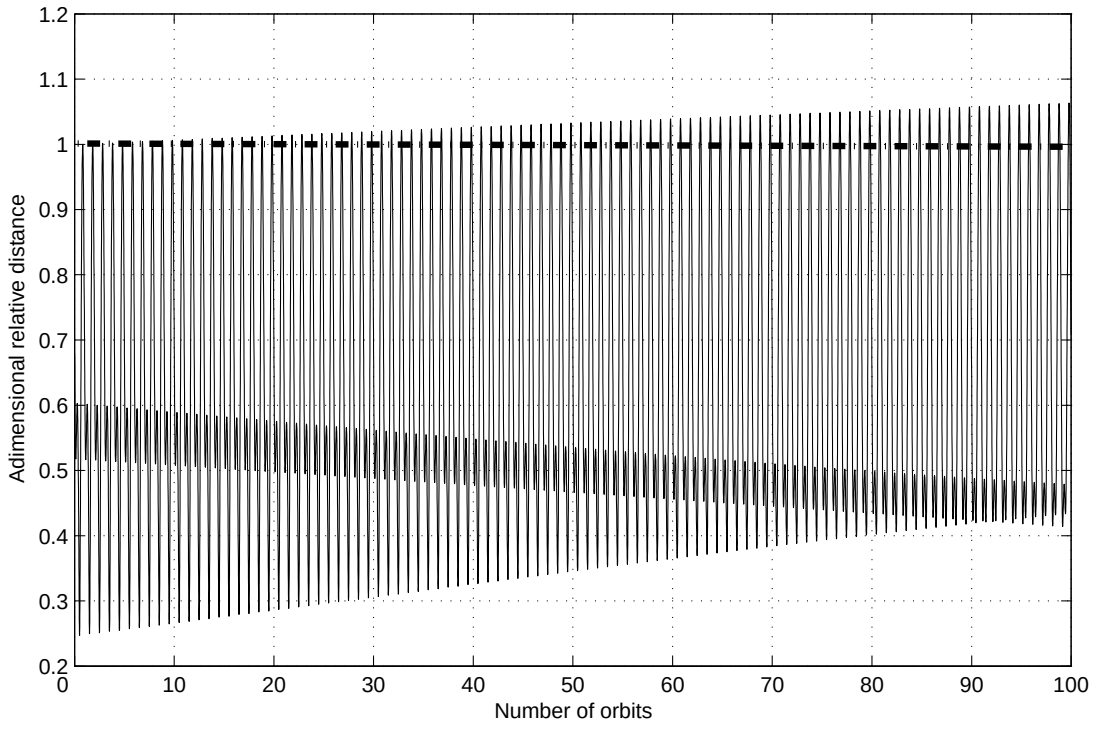

Fig. 110 Adimensional relative distance for a J_2 perturbed orbit

The quantity plotted in Fig. 110 is calculated as:

$$\frac{dist}{\max\left(dist(\text{first orbit})\right)}$$

Eq. 63: adimensional relative distance

The above defined parameter should oscillate between 0 and 1 for closed orbits, or should slightly exceed 1 for bounded, quasi-periodic ones. While a strong divergence from 1 represents not closed relative orbits.

When the drag effects are included into the model and the same initial conditions are propagated for 100 orbits, the results suffer a huge decrease in performances, as illustrated in Fig. 111, Fig. 112, Fig. 113 and Fig. 114

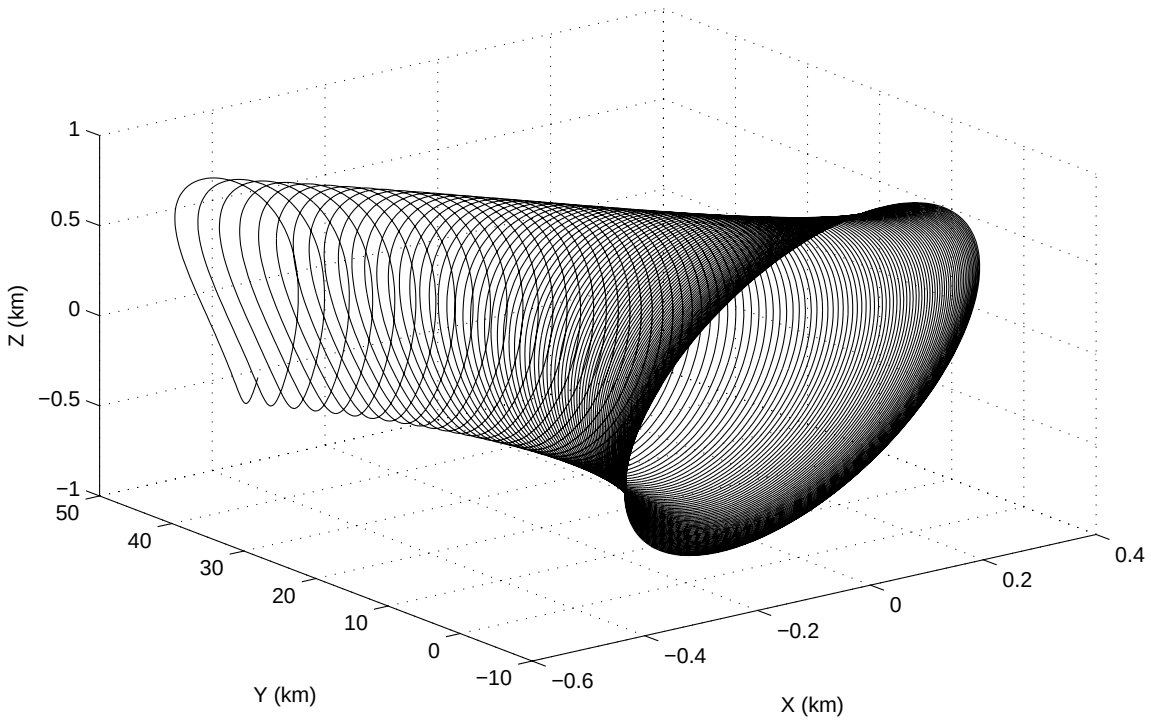

Fig. 111 Relative orbit under combined effects of J2 and drag

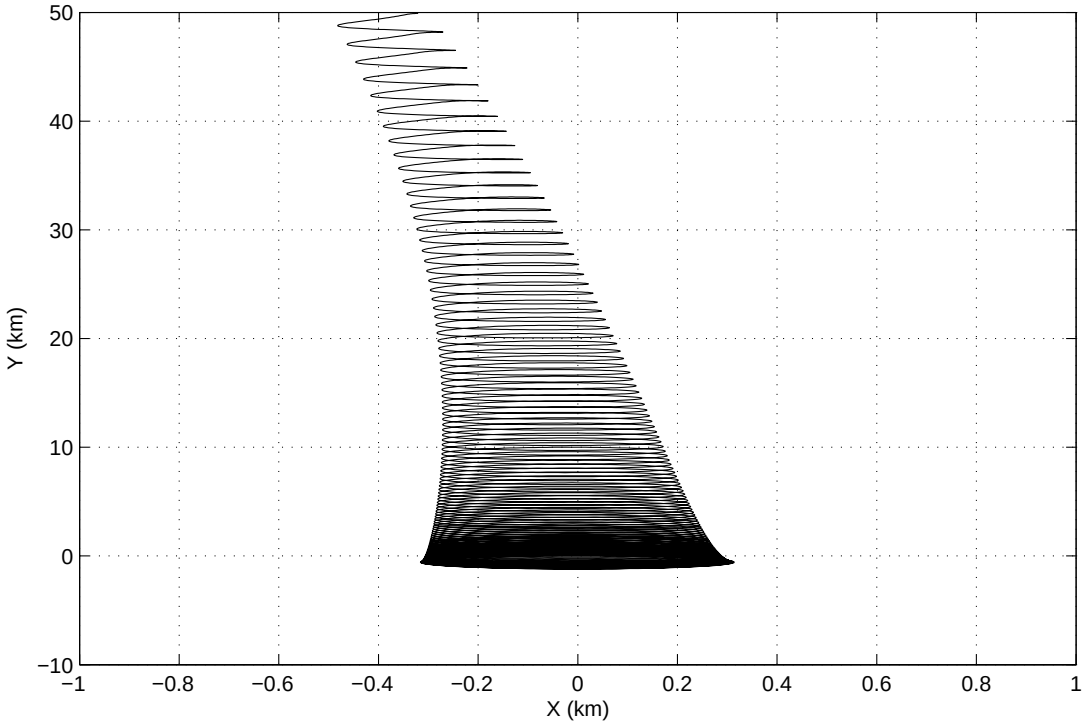

Fig. 112 XY projection of relative orbit under combined effects of J2 and drag

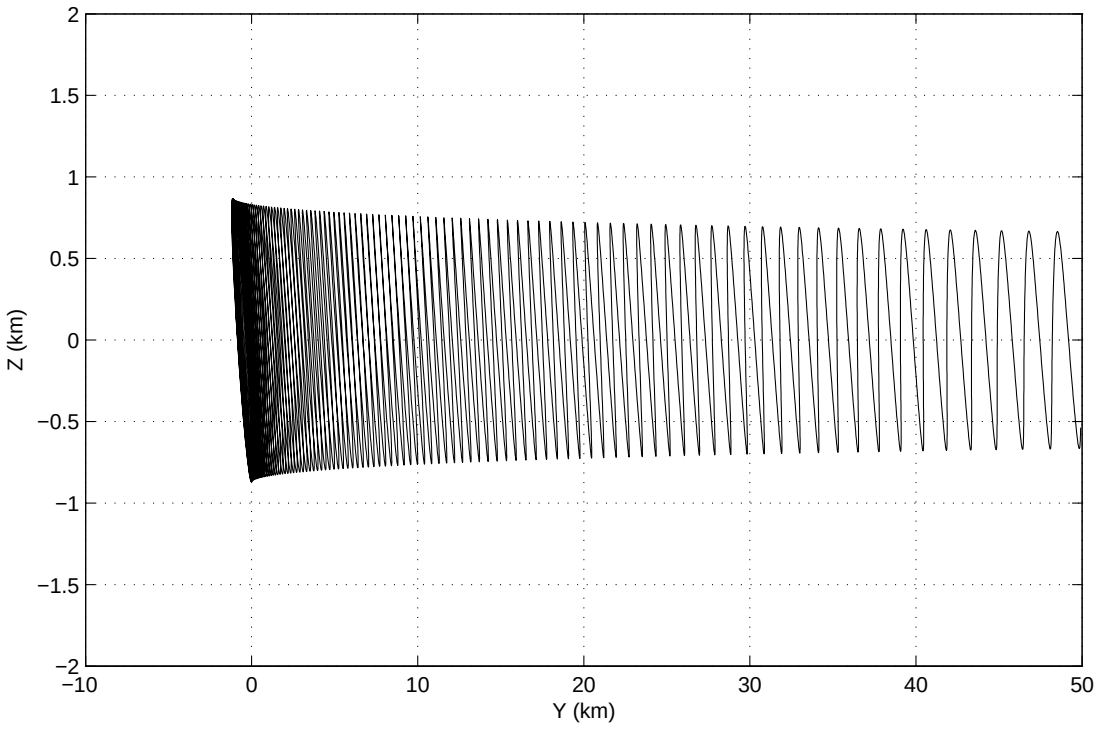

Fig. 113 YZ projection of relative orbit under combined effects of J2 and drag

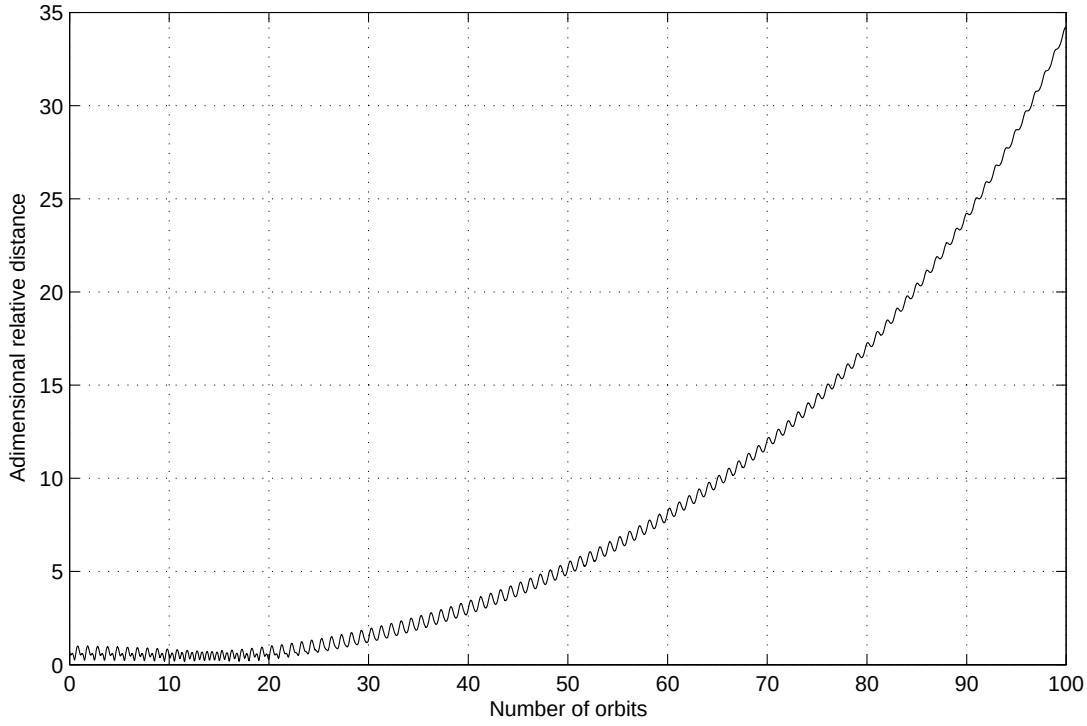

Fig. 114 Adimensional relative distance under J2 and drag perturbation

This shows that at low altitudes drag has a great impact on the formation's dynamics. Then, in the model to be optimized this perturbation must be included. A new set of initial conditions is found:

$$x_0 = \text{-0.420000087999999 km}$$

$$y_0 = \text{-0.910191328000000 km}$$

$$z_0 = \text{-0.156000299999999 km}$$

$$\dot{x}_0 = \text{2.860136740000013E-004 km/s}$$

$$\dot{y}_0 = \text{9.939996700000018E-004 km/s}$$

$$\dot{z}_0 = \text{9.997558140000017E-004 km/s}$$

These conditions are again propagated for 100 orbits in a model including both drag and J_2. If we had expected some significant improvement, we couldn't be satisfied by the results. In fact, the satellites still drift apart quite quickly, and the drag effects are evidently not caught by the initial conditions. Fig. 115, Fig. 116, Fig. 117 and Fig. 118 are in fact not very much different from Fig. 111, Fig. 112, Fig. 113 and Fig. 114 where the initial conditions propagated where found by optimizing a model without drag.

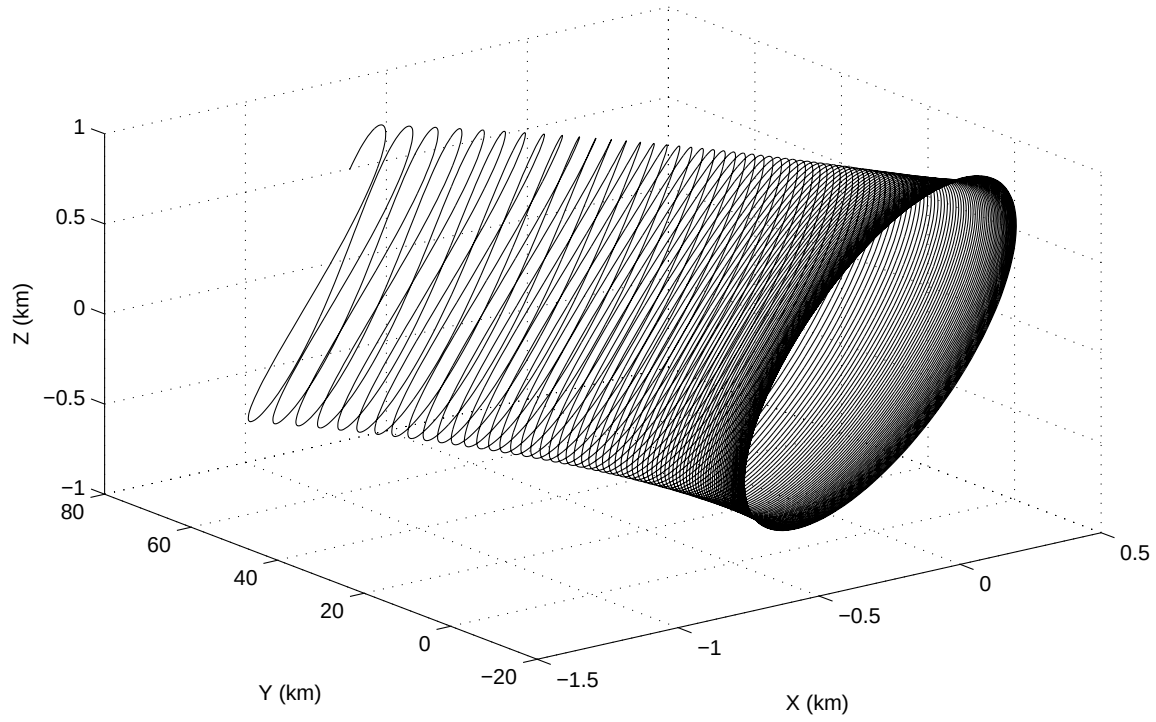

Fig. 115 Relative obit under J2 and drag perturbation

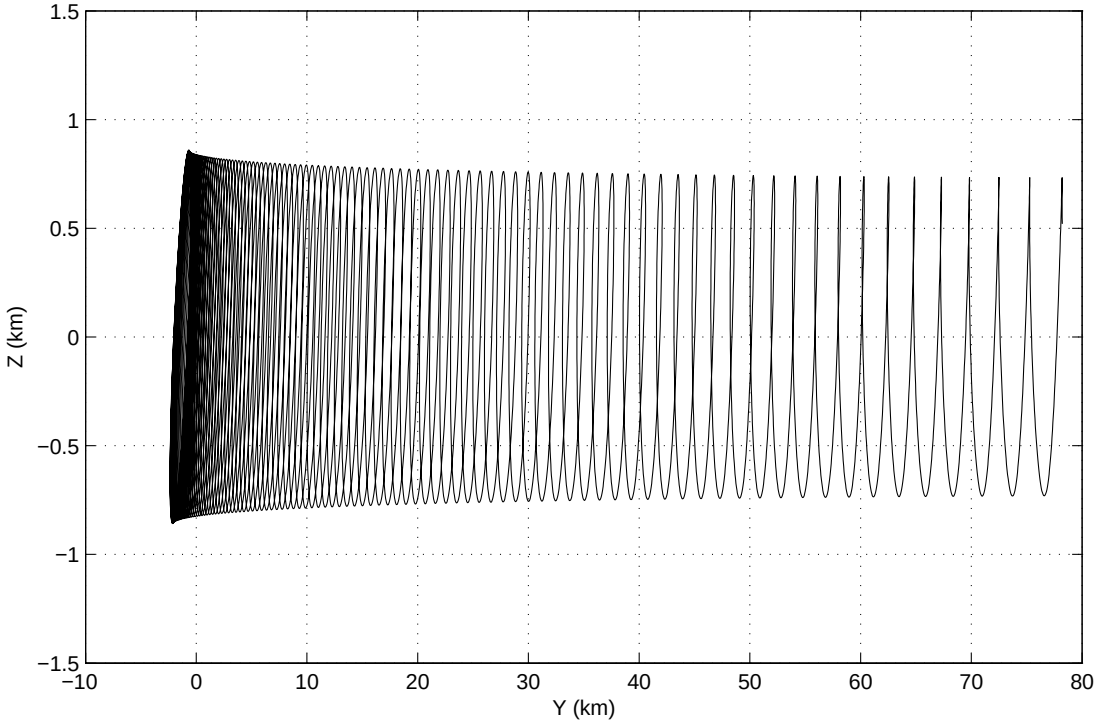

Fig. 116 XY projection of relative obit under J2 and drag perturbation

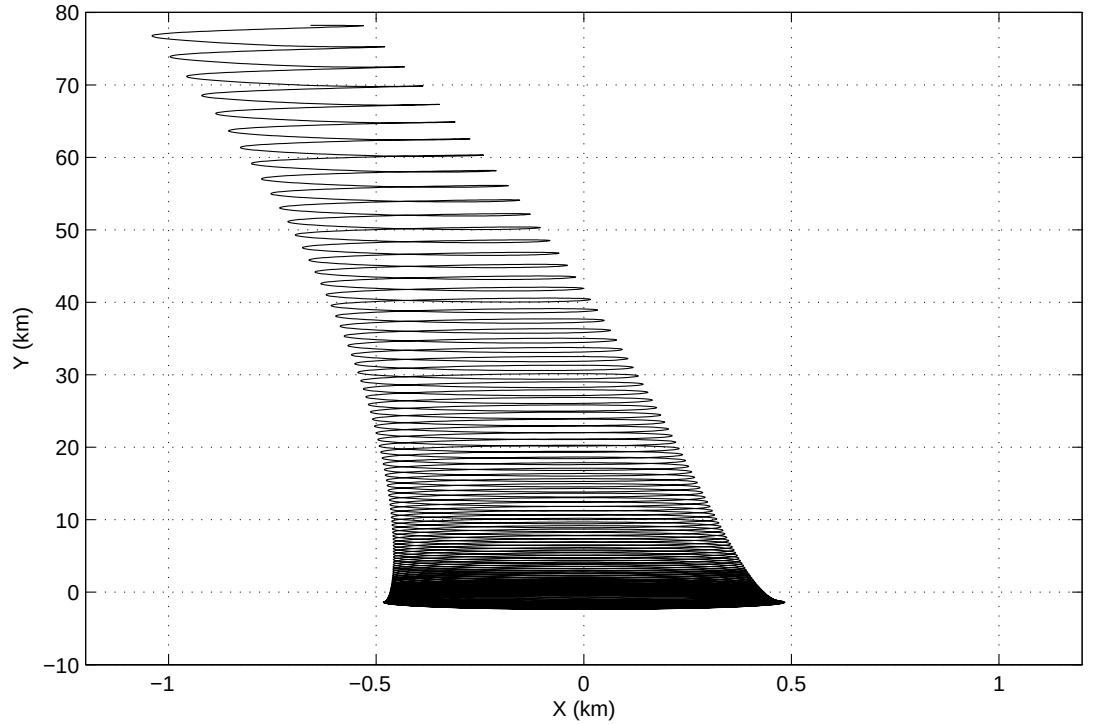

Fig. 117 YZ projection of relative obit under J2 and drag perturbation

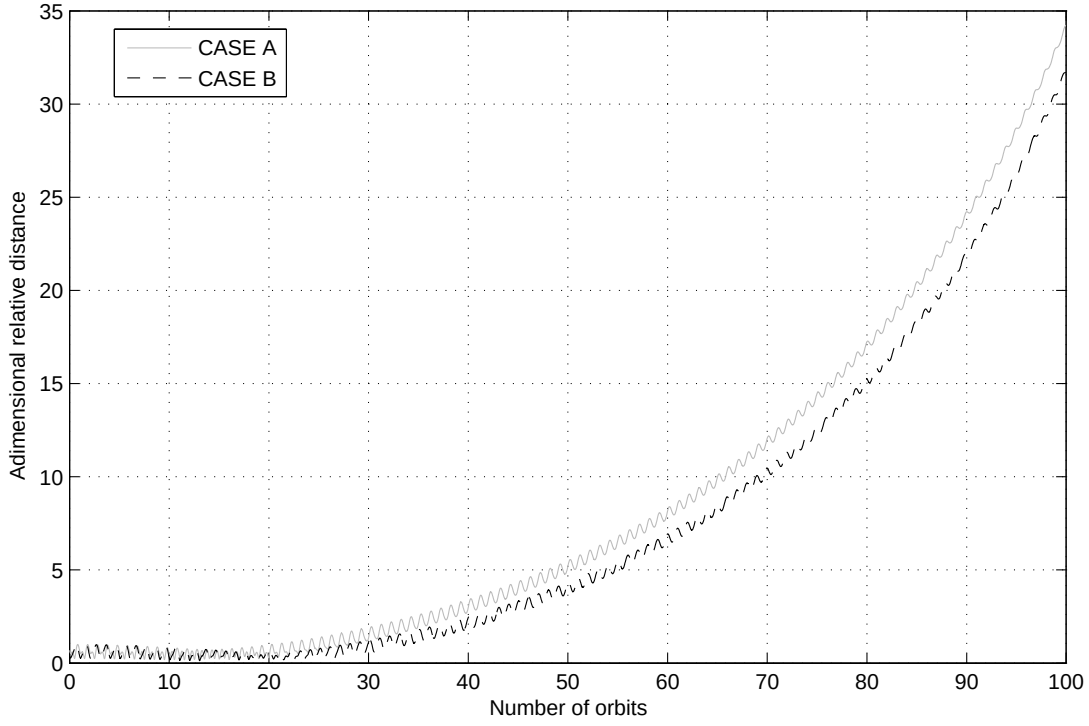

Fig. 118 Comparison between adimensional relative distance between CASE A and CASE B

In Fig. 118, **Case A,** the initial conditions are found optimizing with PIKAIA a model with J_2 and drag perturbations, and then propagated in a simulator including the same two disturbances, while in the **Case B** the initial conditions are found optimizing with PIKAIA a model with just J_2 effects, and then propagated in a simulator with J_2 and drag perturbations.

The improvement obtained in Case A is small. These results could have been foreseen, in fact, under the effects of a dissipative force like air drag, a periodic motion should not be expected.

6.3. An alternative approach for compensating drag effects

A different approach can be implemented. The divergence of the two satellites is clearly due to the drag, in particular to the differential effects. The optimization of the model including drag and J_2 has poor results because it finds a maximum fitness after one orbit. After this period, due to the high non-linearity of the process, the initial conditions found do not compensate the natural drift. On the other hand if the maximum of the fitness is searched after a period of N orbits, the resulting initial conditions could compensate the effects of the drift for a pre-defined number of orbits.

In such way, the relative position is guaranteed to be repeated after N orbits, but not before and after.

A first example is reported for N=50. At a first glance, a propagation for 100 orbits seems to give the same poor results as for the previous cases. This is not true, in fact, focusing on the trajectory corresponding to the first 50 orbits, it can be seen that the formation maintains a bounded trajectory, as shown in Fig. 119 and Fig. 121, and more in detail in the zooms of Fig. 120 and Fig. 122, showing the "go-away-and-come-back" motion.

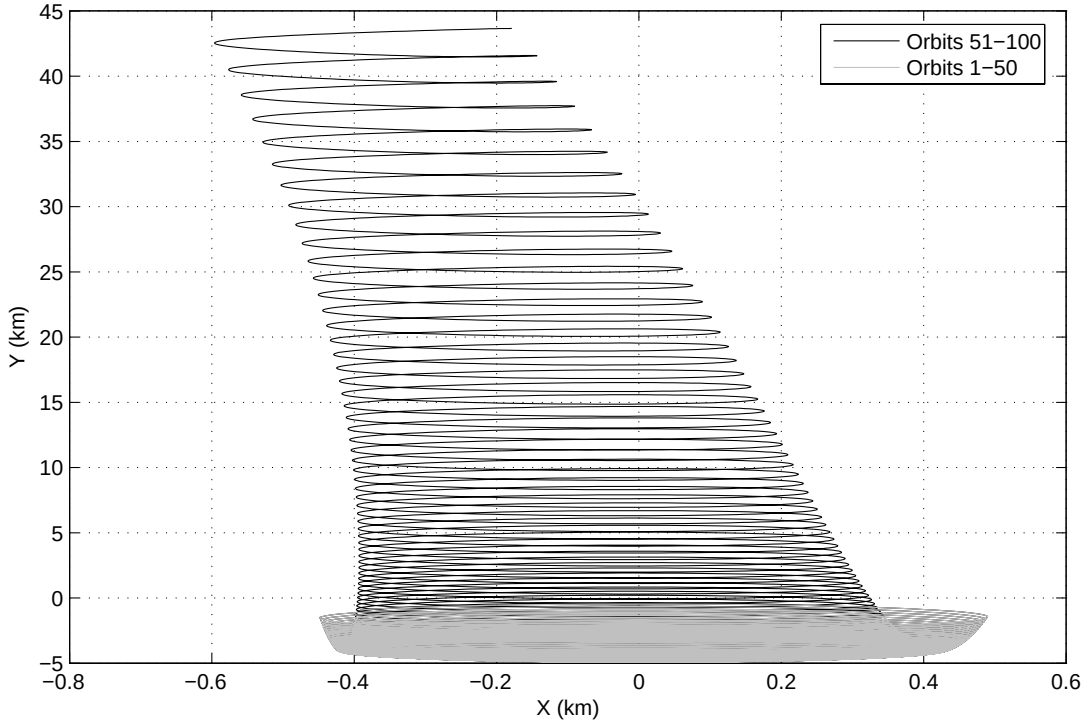

Fig. 119 XY projection of relative orbits obtained by GA conditions with request of being bounded for N=50 orbits

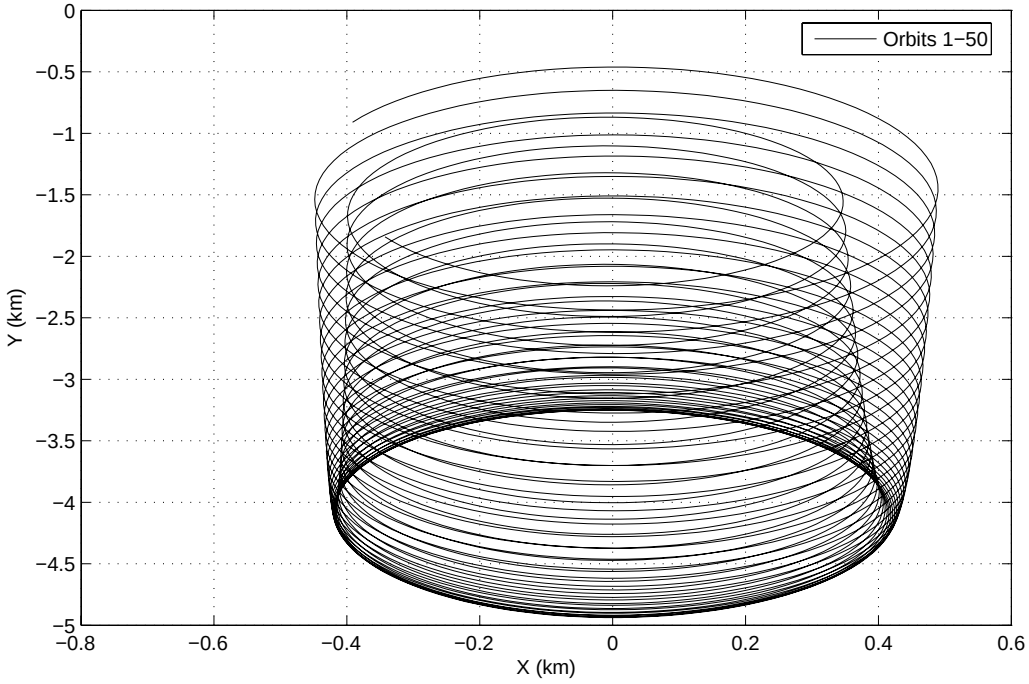

Fig. 120 Zoom of the XY projection of relative orbits obtained by GA conditions with request of being bounded for N=50 orbits

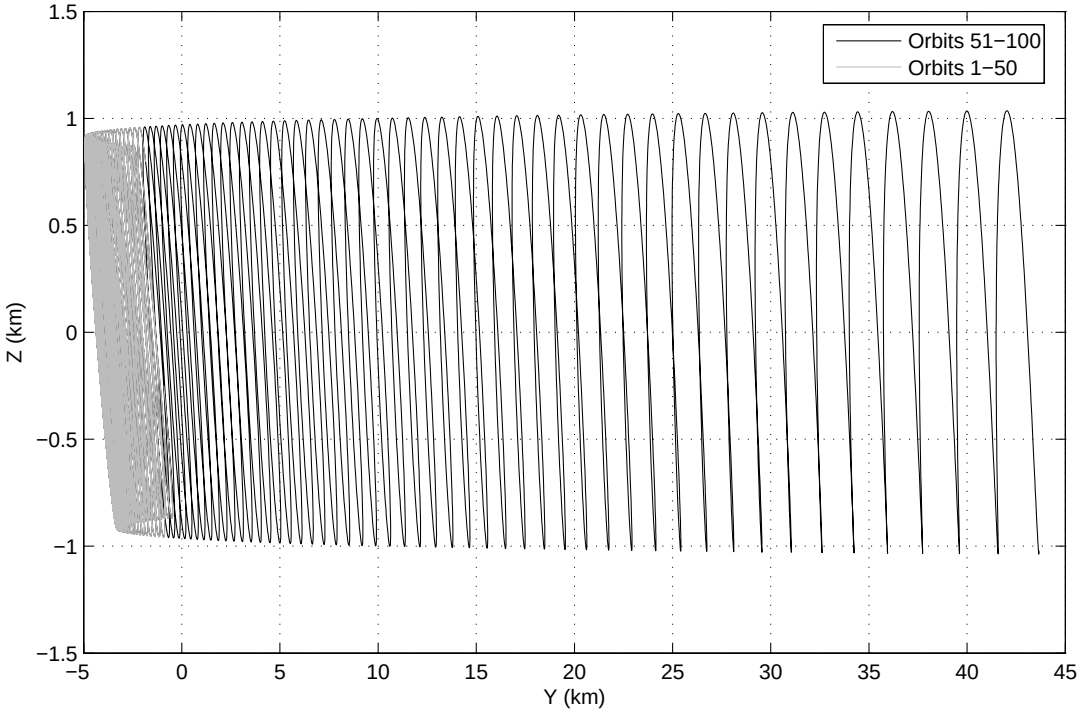

Fig. 121 YZ projection of relative orbits obtained by GA conditions with request of being bounded for N=50 orbits

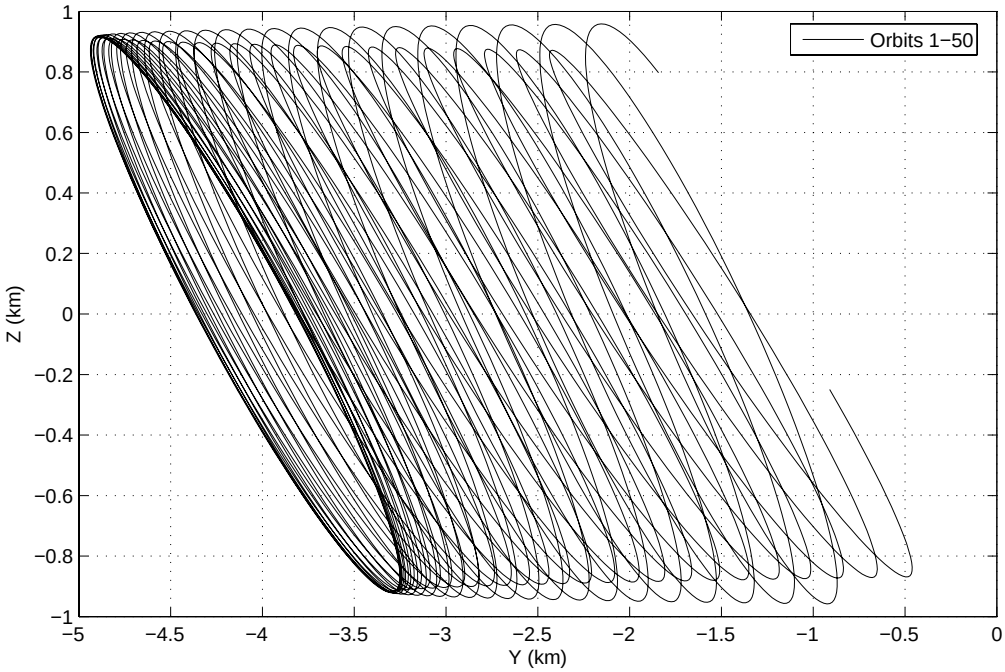

Fig. 122 Zoom of the YZ projection of relative orbits obtained by GA conditions with request of being bounded for N=50 orbits

So the two satellites do not follow a periodic motion, but during the first 50 orbits they drift apart and then get closer again. That's the best one can expect to obtain in this situation. After the first 50 orbits, the formation definitely breaks. Fig. 123 clearly represents this phenomenon.

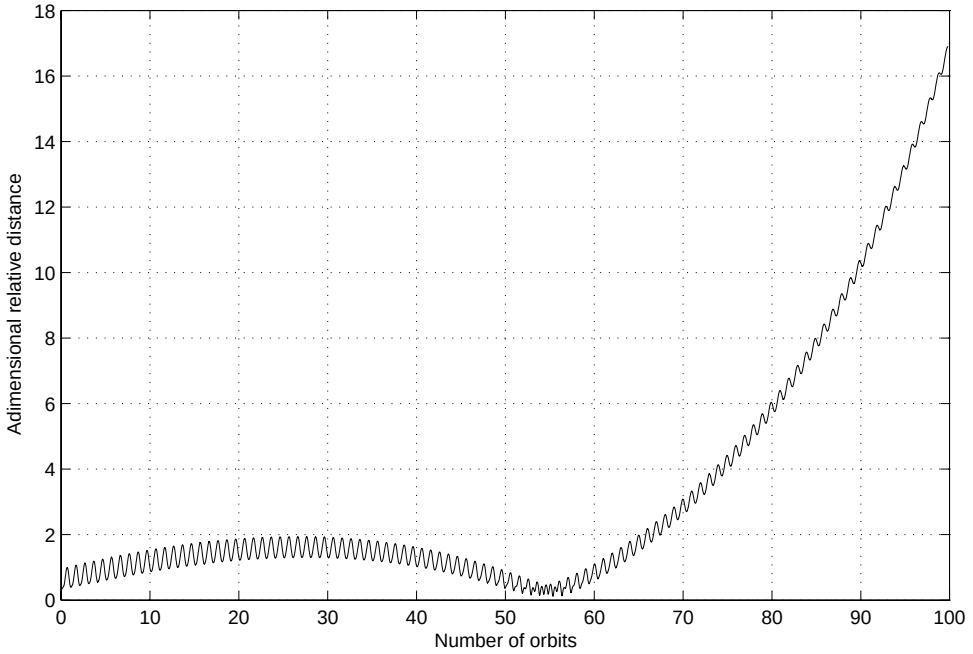

Fig. 123 Adimensional relative distance for N=50 case

Of course one can choose N=100. Fig. 124 and Fig. 125 show again the “going-away-and-coming-back” behaviour.

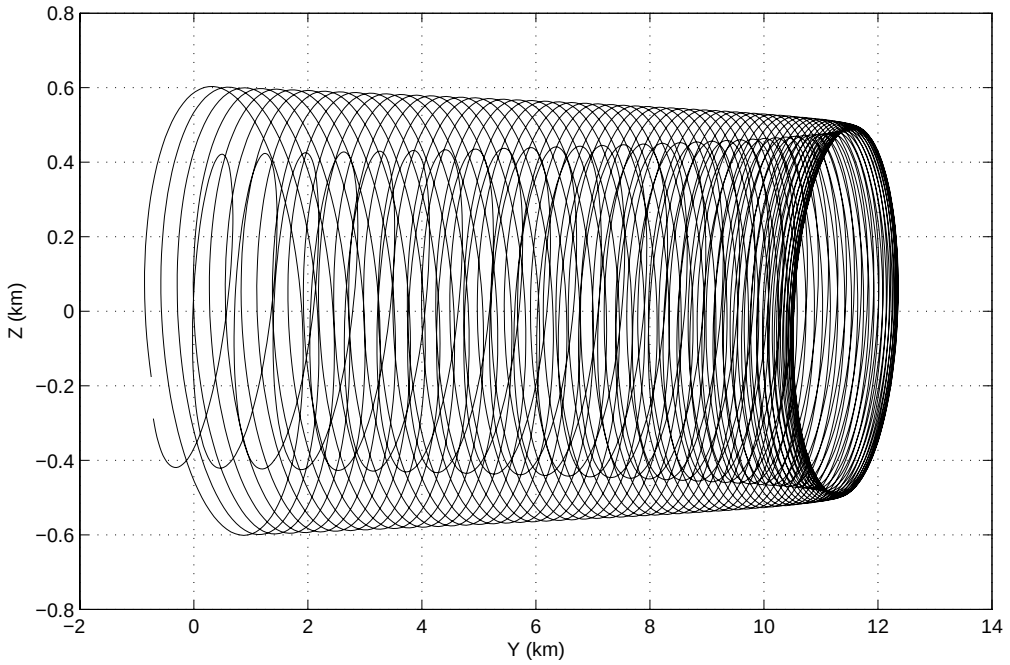

Fig. 124 XY projection of relative orbits obtained by GA conditions with request of being bounded for N=100 orbits

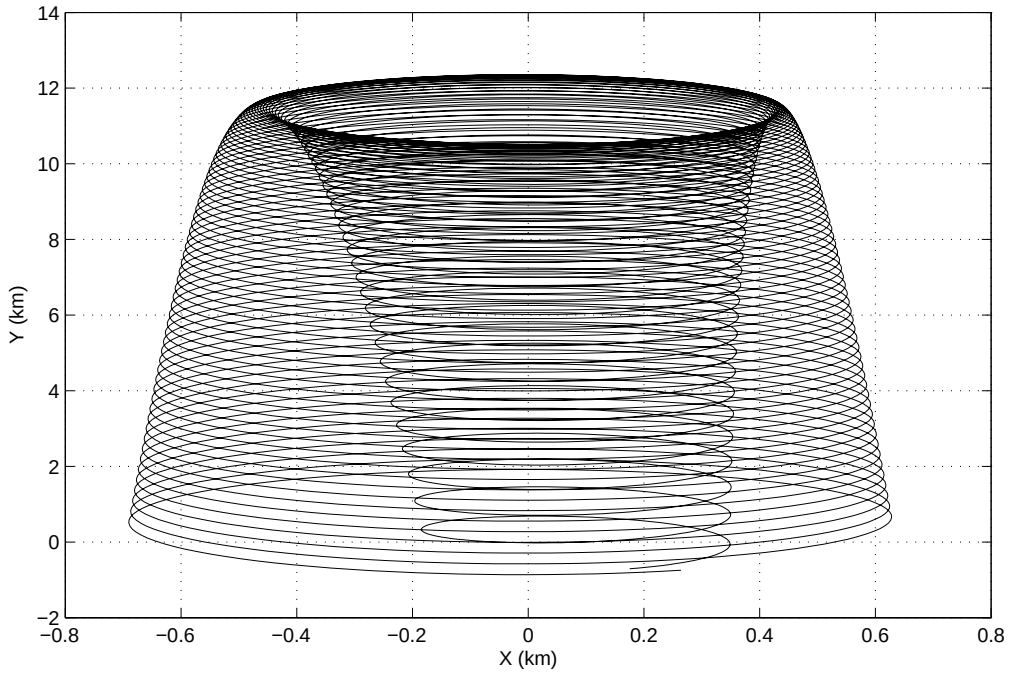

Fig. 125 YZ projection of relative orbits obtained by GA conditions with request of being bounded for N=100 orbits

It is clear that the higher is the number N of orbits considered in the optimization, the harder is to have the satellites close not just at the N^{th} orbit but in every orbit between 0 and N. In other words, the "coming back" is ensured, but it isn't possible to limit how far the satellites go. The ideal number N to be used in the optimizer depends just on the requirements of the particular mission (Fig. 126).

Case A (N=1) is to be preferred if the attention is focused on the first 10, 20 orbits. Case B (N=50) is the right choice is one wants the formation to be bounded for a higher number of orbits, let say 40-70 orbits. Last, if the aim is to have the two satellites close after 70 or more orbits, case C (N=100) has to be chosen.

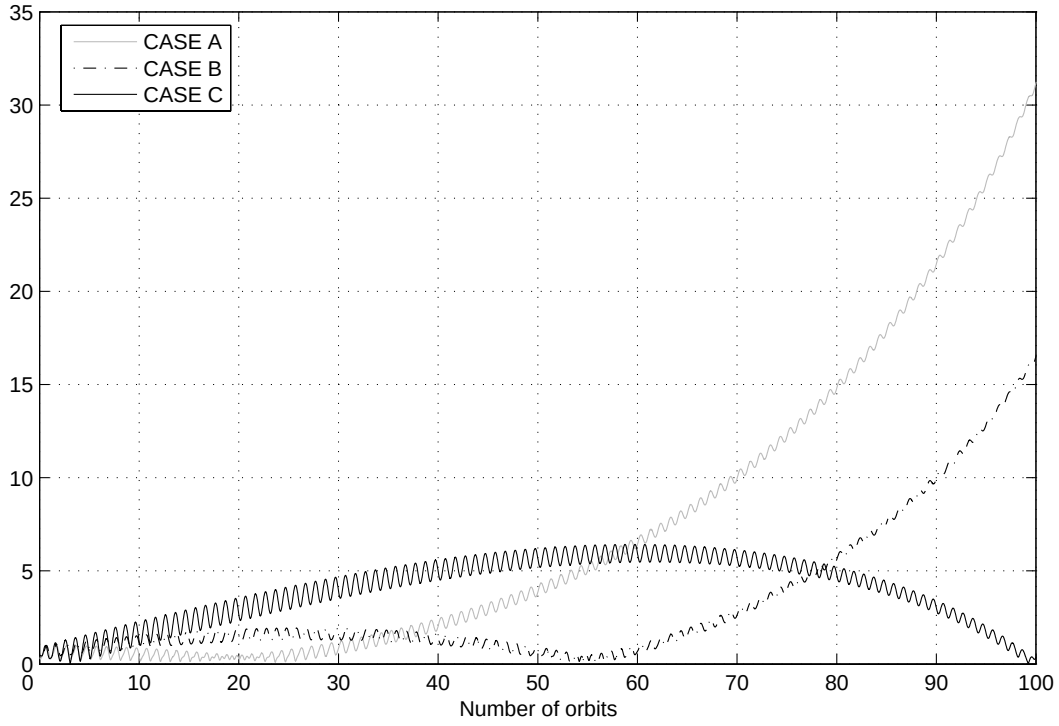

Fig. 126 Comparison among adimensional relative distance for CASE A (N=1), CASE B (N=50) and CASE C (N=100)

6.4. Variations of drag effects for different altitudes.

What deduced in paragraph 6.3 is valid for very low Earth orbits. For these orbits the air density has such a great value that the effects of drag are really evident. But things change rapidly as the study is moved to higher orbits. The orbits considered in this chapter have the following parameters:

$$a=(6378+h)\ \text{km}$$

$$e=0.00118$$

$$i=97.87°$$

$$\omega=90°$$

$$\Omega=270°$$

$$\theta_0=0°$$

where *h* is the altitude above the Earth surface. These altitudes are chosen to be 300 km, 350 km, 400 km, 450 km, and 500 km. As usual, two cases are examined for each altitude:

Case A: the initial conditions are found optimizing with PIKAIA a model with just J_2 perturbation, and then propagated in a simulator with just J_2 perturbation.

Case B: the initial conditions are found optimizing with PIKAIA a model with J_2 perturbation, and then propagated in a simulator with J_2 and drag perturbations.

The aim is to find out when the influence of drag comes at end. Above that altitude, the model optimized in PIKAIA can be chosen to include just J_2 perturbation without introducing significant errors.

h =300 km:

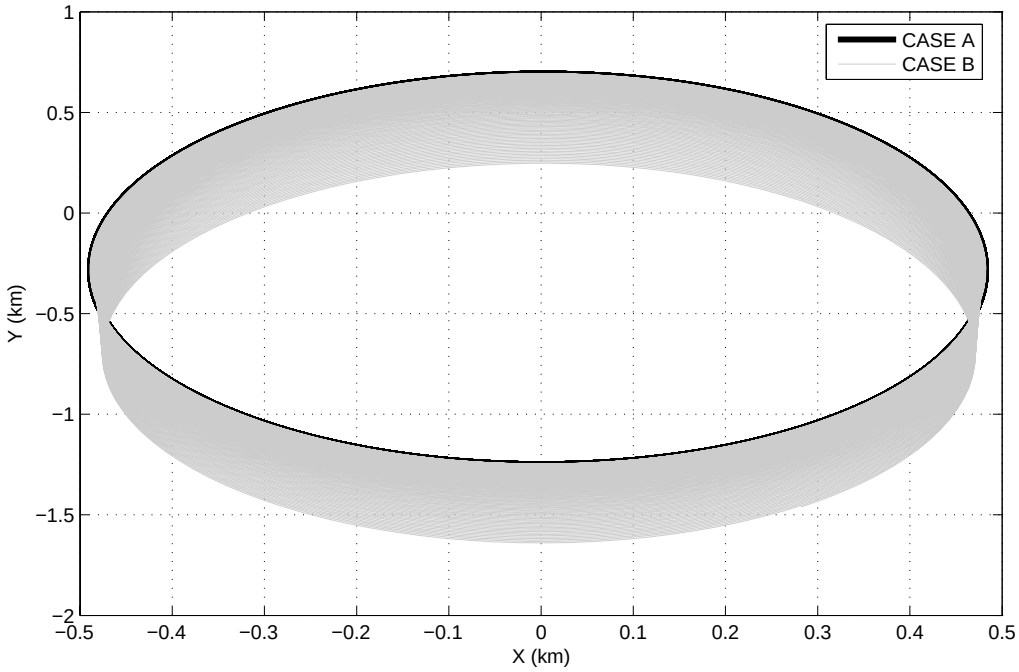

Fig. 127 XY projection of relative orbit with and without including drag perturbation (h=300 km)

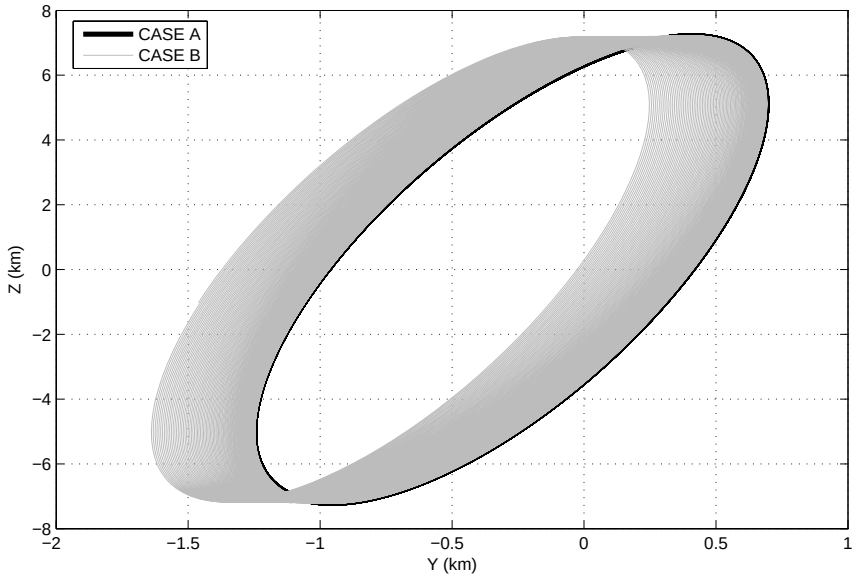

Fig. 128 YZ projection of relative orbit with and without including drag perturbation (h=300 km)

Under the drag effect, the drift appears to be mainly localized on the Y axis. The comparison between the two cases can be then accomplished using the plots of:

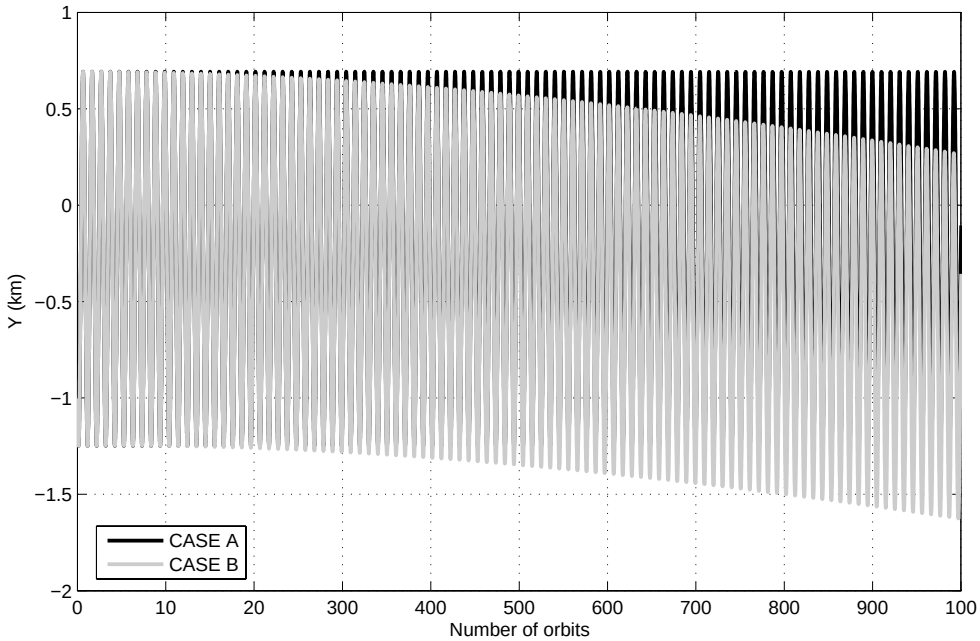

Fig. 129 Y component with and without including drag perturbation (h=300 km)

It is evident how at *h*=300 km the effects of air drag are much weaker.

h= 350 km:

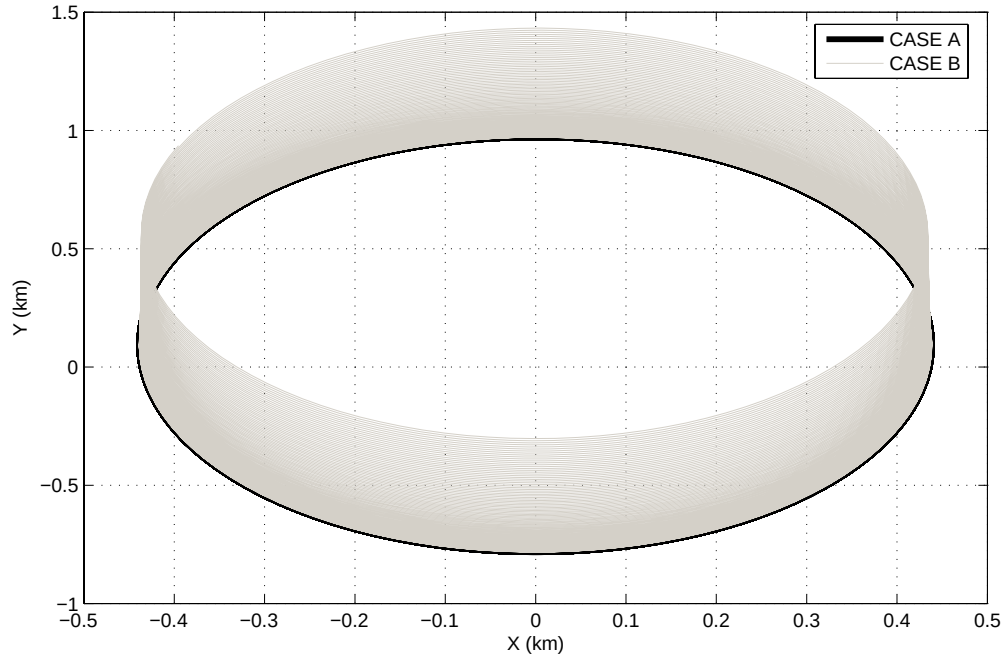

Fig. 130 XY projection of relative orbit with and without including drag perturbation (h=350 km)

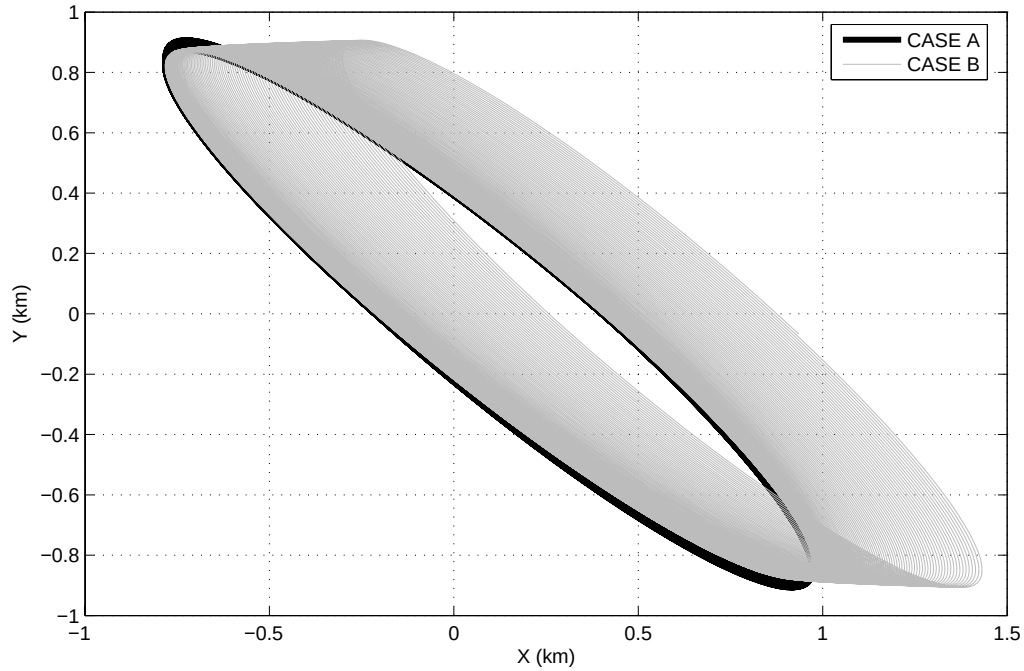

Fig. 131 YZ projection of relative orbit with and without including drag perturbation (h=350 km)

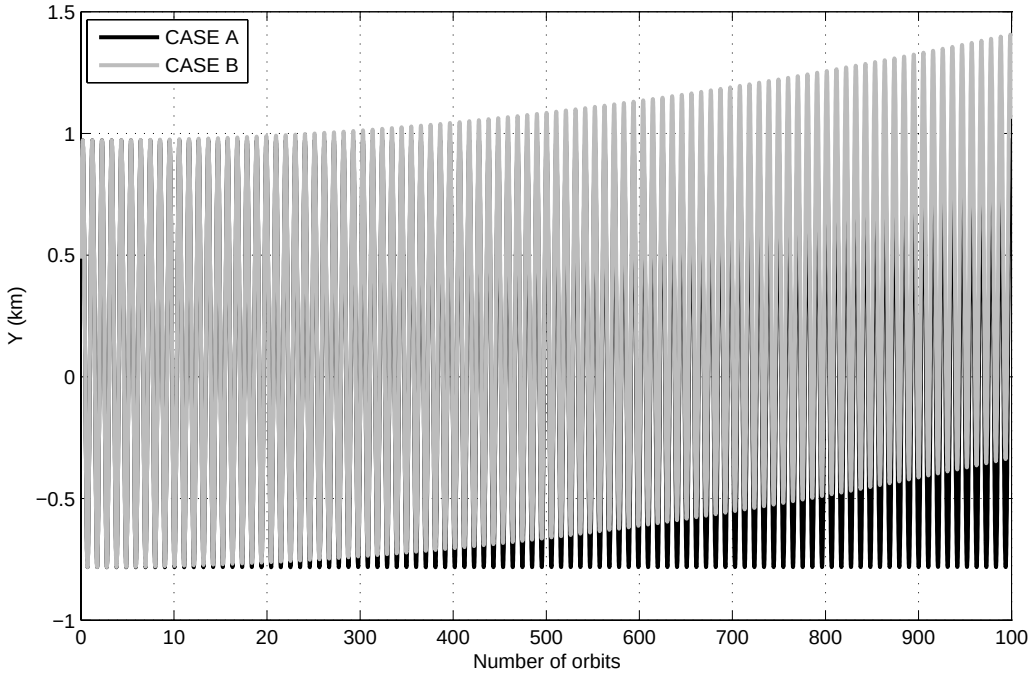

Fig. 132 Y component with and without including drag perturbation (h=350 km)

h= 400 km:

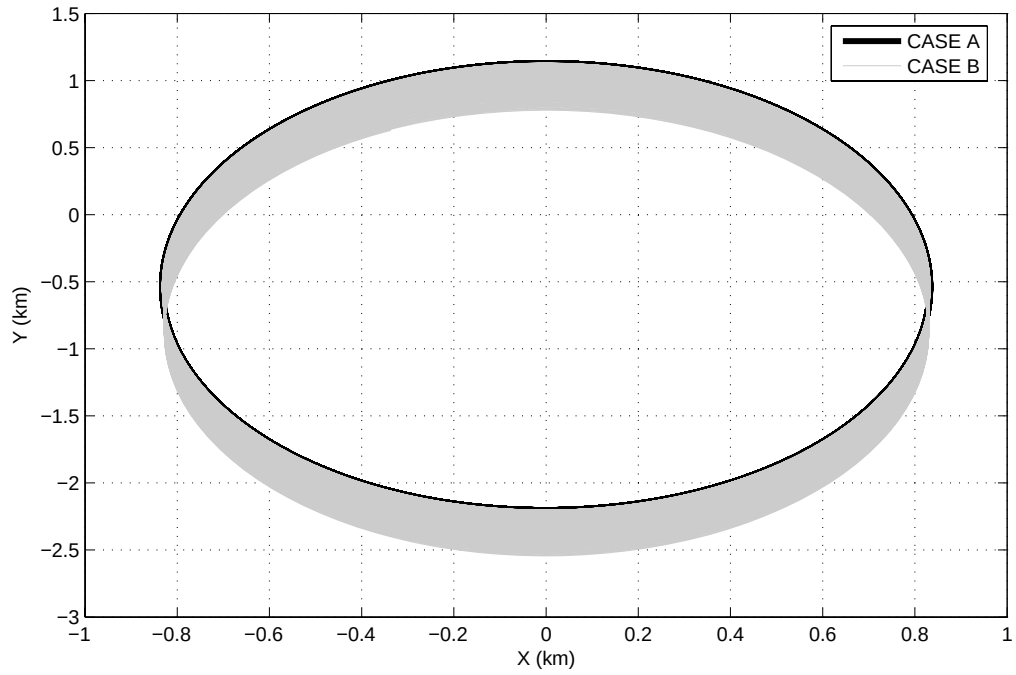

Fig. 133 XY projection of relative orbit with and without including drag perturbation (h=400 km)

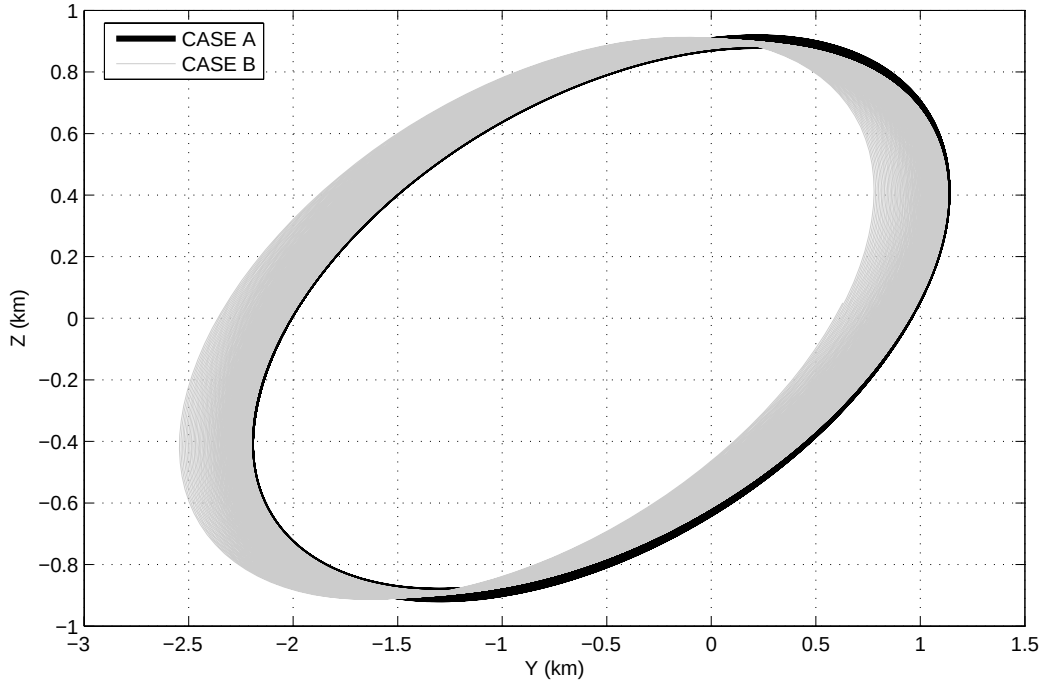

Fig. 134 YZ projection of relative orbit with and without including drag perturbation (h=400 km)

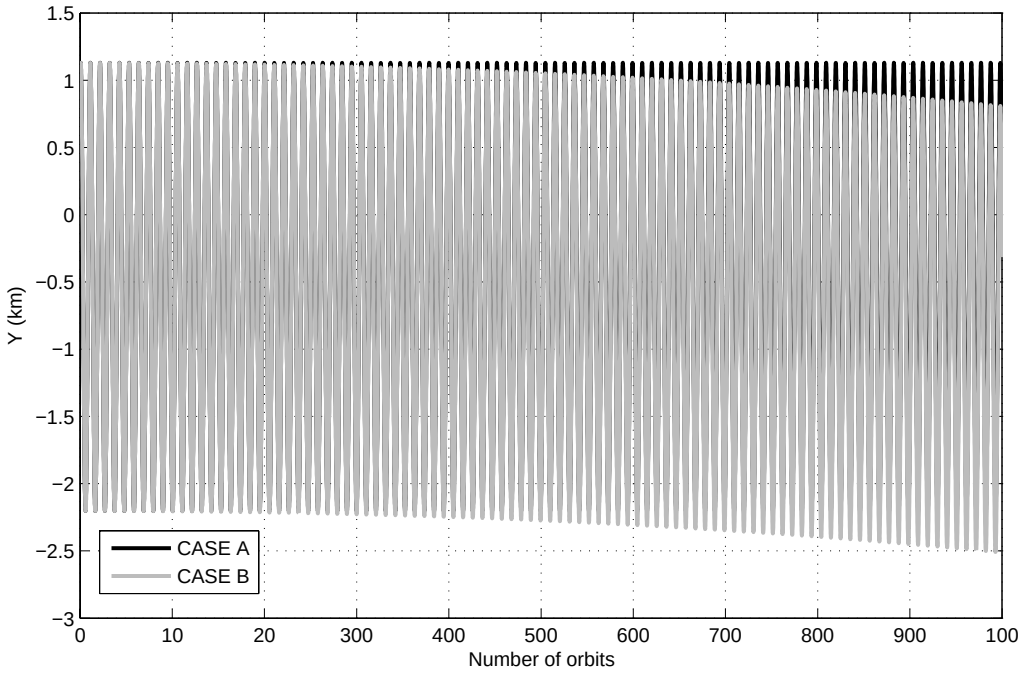

Fig. 135 Y component with and without including drag perturbation (h=400 km)

h= 450 km:

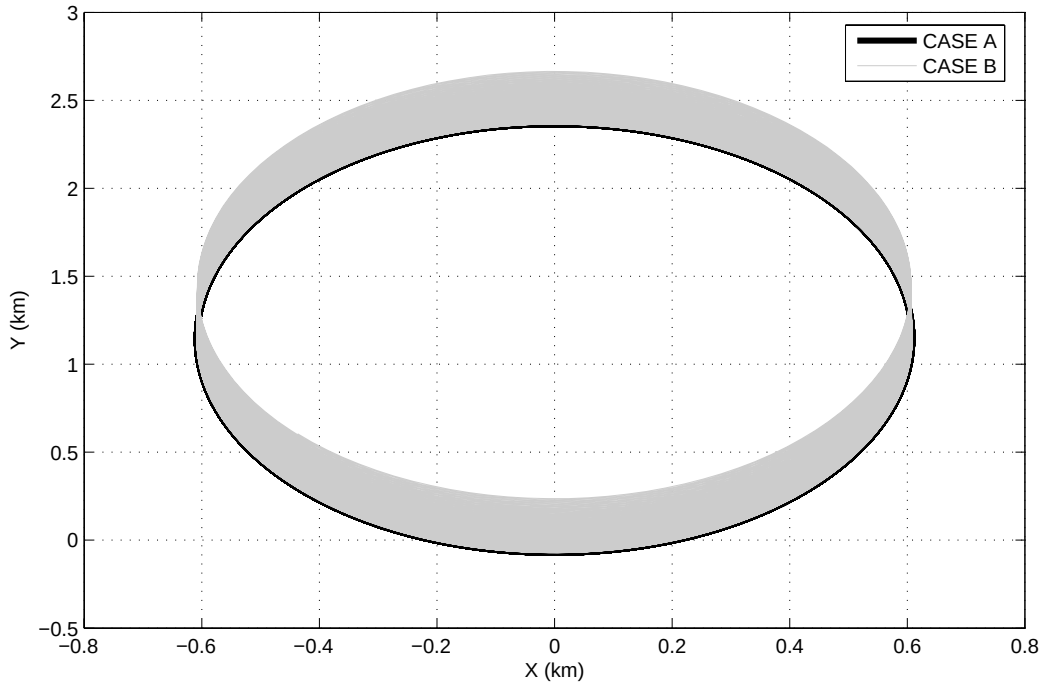

Fig. 136 XY projection of relative orbit with and without including drag perturbation (h=450 km)

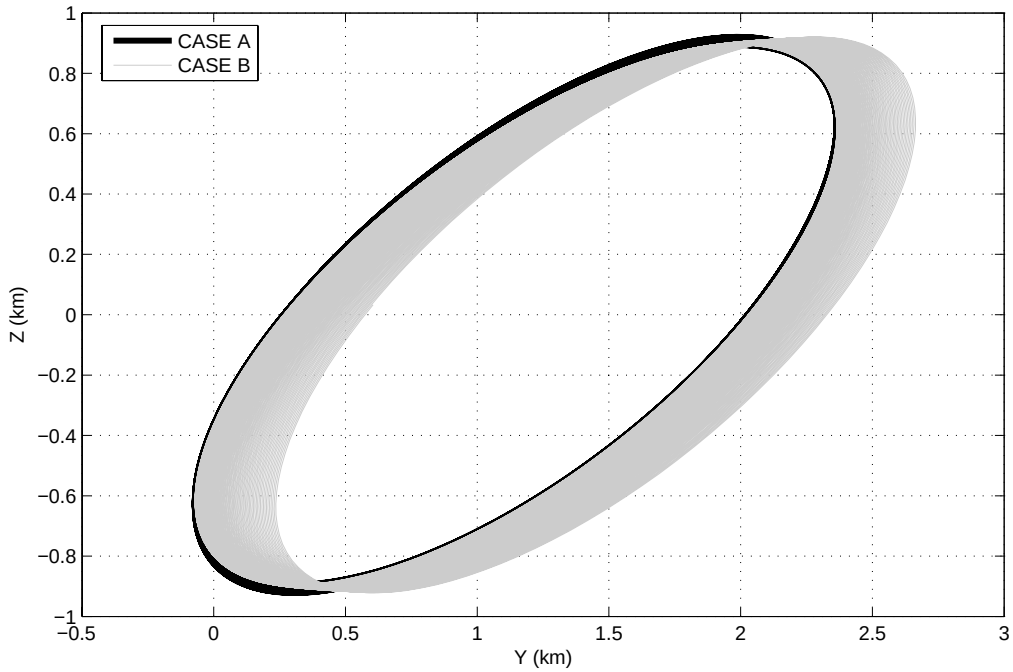

Fig. 137 YZ projection of relative orbit with and without including drag perturbation (h=450 km)

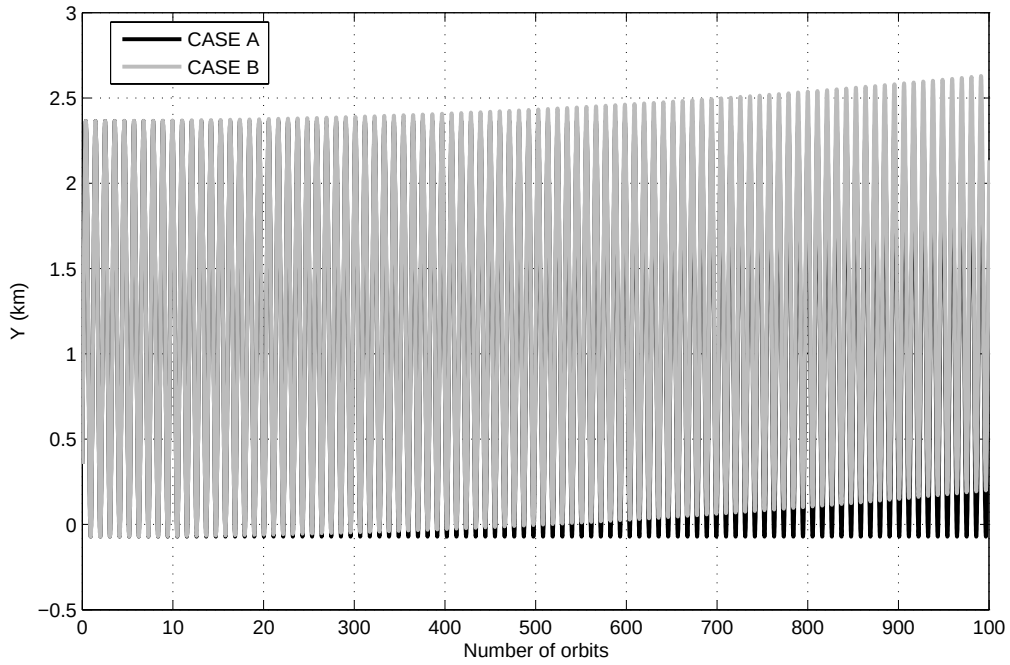

Fig. 138 Y component with and without including drag perturbation (h=450 km)

h= 500 km:

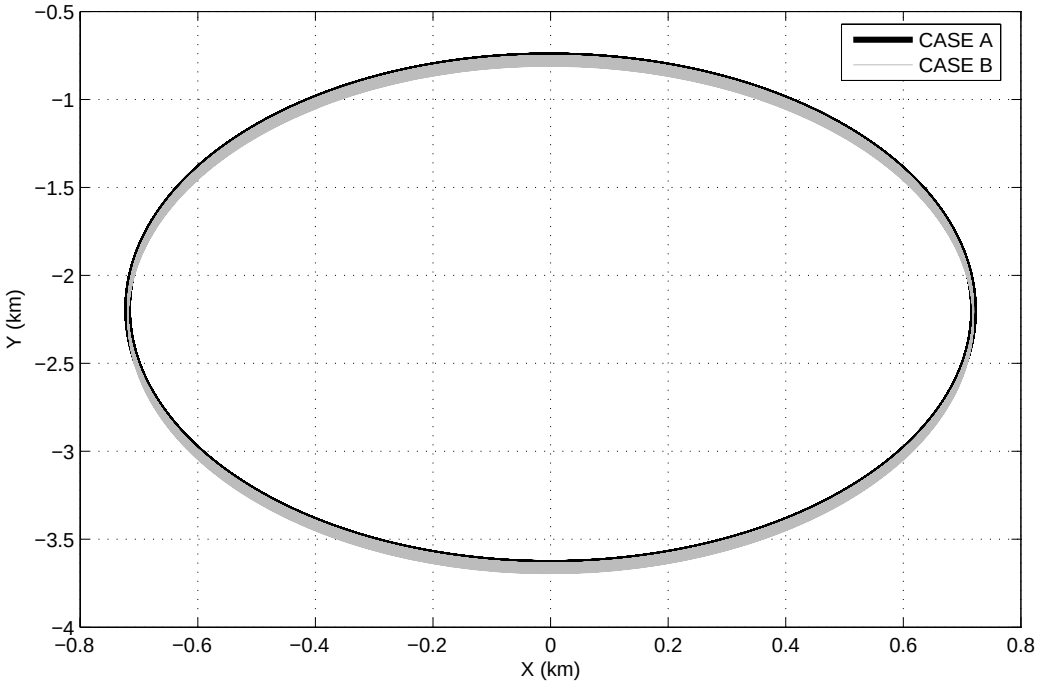

Fig. 139 XY projection of relative orbit with and without including drag perturbation (h=500 km)

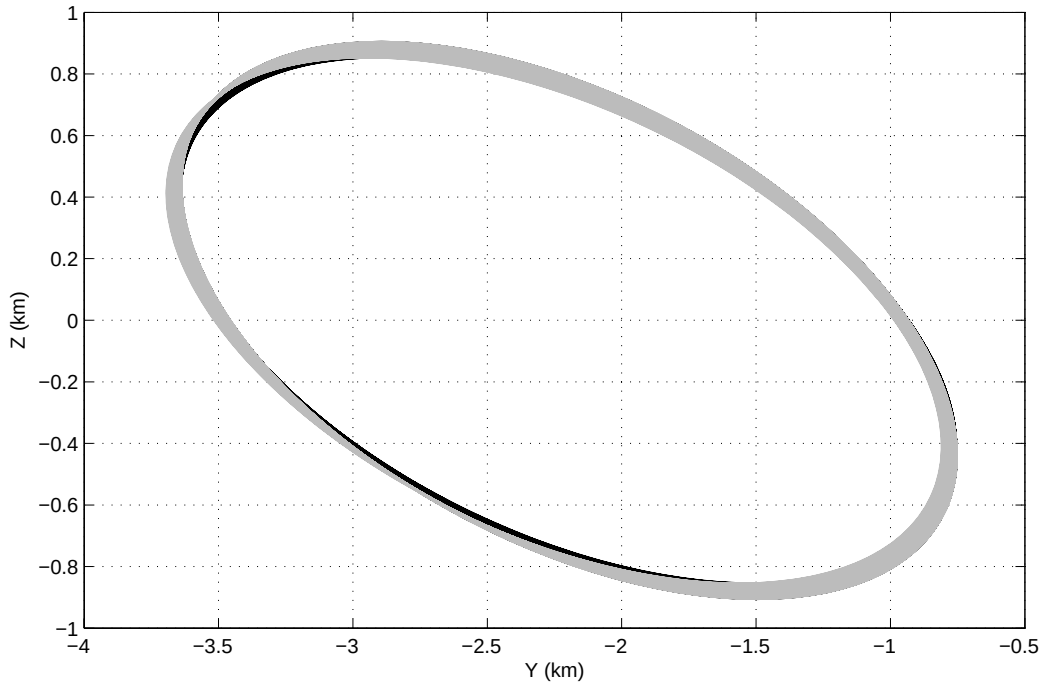

Fig. 140 YZ projection of relative orbit with and without including drag perturbation (h=500 km)

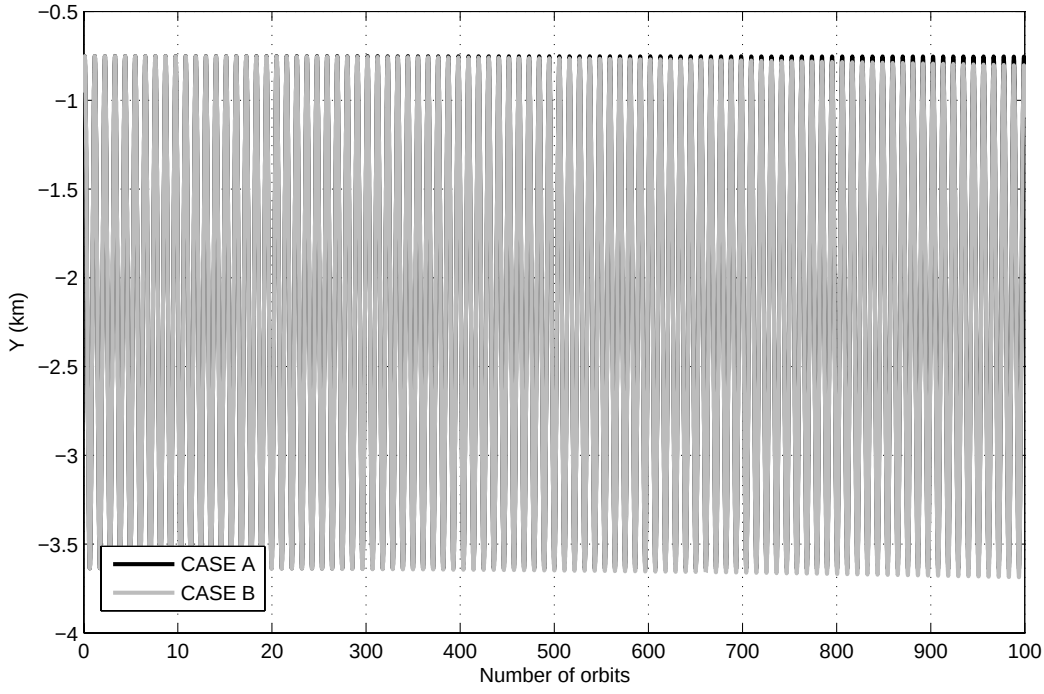

Fig. 141 Y component with and without including drag perturbation (h=500 km)

For this last altitude the two cases are almost completely overlapped. Looking at the adimensional relative distance as defined in

Eq. 63, only a zoom can evidence the small differences, shown in Fig. 142.

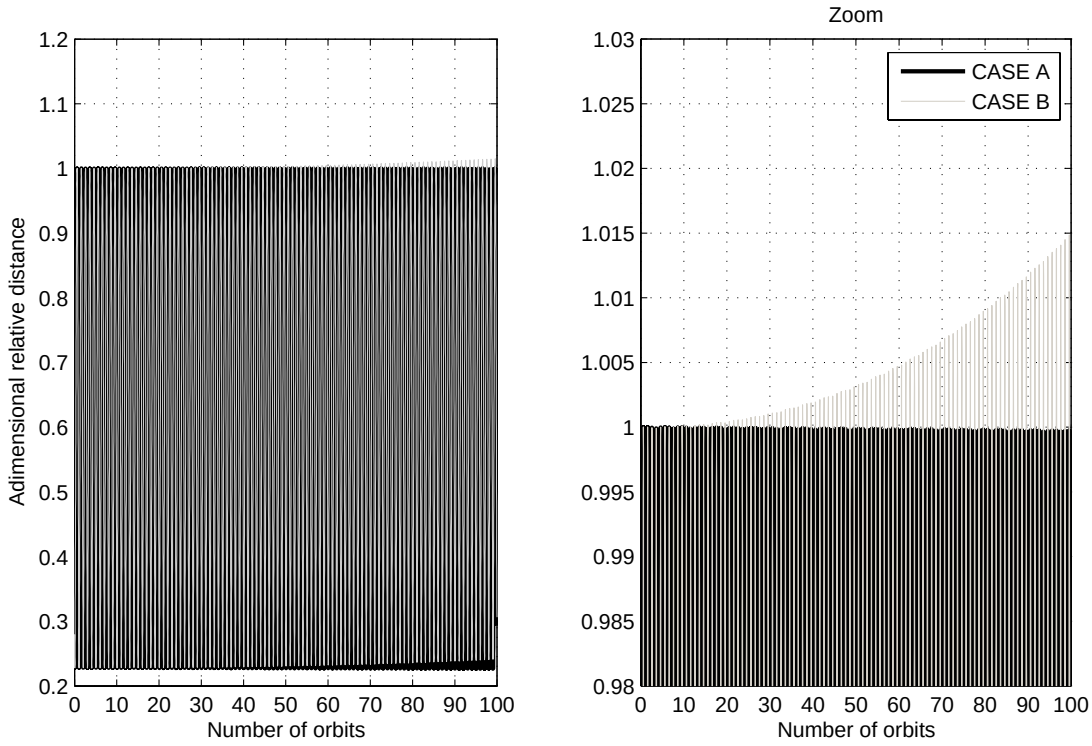

Fig. 142 Adimensional relative distance (left) and a zoom (right) for h=500 km

This results allow one to consider the drag effects irrelevant for $h > 500km$. For lower altitudes, what exposed in Chapter 3 on the existence of invariant orbits must be carefully reviewed. Drag has a very weak dependence on orbit inclination. This means the disturbances shown in the preceding figures are the same for a critical inclined orbit, or for an orbit inclined at the "weak J_2 effect" inclination of 50°.

The considerations and conclusions reported in Chapter 3 are therefore completely valid only for $h > 500km$. For $h < 500km$ there will be disturbs whose intensity grow stronger and stronger as the altitude diminishes.

For $h < 500km$ it is possible to act in various ways. As it was shown for the case of $h = 200km$, the drag is so strong that performing the optimization with just J_2 perturbation would lead to completely breaking formations. The suggested strategy is therefore to include also drag perturbation in the model optimized, but to find the maximum fitness not after one orbit, but after N orbits. It has been underlined that this results in an advantage after N orbits, but that before the N^{th} orbit the satellites can drift apart.

For higher orbits, for example $h = 300km$, drag effect are present but already much weaker. This means the drifting apart of the formation, whose initial conditions are calculated by optimizing a model including just J_2, is not so relevant. Moreover it means that calculating the initial conditions

by the means of an optimization considering drag and N orbits propagation can result in a closer formation after N orbits, but in a worst performance before and after the N^{th} orbit. So, according to the mission requirements, one could prefer to use the conditions calculated considering just J_2 effect even for (not very) low Earth orbits. In fact in this case the drifting apart of the satellites is almost linear and constant. Consider (Fig. 143) four situations in which the propagation is accomplished using a model with drag and J_2, but the initial conditions are calculated optimizing a model with the following characteristics:

CASE A: just J_2 perturbation considered in PIKAIA;

CASE B: J_2 and drag perturbation considered in PIKAIA (fitness function evaluated after 10 orbits);

CASE C: J_2 and drag perturbation considered in PIKAIA (fitness function evaluated after 50 orbits);

CASE D: J_2 and drag perturbation considered in PIKAIA (fitness function evaluated after 100 orbits).

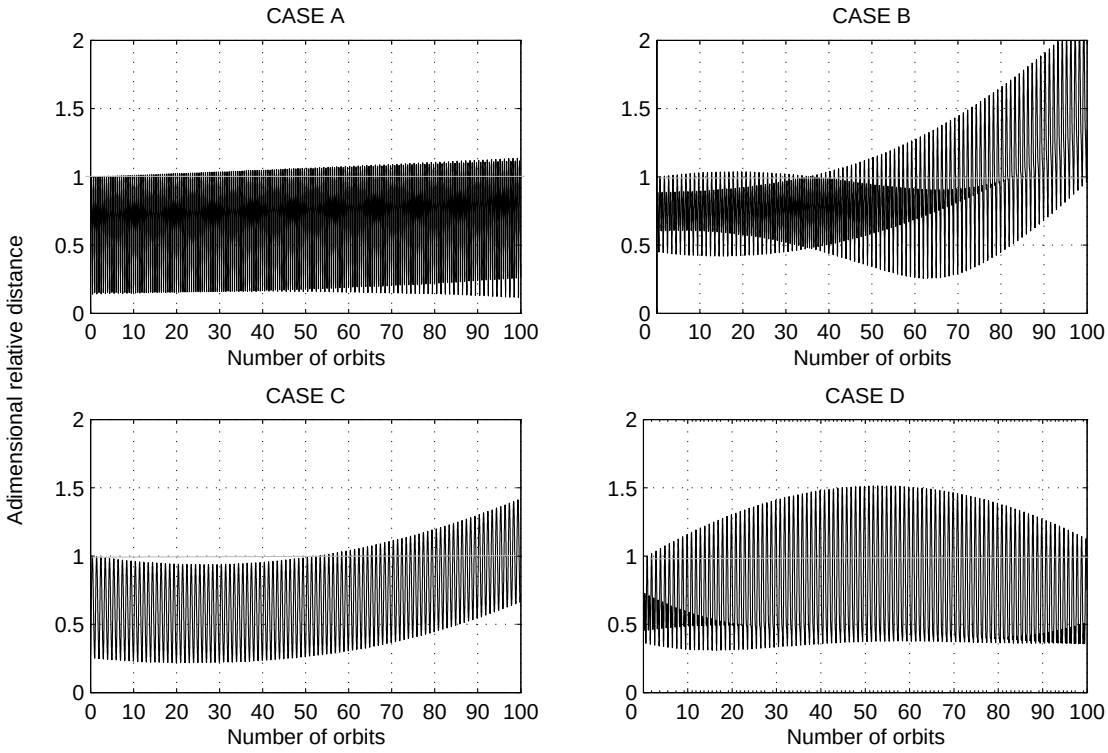

Fig. 143 Four different strategies (h=300 km)

For example, case C is better then case A at the 50^{th} orbit, but not so clearly for the following orbits. At the 100^{th} orbit the initial conditions calculated by neglecting drag give better results. As already stated, choosing the model to be optimized by the GA depends on the mission requirements.

7. Possible applications

7.1. Limits of possible applications: Differential GPS performances

The approach presented in the previous chapters is based on the knowledge of the initial position and velocity of the two satellites of the formation. These are supplied by the genetic algorithm up to the ninth significant digit. This accuracy is sufficient to provide the condition for bounded ness of the relative orbits, when these are physically admissible (see Chapter **Error! Reference source not found.**).

In this paragraph, the actual limits of position and velocity determination are examined. The most used orbit determination method in the past years has been the offline ground tracking. This technique is being replaced by on board GPS sensors, which ensures precision and autonomy to the spacecraft, two characteristics which make GPS ideal for formation flying. For micro or small satellites, as often the members of the formation are intended, this could be the only mean for orbit determination.

With ground tracking, Doppler effect is used to determine satellite's position and velocity; this is not accomplished in real time, because the precision is proportional to $1/\sqrt{Integrating\ time}$. For specific application as well, like interplanetary missions (which are out of the present field of study), with integrating time of 10^3 seconds (in S-band) the precision on velocity is of the order of cm/s.

The performances of a standalone GPS are also sufficient for an orbit determination. The following data are extracted from [15] and confirmed by [19].

For GPS with SA (Selective Availability) turned off and exploiting the code, the order of magnitude of the errors on position (UERE: User Equivalent Range Error) and velocity (UERRE: User Equivalent Range Rate Error) can be inferred from Table 4.

GPS (no SA)	σ_{UERE} , m	σ_{UERRE} , m/s
	0.5	0.01

Table 4: GPS performances

The errors in Table 4 affect the *absolute* position and velocity of the satellite. The errors on the *relative* position and velocity are of the same order of magnitude, according to the equation for errors on the quantity C, difference of to measures A and B:

$$C = A - B \Rightarrow \sigma_C = \sqrt{\sigma_A^2 + \sigma_B^2}$$

Eq. 64: errors relation

So an error of the order of 1 m on the relative position and of the order of 0.01 m/s on the relative velocity is to be expected. These performances become insufficient for the relative orbit determination. In fact, considering again the results of the GA for initial position and velocity in the case of truly closed orbit discussed in Chapter **Error! Reference source not found.**:

$$x_0 = 0.35\underline{2}274198 \text{ km}$$

$$y_0 = 0.97\underline{7}836554 \text{ km}$$

$$z_0 = \text{-}\underline{8}.48000199\text{E-}003 \text{ km}$$

$$\dot{x}_0 = 2.0\underline{0}000348\text{E-}003 \text{ km/s}$$

$$\dot{y}_0 = \text{-}8.\underline{1}7403519\text{E-}004 \text{ km/s}$$

$$\dot{z}_0 = \text{-}5.0\underline{0}083546\text{E-}003 \text{ km/s}$$

the underlined digits are the precision limit imposed by the sensors. It is evident that with these errors no bounded orbits can be obtained, as shown in Fig. 144, where the initial conditions are all affected by $+1\sigma$ error.

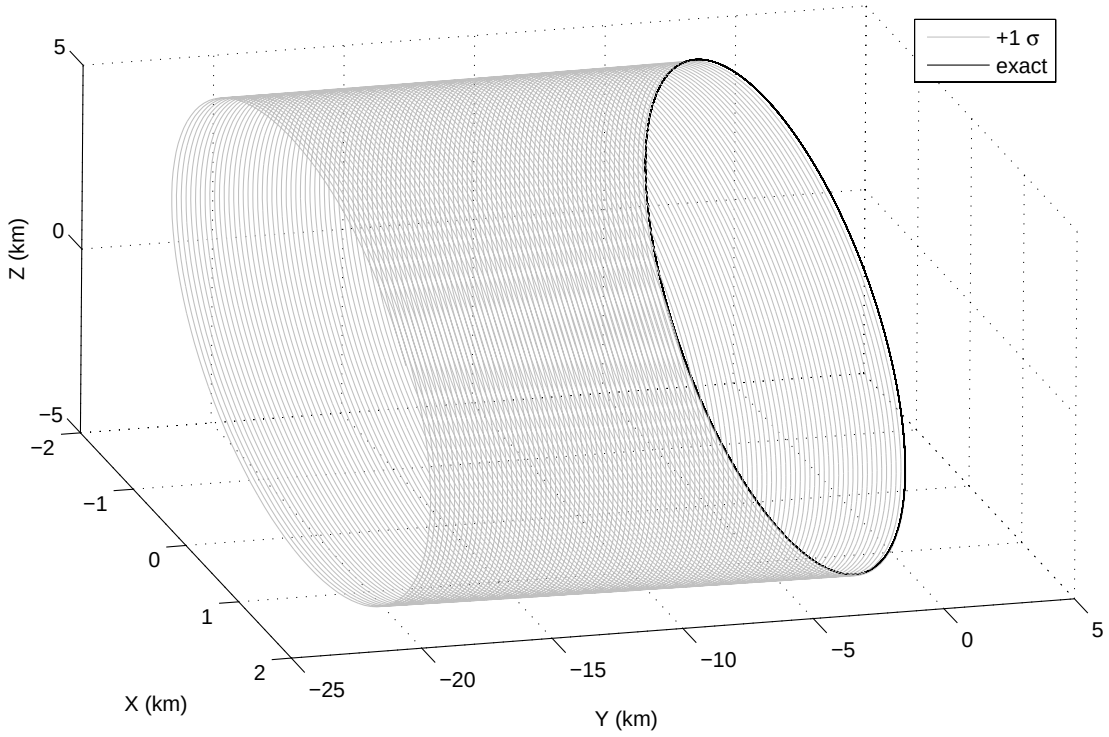

Fig. 144 Propagation of the exact and affected by errors initial conditions

Dealing with GPS sensors mounted on two close orbiting vehicles, the technique of the Differential GPS (DGPS) can be implemented. With this approach, knowing the position of one of the agents, as in the case of large bodies like International Space Station or Space Shuttle (see paragraph 7.2), a certain number of error components can be cancelled being common to both spacecraft (i.e. spatially correlated). More improvements can be achieved exploiting the carrier-phase instead of the GPS signal code. Therefore the best performances are attainable with the CDGPS technique (Carrier Differential Global Positioning System).

The errors in this case are reported in Table 5.

DGPS	σ_{UERE} , m	σ_{UERRE} , m/s
	0.01	0.005

Table 5: CDGPS (Carrier Differential GPS) performances

This precision is still insufficient: the problem is not the error on the position, which is quite low. Fig. 145 and Fig. 146 show how an error of $\pm 1\sigma$ on the initial relative distance doesn't lead to a formation breaking (propagation for 100 orbits).

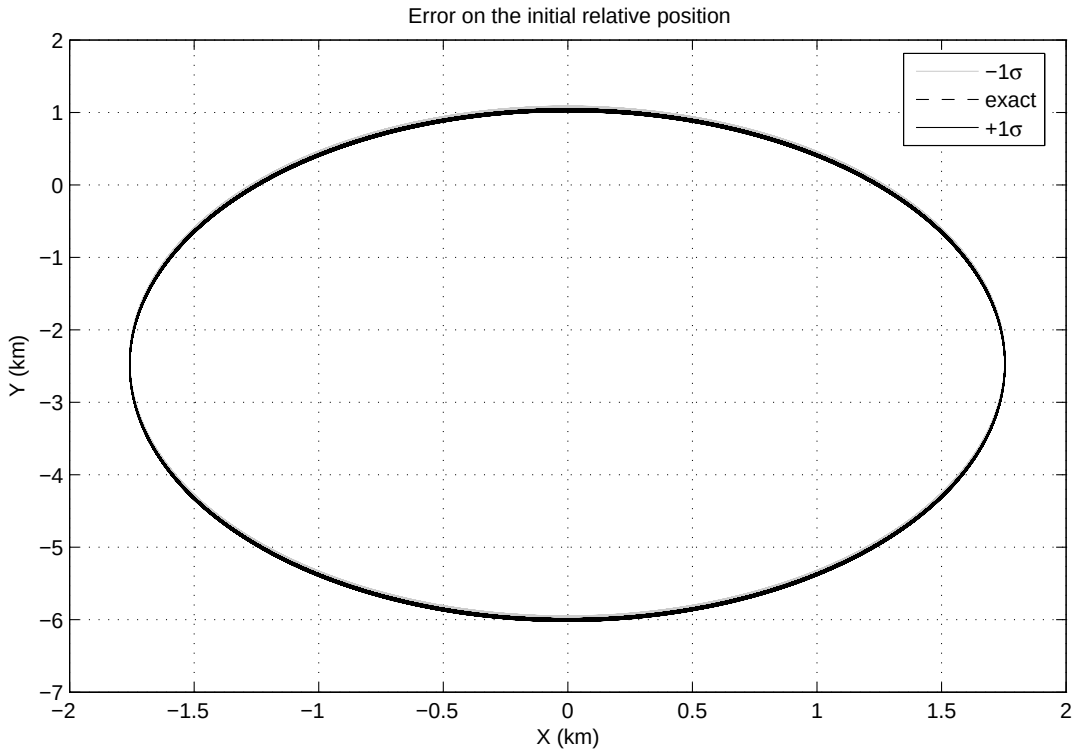

Fig. 145 Propagation of the exact and affected by errors initial position (XY projection)

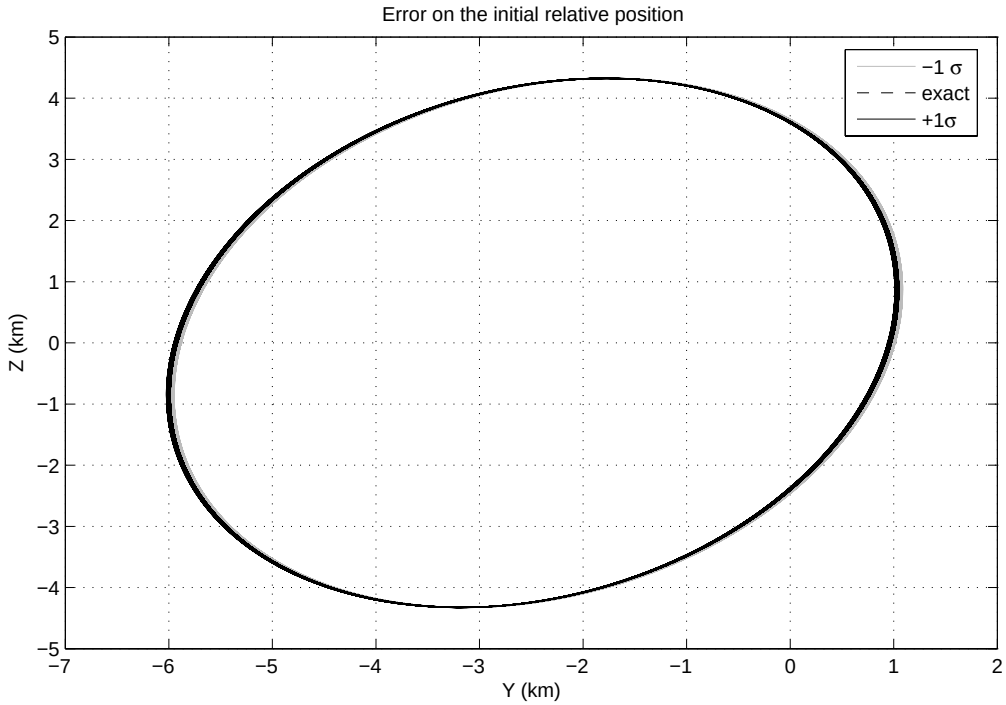

Fig. 146 Propagation of the exact and affected by errors initial position (YZ projection)

The no error case and the ones affected by the truncation on the initial position are almost overlapped. Instead, Fig. 147 and Fig. 148 show that an error of $\pm 1\sigma$ on the initial relative velocity has disruptive consequences on the resulting trajectory (propagation for one hundred orbits).

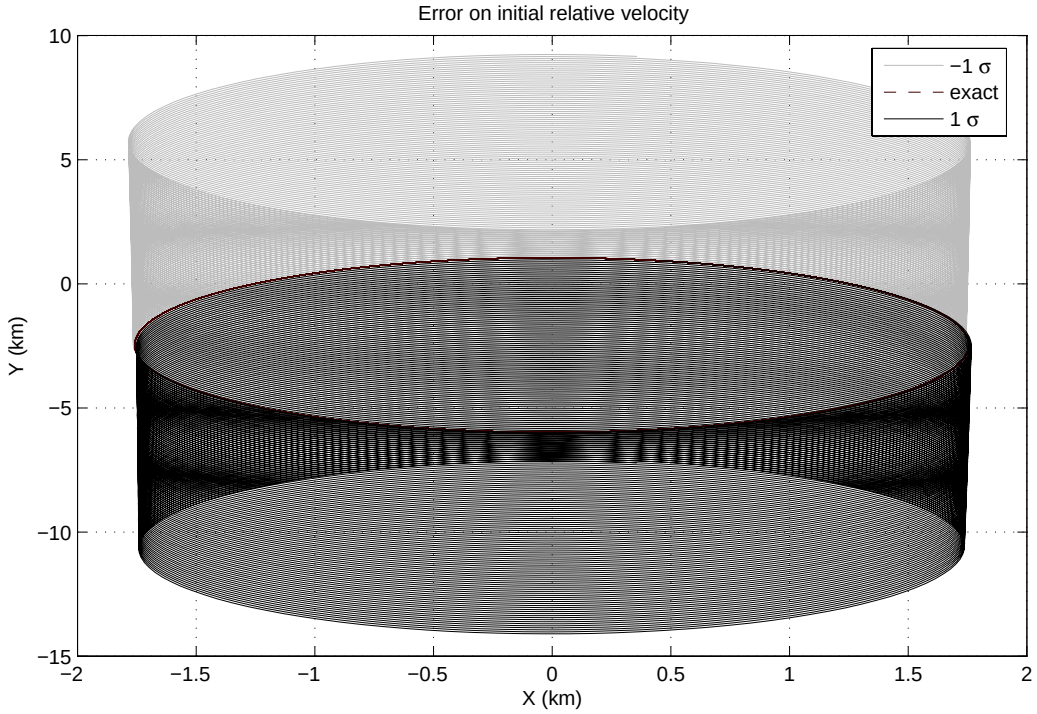

Fig. 147 Propagation of the exact and affected by errors initial velocity (XY projection)

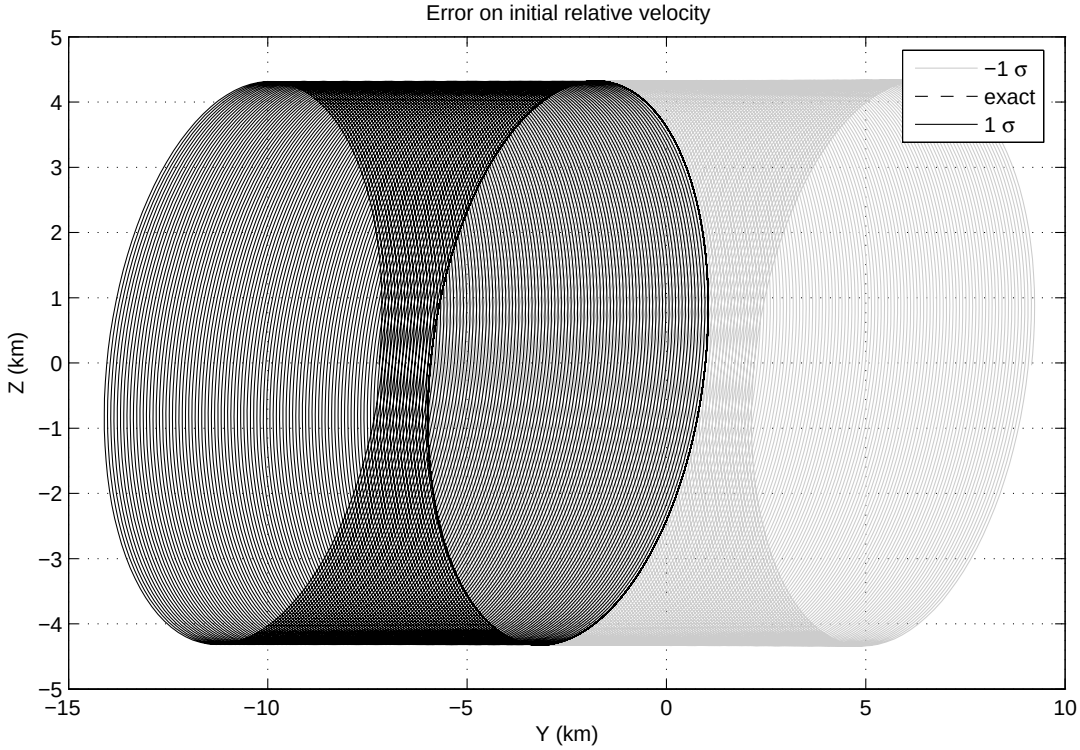

Fig. 148 Propagation of the exact and affected by errors initial velocity (YZ projection)

This analysis brings to an important conclusion: **the initial conditions for bounded relative orbits, as provided by GA or any other numerical or analytical method, need to be necessarily very precise**. With the state-of-the-art technologies, this cannot be achieved. Therefore **the conditions found in Chapters** Error! Reference source not found.**,** Error! Reference source not found. **and 6 have a great theoretic value** but **cannot be used for the actual insertion of the satellites in the proper orbit, wishing they'll keep their periodic motion without control actions.**

Their practical utility is therefore indirect, but still important. When a periodic relative orbit does exist (see Chapter **Error! Reference source not found.**4), a control system must be implemented, because the proper conditions, supplied by GA, cannot be reached with sufficient precision by the GPS sensors. However, **the relative orbits obtained by propagating GA initial conditions can be usefully adopted as reference trajectories for the controller, for example a LQR (Linear Quadratic Regulator)**. In the present work the actual advantages of using the GA orbits as reference for the control system have not been investigated, but we definitely expect a great ΔV saving with respect to other references (generated using other numerical or analytical methods).

7.2. Continuous Visual Health Monitoring of the ISS or STS

In this section a monitoring technique for the Space Shuttle's (STS) external structures is proposed. The approach could be employed to detect dangerous failures representing a serious hazard in the re-entry phases. Not many changes are needed to apply the same method for the International Space Station (ISS) when its altitude is comparable to the altitude of the STS orbit.

The proposed methodology consists of a very small satellite orbiting around ISS or STS. The payload of this nano-satellite should be simply a camera, recording images of the structure's external conditions and transmitting them to the crew. In its trajectory around these large artificial satellites, the camera could detect possible failures in the external structures. Main subsystems which the nano-satellite should be provided of are surely an AOCS (Attitude and Orbital Control System) to keep the right pointing of the camera, a micro-propulsion system to ensure the required manoeuvres and a data-handling and telecommunications subsystems. For simplicity sake, ballistic coefficients of the two members of the formation (ISS or STS and monitoring satellite) are supposed to be the same.

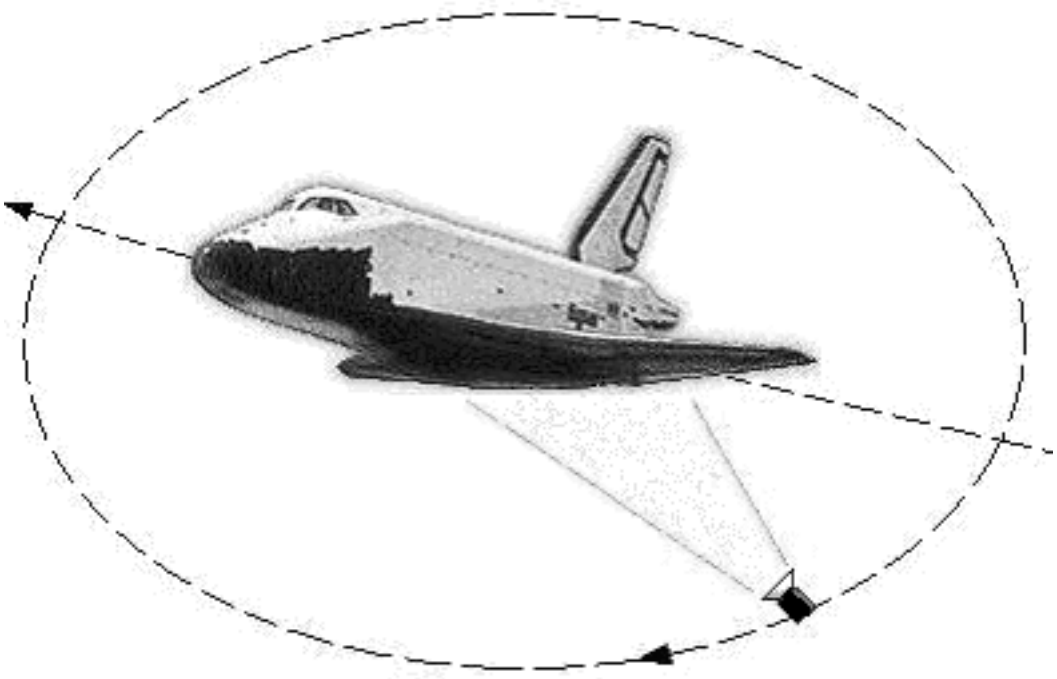

Fig. 149 Simplified scheme of the proposed mission

From the NORAD (North American Aerospace Defence Command) web-site, the Two-Lines Elements (TLE) of the ISS can be easily accessed. Here the TLEs corresponding to a particular epoch are selected. For the ISS:

```
1 25544U 98067A   98324.28472222 -.00003657  11563-4  00000+0 0    10
2 25544  51.5908 168.3788 0125362  86.4185 359.7454 16.05064833    05
```

The corresponding orbit parameters are:

$$a = 6638.551 \text{ km}$$
$$e = .012536$$
$$i = 51.5908°$$
$$\varpi = 86.419°$$
$$\Omega = 168.379°$$
$$M_0 = 359.745°$$

At this epoch the ISS is at a quite low altitude; usually it ranges between 250 km and 400 km. Obviously what we consider at 250 km is not valid for a 400 km height case, where the drag is much less important. The following simulations will be based on this set of orbital parameters.
The TLE of the Space Shuttle can be treated the same way:

```
1 27647U 03003A   03016.64683704  .00000000  00000-0  00000+0 0    13
2 27647  39.0169 229.2417 0012696 352.7112   7.4097 15.97530540    04
```

Again the orbital parameters:

$$a = 6659.407 \text{ km}$$
$$e = .0012696$$
$$i = 39.0169°$$
$$\omega = 352.711°$$
$$\Omega = 229.242°$$
$$M_0 = 7.41°$$

These are two reference orbits in which both J_2 and drag perturbations have a great impact. As exposed in Chapter **Error! Reference source not found.**, for altitudes below 300 km, any attempt to find bounded orbits without including drag effect result in a complete failure. So the employment of analytical formulations such as Schaub's J_2 invariant orbits [7], or Kolemen et al. epicyclic elements [14] or [22] is not useful. Moreover remember that a GA optimization where the fitness function is calculated after one orbit doesn't give any advantage, for the reasons explained in Chapter **Error! Reference source not found.**. In Fig. 150, Fig. 151 and following figures the black dots represent the STS and ISS.

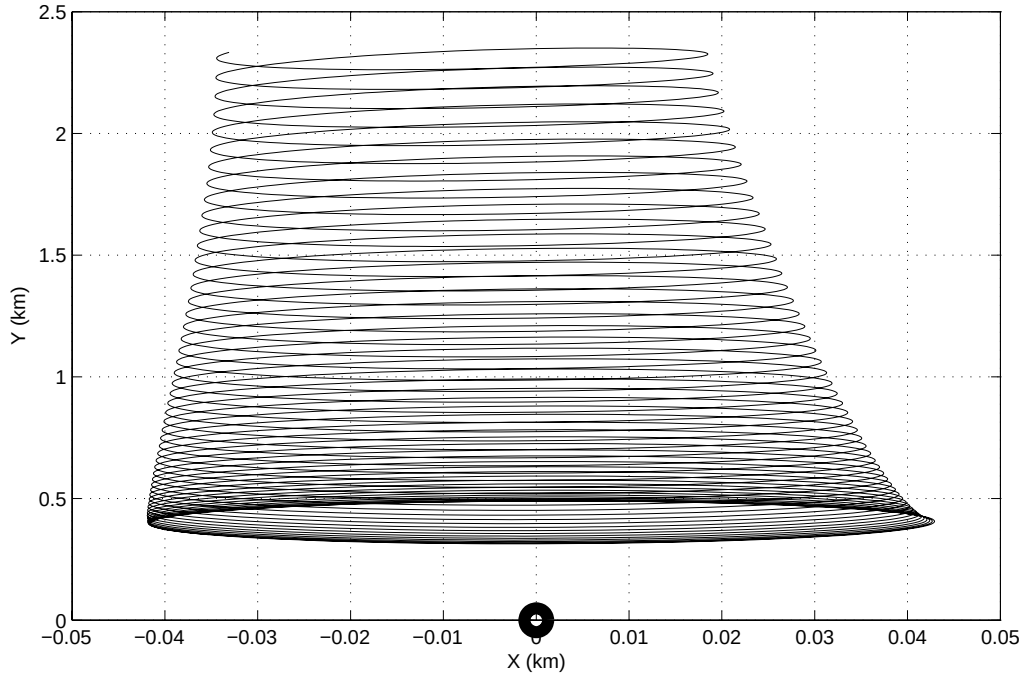

Fig. 150 Drifting of the camera-satellite due to drag (XY projection)

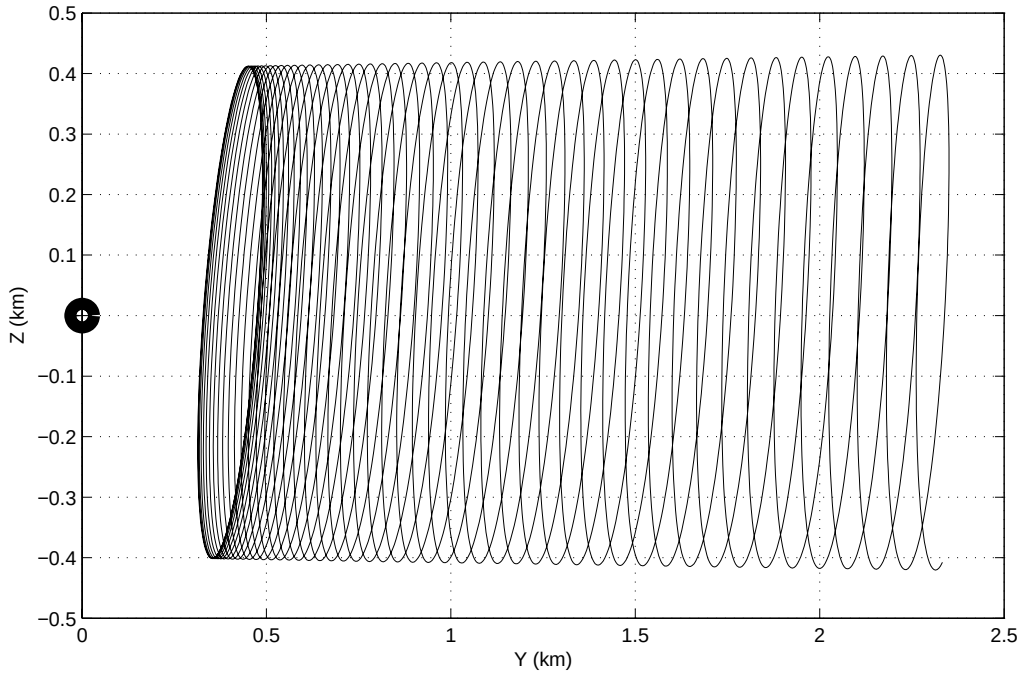

Fig. 151 Drifting of the camera-satellite due to drag (YZ projection)

The camera doesn't move around the object but quickly drift away during the 50 orbits of the simulation. Following the results of Chapter **Error! Reference source not found.**, what can be done is to run an optimization where the fitness function is evaluated after 50 orbits. In this way

during this period (about three days), the camera will be orbiting in the neighbourhoods of the object to be monitored:

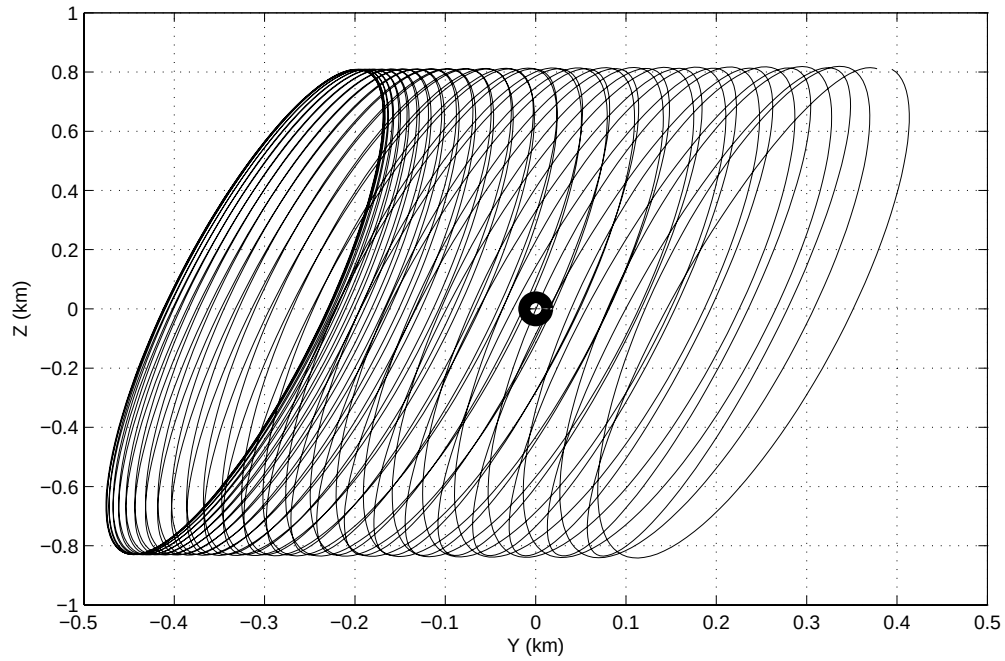

Fig. 152 Strategy of maintaining the formation compact for 50 orbits (XY projection)

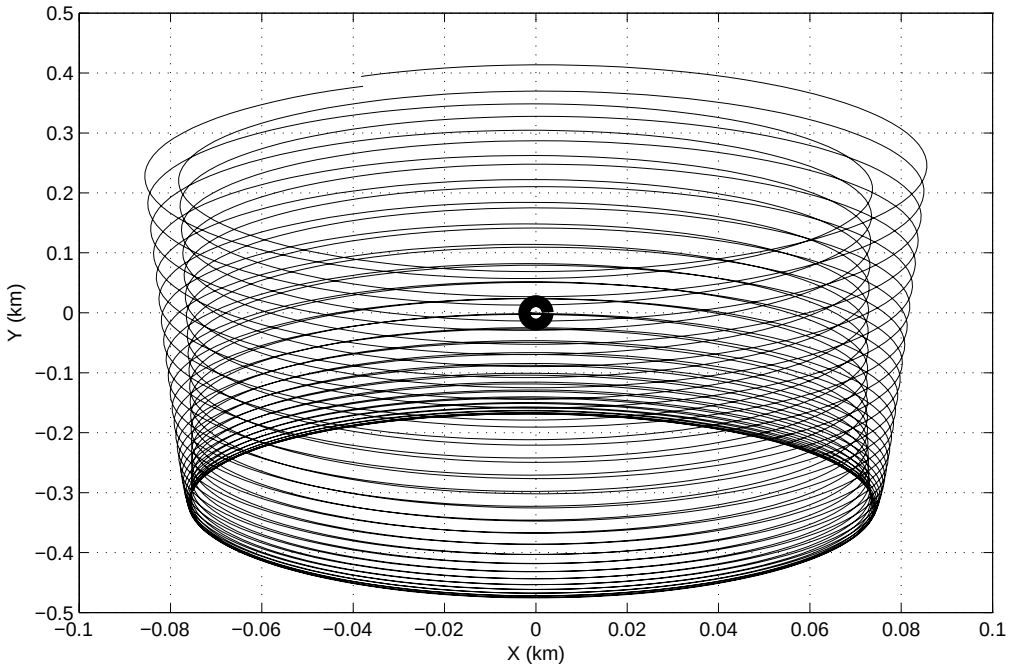

Fig. 153 Strategy of maintaining the formation compact for 50 orbits (YZ projection)

After that period, the nano-satellite will drift away as in the previous case. From Fig. 154, Fig. 155 and Fig. 156 it is possible to see how the responsible for the formation breaking is mainly the behaviour of the component along Y axis.

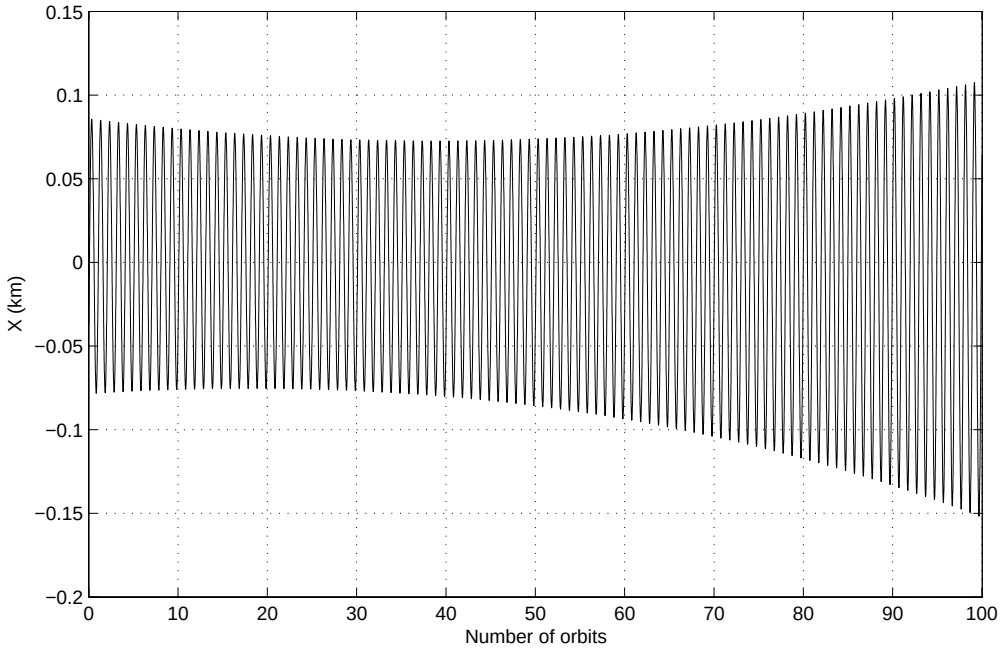

Fig. 154: 100 orbits propagation of the strategy maintaining the formation compact for 50 orbits (X component)

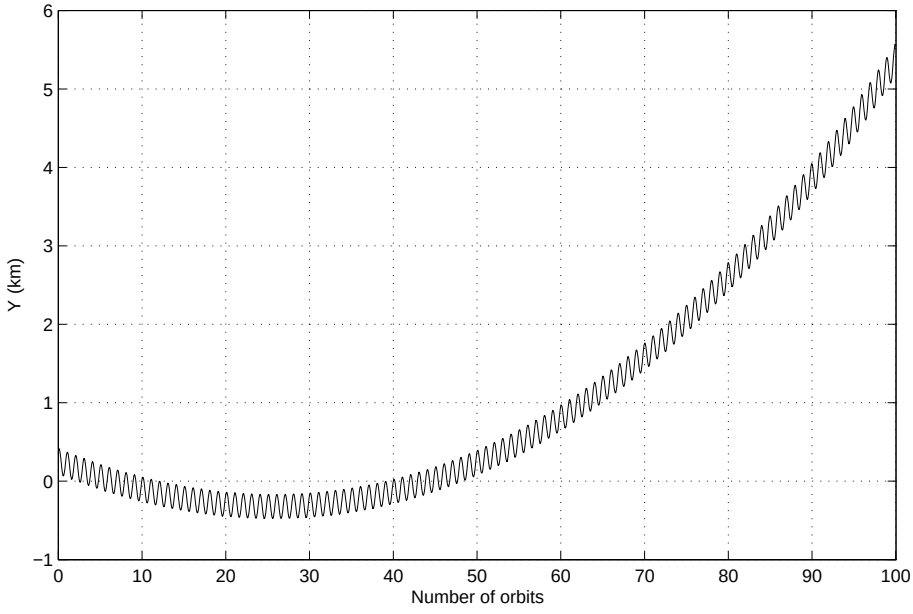

Fig. 155: 100 orbits propagation of the strategy maintaining the formation compact for 50 orbits (Y component)

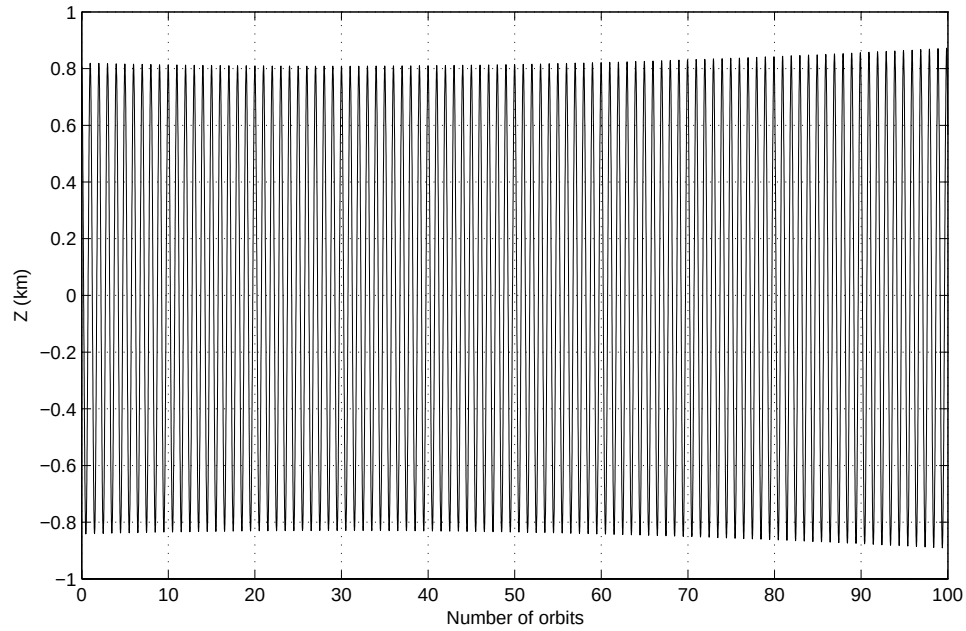

Fig. 156 : 100 orbits propagation of the strategy maintaining the formation compact for 50 orbits (Z component)

A manoeuvre is therefore necessary. The manoeuvre performed is accomplished in order to start again the "go away and come back" motion. The position of the camera after 50 orbits is assigned, and we want to calculate the necessary ΔV to modify the relative trajectory and avoid the drift after the 50th orbit. As x and z components have not a tendency to diverge, the manoeuvre will be performed just along the *y* axis, in order to avoid the drift along that direction. This means that the optimization is performed assuming $\dot{y}_0$ and T as the only two variables, while $\dot{x}$ and $\dot{z}$ are considered fixed. For example, after the first 50 orbits the relative state is given by:

$$x_f = \text{-}0.037852 \text{ km}$$

$$y_f = 0.377946 \text{ km}$$

$$z_f = 0.810730 \text{ km}$$

$$\dot{x}_f = 6.75025\text{e-}5 \text{ km/s}$$

$$\dot{y}_f = 7.66726\text{e-}5 \text{ km/s}$$

$$\dot{z}_f = 5.92971\text{e-}5 \text{ km/s}$$

x_f , y_f , z_f , $\dot{x}_f$ and $\dot{z}_f$ are assigned and fixed in the GA for two different reasons: the relative distances x_f , y_f , z_f are fixed to keep the space vector continuous; the relative velocities $\dot{x}_f$ and $\dot{z}_f$ have a negligible effect with respect to $\dot{y}$.

As a result of the optimization, in order bound the relative motion, the state must assume these values:

$$x_0 = \text{-}0.037852 \text{ km}$$

$$y_0 = 0.377946 \text{ km}$$

$$z_0 = 0.81073 \text{ km}$$

$$\dot{x}_0 = 6.75025\text{e-}5 \text{ km/s}$$

$$\dot{y}_0 = \underline{8.83999\text{e-}5 \text{ km/s}}$$

$$\dot{z}_0 = 5.92971\text{e-}5 \text{ km/s}$$

In other words, the final state vector after the first 50 orbits is the same as the initial state vector of the following 50 orbits with the exception of the relative velocity along *y* axis.

This change in the $\dot{y}$ component is sufficient to eliminate the drift during the orbits 51-100 (as instead it would be without manoeuvring). The resulting trajectory is shown in Fig. 157 and Fig. 158.

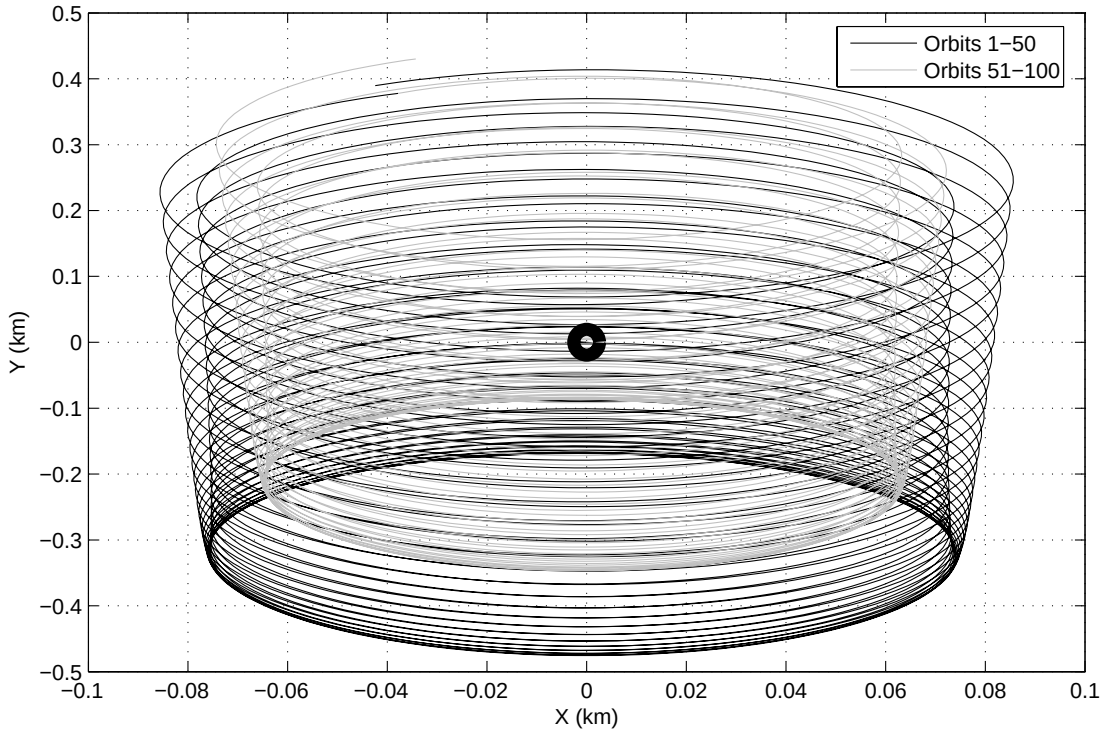

Fig. 157: Strategy manoeuvring every 50 orbits (XY projection)

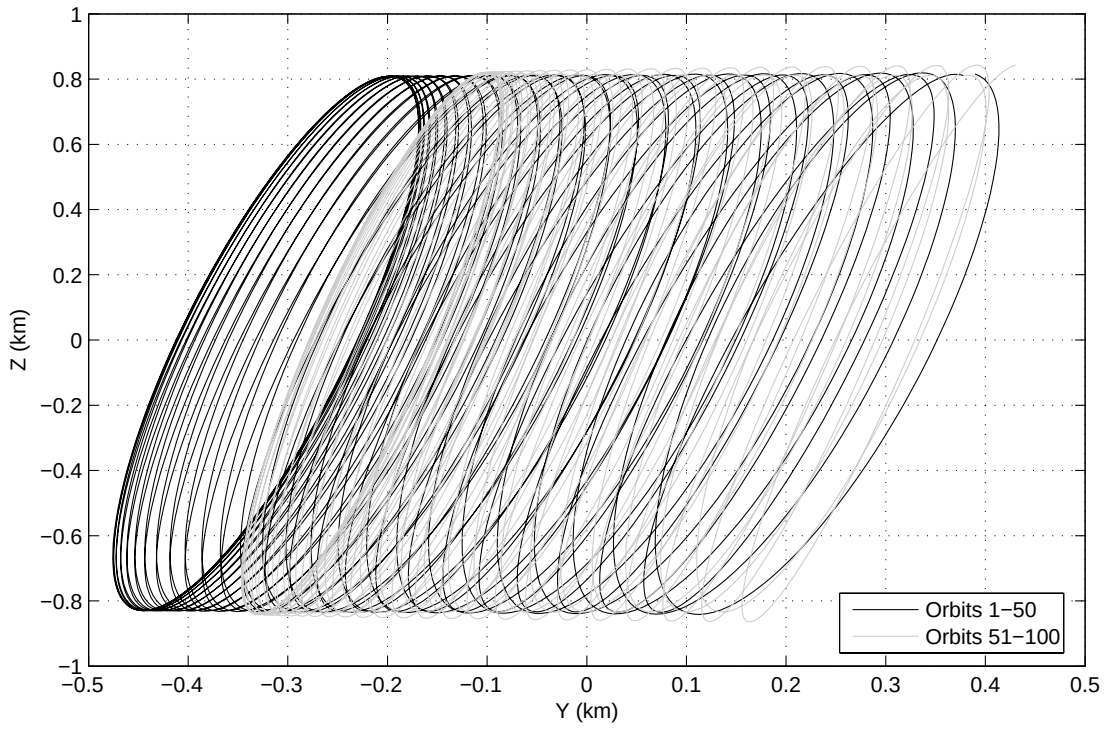

Fig. 158: Strategy manoeuvring every 50 orbits (YZ projection)

Fig. 159 zooms Fig. 157 in order to see the manoeuvre point.

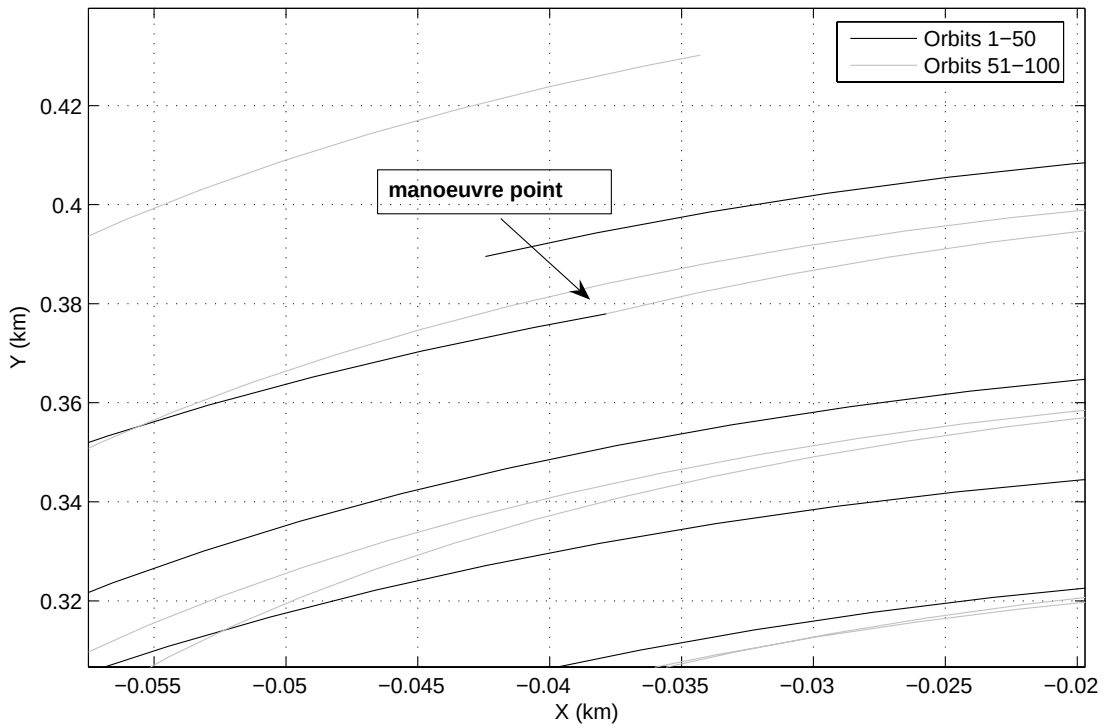

Fig. 159: Strategy manoeuvring every 50 orbits (zoom of the manoeuvring point)

In this way, the object of the observation is always in the neighbourhoods of the monitoring satellite. The ΔV required is simply calculated by the difference between the $\dot{y}_0$ and the $\dot{y}_f$:

$$\Delta V_1 = \text{-1.125323740000002e - 005 km/s}$$

The preceding can be repeated without any modification. Two more manoeuvres are simulated, at the100th and at the 150th orbits. The resulting ΔV are smaller then in the first case:

$$\Delta V_2 = 3.897508027203157\text{e - 006 km/s}$$

$$\Delta V_3 = 3.306446315298140\text{e - 006 km/s}$$

Fig. 160 shows the behaviour along the y axis, where the drift mainly locates without control:

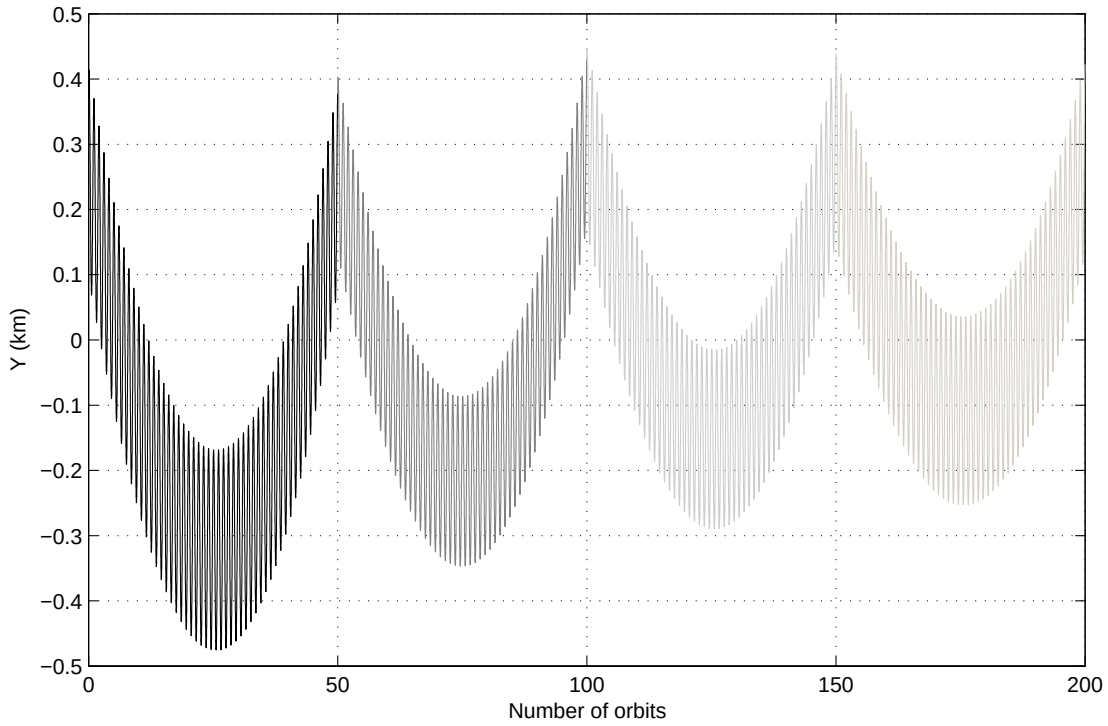

Fig. 160 Y component behaviour for 200 orbits (3 manoeuvres)

The trajectory followed by the camera-satellite for 200 orbits is plotted in Fig. 161: it emphasizes how the formation keeps bounded in time, using very low ΔV demanding manoeuvres.

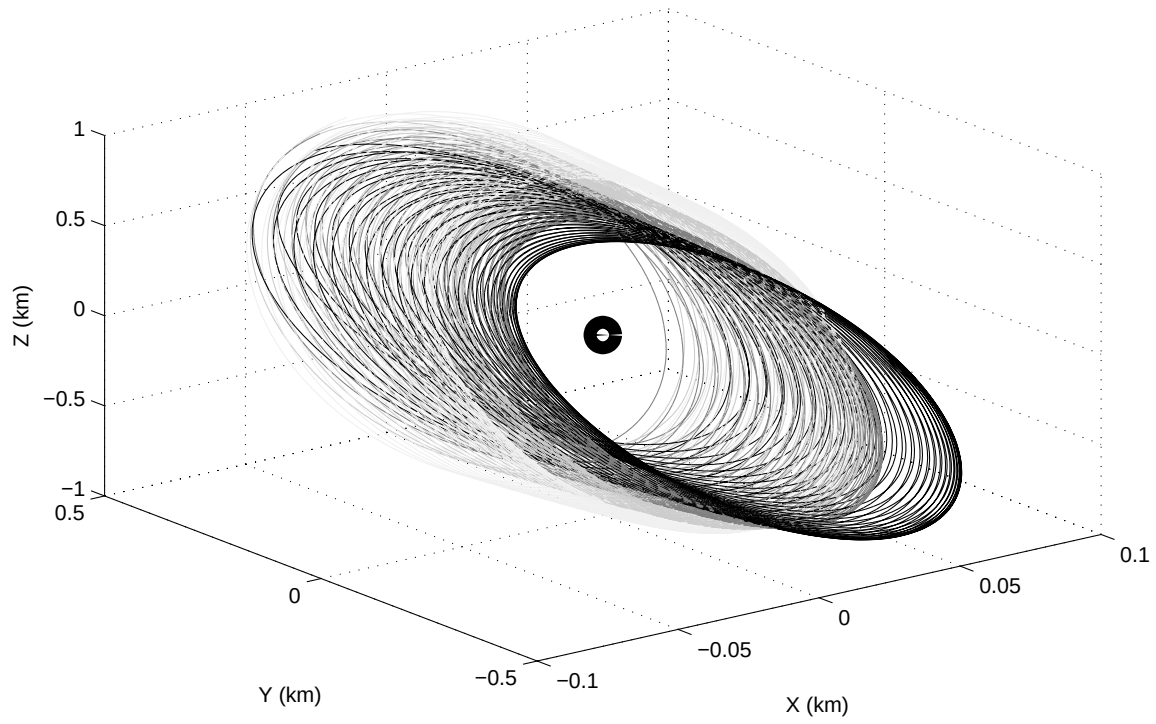

Fig. 161 Relative orbits with 3 manoeuvres

7.3. Very large structures assembly

In the latest years it became evident that the most demanding missions can be accomplished only operating outside of the Earth's atmosphere. Doing so the great amount of ΔV needed for the take-off is saved. For instance, an ESA project of a mission to mars (HMM: Human Mission to Mars, from the Concurrent Design Facility) plans the in orbit assembly of the spacecraft's structure [24].

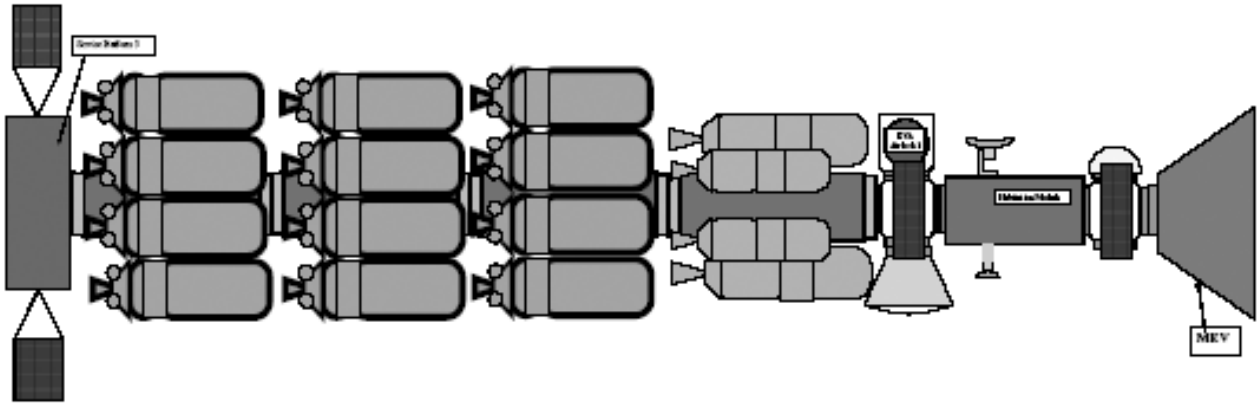

The space vehicle is so large that about 25 launches would be necessary in order to put in orbit the foreseen one thousand tons of materials. The parking orbit could be a LEO, a nuclear safe orbit, a MEO, a GEO, or a HEO. When choosing the orbit for the assembly operations, nuclear safe orbits

will only be considered if nuclear devices are present in the composite, currently none are base lined. Elliptical orbits are discarded due to the complexity of the RDV manoeuvre. GEO and HEO are discarded due to the loss of performance of the launchers and the (potentially) more hostile environment.

LEO is the preferred assembly orbit. An altitude of 400 km (similar to that of the ISS, where drag has to be taken into account) has been selected.

We can imagine a situation requiring two components to not dock immediately but waiting for a collector. In this situation, a strategy similar to that discussed in Chapter 5 can be implemented. In fact a launch frequency between one and three months is given. For our simulation we choose a mean period of two months.

The two components, close after their release in orbit, must be again close to each other after two months, that's about one thousand orbits, in order to accomplish rendezvous with the collector. Referring to the notation of paragraph 6.3, the fitness function is evaluated by GA after N=1000 orbits. Inserted with the right initial conditions and with no other control, the two agents will drift apart and than get close again after two months, ready for the rendezvous with the last component launched.

In the Low Earth Orbit characterized by:

$a = 6778$ km

$e = 0.00118$

$i = 50°$

$\omega = 90°$

$\Omega = 270°$

$\theta = 0°$

the projections along the three axes are reported in Fig. 162, Fig. 163 and Fig. 164.

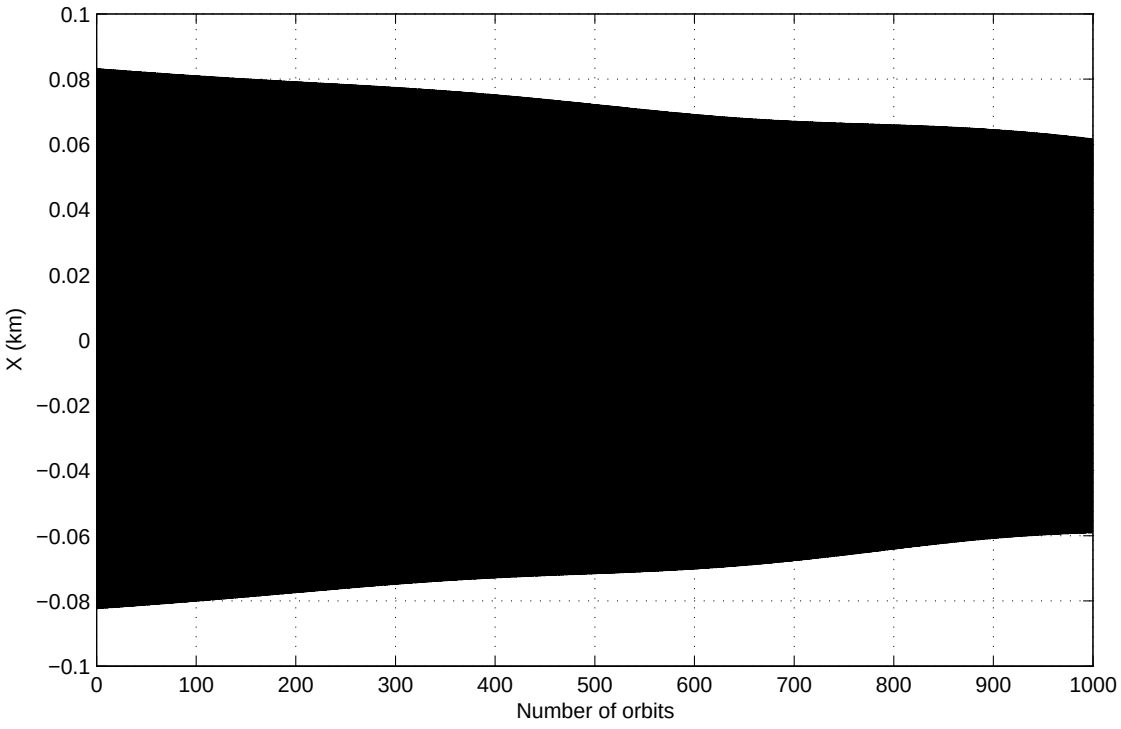

Fig. 162 Fixing rendezvous after 1000 orbits (X component)

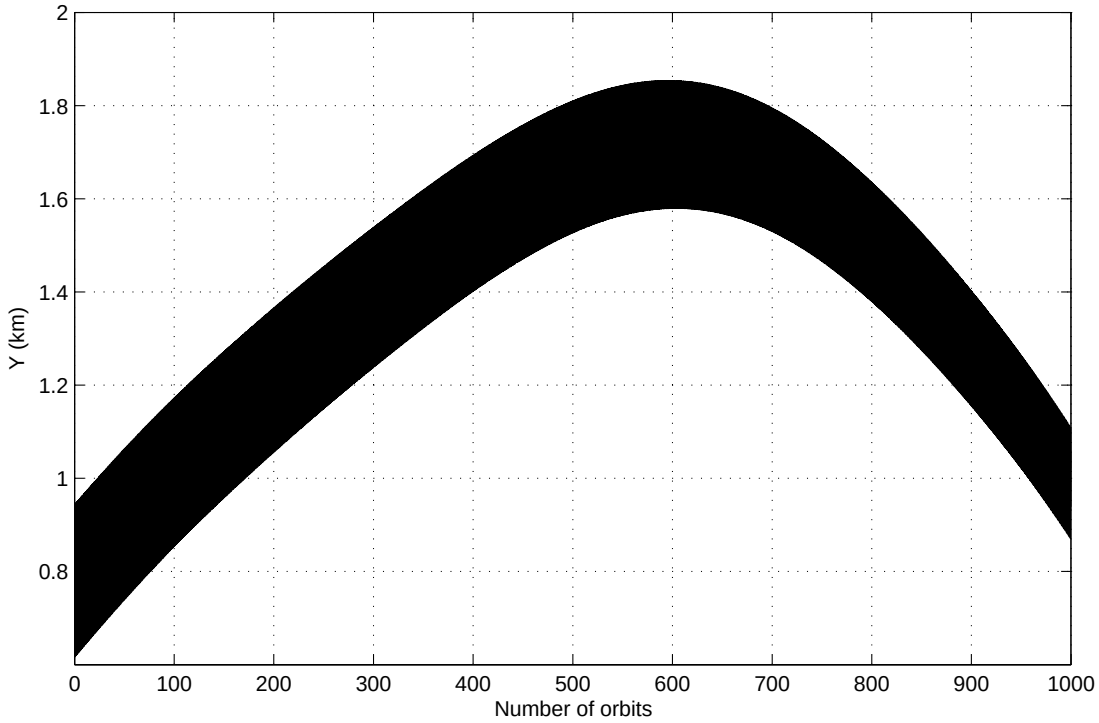

Fig. 163 Fixing rendezvous after 1000 orbits (Y component)

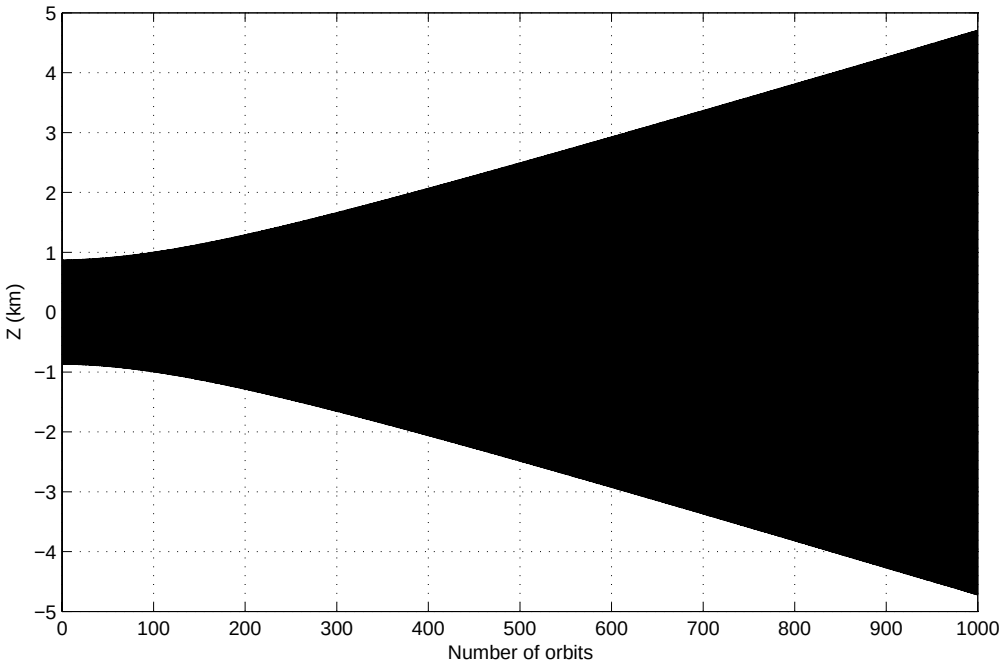

Fig. 164 Fixing rendezvous after 1000 orbits (X component)

After 1000 orbits the vehicles are close enough and ready for rendezvous.

Of course if the parking orbit is intended to be at a lower altitude, for example 300 km, the separation of the two components would be much greater, as Fig. 165 shows referring to the behaviour along Y axis.

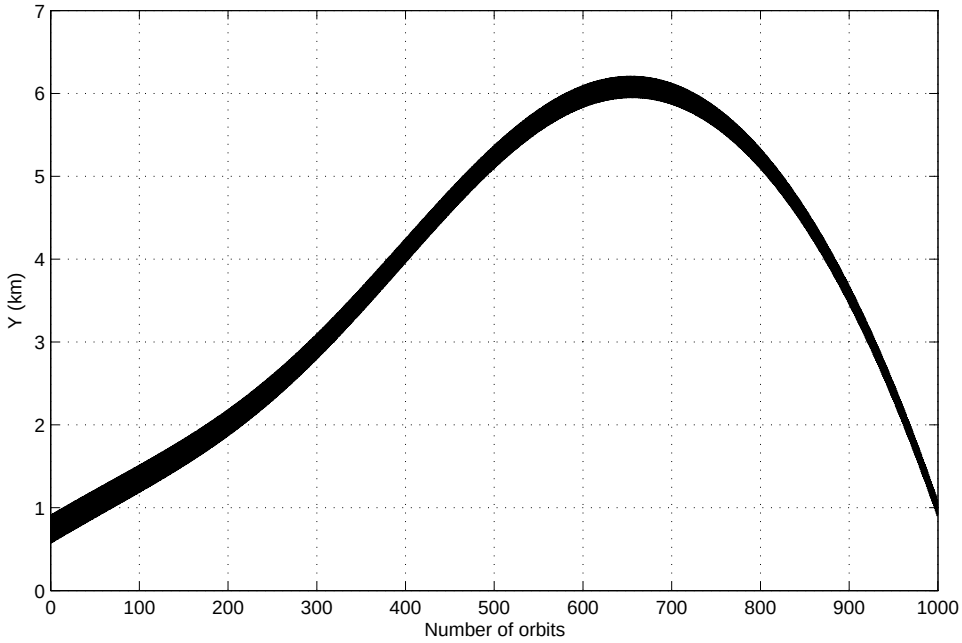

Fig. 165 Fixing rendezvous after 1000 orbits (Y component, h=300 km)

8. Conclusions

In the present work the invariance of relative satellite motion has been numerically analysed through a genetic algorithm based on the PIKAIA freely on line available software, modified in order to fulfil the precision and data handling requirements imposed by the study.

In Chapter **Error! Reference source not found.** the basic principles and main characteristic of a genetic algorithm are illustrated, and the tool has been tuned. The tuning has been time demanding, because of some random behaviour unavoidable when using GAs. Results can be satisfying in 9 cases on 10 and then be failing in the last attempt. The conclusion of the tuning has led to a set of parameters which minimize the possibility for the algorithm to fail in the optimization, but without cancelling it completely.

In Chapter **Error! Reference source not found.** the GA is used to study the unperturbed reference orbit case. A number of models are available in literature: from the classical HCW equations for circular orbit to the TH equations for the elliptical ones. These linear models supply a good approximation for the closing conditions in low dimensions formations. Other models try to include higher order terms of the gravitational potential. For circular orbits the most complete analytical model results to be sufficient to ensure bounded ness of relative orbits. So, the circular unperturbed reference orbit is just a test case for the GA, successfully passed. Introducing eccentricity results in a much more important impact of non-linearities, and analytical models can fail to catch the right initial conditions to obtain closed relative orbits. GA, on the other hand, results to perform well for every eccentricity and orbit dimension. The most important conclusion of Chapter **Error! Reference source not found.** is the fact that when a closing condition exists, GA is able to find it.

In Chapter **Error! Reference source not found.** a very important case is studied: satellites subject to J_2 perturbation. The above mentioned problem has been deeply studied in the latest years, as J_2 is the main perturbation affecting satellites orbiting around the Earth at altitudes higher then 400 kilometres. There exist a variety of models supplying conditions for invariant J_2 motion. Some of them, in spite of some limitations, work pretty well. But only a numerical research has led to the conclusion that invariant J_2 orbits are not caught by these models; not because of their approximations, rather because these invariant orbits simply do not exist. The cause is the non-periodic behaviour of the J_2 harmonic; only cancelling this effect initial conditions for a periodic relative orbit can be found.

When the reference orbit is critically inclined, this means when the argument of perigee shows no secular drift, i.e. at 63.434° and 180°-63.434°= 116.565°, a periodic relative motion is possible and the proper initial conditions are obtained.

Surprisingly, also other two inclinations where it is possible to obtain quasi-periodic orbits are found. For the very common case of LEO, this is about at 50° and at 180°-50°=130°. The physical explanation for these two more results is still unexplained. At present we can only say they are maybe particular inclinations where the non-periodic effects of the perturbation are somehow much weaker, but they are no more valid when the eccentricity grows.

In Chapter **Error! Reference source not found.** the effects of other minor gravitational perturbations are analysed. The presence of other celestial bodies (called third body effect) and the higher harmonics of the geopotential are analysed. Their influence is minimal, and they neither break the bounded ness of the relative orbit, if this is truly periodic, nor they make the situation worst for the cases when the relative orbits are bounded but not periodic. This is shown to be valid both for LEO and for GEO orbits. Therefore, these perturbations are not taken into consideration in the subsequent part of the work.

In Chapter **Error! Reference source not found.** an important perturbation for low orbits is considered: air drag. The presence of this non-conservative force makes any attempt to find closed relative orbits vain.

In fact, satellites will always drift apart when subject to differential drag. A different use of the GA is then implemented. The aim now is not to have the satellite passing for the same point, with the same velocity after a certain time, as it has been imposed when searching for periodic motion. The purpose is instead to maintain the formation compact for a given number of orbits. This means the satellites are free to drift apart, but in such a way that after the imposed time they will be close again. Of course, the longer is the period for the formation to be bounded, the bigger is the distance between satellites during that period. The mission requirements will drive the strategy's choice (formation more compact but for brief time span or looser spatial constraints but for longer periods). The influence of drag is affecting formation dynamics up to 500 km of altitude. Though never disappearing entirely, in theory, above that altitude its effects can be neglected without heavy approximations.

In Chapter 7 limits and possible applications of the presented approach are analysed. Imposing initial conditions to a satellites in order to ensure a periodic motion for the formation requires a great precision. Global Positioning System (GPS) sensors are verified to be incapable to supply the necessary performances, even when implementing Carrier Differential GPS (CDGPS). Ground-tracking is even less performing. This leads to two conclusions: 1) the conditions found by GA as in

this work have an important theoretic value, because thanks to them it has been possible to recognize *when* an invariant motion is possible, and what can be done when it is physically impossible; 2) the initial conditions found cannot be used directly, but they generate a relative orbit that can be usefully taken as reference trajectory for a controller such as a Linear Quadratic Regulator (LQR) with a probable great saving of ΔV .

Two possible scenarios have been presented. In the first one, a continuous visual health status monitoring of the structures of large spacecraft like Space Shuttle (STS) or International Space Station (ISS) has been implemented using the technique of maintaining the formation compact for a certain number of orbits, in order to counteract the effects of drag. After the established number of orbits, a very weak control is necessary to avoid breaking of the formation. The direction of the control has been argued by physical considerations, its intensity through the GA.

A final application suggested is the in orbit assembly of large structures. In some cases, it would be preferable to have more bodies waiting for a collector, instead of performing the docking each time a component is launched. Of course, the bodies can be orbiting very far from each other, but it's important to have them close when the collector is launched, and this could happen two months after the first components. The usual strategy of leaving the formation free to break with the condition of being compact after a given period (two months, in this case) is successfully implemented.

Future developments of the present work can be:

1) a deep study in the J_2 perturbed case of the existence of the apparent periodicity inclinations (though they are not the critical ones);
2) the implementation of a controller exploiting the results obtained in terms of reference trajectory;
3) searching for other possible applications, mainly in the field of scientific research (study of Earth magnetic field, astronomy, remote sensing).

REFERENCES

[1] Charbonneau P., Knapp B., “A user’s guide to PIKAIA 1.0”, NCAR Technical note 418+1A (Boulder: National Centre for Atmospheric Research), 1995.

[2] Myatt, D.R., Becerra, V.M., Nasuto, S.J., and Bishop, J.M., “Advanced Global Optimisation for Mission Analysis and Design.” Final Report. Ariadna id: 03/4101. Contract Number: 18138/04/NL/MV, 2004. Available on-line: http://www.esa.int/gsp/ACT/doc/ACTRPT-ARIADNA-03-4101-Reading.pdf.

[3] Inalhan G., Tillerson M., How J. P., “Relative dynamics and control of spacecraft formations in eccentric orbits”, Journal of Guidance, Control and Dynamics, Vol. 25, No. 1, 2002, pp. 48-59.

[4] Izzo D, “Formation Flying linear modelling ”, Proceedings of the 5th International Conference On Dynamics and Control of Systems and Structures in Space held in Cambridge , UK , 14-18 July 2002, pp. 283-289.

[5] Kim Y. H., Spencer D. B., “Optimal Spacecraft Rendezvous Using Genetic Algorithms”, Journal of Spacecraft and Rockets, vol. 39, No. 6, November-December 2002.

[6] Izzo D., Sabatini M., Valente C., “A new linear model describing formation flying dynamics under J_2 effects”, Proceedings of 17th AIDAA national congress held in Rome, ITA, 15-19 September 2003, Vol.1, pp.493-500.

[7] Schaub H., Alfriend K.T**.,** **“**J_2 invariant relative orbits for spacecraft formations,” Celestial Mechanics and Dynamical Astronomy, Vol. 79, 2001, pp. 77-95.

[8] Tschauner J., “Elliptic orbit rendezvous”, AIAA journal, vol.5, no.6, pp. 1110-1113, 1967.

[9] Vadali S. R., “An analytical solution for relative motion of satellites”, Proceedings of the 5th International Conference on Dynamics and Control of Structures and Systems in Space held in Cambridge , UK , 14-18 July 2002.

[10] Clohessy W. H., and Wiltshire R. S., “Terminal Guidance System for Satellite Rendezvous,” Journal of the Aerospace Sciences, Vol. 27, No. 9, 1960, pp. 653-658.

[11] Tshauner J., and Hempel P., “Rendezvous zu einem in Elliptischer Bahn Umlaufenden Ziel,” Acta Astronautica, Vol. 11, 1965, pp. 104-109.

[12] Rimrott, Fred P.J., “Introductory Orbit Dynamics”, Braunschweig; Wiesbaden: Vieweg,1989.

[13] Lovell T.A., “Analysis of the reconfiguration and maintenance of close spacecraft formations“, 13th AAS/AIAA Space Flight Mechanics Meeting, Puerto Rico, 9-13 February 2003

[14] Kasdin J. and Gurfil P., “Hamiltonian Modelling of Relative Motion”, Ann. N. Y. Acad. Sci., 2004, pp. 138-1157.

[15] Parkinson B. W. and Spilker J.J. Jr., “Global Positioning System: Theory and Applications”, published by AIAA, 1995.
[16] Strang G. and Borre K., “Linear Algebra, Geodesy, and GPS”, Wellesley-Cambridge Press, 1997.
[17] Vaddi S. S., Vadali S.R., and Alfriend K.T., “Formation Flying: Accommodating Nonlinearities and eccentricity Perturbations”, Journal of Guidance, Control, and Dynamics, Vol. 26, No. 2, March-April 2003, pp. 214-223.
[18] Williams T., “Determination of Satellite Formation Geometry and Phasing From Range Data”, 13th AAS/AIAA Space Flight Mechanics Meeting, Puerto Rico, 9-13 February 2003.
[19] Ebinuma T., Bishop R.H. and Lightsey E.G., “Integrated Hardware Investigations of Precision Spacecraft Rendezvous Using the Global Positioning System”, 13th AAS/AIAA Space Flight Mechanics Meeting, Puerto Rico, 9-13 February 2003.
[20] Schweighart S.A and Sedwick Raymond, “A high fidelity linearized model for satellite formation flying”, AIAA Journal of Guidance, Control, and Dynamics, 2003.
[21] Martin M., Kilberg S., “Techsat21 and revolutionizing space missions using microsatellites”, American Institute of Aeronautics and Astronautics, SSC01-1-3.
[22] kasdin e koleman
[23] Schaub H., Junkins J.L., “Analytical Mechanics of Space Systems”, AIAA Education Series, 2003.
[24] HMM Assessment Study, ESA Technical Report CDF-20(A), pp. 89- 101 February 2004.